STRUCTURAL, METAMORPHIC AND TECTONIC STUDIES IN CENTRAL GAGNON TERRANE, GRENVILLE PROVINCE

STEVEN H. SCHWARZ

National Library
of Canada

Acquisitions and
Bibliographic Services

395 Wellington Street
Ottawa ON K1A 0N4
Canada

Bibliothèque nationale
du Canada

Acquisitions et
services bibliographiques

395, rue Wellington
Ottawa ON K1A 0N4
Canada

Your file Votre référence

Our file Notre référence

0-612-47431-3

Canada

STRUCTURAL, METAMORPHIC AND TECTONIC STUDIES IN CENTRAL GAGNON TERRANE, GRENVILLE PROVINCE

by

©Steven H. Schwarz, B.Sc. (Hons)

A thesis submitted to the School of Graduate Studies

in partial fulfilment of the

requirements for the degree of

Master of Science

Department of Earth Sciences
Memorial University of Newfoundland

1998

St. John's Newfoundland

ABSTRACT

The Gagnon terrane, comprising the lower deck of the Parauthochthonous belt in northeastern Grenville Province, is a metamorphic fold-thrust and nappe belt consisting of Paleoproterozoic supracrustal rocks (Knob Lake Group) and their reworked Archean basement (Ashuanipi Metamorphic Complex) that is tectonically overlain by the Molson Lake terrane. This thesis comprises a structural-metamorphic-geochronologic study of an area in the central Gagnon terrane in eastern Québec, some 80km south of the Grenville Front.

The structural component of the study involved the division of the area into thrust sheets utilizing stratigraphic, younging and fabric criteria, evaluation of the structural architecture, and interpretation of the structural evolution. Ductile thrusts bounding the thrust sheets have steep dips in the northern part of the map area, whereas those farther south have intermediate dips towards the north and a southerly vergence. This southerly vergence is in contrast to the well-developed northerly (-northwesterly) vergence that has been reported previously in the northern Gagnon terrane, and is interpreted in terms of backthrusting due to the incorporation of a major wedge of basement rocks into the thrust stack during its construction.

Overall within the study area, there is evidence for four phases of deformation (D_1-D_4). D_1 involved development of the regional, penetrative foliation (S_1), that is subparallel to relict compositional layering (S_0) in most outcrops. F_1

folds vary from outcrop- to map-scale; large-scale F_1 folds had approximately E-W trending axes and are overturned towards the south or recumbent in different thrust sheets. In the northern thrust sheets, D_1 fabrics are refolded by outcrop- and map-scale F_2 folds with variably penetrative S_2 fabrics and generally SE-plunging axes. F_3 folds, previously unrecognized within Gagnon terrane, are local small-scale recumbent structures that occur in the northern thrust sheets and are interpreted to have developed as a result of gravitational collapse of the overthickened, thermally-weakened crust. F_4 folds are large-scale upright variably plunging cross-folds best developed in the southern part of the study area. Overprinting of folds of different generations has led to a wide range of structural interference patterns on all scales within the map area.

Metamorphic rocks within the study area are composed of amphibolite facies mineral assemblages, and evidence of partial melting in rocks of pelitic and quartzofeldspathic composition is widespread. Field and microstructural relationships indicate that peak metamorphism and porphyroblast growth occurred syn- to post-D_1 and pre- to syn D_2, although there are local variations according to thrust sheet. The Lac Don thrust sheet in the northern part of the map area contains the assemblage Qtz-Ms-Grt-Bt-Pl±Kfs-L, whereas the Lac Gull thrust sheet farther south contains the assemblages Qtz-Kfs-Ky-Bt-Grt-L or Qtz-Ms-Kfs-Ky-Bt-Grt-L. Garnet zoning profiles from the Lac Don thrust sheet exhibit relict growth zoning that was significantly altered by post-peak re-equilibration,

suggesting that temperature remained high for a prolonged period of time and that exhumation was relatively slow in this area. In contrast, garnets in the Lac Gull thrust sheet exhibit well-preserved growth profiles with very narrow retrograde rims, suggesting a hairpin shaped P-T path as a result of rapid, tectonically-driven exhumation. P-T estimates from both samples are in the range of 710-800^{0}C and between 12-15 kbars.

Thrusts faults are locally intruded by pegmatites, one of which shows evidence of syntectonic (post-D_1/pre-D_2) intrusion. This pegmatite has been dated by the U/Pb zircon method at 995 ± 2 Ma, thus providing the first direct estimation of the age of peak metamorphism and crustal thickening within this part of Gagnon terrane.

These structural, metamorphic and geochronologic data are compatible with existing tectonic models for the northeastern part of Gagnon terrane in which NW-directed transport of a thrust wedge (Molson Lake terrane) over its foreland (Gagnon terrane) resulted in the progressive accretion of Gagnon terrane to the base of a thickening thrust wedge. However, the data from this thesis suggest that the tectonic evolution in central Gagnon terrane differed significantly in detail from that farther north. Metamorphic grade (both P and T) is higher, map-scale recumbent fold nappes are present, and northerly vergence and back-thrusting, due to the incorporation of a thick slice of basement rocks into the thrust pile, is important. These features have been incorporated into a revised tectonic model for the evolution of Gagnon terrane.

ACKNOWLEDGEMENTS

There are many people to be acknowledged for contributing to the completion of this thesis and to my studies at Memorial University. First I would like to thank my supervisors, Toby Rivers and Aphordite Indares, for their encouragement and support over the course of my M.Sc program, and for allowing me to pursue valuable non-academic employment during my time at MUN.

The thesis also benefited significantly from discussions with Jeroen van Gool and Pablo Valverde-Vaquero. My thanks as well to John Ketchum for helpful comments on the metamorphic section, and to Greg Dunning and Pablo Valverde-Vaquero for their assistance in the geochronology lab. Special thanks to Maria and Lydia Smirnova for their help in drafting the figures.

I would like to thank the administrative and technical staff in the Department of Earth Sciences, and particularly Gerri Starkes and Pat Browne for their help throughout my stay. Thank you to Steve House, Lori Dwyer and Laurel McDonald for their assistance in the field, and Rick Small of the Carol Inn in Labrador City for help with logistics.

I am extremely grateful to my mother and to John Glynn, for their incredible support and help throughout this sometimes difficult period. I also want to thank my friends, specifically those who have not yet finished their theses: Michèle, Laurel, Jason, Ian "grey/green guy", Kevin and Lori. Finally, I am especially

indebted to "Mimi", who has shown me that there is life during the writing of a thesis.

FRONTISPIECE

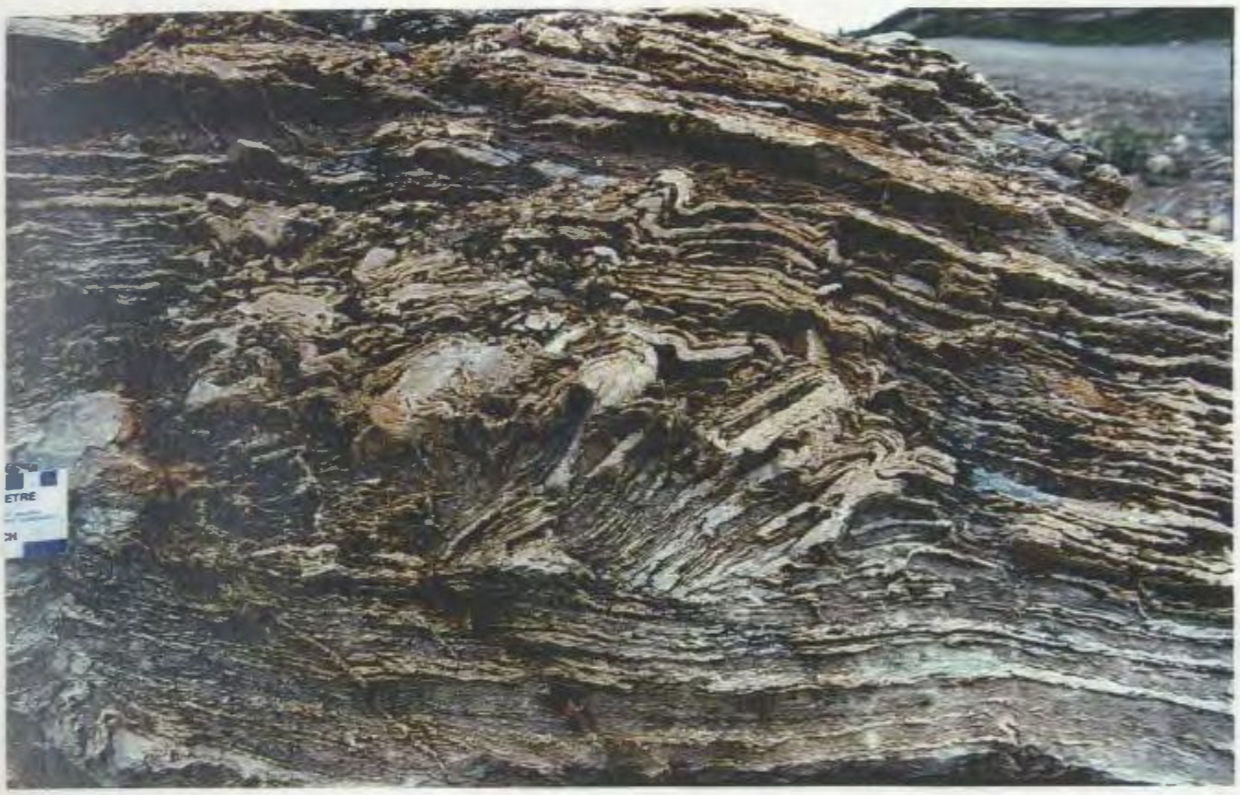

Brittle and ductile deformation, in marble of Denault Formation, that bears a remarkable similarity to the proposed tectonic model of central Gagnon terrane. Of particular interest in the photograph are the subvertical axial surfaces which steepen towards the left. Similar, but large-scale, south vergent structures have been observed in the field area, in contrast to northerly (- northwesterly) vergence in the northern Gagnon terrane. Southerly vergent structures are inferred to have developed as a result of backthrusting due to incorporation of a thrust wedge into the thrust stack, as seen in the lower right of the photograph.

TABLE OF CONTENTS

ABSTRACT ii

ACKNOWLEDGEMENTS v

FRONTISPIECE vii

TABLE OF CONTENTS viii

LIST OF TABLES xiii

LIST OF FIGURES xiv

LIST OF PLATES xvii

CHAPTER 1: THE GRENVILLE OROGEN 1

1.1 LOCATION AND SIGNIFICANCE OF THE GRENVILLE OROGEN 1

1.2 HISTORY OF THOUGHT 3

1.3 THE PARAUTOCHTHONOUS BELT OF GRENVILLE PROVINCE IN WESTERN LABRADOR AND EASTERN QUÉBEC 7

1.4 AIMS OF STUDY 12

1.5 LOCATION OF STUDY AREA 13

1.6 METHODOLOGY EMPLOYED IN GEOLOGICAL MAPPING 14

CHAPTER 2: STRATIGRAPHY 16

2.1 LITHOLOGIES OF THE GAGNON TERRANE 16

2.2 DESCRIPTION OF ROCK TYPES IN THE FIELD AREA 18
- 2.2.1 Attikamagen Formation 18
- 2.2.2 Denault Formation 23
- 2.2.3 Wishart Formation 23

2.2.4 Sokoman Formation 26
2.2.5 Menihek Formation 31
2.2.6 Lac Gull Formation 31
2.2.7 Gabbro And Related Lithologies 34
2.2.8 Granitoid Rocks 37

2.3 PALINSPASTIC RECONSTRUCTION OF SHELF 37

CHAPTER 3: STRUCTURAL GEOLOGY 44

3.1 INTRODUCTION 44

3.2 PREVIOUS WORK IN AND ADJACENT TO THE STUDY AREA 45

3.3 THIS STUDY 47

3.4 DIVISION OF AREA INTO THRUST SHEETS 48
3.4.1 Lac Audréa Shear Zone 48
3.4.2 Gueslis Shear Zone 55
3.4.3 Lac Don Shear Zone 56
3.4.4 Lac Gull Shear Zone 59
3.4.5 Lac Lamêlée Shear Zone 59

3.5 THRUST SHEET STRATIGRAPHY 61
3.5.1 Gueslis Thrust Sheet 61
3.5.2 Lac Don Thrust Sheet 64
3.5.3 Lac Gull Thrust Sheet 65
3.5.4 Lac Lamêlée Thrust Sheet 65
3.5.5 Lac Hippocampe Thrust Sheet 66

3.6 COMPARISON OF THE STRATIGRAPHIES OF THE THRUST SHEETS 66

3.7 PHASES OF DEFORMATION IN THE STUDY AREA 68
3.7.1 Primary (D_0) Structures 71
3.7.2 D_1 Structures 77
3.7.3 D_2 Structures 84
3.7.4 D_3 Structures 89
3.7.5 D_4 Structures 89

3.8 STRUCTURE OF THRUST SHEETS 89
3.8.1 Gueslis Thrust Sheet 90

3.8.2 Lac Don Thrust Sheet 93
3.8.3 Lac Gull Thrust Sheet 95
3.8.4 Lac Lamêlée Thrust Sheet 95
3.8.5 Lac Hippocampe Thrust Sheet 95

3.9 RE-INTERPRETATION OF PUBLISHED MAPS ADJACENT TO THE STUDY AREA 96
3.9.1 Gueslis-Lac Don Thrust Sheet 102
3.9.2 Lac Gull Thrust Sheet 106
3.9.3 Lac Lamêlée Thrust Sheet 109
3.9.4 North Lamêlée Thrust Sheet 113
3.9.5 Lac Kendrick Thrust Sheet 114
3.9.6 Lac Hippocampe Thrust Sheet 115

3.10 MAP-SCALE INTERFERENCE PATTERNS 115

3.11 ARCHITECTURE OF THE THRUST STACK 120

3.12 STRUCTURAL SUMMARY 123

CHAPTER 4: METAMORPHISM 124

4.1 INTRODUCTION 124

4.2 PETROGRAPHIC MINERAL DESCRIPTIONS 124
4.2.1 Denault Formation 128
4.2.2 Wishart Formation 128
4.2.3 Sokoman Iron Formation 128
4.2.4 Attikamagen and Menihek Formation 129
4.2.5 Granitic Rocks 134
4.2.6 Garnet Amphibolites 134
4.2.7 Shabagamo Gabbro 135

4.3 RELATIVE TIMING OF PORPHYROBLAST GROWTH AND DEFORMATION 135
4.3.1 Gueslis Thrust Sheet 136
4.3.2 Lac Don Thrust Sheet 138
4.3.3 Lac Gull Thrust Sheet 141
4.3.4 Lac Lamêlée Thrust Sheet 141
4.3.5 Summary 141

4.4 P-T ESTIMATION OF MINERAL ASSEMBLAGES IN METAPELITIC AND QUARTZOFELDSPATHIC ROCKS 144
4.4.1 Assemblage: Ms_{ss}-Bt_{ss}-Qtz-Kfs(-Pl)±L 147
4.4.2 Assemblage: Ms_{ss}-Bt_{ss}-Qtz (-Pl)-Ky+L 147
4.4.3 Assemblage: Bt_{ss}-Ms_{ss}-Qtz (-Pl)-Ky-Kfs±L 148
4.4.4 Sub-Assemblage: Bt_{ss}±Ms_{ss}-Qtz (-Pl)-ky-Grt±Kfs± L 148

4.5 QUALITATIVE ESTIMATION OF P-T CONDITIONS IN DIFFERENT THRUST SHEETS 149
4.5.1 Gueslis And Lac DonThrust Sheets 149
4.5.2 Lac Gull Thrust Sheet 149
4.5.3 Lac Lamêlée Gull Thrust Sheet 150
4.5.4 Summary 150

4.6 P-T PATHS AND THERMOBAROMETRY 150
4.6.1 Introduction 150
4.6.2 Garnet Zoning And P-T Paths Theory 151
4.6.3 Studied Samples 153
4.6.4 Analytical Conditions 154
4.6.5 Mineral Compositions: S-11 155
4.6.5.1 Orthopyroxene 155
4.6.5.2 Plagioclase 155
4.6.5.3 Garnet 155
4.6.6 Qualitative Interpretation Of Mineral Zoning S-11 158
4.6.7 Mineral Compositions: S-218 161
4.6.7.1 Biotite 161
4.6.7.2 Plagioclase 161
4.6.7.3 Garnet 161
4.6.8 Qualitative Interpretation Of Mineral Zoning S-218 167

4.7 GEOTHERMOBAROMETRY 168
4.7.1 Methods 168
4.7.2 Selection Of Analyses 169
4.7.3 Quantitative P-T Results 171
4.7.3.1 Sample S-11 171
4.7.3.2 Sample S-218 172
4.7.4 Discussion And Comparison Of Results 175

4.8 CONCLUSION 177

CHAPTER 5: GEOCHRONOLOGY 179

5.1 INTRODUCTION 179

5.2 ANALYTICAL PROCEDURE 179

5.3 RESULTS 180

CHAPTER 6: TECTONIC MODEL FOR CENTRAL GAGNON TERRANE . . 182

6.1 INTRODUCTION: EXISTING MODEL NORTHERN GAGNON TERRANE 182

6.2 COMPARISON WITH EXISTING MODEL 186

6.3 REVISED TECTONIC MODEL FOR CENTRAL GAGNON TERRANE . . 188

6.4 CONCLUSION 193

REFERENCES 195

APPENDIX A_1: Outcrop locations in Field Area 207
APPENDIX A_2: Outcrop locations in Re-interpreted Area 208
APPENDIX B: U/Pb Data 209

LIST OF TABLES

Table 3.1 Distribution and orientation of map-scale structures by thrust sheet 117

Table 3.2 Summary of shear zone relationships 121

Table 4.1 Mineral assemblages in non-pelitic rocks 126

Table 4.2 Mineral assemblages in Attikamagen and Menihek formations . . . 127

Table 4.3 Representative orthopyroxene rim-core-rim compositions, S-11 . . 156

Table 4.4 Representative plagioclase rim-core-rim compositions, S-11 157

Table 4.5 Representative garnet compositions, S-11 159

Table 4.6 Representative matrix biotite compositions, S-218 162

Table 4.7 Representative plagioclase rim-core-rim compositions, S-218 164

Table 4.8 Representative garnet compositions, S-218 165

Table 4.9 Thermobarometric results 176

LIST OF FIGURES

Figure 1.1 Lithotectonic map of the northeastern Grenville Province in eastern Québec and western Labrador 6

Figure 1.2 Schematic cross-section of the Parautochthonous Belt in northeastern Grenville Province (modified from Rivers, 1992 and Rivers et al., 1993) 10

Figure 1.3 Map of the study area showing the major topographic features described in the text 15

Figure 2.1 Schematic palinspastic reconstruction of the Paleoproterozoic continental margin of the Superior Craton on which the Knob Lake Group was deposited 42

Figure 3.1 An outline of the major geological features and subdivision of the field area into five distinct thrust sheets, separated by shear zones 49,50

Figure 3.2 Location map for plates described in text 51

Figure 3.3 Schematic stratigraphic columns illustrating the variations in the Knob Lake Group stratigraphy and unit thickness within each thrust sheet in the field area 63

Figure 3.4 Geological map of the study area illustrating the distribution of lithologic units and planar fabrics (S_1 and S_2) in the Knob Lake Group . 72

Figure 3.5 Geological map illustrating the distribution of measured fold axes in the study area 73

Figure 3.6 Geological map illustrating the distribution of measured linear fabrics (L_x) in the study area 74

Figure 3.7 Summary of the large-scale ductile structures within the study area 75

Figure 3.8 Two possible schematic cross-sections through the F_1 fold pair, south of Lac Audréa 92

Figure 3.9 Block diagram of the NW-trending, SW-verging D_2 Lac Don anticline -syncline pair that has been refolded by N-trending F_4 folds 94

Figure 3.10 Compilation of previous mapping in the surrounding area using the style and nature of deformation observed in the area mapped by the author 97,98

Figure 3.11 Schematic stratigraphic columns illustrating the variations in the Knob Lake Group stratigraphy and lithological thickness in each thrust sheet based on the reinterpretation of maps of previous workers 100

Figure 3.12 Geologic map (A) and schematic cross-sections (B) through the Gueslis-Lac Don thrust sheet 102,103

Figure 3.13 Geologic map (A) and schematic cross-sections (B) through the Lac Gull thrust sheet 106,107

Figure 3.14 Geologic map (A) and schematic cross-sections (B and C) through the Lac Lamêlée, Lac Kendrick and North Lamêlée Hill thrust sheets 109,110,111

Figure 3.15 Geological map of the Archean basement dominated Lac Hippocampe thrust sheet 115

Figure 3.16 Summary of map-scale deformation in the compiled field area . . 116

Figure 4.1 Map of sample locations described in the text 125

Figure 4.2 Schematic AFM diagrams projected from muscovite and/or K-feldspar 133

Figure 4.3 Schematic representation of garnet porphyroblast-fabric relations in GTS 137

Figure 4.4 Schematic representation of garnet porphyroblast-fabric relations in LDTS 140

Figure 4.5 Schematic representation of garnet porphyroblast-fabric relations in LGTS 140

Figure 4.6 Schematic representation of a garnet porphyroblast-fabric relations in LLTS 143

Figure 4.7 Schematic petrogenetic grid for quartz-saturated melting in metapelitic and metagreywacke (X_{Mg} ~0.5) in the model KFMASH system (after Vielzeuf and Holloway, 1988) 146

Figure 4.8 Zoning profile of garnet in sample S-11 160

Figure 4.9 Zoning profile of garnet in sample S-218 166

Figure 4.10 Grt-Opx and Grt-Opx-Pl-Qtz geothermobarometry in sample S-11 suggests peak P-T conditions between 750-770 ^{0}C and 12-13kbars . . 173

Figure 4.11 Grt-Bt and Grt-Ky-Qtz-Pl geothermobarometry in sample S-218 suggests rapid post-metamorphic peak uplift to lower temperatures . . 174

Figure 5.1 U/Pb concordia diagram for two fractions of abraded zircons from sample SS-11B, a syntectonic Grt-Cpx bearing S-type granite 181

Figure 6.1 Detailed schematic cross section of the van Gool (1992) and Rivers et al. (1993) tectonic model of northeastern Grenville Province (modified from van Gool, 1992 and Rivers et al., 1993) 184

Figure 6.2 Detailed schematic cross section of a thin-skinned, upper-level thrust stack 185

Figure 6.3 Detailed schematic cross section of basement involved thrusts . . 185

Figure 6.4 Detailed view of an area shown in Figure 6.3 illustrating the large scale fold structures in the area now termed the Gagnon terrane nappe belt (Rivers et al., 1993) 189

LIST OF PLATES

Plate 2.1 Well foliated biotite-garnet quartzofeldspathic gneiss of the Attikamaken Formation containing coarse-grained leucocratic veins parallel to the main foliation (S_1) 19,20

Plate 2.2 Highly strained biotite-rich quartzofeldspathic gneiss of the Attikamagen Formation with cm-scale granitic pods and veins parallel to the main fabric (S_1) 19,20

Plate 2.3 Homogeneous biotite schist of the Attikamagen Formation containing relict compositional layering (S_0), subparallel to the S_1 foliation 21,22

Plate 2.4 Well-layered marble of the Denault Formation 21,22

Plate 2.5 Well-layered marble with coplanar and colinear tight to-isoclinal F_1 and F_2 folds, refolded by steeply plunging F_3 crenulations 24,25

Plate 2.6 Elongation lineation (L_x) defined by the preferred orientation of tremolite in marble of the Denault Formation 24,25

Plate 2.7 Two varieties of Sokoman silicate-carbonate iron formation 27,28

Plate 2.8 Quartzite layers within Sokoman silicate-carbonate iron formation 29,30

Plate 2.9 Strongly lineated quartz-rich oxide iron formation containing quartz, magnetite and local specular hematite 29,30

Plate 2.10 Layered garnet quartz-muscovite schist of the Menihek Formation, containing medium-grained leucocratic veins parallel to the main foliation (S_1) 32,33

Plate 2.11 Rounded to subrounded pebble to cobble conglomerate (Lac Gull formation) containing clasts of quartzofeldspathic gneiss, marble and iron formation 35,36

Plate 2.12 Garnet amphibolite dyke (at left) cross-cutting ductile fabric in marble (Denault Formation) 35,36

Plate 2.13 Detail of amphibolite dyke in Plate 2.12, showing 2 cm garnet porphyroblasts with plagioclase decompression rims 38,39

Plate 2.14 Relict intrusive relationships between homogeneous, coarse grained granitic pegmatite and biotite gneiss (Attikamagen Formation) 38,39

Plate 2.15 Layer parallel intrusion of pegmatitic granite into thinly layered Sokoman oxide formation in the Lac Lamêlée thrust sheet 40,41

Plate 2.16 Coarse-grained granitic pegmatite cross-cutting silicate-carbonate iron formation of the Gueslis thrust sheet, at the location sampled for U/Pb zircon geochronology 40,41

Plate 3.1 Stream-washed outcrop of porphyroclastic biotite hornblende quartzofeldspathic gneiss of Attikamagen Formation along the Lac Audréa shear zone 53

Plate 3.2 Quartzofeldspathic schist of the Attikamagen Formation containing relict compositional layering (S_0) and disrupted quartz veins preserved as boudins 54

Plate 3.3 High strain straight gneiss along the Lac Don shear zone 57,58

Plate 3.4 Strong down-dip quartz stretching lineation, parallel to pencil, in granitic layer along the Lac Don shear zone 57,58

Plate 3.5 High strain in boudinaged biotite-quartzofeldspathic gneiss along the Lac Gull shear zone 60

Plate 3.6 Well layered biotite quartzofeldspathic gneiss with interleaved amphibolite and rare, dextrally rotated granitic anatectic vein with down-dip quartz stretching lineation 62

Plate 3.7 Boudinage in quartz-rich 'lean' iron formation (Sokoman Formation) on the western side of Lac Gull, showing $S_0//S_1$ and implying a very large layer-parallel D_1 strain 76

Plate 3.8 Layered garnet-biotite gneiss (Menihek Formation) with coarse-grained quartzofeldspathic veins interpreted to be of anatectic origin 78,79

Plate 3.9 Tight to isoclinally folded pelitic to semi-pelitic biotite-muscovite-garnet-kyanite quartzofeldspathic schist of the Attikamagen Formation . 81

Plate 3.10 Detail view of an area in the upper right corner of Plate 3.9 illustrating the well developed axial planar foliation (S_1) defined by biotite, as well as the tightly folded compositional layering (S_0) 82

Plate 3.11 Oblique section through isoclinal F_1 folds defined by quartz ribbons in granite along the Lac Don shear zone, north of Lac Gull 83

Plate 3.12 Folded (F_2) bedding parallel quartz lens in homogeneous, fine grained biotite quartzofeldspathic schist (Menihek Formation) 85,86

Plate 3.13 Layered quartzofeldspathic biotite gneiss of the Attikamagen Formation containing 1-10 cm leucocratic veins parallel to S_1, and deformed by F2 85,86

Plate 3.14 F_2 refolding of isoclinal, intrafolial F_1 fold in marble of the Denault Formation 87,88

Plate 3.15 A rare F_3 fold deforming both the S_1 foliation and a lineation . . . 87,88

Plate 4.1 Photomicrographs of kyanite and quartz replacement by muscovite and K-feldspar in a quartz-rich muscovite-kyanite schist 132

Plate 4.2 Photomicrographs of two garnet porphyroblasts (S-107) from Gueslis thrust sheet 139

Plate 4.3 Photomicrograph of garnet (bottom right) and kyanite (centre bottom) porphyroblasts in pelitic schist from Lac Gull thrust sheet (S-218) 142

CHAPTER 1: THE GRENVILLE OROGEN

1.1 LOCATION AND SIGNIFICANCE OF THE GRENVILLE OROGEN

The Grenville Orogen, which extends from Mexico through eastern North America to Scandinavia (Hoffman, 1988), is a deeply eroded orogenic belt interpreted to be the result of a continental collision that occurred ~1200-1000 Ma between Laurentia (i.e. Proterozoic North America) and an unknown continent (possibly South America, Moores 1991). In North America, the Grenvillian Orogeny involved the Laurentian paleo-continental margin comprising the Grenville Province and terranes of unknown provenance to the southeast, now in part obscured in the Appalachian Orogen (Wynne-Edwards, 1972; Dewey and Burke, 1973; Baer, 1974, 1976; Moore, 1986; Windley, 1986, 1989; Rivers et al., 1989). The Grenville Province, i.e. that part of the Grenville Orogen exposed in the southeastern Canadian Shield, is bordered to the north by the Grenville Front (Wynne-Edwards, 1972) that separates it from adjacent older provinces of the Canadian shield. Exposed for a length of 2000 km, the Grenville Province comprises reworked polycyclic Archean, Paleo- and Meso-Proterozoic rocks derived from Laurentia as well as monocyclic rocks accreted just prior to the Grenvillian Orogeny (Rivers et al., 1989, 1993; Corrigan et al., 1994; Corrigan and van Breeman, 1996). The Grenville Province is largely characterized by high grade (amphibolite and granulite facies) rocks (Jamieson et al., 1992, 1995; Ketchum et al., 1994; Corfu and Easton, 1995; Wodicka et al., 1996), and eclogite facies rocks have recently been reported from widely spaced locations across the orogen (Davidson, 1990, 1991; Indares, 1993; Indares and Rivers,

1995; Indares and Dunning, 1997). Greenschist facies rocks are principally restricted to the areas of monocyclic rocks in the eastern and western Grenville Province (Rivers, 1983a, 1983b; Brown, 1990; Brown et al., 1991; van Gool, 1992). The overall high grade of metamorphism throughout much of the orogen suggests that a section through the lower crust is now exposed at the surface.

Structural trends within the Grenville Province are highly variable, although locally portions of the orogen are characterized by northeast-trending, southeast -dipping thrust slices, and several lithotectonic terranes are separated by ductile shear zones with kinematic indicators suggesting NW-directed tectonic transport (Davidson et al., 1982; Rivers, 1983a; Davidson, 1984, 1986; Hanmer, 1984; Rivers and Chown, 1986; Wardle et al., 1986; Rivers et al., 1989; Jamieson et al., 1992, 1995; Corrigan et al., 1994; Culshaw et al., 1994; Davidson, 1995; Cureton et al., 1997; Hanmer and McEachern, 1997). The increasing metamorphic grade towards the southeast, away from the Grenville Front, in parts of the orogen is now recognized to be a combination of (i) tectonic uplift of previously metamorphosed (i.e.: pre-Grenvillian) metamorphic rocks and (ii) the result of overthrusting of deeper (higher Grenvillian metamorphic grade) thrust sheets or terranes on lower grade rocks.

At present most of the generic understanding of the tectonic evolution of major collisional orogens is derived from Paleozoic or Phanerozoic examples (e.g. the Himalayas, Alps, Cordillera and Caledonides) where the middle to upper parts of the crust are typically exposed and the mechanisms of crustal stacking

can be relatively easily studied. The deeply eroded northeastern Grenville Province, in contrast, provides an opportunity for detailed studies of the tectonic processes in collisional orogens that take place within the lower crust. Since the Grenville Province is distinguished by high metamorphic grades, the thermal evolution (P-T paths) of various crustal segments can also be used to constrain the mechanisms of crustal thickening and subsequent unloading, permitting new insights on the tectonic evolution of deeply eroded continental collision orogens.

1.2 HISTORY OF THOUGHT

Wilson (1918, 1925) was the first to recognize the Grenville Province in terms of contrasting metamorphic grade across the Grenville Front and its regionally extensive high grade metamorphic assemblages. Since that time, numerous tectonic models of the Grenville Province have been proposed which have encapsulated the current understanding of its tectonic evolution. Wynne-Edward's (1972) regional synthesis of mapping and available geochronological data led to the recognition that the Grenville Orogen was affected by a large-scale tectono-metamorphic and plutonic event that involved both reworked and newly accreted material to the Canadian Shield (see also Gastil and Knowles, 1960; Stockwell, 1961, 1964; Walton and de Waard, 1963; Wynne-Edwards, 1964, 1969) followed by erosion to deep crustal levels. Wynne-Edward's (1972) compilation of previous work also led to the first subdivision of the Grenville Province into distinct structural and metamorphic zones. During the second Grenville Symposium, several possible tectonic

models, not all mutually exclusive, were proposed to explain the evolution of the Grenville Orogen (summarized in Baer, 1974). The models were based on: (1) the role of hot-spots and anorthosites, the so called 'millipede' model of Wynne-Edwards, which was subsequently published in 1976; (2) paleo-magnetic polar wandering data, the Grenville Loop (Fahrig et al., 1974; Irving et al., 1974); (3) structural styles, leading to inferences that the Grenville Province was part of a continent-continent collisional orogen (Dewey and Burke, 1973); and (4) shear zone analogies, relating to Baer's (1976, 1981) megashear models that the whole Grenville Orogen is a sinistral shear zone.

In the late 1970's and throughout the 1980's and 1990's, there have been ongoing programs of detailed mapping combined with structural, petrological and geochronological studies throughout much of the Grenville Province, especially in Labrador and Ontario, leading to considerable convergence of thought concerning the nature of the tectonic environment of the Grenville Orogen. Most workers now agree with Dewey and Burke (1973) that the orogen developed as a result of continent-continent collision, and efforts are currently directed towards investigating the details of that process.

Since the late 1970's, regional mapping programs in various parts of the Grenville Province have resulted in major revisions to previous interpretations. Davidson et al. (1982) and Davidson (1984, 1986), working in the Central Gneiss Belt of the southwestern Grenville Province in Ontario, recognized a thrust stack composed of distinct high grade crustal domains separated by mylonitic high

strain zones. Shear sense indicators throughout the Central Gneiss Belt and the inverted metamorphic isograds were found to be consistent with NW-directed thrust movement and the stacking of deeper, higher metamorphic grade thrust-bound domains on top of lower grade domains. At about the same time, Rivers (1983a, 1983b) reported the existence of a foreland fold-thrust belt immediately south of the Grenville Front in western Labrador, with an inverted metamorphic gradient in the thrust stack. Subsequently, Windley (1984, 1986) published a tectonic model incorporating the results of Davidson et al. (1982), Davidson (1984, 1986) with the previously-inferred existence of a Mesoproterozoic island arc in southeast Grenville Province (Brown et al., 1975), and suggested that there was an overall similarity between the geological and tectonic framework of the western Grenville Province and the Asia-India collision that formed the Himalayas.

As a result of increased understanding of crustal-thickening mechanisms and new structural, metamorphic, geophysical and geochronologic data (e.g. Rivers, 1983a, 1983b; Davidson, 1984, 1986; Wardle et al., 1986; Green et al., 1988; Indares and Martignole, 1989), Rivers and Chown (1986) and Rivers et al., (1989) proposed a new tectonic subdivision of the Grenville Province (Figure 1.1) into three first-order, northeast-trending tectonic belts. These belts, the Parautochthonous Belt, Allochthonous Polycyclic Belt, and the Allochthonous Monocyclic Belt, were defined on the basis of lithological affinity to the units in the adjacent foreland to the north and on the polycyclic or monocyclic character of

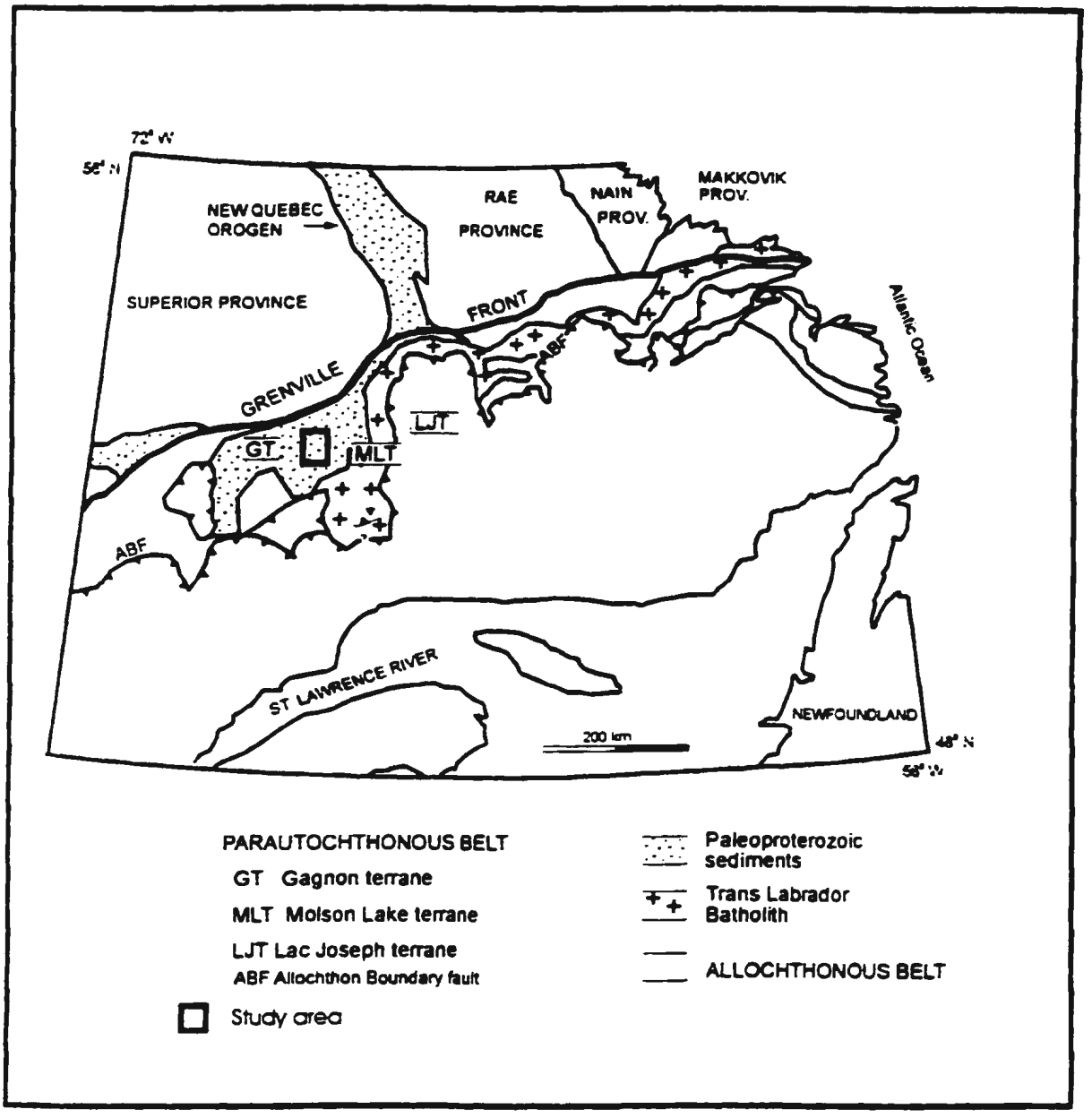

Figure 1.1 Lithotectonic map of the northeastern Grenville Province in eastern Québec and western Labrador. The Parautochthonous belt is bounded by the Grenville Front in the northwest and the Allochthon Boundary Fault (ABF) in the southeast. The box outlines the location of the study area. Modified from Rivers and Chown (1986), Rivers et al. (1989) and Indares (1995).

the material involved (Figure 1.1). The belts are separated by three crustal-scale ductile shear zones (Davidson et al., 1982; Davidson, 1984; Rivers et al., 1989; van Gool, 1992). The most northerly of these ductile shear zones, the Grenville Front (Wynne-Edwards, 1972; Rivers, 1983a; Rivers et al., 1989) represents the northwest limit of penetrative Grenvillian overprint and separates the Archean to Proterozoic foreland, the autochthon of Rivers and Chown (1986), from the structurally overlying Parautochthonous Belt. The Parautochthonous Belt is characterized by lithological continuity with the foreland and is tectonically overlain by the allochthonous belts (Rivers and Chown, 1986; Rivers et al., 1989). Both the Allochthonous Polycyclic Belt and the Allochthonous Monocyclic Belt contain transported rocks which do not have an obvious source relationship with the foreland. The Allochthonous Polycyclic Belt is composed of pre -Grenvillian rocks reworked during the Grenville Orogen and the Allochthonous Monocyclic Belt consists of rocks deformed for the first time during the Grenville Orogen.

With reference to the tectonic subdivision of Rivers et al. (1989), the study area lies within the Parautochthonous belt, specifically Gagnon terrane, which is located in western Labrador and adjacent eastern Québec (Figure 1.1).

1.3 THE PARAUTOCHTHONOUS BELT OF GRENVILLE PROVINCE IN WESTERN LABRADOR AND EASTERN QUÉBEC

In southwestern Labrador-eastern Québec, the Parautochthonous belt (Rivers and Chown, 1986; Rivers et al.,1989) is subdivided into the Gagnon terrane, containing lithological correlatives of the Knob Lake Group of the

Labrador Trough (Rivers, 1983a), and the structurally overlying Molson Lake terrane (Connelly et al., 1989) composed mainly of Middle Proterozoic (1650 Ma) rocks of the Trans-Labrador batholith (Figure 1.1). Both terranes are intruded by Shabogamo Gabbro (Connelly et al., 1993).

The Gagnon Terrane contains reworked Archean basement gneisses correlated with the adjacent Ashuanipi Metamorphic Complex of the northeastern Superior Province and a metamorphosed continental margin sedimentary sequence, the Knob Lake Group, part of the Paleoproterozoic Kaniapiskau Supergroup that was deposited unconformably on the margin of the Superior Province basement and which further north is incorporated in the New Québec Orogen (Dimroth, 1972; Wardle & Bailey, 1981). Characteristic lithologies in the Knob Lake Group stratigraphic sequence in Gagnon terrane include pelitic and semi-pelitic metasediments, marble, quartzite and iron formation which are intruded by granitic veins and dykes of Shabogamo Gabbro (Rivers, 1980, 1983a). Archean rocks do not contain earlier (pre-Grenvillian) fabrics, and pre-Grenvillian fabrics have not been found in the Knob Lake Group except in the extreme northeastern parts (Brown, 1990). In this way, metamorphic assemblages and fabrics preserved in the Knob Lake Group provide a means to characterize the Grenvillian orogenic event (Rivers, 1983a; Rivers et al., 1989; Brown et al., 1992; van Gool, 1992).

Fieldwork in the northern part of Gagnon terrane near Labrador City and Wabush (Rivers, 1978, 1980) led to the proposal that the northern margin of

Gagnon terrane is a metamorphic foreland fold-thrust belt (Rivers, 1983a; Rivers and Chown, 1986; Rivers et al., 1993) and the character of the fold-thrust belt was subsequently investigated in detail by van Gool et al. (1987, 1988), van Gool (1992) and Rivers et al. (1993). According to their model, northwest-directed Grenvillian tectonic transport along southeast-dipping ductile shear zones resulted in the imbrication and polyphase ductile deformation of the upper part of the Archean basement gneisses as well as in the metasedimentary cover. To the southwest near Mount Wright, Roach and Duffell (1974) and later Rivers and Chown (1986) compiled previous mapping by Phillips (1958, 1959), Duffell and Roach (1959), Murphy (1959, 1960), Clarke (1960, 1967, 1968, 1977), Gastil and Knowles (1960), Sinclair (1961), Gross (1988) and Roach and Duffell (1968) to characterize the large-scale structural features defined by the Knob Lake Group sequence. In this region Rivers and Chown (1986) recognized several styles of dome and basin fold interference structures that they inferred were the result of refolding of large-scale recumbent nappes. This area, informally termed the nappe belt (Rivers et al., 1993), structurally overlies the fold-thrust belt and is presumed to have developed as a result of the thrust emplacement of Molson Lake terrane over the fold-thrust belt (van Gool, 1992; Rivers et al., 1993) (Figure 1.2).

In general, Grenvillian deformation in northwestern Gagnon terrane began with foliation development and isoclinal folding (F_1) inferred to be associated with thrust imbrication and possibly fold nappe development. Near the Grenville Front,

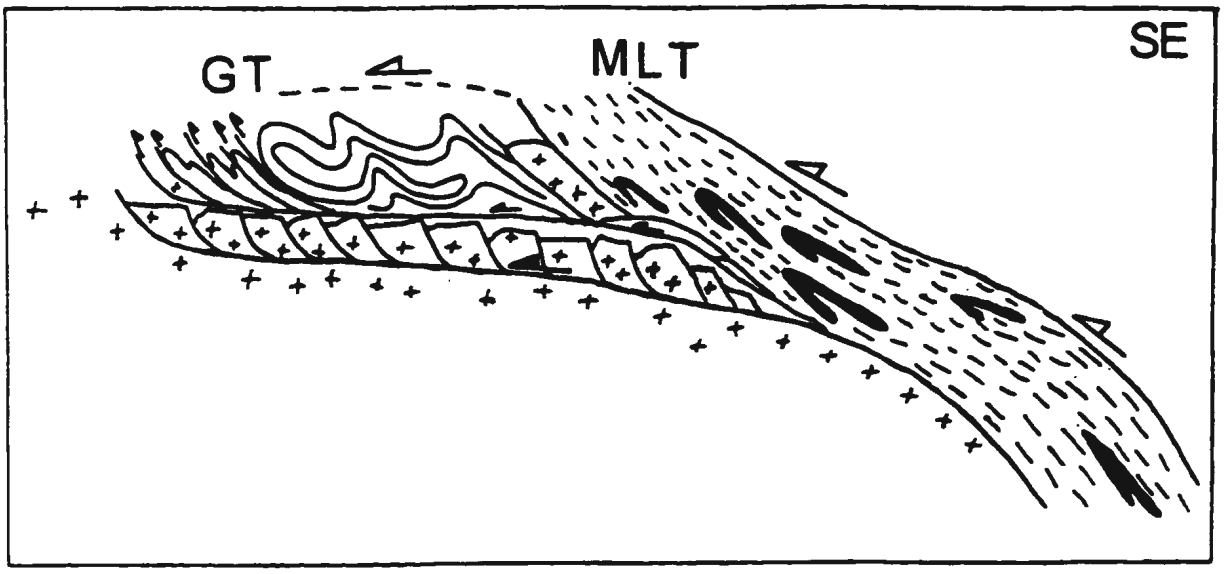

Figure 1.2 Schematic cross-section of the Parautochthonous Belt in northeastern Grenville Province (modified from Rivers, 1992; Rivers et al., 1993). The cross-section is modified to show large-scale fold structures, in the area now termed the Gagnon terrane nappe belt (Rivers et al., 1993). This area is the approximate location of the study area. According to the tectonic model of van Gool, (1992) and Rivers et al. (1993), northwest-directed emplacement of Molson Lake terrane over Gagnon terrane (white thrust arrows) resulted in the imbrication and polyphase ductile deformation of the upper part of the Archean basement gneisses as well as in the metasedimentary cover. In Gagnon terrane, two levels of thrusting are recognized (van Gool, 1992). Upper level involves thin-skinned thrusting of cover rocks (small black thrust arrows), whereas lower level involves thick-skinned thrusting of extensionally rifted Paleoproterozoic continental margin (large black thrust arrows). The cross section is drawn with considerable vertical exaggeration, and the length of section is approximately 100 km.

Brown (1990), Brown et al. (1991, 1992) and van Gool (1992) recognized evidence of thrust imbrication at two crustal-levels, and in the same area van Gool et al. (1987, 1988) and van Gool (1992) documented both foreland and hinterland (out-of-sequence) thrusting. According to these workers, thin-skinned, penetratively deformed upper-level thrusts developed mostly within the metasedimentary sequence of the Knob Lake Group, and locally within some slices of basement, whereas basement-involved thrusts exclusively involved thick slices of Archean basement gneisses. The second phase of Grenvillian deformation (D_2) is represented by northwest-vergent, northeast-trending F_2 fold structures that refolded earlier folds and thrusts. Late large-scale northwest -trending F_3 cross-folds (Roach and Duffell, 1974; Rivers, 1983a; Rivers and Chown, 1986; van Gool et al., 1988; van Gool, 1992) are more pervasive towards the southeast. Within the northern Gagnon terrane, the metamorphic grade increases from greenschist facies at the Grenville Front to upper amphibolite and eclogite facies to the south (Rivers, 1983a, 1983b; Rivers and Chown, 1986; Brown et al., 1992; van Gool, 1992; Indares, 1993; Rivers et al., 1993; Indares and Rivers, 1995; Indares and Dunning, 1997). Hairpin-shaped P-T-t paths (van Gool, 1992) in the same area indicate rapid tectonic decompression from mid-amphibolite facies. In southern part of the Parautochthonous Belt where Molson Lake terrane tectonically overlies part of the Gagnon terrane, Indares (1993), Indares and Rivers (1994) and Indares and Dunning (1997) observed eclogite facies mineral assemblages in the Shabogamo Gabbro and high

pressure assemblages in metapelites. Preservation of eclogitic rocks, combined with hairpin-shaped P-T-t paths, are consistent with tectonic uplift of Molson Lake terrane over Gagnon terrane along a crustal-scale ramp (van Gool, 1992; Rivers et al., 1993) (Figure 1.2). This interpretation has recently been confirmed by seismic investigation (Eaton et al., 1994, 1996) along the Wabush-Baie Comeau AG-Lithoprobe transect.

Uplift of Molson Lake terrane along a crustal ramp (Rivers et al., 1993) is interpreted to be responsible for northwest-directed thrusting and the development of fold-thrust and nappe belts in the Gagnon terrane (Rivers, 1983a; Brown et al., 1992; van Gool, 1992; Rivers et al., 1993). The structural and metamorphic studies described above suggest that the inverse metamorphic gradient and telescoped thrust stack in the northeastern Grenville Province developed during the stacking of higher metamorphic grade slices on top of lower grade slices during-build up of critical topography required for the thrust belt to advance into the foreland. Also, the presence of high grade mineral assemblages in the fold-thrust belt, and the predominance of ductilely deformed rocks implies that this belt was developed at deep crustal levels (Rivers, 1983b; Brown, 1990; Brown et al., 1992; van Gool, 1992), as shown in Figure 1.2.

1.4 AIMS OF STUDY

Although the fold-thrust belt of Gagnon terrane is well documented immediately south of the Grenville Front in Labrador (i.e. Rivers, 1983a, 1983b; Rivers and Chown, 1986; van Gool et al., 1987, 1988; Brown, 1991; Brown et al.,

1992; Rivers et al., 1992; van Gool, 1992) the nappe belt was provisionally identified only on the basis of the compilation of regional maps. The objective of this thesis is to investigate the structural and metamorphic evolution of the nappe belt in central Gagnon terrane. Macroscopic and mesoscopic structural data are combined with detailed lithological maps to construct schematic cross-sections in order to present the relationship between mid-to deep crustal level folding and thrusting processes. Thermobarometric studies of suitable metapelitic rocks for the construction of P-T-t paths are combined with the first U/Pb zircon radiometric age of metamorphism from within the Gagnon Terrane. These results, when compared with the well-studied areas farther to the north near the Grenville Front, will constrain the structural and metamorphic variation across the Gagnon terrane and lead to a more thorough understanding of the nature, stacking order and kinematics of mid-to deep crustal deformation of a thrust wedge under conditions ranging from greenschist to eclogite facies.

1.5 LOCATION OF STUDY AREA

The map area is situated along the Baie Comeau-Fermont road (Route 389), approximately 25 km south of Fermont (Québec). The area covers approximately 131 km^2 between latitudes $52^0$40' and $52^0$25' and longitudes $67^0$15' and $67^0$45', and lies within the 23B/15 NTS map sheet (Figure 1.3). The landscape is hilly with elevations ranging from 2000 to 2650 ft. Transmission lines and the railway trend north-south, approximately parallel to the main road, and local gravel roads provide easy access to much of the area. There are many

lakes and small ponds in the area and the larger ones are labelled in Figure 1.3. Vegetation varies from dense bush to rare open areas that contain evidence of having been burned some tens of years previously.

1.6 METHODOLOGY EMPLOYED IN GEOLOGICAL MAPPING

Geological mapping was carried out on foot from the road, railroad and lake network. Aerial photographs were used for location and data were plotted on enlarged versions of the 1:50,000 topographic map. Traverses were spaced approximately 500-800m apart, but in areas of dense outcrop and/or complex structure, traversing was designed to include all available outcrops. It was not possible to reach all of the outlying outcrops in the map area, however, and a few of these were compiled from the maps of Phillips (1958, 1959), Murphy (1959) and Clarke (1967). Geological contacts were interpreted using aerial photographs and available aeromagnetic maps. Areas of iron formation show up very clearly on the aeromagnetic maps, but the maps were not useful for precisely determining the boundaries of iron formation units as the aeromagnetic anomalies extend significantly beyond the limit of the units themselves. Sampling was conducted with several aims in mind; (a) to obtain representative samples of all the units; (b) to obtain maximum phase assemblages in pelites for metamorphic petrology and thermobarometry; and (c) to obtain samples with clear cross-cutting relationships for geochronology.

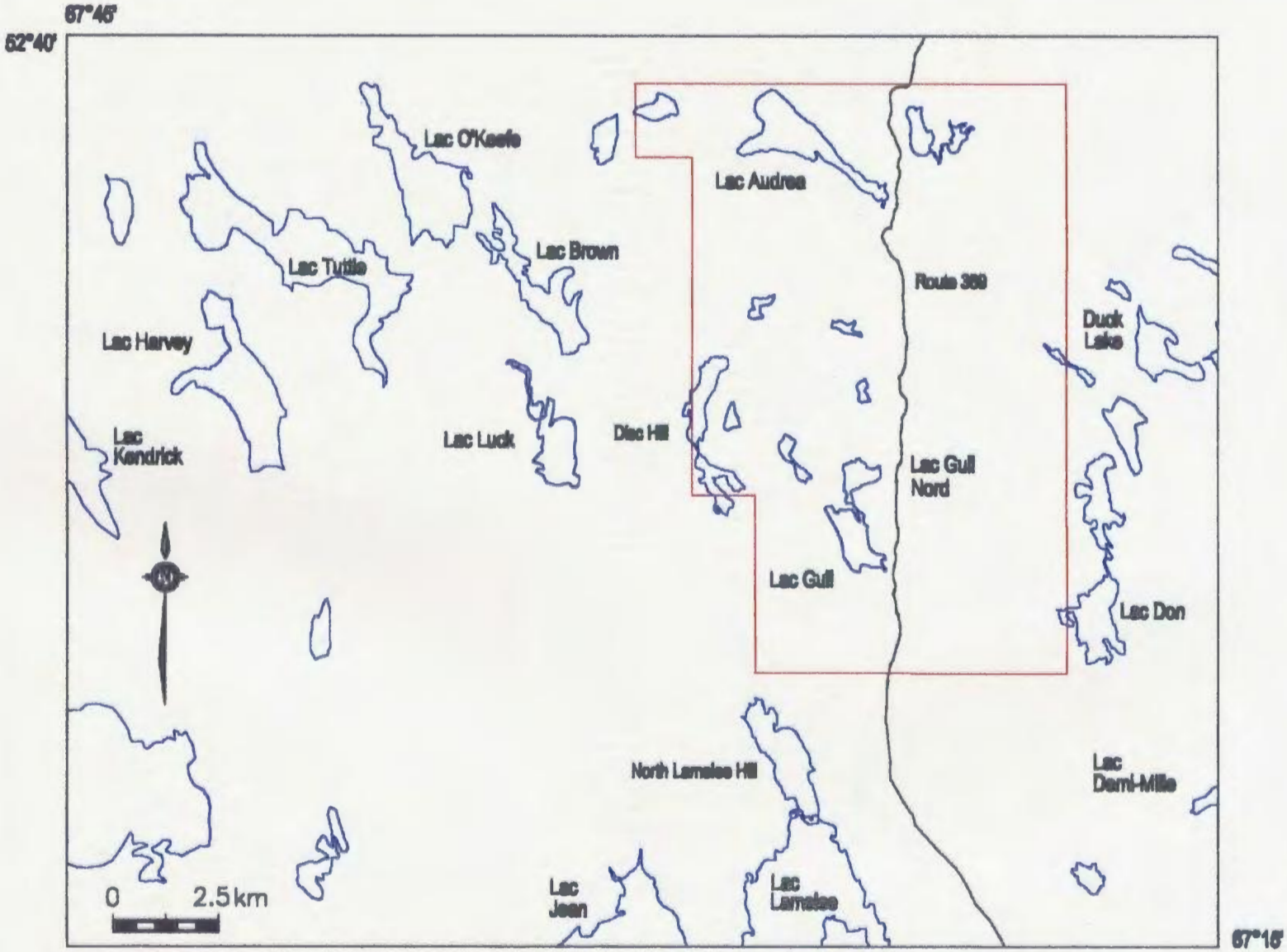

Figure 1.3 Map of study area showing the major topographic features described in the text. The area outlined in red was mapped by the author, whereas the adjacent areas are based on reinterpretation of maps and structural information by Phillips (1958, 1959), Murphy (1959) and Clarke (1967).

CHAPTER 2: STRATIGRAPHY

2.1 LITHOLOGIES OF THE GAGNON TERRANE

In Gagnon terrane, the Archean crystalline basement is overlain by Paleo -proterozoic continental margin sediments which have been intruded by Mesoproterozoic granitoid rocks and the Mesoproterozoic Shabogamo gabbros. With the exception of the granitoids, all of these units can be traced north of the Grenville Province into the New Québec Orogen.

The Archean basement is correlated with the Ashuanipi Metamorphic Complex (AMC) of the adjacent Superior Province, and is composed of variably retrogressed two-pyroxene quartzofeldspathic gneisses and mafic granulites that contain evidence of having undergone at least two contrasting metamorphic episodes. In zones of Grenvillian reworking, rocks of the AMC are characterized by speckles or clusters of fine-grained secondary biotite, garnet and quartz replacing pyroxenes that formed during the superimposed lower grade conditions in the Grenvillian Orogeny (Phillips, 1958; Clarke, 1967, 1977; Roach and Duffell, 1968; van Gool, 1992; Perreault, 1994). In zones of high Grenvillian strain, the AMC is completely transformed into phyllonitic schists at low grade, near the Grenville Front, and into quartzofeldspathic gneisses at higher grade farther to the south (van Gool, 1992). Reworked Archean rocks have not been definitively identified within the field area since these would have been strongly reworked and are likely indistinguishable from cover rocks. A dating program is in progress to determine if Archean rocks are present.

The Paleoproterozoic continental margin metasediments are part of the Kaniapiskau Supergroup (KSG) that was in part derived from and was unconformably deposited on Superior Province basement. The stratigraphy of the KSG in the Labrador Trough was defined by Fahrig (1967), Dimroth (1968, 1971, 1972, 1978), Dimroth et al. (1970) and Wardle and Bailey (1981) where the metamorphic grade is low and primary features are still visible. The continental-margin-shelf-slope units that extend from south-central Labrador Trough into the Gagnon Terrane are known as the Knob Lake Group (KLG) (Rivers, 1983a). On the basis of interpretation from low grade areas, these metasediments are characterized by a younging upward progression beginning with deep-water greywacke to shale sedimentation (Attikamagen Formation) on the extensionally rifted Archean basement (Donaldson, 1966; Wardle and Bailey, 1981). Carbonate buildups in the form of calcitic and dolomitic barrier reefs formed the Denault Formation, which was an approximate time equivalent to the near shore aeolian to fluviatile quartz-rich sand- and siltstones of the Wishart Formation (Donaldson, 1966; Wardle and Bailey, 1981). Banded oxide, silicate and carbonate iron formations (Sokoman Formation) were deposited in a the restricted basin situated between the carbonate reef and the shore. Submarine pillows and pyroclastic volcanic rocks, of the McKay River Formation, are locally interbedded with marble and the overlying iron formation (Wardle and Bailey, 1981). The immediately overlying black shales and slates of the Menihek Formation are characteristic of a relatively quiet water environment, and gradually

give way upwards to less well sorted greywacke sediments, suggesting a rapid deepening of the basin (Wardle and Bailey, 1981).

2.2 DESCRIPTION OF ROCK TYPES IN THE FIELD AREA

Lithologic units of the KLG in the field area are described below. Additional details concerning these units may be found in Phillips (1958, 1959), Murphy (1959), Clarke (1967, 1977) and Roach and Duffell (1968).

2.2.1 Attikamagen Formation

The principal lithology is a medium to coarse grained, white to grey, well-foliated biotite ± garnet quartzofeldspathic gneiss (Plate 2.1), containing variable proportions of cm-scale leucocratic tonalitic (quartz - plagioclase) to granitic (quartz - plagioclase - microcline) veins or pods subparallel to the main fabric (Plate 2.2). The meta -sedimentary origin of this unit is inferred from the presence of interlayered pelitic schist composed of quartz - plagioclase - biotite + muscovite ± garnet ± kyanite with locally preserved relict compositional layering (Plate 2.3), and from the presence of sparse concordant layers of calc-silicate, marble and garnet amphibolite (Plate 2.3). The origin of the leucocratic veins and pods that characterize much of the unit is not everywhere clear, but their absence in aluminumous schists suggests that at least some were derived from *in situ* partial melting of the quartzofeldspathic metasediments.

Much of what is now interpreted to be Attikamagen Formation was originally mapped by Phillips (1958, 1959) and Murphy (1959) as the upper gneiss unit (Menihek Formation). However, recognition of the KLG stratigraphy by

Plate 2.1 Well foliated biotite quartzofeldspathic gneiss of the Attikamagen Formation containing coarse-grained leucocratic veins parallel to the main foliation (S_1).

Plate 2.2 Highly strained biotite-rich quartzofeldspathic gneiss of the Attikamagen Formation with cm-scale granitic pods and veins parallel to the main fabric (S_1).

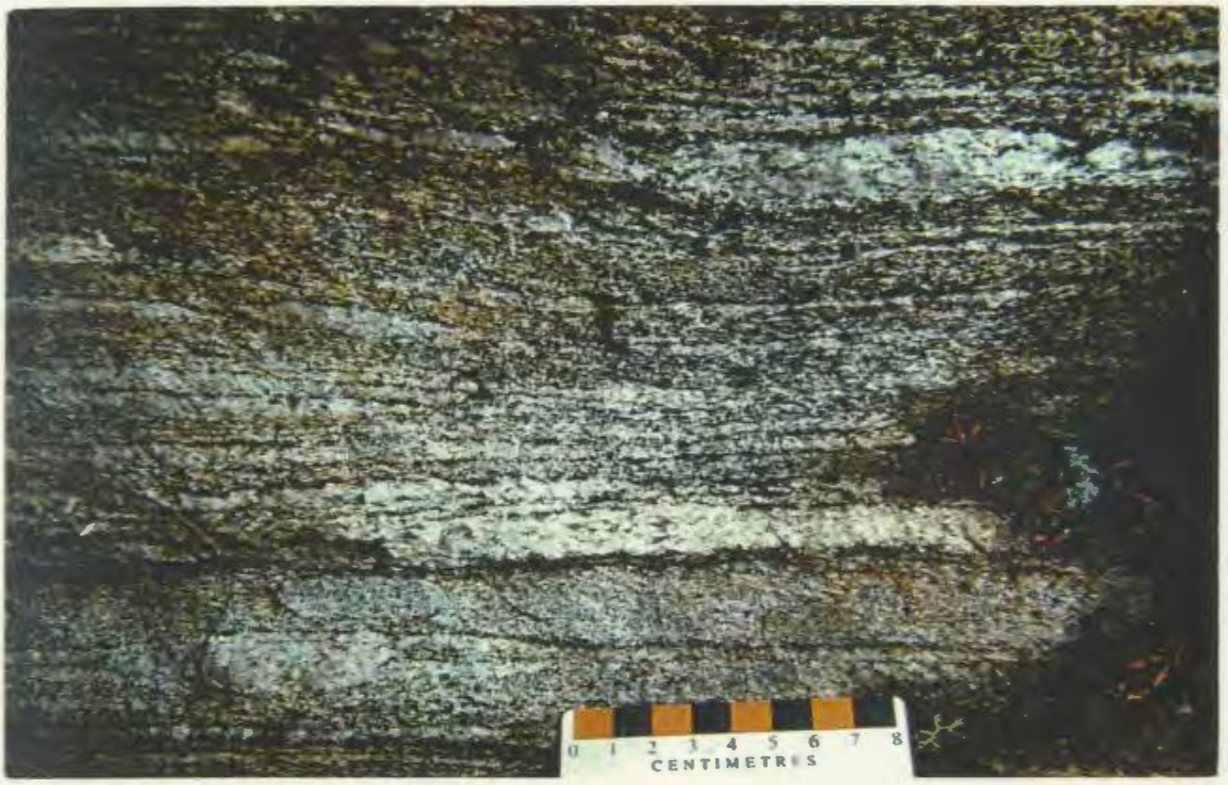
0 1 2 3 4 5 6 7 8
CENTIMETRES

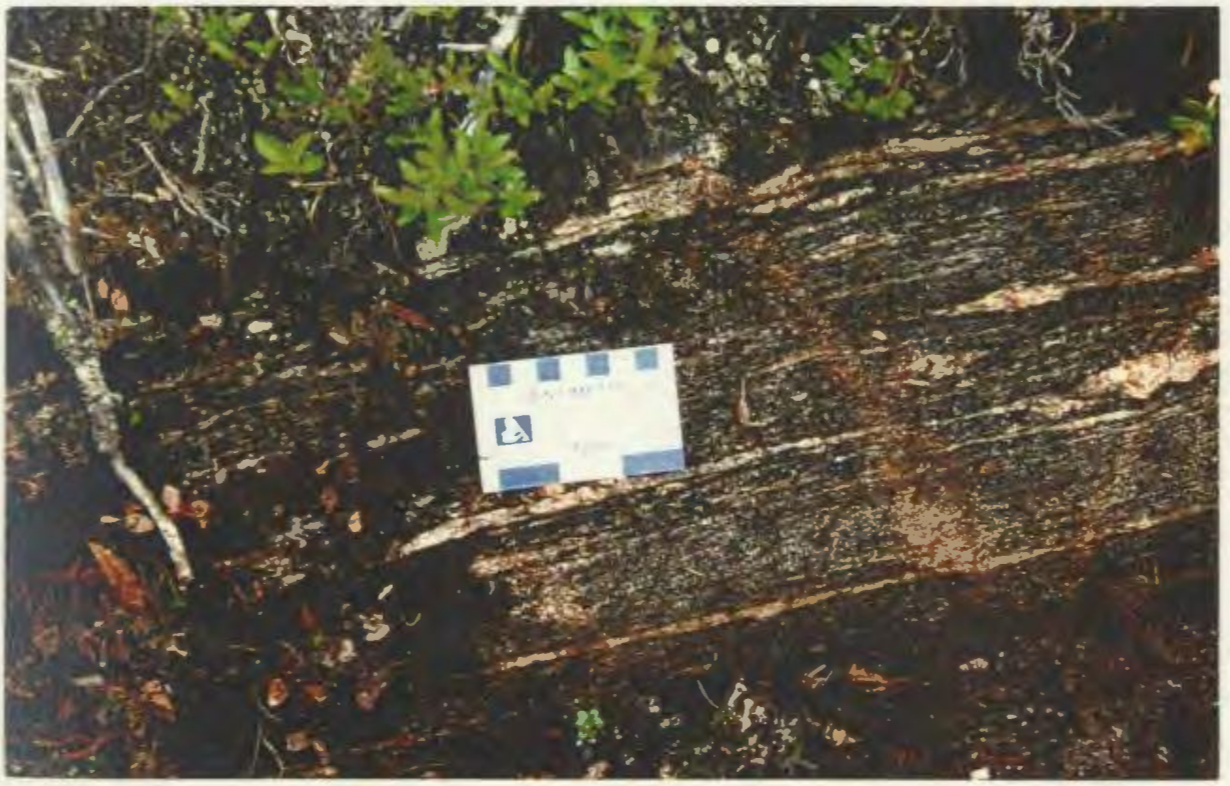

Plate 2.3 Homogeneous biotite schist of the Attikamagen Formation containing relict compositional layering (S_0), subparallel to the S_1 foliation.

Plate 2.4 Well-layered marble of the Denault Formation. The layering, defined by alternating quartz and carbonate layers is a combined $S_0//S_1$ fabric, as shown by the presence of small isoclinal folds in the bottom of the picture.


CENTIMETRE
CANADA-NWT MINERAL DEVELOPMENT AGREEMENT
INCH

Roach and Duffell (1974) and Rivers (1983a) has shown that it occupies the stratigraphically lowest part of the succession within the field area.

2.2.2 Denault Formation

The Denault Formation is typically a dark-weathering calcite and dolomitic marble, with subordinate layers of quartz and calc-silicates having positive relief on the weathered surface due to differential erosion. Thin quartz layers commonly record evidence of polyphase deformation (Plates 2.4 and 2.5), whereas the more thickly bedded units display less evidence of polyphase deformation, and are characterized by randomly oriented coarse-grained calc-silicate minerals (tremolite-actinolite, diopside and forsterite) (Plate 2.6). Cream-coloured massive dolomitic layers are variable in thickness (cm to m-scale), and show evidence of tectonic thickening by plastic deformation, but are internally recrystallized and do not record significant microstructural information.

2.2.3 Wishart Formation

The Wishart Formation is characterized by coarsely recrystallized, massive or thick-bedded quartzite. Grain size is typically less than 0.5 cm and the principal accessory phases include magnetite and hematite. The large quartzite body south of Lac Audréa (Figure 1.3) is associated with a significant aeromagmetic anomaly suggesting a close spatial link with the iron formation.

Also at this location, there are also outcrops of a recrystallized quartz-pebble conglomerate containing distinctive finely disseminated specular hematite. About 0.5 km east of Lac Audréa (Figure 1.3) a light grey, well layered quartzite

Plate 2.5 Well-layered marble with coplanar and colinear tight to-isoclinal F_1 and F_2 folds that have been refolded by steeply plunging F_3 crenulations. Evidence of F_1 is locally limited to relict intrafolial fold hinges.

Plate 2.6 Elongation lineation (L_x) defined by the preferred orientation of tremolite in marble of the Denault Formation. Although variable, tremolite generally plunges towards the right. The calc-silicate rich layers define the $S_0//S_1$ surface.

pod (10-12m) in the Lac Audréa shear zone contains minor amounts of muscovite and hematite, and stretched quartz grains that define a sub horizontal lineation.

2.2.4 Sokoman Formation

The Sokoman Formation consists of two sub-units in the field area: silicate -carbonate iron formation (S-CIF) and oxide iron formation (OIF).
Silicate-carbonate iron formation is well layered and composed of medium- to coarse-grained white to grey quartzite, up to a few cm wide, alternating with layers of Fe-silicate and carbonate (Plates 2.7 and 2.8). Quartzite layers are extensively boudinaged and irregular layers of rusty-weathering Fe-silicates (grunerite-cummingtonite, actinolite, Fe Cpx Fe Opx) occur in a matrix of carbonates (siderite and ankerite) with minor amounts of garnet and magnetite. Accessory minerals include apatite and the retrograde phase stilpnomelane, minnesotaite and goethite (Clarke, 1967, 1977). S-CIF units are of variable thickness (5 to 200 m) and locally contain carbonate pisoliths expressed on the weathered surface by 0.5 to 1 cm pits (Plate 2.8). Thin pelitic layers within the S-CIF consist of Fe-rich garnet-biotite-orthopyroxene schist.

The oxide iron formation occurs in two modes: (i) sharply bounded layers up to a few cm thick, and varying little in thickness along strike, composed of quartz and blue-grey specularite (hematite) and lesser amounts of magnetite alternating with medium-grained glassy quartz (Plate 2.9); and (ii) as magnetite-rich lens-shaped bodies with gradational contacts with banded silicate-carbonate iron formation.

Plate 2.7 Two varieties of Sokoman silicate-carbonate iron formation. A) Distinctive layering consists of light coloured quartz-rich layers, with locally preserved isoclinal F_1 folds, in a matrix of Fe-silicates (grunerite-cummingtonite, actinolite-tremolite, ortho- and clinopyroxene). B) Silicate-carbonate iron formation from the Lac Gull thrust sheet. Quartz-rich pods (or boudinaged layers) are surrounded by dark brown Fe-silicates in a light brown carbonate (siderite and ankerite) matrix. Intrafolial F_1 fold hinges are locally preserved in the light coloured quartzite boudins (e.g. Plate 2.7A).


CENTIMETRE
INCH

Plate 2.8 Quartzite layers within Sokoman silicate-carbonate iron formation. These layers locally contain recessive, flattened pits, interpreted to be deformed carbonate pisoliths, subparallel to the axial surface of the steeply plunging F_4 fold (subparallel to marker). Marker is oriented parallel to NNW-trending F_4 folds.

Plate 2.9 Strongly lineated quartz-rich oxide iron formation containing quartz, magnetite and local specular hematite. Recessive weathering pits (~0.5 cm), visible to the left of the scale card, are interpreted to be deformed carbonate pisoliths.

2.2.5 Menihek Formation

In the field area, the Menihek Formation is lithologically indistinguishable from the Attikamagen Formation and the two units are identified on the basis of the younging direction of the intervening members of the KLG stratigraphy. The dominant lithology is a medium-grained quartzofeldspathic gneiss, with rare interstratifications of more aluminous quartz-muscovite±plagioclase schist (Plate 2.10), quartzite and mica schist with porphyroblasts of garnet and kyanite. Layers of mafic gneiss composed of garnet-hornblende-plagioclase-pyroxene or garnet-plagioclase-pyroxene-biotite assemblages occur locally. Accessory phases include titanite, ilmenite, apatite, rutile and zircon. Near the southern end of Lac Audréa, biotite-garnet -bearing quartzofeldspathic gneiss can be seen to grade across strike into muscovite-biotite±garnet±kyanite schist, locally with coarse-grained layers, pods and stringers of injected pink granite.

2.2.6 Lac Gull formation

On the basis of younging direction, the stratigraphically youngest unit in the field area appears to be a conglomerate that occurs in a single outcrop, approximately 3 km north of Lac Gull. The outcrop is composed of well-rounded to angular, ellipsoidal pebble size (10-25cm) clasts of quartzite, silicate-carbonate iron formation, marble, and quartzofeldspathic gneiss in a fine grained matrix (Plate 2.11). This unit has not been previously reported from the Lac Audréa area, and is part of a separate unite, informally known as the Lac Gull Formation. It may be correlated with the Equus Formation, another conglomerate unit

Plate 2.10 Layered garnet quartz-muscovite schist of the Menihek Formation, containing medium-grained leucocratic veins parallel to the main foliation (S_1). To the left of the clipboard, garnet porphyroblasts (0.5 cm) are macroscopically zoned. A) Shows the well-developed planar fabric with flattened leucosomes, whereas B) shows disaggregated quartz veins with tails. Note that both show $S_0//S_1$.


CENTIMETRE
INCH

described by Brown (1990) from the northeastern Gagnon terrane.

2.2.7 Gabbro and Related Lithologies

Gabbroic rocks occur as sills (3-8 m wide and traced for up to 20m) and dykes subparallel to and crosscutting relict bedding in the Knob Lake Group. Centres of the intrusions retain original igneous textures which have been overprinted by Grt-Cpx bearing metamorphic coronas, whereas the margins are retrogressed to foliated garnet amphibolite (Grt+Hbl+Pl±Bt), as shown in Plates 2.12 and 2.13. Some dykes cut the main fabrics in the gneisses and are therefore presumably younger than the Shabogamo Gabbro (Plate 2.12). These units are undated, but are affected by a pervasive amphibolite facies metamorphism (Plate 2.13) suggesting that they are syn-Grenvillian. These differences in structural relationships with the host rocks suggests that there may be more than one age of dykes in this unit. Whether any of these dykes can be correlated with the 1459+23-22 Ma Shabogamo Gabbro (Connelly and Heaman, 1993) is uncertain in the absence of precise dating, although the field relations and mineralogical character of the sills that have been deformed with the KLG suggest that these bodies are good candidates to be included in this unit. The significance of the dyke that cross-cuts deformed KLG strata is also uncertain without additional chemistry and dating. If it were a Shabogamo Gabbro, then this would be the first unequivocal evidence for pre-Shabogamo deformation in the interior part of Gagnon terrane, and would indicate that it is located in a window of previously unrecognized post-tectonic dyke. Since there is no evidence to suggest that

Plate 2.11 Rounded to subrounded pebble to cobble conglomerate (Lac Gull formation) containing clasts of quartzofeldspathic gneiss, marble and iron formation. View to north on steep rock face.

Plate 2.12 Garnet amphibolite dyke (at left) cross-cutting ductile fabric in marble (Denault Formation). View to northeast. Hammer for scale.

Grenvillian strain is lower in the area of the cross-cutting dyke, and since the dyke appears much different in character to the Shabogamo Gabbros (the Shabogamo Gabbros are characterized by garnet in a corona texture, not by garnet porphyroblasts), the latter hypothesis is favored by the author.

2.2.8 Granitoid Rocks

Various granitoid rocks intrude the supracrustal gneisses. On the eastern side of Lac Gull, a large body of foliated, medium-grained, homogeneous biotite granodiorite to granite intrudes the gneisses of the Attikamagen Formation and preserves evidence of assimilation of the gneisses near its margins (Plate 2.14). A second body of similar composition occurs farther to the south, within the oxide unit of the Sokoman Formation, where a homogeneous pegmatitic granite (Plate 2.15) exhibits contacts parallel to $S_0//S_1$ in the iron formation.

The third location is approximately 4 km south of Lac Audréa, where a small body of pegmatitic granitic cross-cuts the main regional fabric in the silicate-carbonate iron formation and is itself weakly to moderately deformed (Plate 2.16). It contains Cpx-Hbl-Grt as mafic minerals and displays graphitic intergrowths between quartz and potassium feldspar. A sample of this rock has been dated by U/Pb geochronology (see Chapter 5).

2.3 PALINSPASTIC RECONSTRUCTION OF SHELF

An interpretive diagram indicating the author's concept of the tectonic setting of the KLG before the Grenvillian Orogeny is illustrated in Figure 2.1. It has been drawn on the assumption that local facies changes are at least a

Plate 2.13 Detail of amphibolite dyke in Plate 2.12, showing 2 cm garnet porphyroblasts with plagioclase decompression rims.

Plate 2.14 Relict intrusive relationships between homogeneous, coarse grained granitic pegmatite and biotite gneiss (Attikamagen Formation) (see also Plate 2.2). Notice that the granite is dominantly parallel to the S_1 fabric in the host rock and contains evidence of assimilation of the gneisses near its margins.

Plate 2.15 Layer parallel intrusion of pegmatitic granite into thinly layered Sokoman oxide formation in the Lac Lamêlée thrust sheet. Notice that the granite is massive and does not contain a planar fabric.

Plate 2.16 Coarse-grained granitic pegmatite cross-cutting silicate-carbonate iron formation of the Gueslis thrust sheet, at the location sampled for U/Pb zircon geochronology. Notice that the granite is dominantly parallel to the S_1 fabric but also truncates S_1, suggesting that granite emplaced occurred post D_1 and pre-D_2. View to the west. Field of view is approximately 3 m.

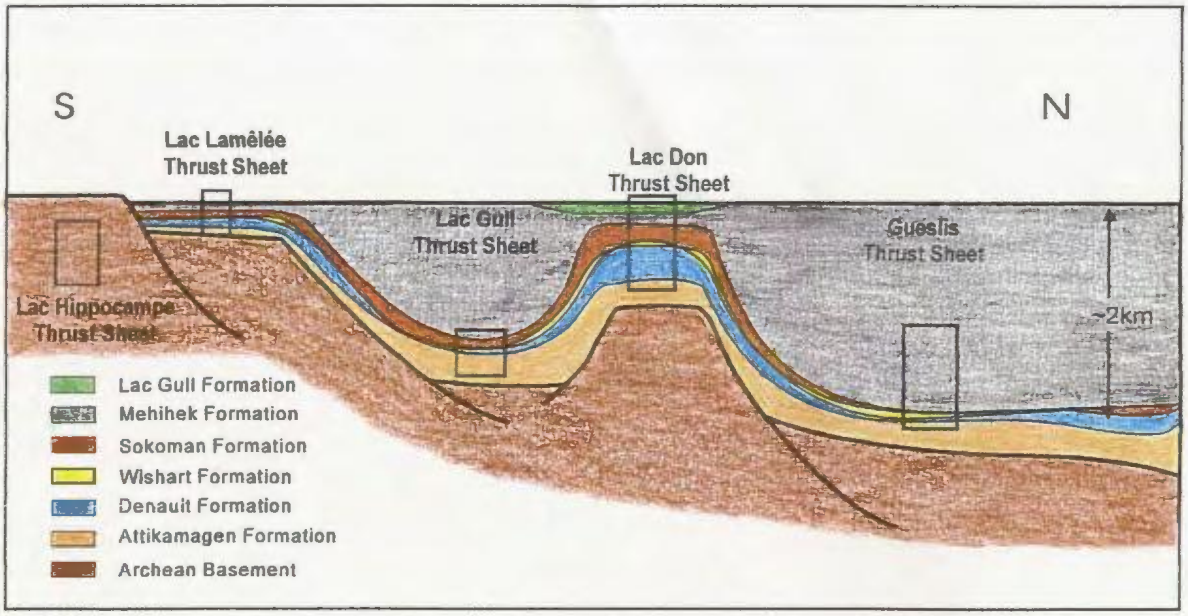

Figure 2.1 Schematic palinspastic reconstruction of the Paleoproterozoic continental margin of the Superior Craton on which the Knob Lake Group was deposited. It is assumed that facies changes in the major stratigraphic units were controlled by basement topography. Location of pre-thrusting stratigraphic sections forming each thrust sheet in the study area are shown by boxes. Estimated thickness of section is at least 2 km, as indicated, and the length of section is unknown.

contributing factor to the observed distribution in lithologies and thicknesses. This has been established in the New Québec Orogen to the north of the Grenville Province (Wardle and Bailey, 1981). However, the role of tectonic thickening and thinning of the stratigraphy is clearly not insignificant, although it has not been quantified. Assumptions made in drawing the figure are that: (a) quartzite (Wishart Formation), thick carbonate units (Denault Formation) and silicate carbonate iron formation of (Sokoman Formation) are shallow water deposits that formed on formed on horsts; (b) thin carbonate units formed in deeper water; and (c) muds and sands (quartzofeldspathic gneisses and schists) of the Attikamagen and Menihek formations formed thicker accumulations in the grabens than on the horsts. Unfortunately, these assumptions cannot be rigorosly quantified because there are no undeformed sections in Gagnon terrane with which they can be compared. This reconstruction differs from previous less well-constrained restorations of Gagnon terrane for two reasons. (1) It takes into account of the observation that the variability of sedimentary facies assumed by Rivers (1983a). (2) It allows for a much greater role for reworked basement in much of the terrane, due to the inference that the thickness of the cover sequence does not increase monotonically towards the southeast. Evidence supporting these two observations has emerged from recent work in various parts of Gagnon terrane (e.g. van Gool, 1992; T. Rivers and A. Indares, personal communication 1996).

CHAPTER 3: STRUCTURAL GEOLOGY

3.1 INTRODUCTION

Since the work of Rivers (1983a) it has been recognized that the northern margin of Gagnon terrane is a metamorphic fold-thrust belt that developed during the Grenvillian Orogeny, and the recent studies of van Gool et al. (1987, 1988), Brown (1990), Brown et al (1992), van Gool (1992) and Rivers et al. (1993) have provided a wealth of detail concerning its structural and metamorphic evolution. Fold-thrust development is interpreted to have occurred at mid-crustal depths as a result of over-thrusting by the high pressure Molson Lake terrane, resulting in accretion of the underlying Gagnon terrane in a NW-directed thrust wedge. Three regionally developed phases of Grenvillian deformation have been recognized in northern Gagnon terrane, the first two of which are related to the development of the accretionary thrust wedge, i.e. (i) a bedding-parallel foliation (S_1), interpreted to be a result of D_1 thrust imbrication and isoclinal F_1 folding; (ii) folding of the S_1 fabric into initially NE-trending, NW-vergent F_2 folds with variable development of an S_2 axial planar schistosity; and (iii) late northwest-trending large-scale F_3 cross-folds with no associated axial planar fabric, that are generally most easily inferred from the map pattern. This generalized structural pattern appears to be widespread across those parts of northern Gagnon terrane that have been examined in detail.

However, despite the well-characterized style of Grenvillian deformation

near the Grenville Front, there has been no modern structural analysis of the interior of Gagnon terrane, which has been tentatively referred to by Rivers et al. (1993) on the basis of mapping by Clarke (1967, 1977) and reconnaissance studies, as a 'nappe belt' that tectonically overlies the foreland fold-thrust belt. It is therefore one of the aims of this study to provide an interpretation of the structural architecture and evolution of a representative part of the nappe belt, and to relate this to the better-known evolution of the foreland fold-thrust belt in the northern part of Gagnon terrane.

Gagnon terrane has special significance to the understanding of Grenvillian orogenesis because most of the terrane was undeformed and unmetamorphosed prior to the Grenvillian Orogeny, and is thus monocyclic. This contrasts with much of the Grenville Province, in which pre-Grenvillian deformation was overprinted by Grenvillian effects during Grenville Orogeny, making characterization of the latter a much more difficult and contentious matter.

3.2 PREVIOUS WORK IN AND ADJACENT TO THE STUDY AREA

Early mapping in this and adjacent areas of Gagnon terrane by personnel of Québec's Ministry of Natural Resources was designed primarily to outline the distribution of iron formation and to assess its economic potential. The 1":1 mile scale maps of Phillips (1958, 1959) and Murphy (1959) were the first published geological maps of the study area and show the broad distribution of units. These maps were subsequently compiled into a 1:256, 630 scale map of a larger area

by Duffell and Roach (1959), following which Roach and Duffell (1974) published the first structural interpretation of what is now known as Gagnon terrane. In their regional compilation, these authors recognized three phases of ductile deformation on the basis of fold style and trend. According to their interpretation, approximately E-W trending large scale folds (F_1 in their terminology) were deformed by NW-NNW trending F_2 folds that increase in intensity towards the central part of the map area. Their third generation of folds, characterized by steeply dipping NE to N-NE trending axial planes, also developed large fold interference patterns.

At about the same time as the work of Roach and Duffell (1974), geological mapping by Clarke (1967, 1968) and others was continuing elsewhere in Gagnon terrane, and the widespread continuity of the stratigraphy became apparent. Considerably later, Rivers and Chown (1986), on the basis of compilations of existing mapping, drew a series of cross-sections in key areas of Gagnon terrane. Of particular interest to this study was a cross-section located in the vicinity of the Grenville Front immediately north of the present field area. Rivers and Chown (1986) observed that in this section structural vergence is towards the southeast, in contrast to northwest vergence observed elsewhere in the terrane in the vicinity of the Grenville Front. This led Rivers and Chown (1986) to propose the existence of a basement buttress and associated backfolding, an interpretation that was supported by the recent mapping of

Perreault (1994) in the Lac Gensart area immediately northwest of the study area. The most recent work in the vicinity of the study area took place in the southern part of Gagnon terrane, which was imaged in a LITHOPROBE multichannel seismic reflection experiment conducted along the Baie Comeau-Wabush road (Eaton et al., 1995). The results of this survey show that Gagnon terrane is structurally overlain by the Manicouagan Shear Belt, a composite thrust slice containing abundant eclogite facies rocks (Indares, 1993, 1994; Indares and Dunning, 1997). The significance of these interpretations will be discussed in Chapter 6, where they are related to the results obtained from this study.

3.3 THIS STUDY

The remainder of this chapter is divided into 5 parts. (a) Division of the area into thrust sheets; (b) an examination of the geometry of Grenvillian deformation in the study area based on an analysis of structural data obtained in the field by the author; and (c) an interpretation of structural style and sequence of deformation in this part of Gagnon terrane. This is followed by (d) a reinterpretation of the maps and structural information from adjacent areas that were published some 20-30 years ago by geologists of Québec's Ministry of Natural Resources and (e) construction of a model for the structural evolution of the region.

3.4 DIVISION OF AREA INTO THRUST SHEETS

On the basis of detailed remapping by the author, there is evidence to indicate that the map area is transected by four major ductile faults, three of which can be shown to duplicate the stratigraphy and are therefore interpreted as thrusts. In the field, these thrust zones are locally observed in areas of suitable outcrop and are characterized by the presence of high strain fabrics associated with straight gneiss. However, kinematic indicators are not widespread due to subsequent annealing, so the sense of displacement has not everywhere been unequivocally established in the field. Elsewhere, ductile shear zones have been inferred from the map pattern in the supracrustal sequence and the relative sense of displacement has been estimated from the stratigraphic cut offs in the adjacent thrust sheets. Figure 3.1 shows the division of the area into five thrust sheets, each of which, in keeping with convention, is named after the thrust fault at its base. They are described below from north to south. The location of geological features, and photographs (Plates) described in the text are shown in Figures 3.1 and 3.2 respectively.

3.4.1 Lac Audréa Shear Zone

The Lac Audréa shear zone is a WNW-ESE trending subvertical zone of high strain rocks in the northern part of the map area (Figure 3.1). Compared to the other high strain zones described below, the Lac Audréa shear zone does not define the boundary of a thrust sheet, and it may be a later structure. Two areas

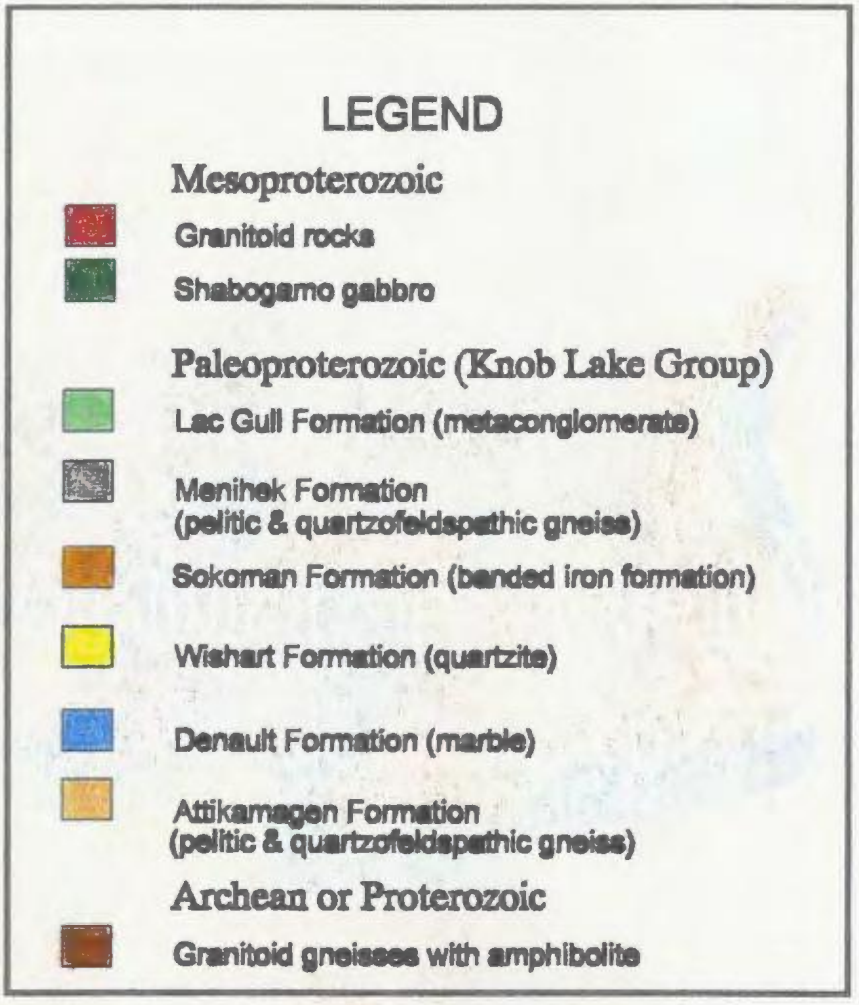

Figure 3.1 An outline of the major geological features and subdivision of the field area into five distinct thrust sheets, separated by shear zones. Abbreviations: GTS - Gueslis thrust sheet, LDTS - Lac Don thrust sheet, LGTS - Lac Gull thrust sheet, LLTS - Lac Lamêlée thrust sheet, LHTS - Lac Hippocampe thrust sheet, GSZ - Gueslis shear zone, LASZ - Lac Audréa shear zone, LGSZ - Lac Gull shear zone, LLSZ - Lac Lamêlée shear zone, LAS - Lac Audréa syncline, DLA - Duck Lake anticline, LDA - Lac Don anticline, LDS - Lac Don syncline.

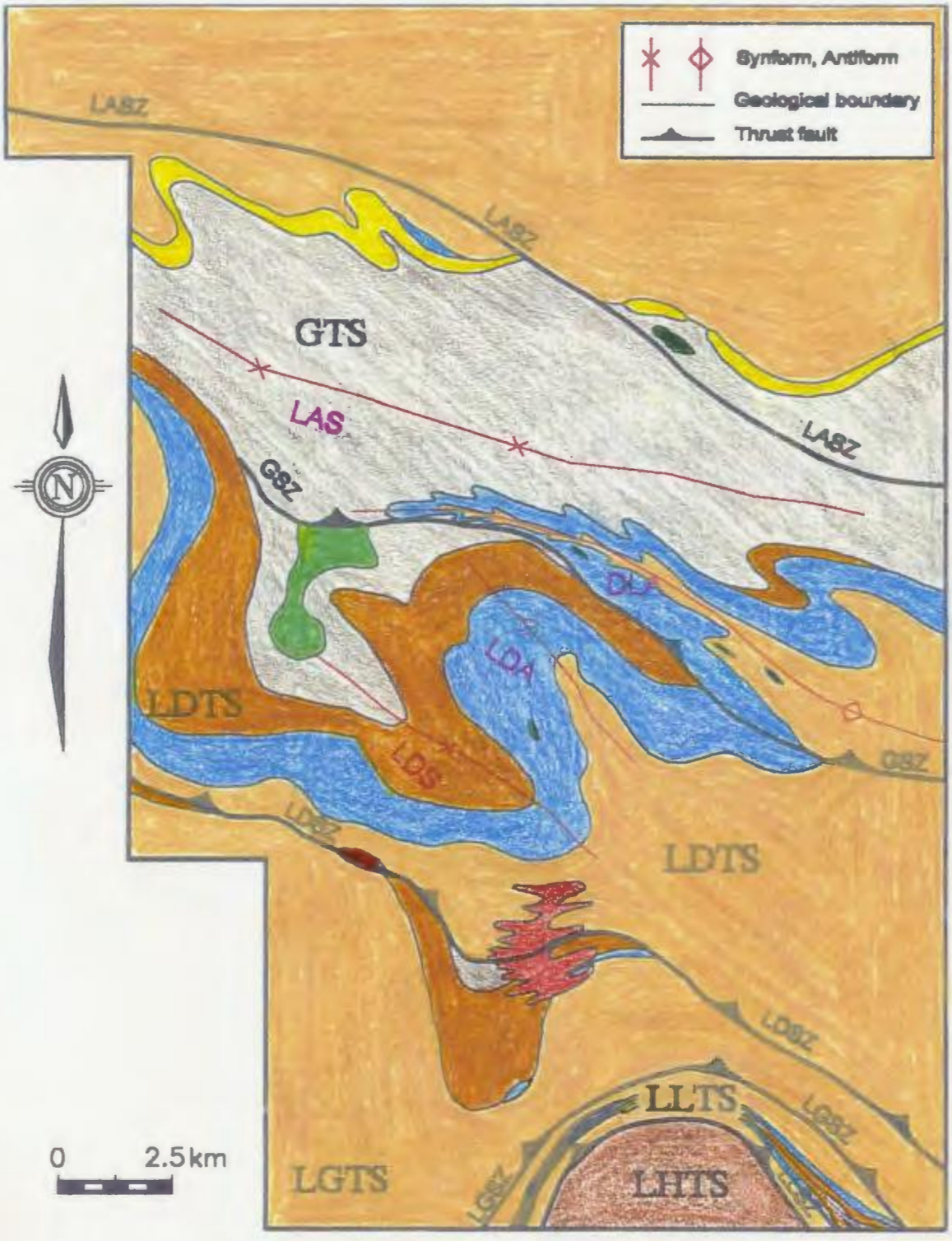
Synform, Antiform
Geological boundary
Thrust fault
LASZ
LASZ
GTS
LAS
LASZ
GSZ
DJ
LDA
LDTS
LDS
GSZ
LDSZ
LDTS
LDSZ
LLTS
LGSZ
LGTS
LHTS
LGSZ
N
0
2.5km

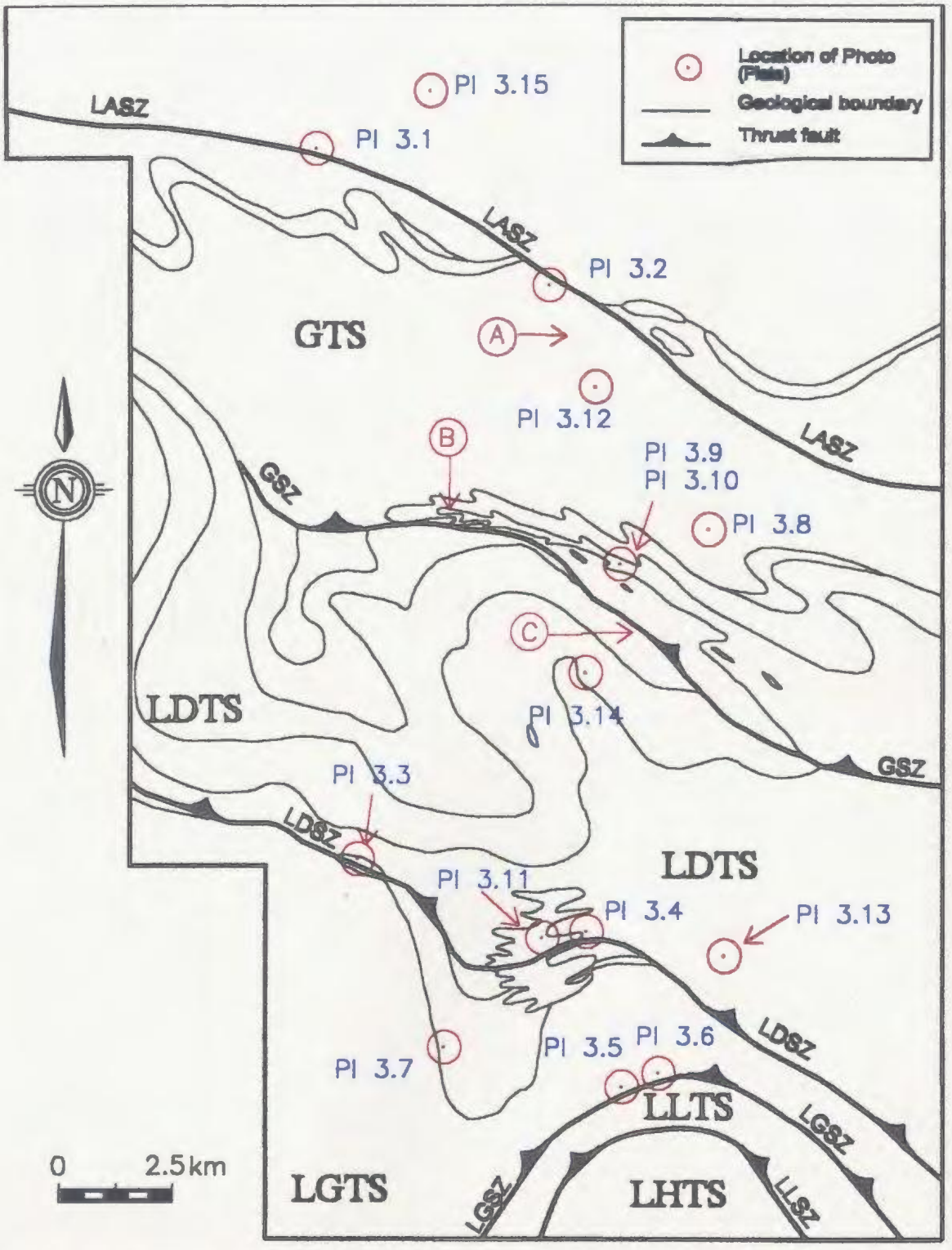

Figure 3.2 Location map for plates described in text (refer to Figure 3.1 for abbreviations).

of good exposure along the shear zone will be discussed.

Near the southern shore of Lac Audréa, shear zone fabrics comprise heterogeneously foliated quartzofeldspathic biotite gneisses which locally contain lens-shaped calc-silicate pods (4-8 cm) and highly disaggregated layer-parallel granitic veins (Plate 3.1). More intense deformation is expressed by a concordant straight gneiss fabric consisting of 1-10 cm wide layers of quartzofeldspathic gneiss with quartz augen alternating with layers of amphibolite. A stretching lineation, defined by quartz and feldspar, plunges moderately towards the southeast, oblique to the strike of the main foliation, suggesting a component of dip-slip movement on the shear zone. The highest strain areas are characterized by symmetrical K-feldspar and plagioclase augen in a matrix of parallel quartz ribbons.

Farther southeast along the shear zone, at 'A' (Figure 3.2), pelitic and semi-pelitic gneisses are locally interleaved with competent calc-silicate fragments, boudinaged mafic pods and cm-scale granitic veins transposed into parallelism with the shear foliation. Aligned cm-scale quartz boudins may represent (at least in part) boudinaged F_1 isoclinal fold hinges (Plate 3.2) (see also Section 3.7.2). Outcrop-scale anastomosing high strain fabrics enclose lenses of lower strained rocks, indicating that shear motion was not concentrated along a single zone. A weak mineral stretching lineation marked by elongate quartz grains plunges to the southeast, as elsewhere in the shear zone,

Plate 3.1 Stream-washed outcrop of porphyroclastic biotite hornblende quartzofeldspathic gneiss of Attikamagen Formation along the Lac Audréa shear zone. Local evidence of layer parallel shear is suggested by asymmetrically boudinaged feldspar porphyroclasts (0.25-2 cm) and layering of felsic and mafic lithologies. Lineations plunge steeply down dip. View to the south.

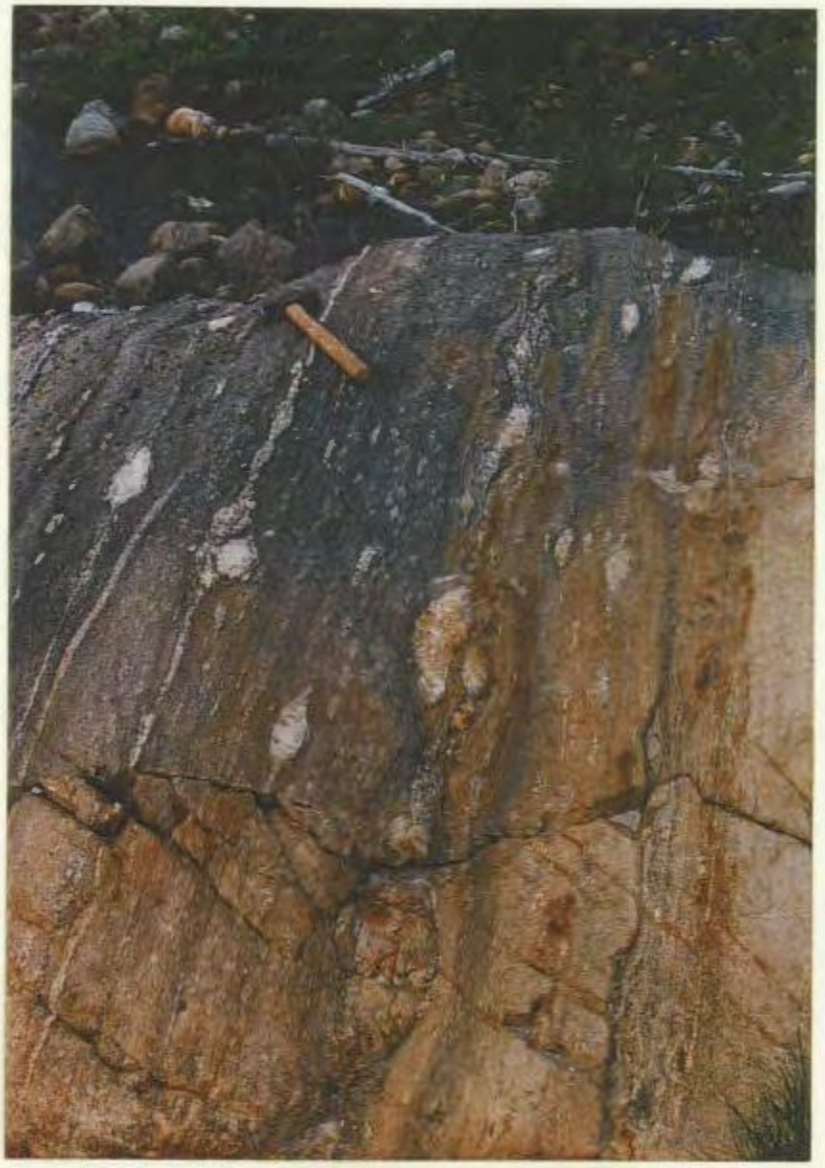

Plate 3.2 Quartzofeldspathic schist of the Attikamagen Formation containing relict compositional layering (S_0) and disrupted quartz veins preserved as boudins. Note that compositional layering, defined by slight contrasts in colour and grain size, is parallel with the tectonic fabric (S_1). The majority of the boudins in this photograph do not contain evidence of folding, however it is possible that some may be relict F_1 fold hinges, as is suggested by the layer parallel fabric and down-dip quartz stretching lineation. View to the northwest.

suggesting an overall NNW-SSE direction of movement. However kinematic indicators are rare and ambiguous as both sinistral and dextral shear senses were observed, along with symmetrically recrystallized feldspar tails around garnet porpyroclasts.

On the basis of the map pattern the Lac Audréa shear zone is considered to have only minor displacement across it, and it may be a relatively late feature compared to the shear zones discussed below.

3.4.2 Gueslis Shear Zone

The Gueslis shear zone separates the Gueslis thrust sheet from the Lac Don thrust sheet to the south (see Figure 3.1). The location of the shear zone is largely inferred from the map pattern, and it is only well exposed within 0.5 km of the road (Hwy 389) (see Figure 1.3), but its trace has been extended to the east and west along distinct airphoto and topographic trends. To the east of the road, at 'B' (see Figure 3.2), a heterogeneously deformed granite appears to have intruded into the shear zone. Planar fabrics in the granite are generally concordant with those in the surrounding silicate-carbonate iron formation (Sokoman Formation), however, local cross-cutting fabrics as shown in Plate 2.16, suggest that the emplacement into the shear zone was syn- to post-D_2. A sample of this granite was collected for U/Pb geochronology, and is discussed in Chapter 5. Approximately 1.5 km to the southeast, the Gueslis shear zone is inferred to truncate the silicate-carbonate iron formation of the Lac Don thrust

sheet along a prominent airphoto lineament, and near the eastern margin of the map the shear zone separates zones of contrasting strike in marble and quartzofeldspathic gneisses of the Denault and Attikamagen formations respectively (see Figure 3.1).

On the western side of the road, the Gueslis shear zone is not exposed, but is interpreted to follow a prominent E-W trending valley (location 'C', Figure 3.2) to the south of marble (Denault Formation) outcrops in the Gueslis thrust sheet. Farther west, the shear zone is interpreted to die out, as structural continuity between the Gueslis and Lac Don thrust sheets is suggested by the trends of the lithological units and S_1 measured by Phillips (1958), Murphy (1959) and the author.

3.4.3 Lac Don Shear Zone

The location of the Lac Don shear zone, which separates the Lac Don thrust sheet from the Lac Gull thrust sheet, is difficult to define precisely, especially where the distinctive platformal stratigraphy of the Knob Lake Group is absent. However, it coincides with a well exposed zone of straight gneiss (up to 2 m wide) in the vicinity of Lac Gull (Plates 3.3 and 3.4), consisting of white to pink weathering granite with elongate quartz and stretched out feldspar aggregates tectonically interleaved with amphibolite and quartzofeldspathic biotite gneiss. The sense of displacement is not apparent at these outcrops due to the pervasive annealing and the lack of asymmetrical kinematic indicators.

Plate 3.3 High strain straight gneiss along the Lac Don shear zone. At this location, the shear zone separates gneisses of the Attikamagen Formation of the Lac Don thrust sheet (top of photograph) from lithologically similar gneisses of the Menihek Formation (Lac Gull thrust sheet). View looking northeast.

Plate 3.4 Strong down-dip quartz stretching lineation, parallel to pencil, in granitic layer along the Lac Don shear zone. View to southeast.

In the central part of the map area, the location of the Lac Don shear zone is inferred from truncation of the iron formation unit and the opposing stratigraphic younging directions (see Section 3.5) on either side of the shear zone.

3.4.4 Lac Gull Shear Zone

The Lac Gull shear zone separates the Lac Gull thrust sheet from the underlying Lac Lamêlée thrust sheet (see Figure 3.1). Shear fabrics in the well foliated biotite quartzofeldspathic gneisses of the Attikamagen Formation are moderately to steeply dipping and locally include dextrally rotated plagioclase porphyroclasts (Plate 3.5), folded granite anatectic veins and local strong down-dip quartz stretching lineation. These kinematic indicators suggest a top-to-the-south sense of displacement along the shear zone. Other evidence of layer parallel shear includes tension gashes in calc-silicate rich marble, now infilled with quartz and actinolite.

3.4.5 Lac Lamêlée shear zone

As shown in Figure 3.1, the Lac Lamêlée shear zone separates the Lac Lamêlée thrust sheet from the Lac Hippocampe thrust sheet to the south. Due to the absence of distinct KLG stratigraphy in the Lac Hippocampe thrust sheet (Section 3.5.5), the location of the shear zone is based on structural trends in quartzofeldspathic gneisses from Clarke (1977). Where mapped by the author, at the southern extent of the field area, the Lac Lamêlée shear zone consists of strongly layered biotite quartzofeldspathic gneiss with variably interleaved

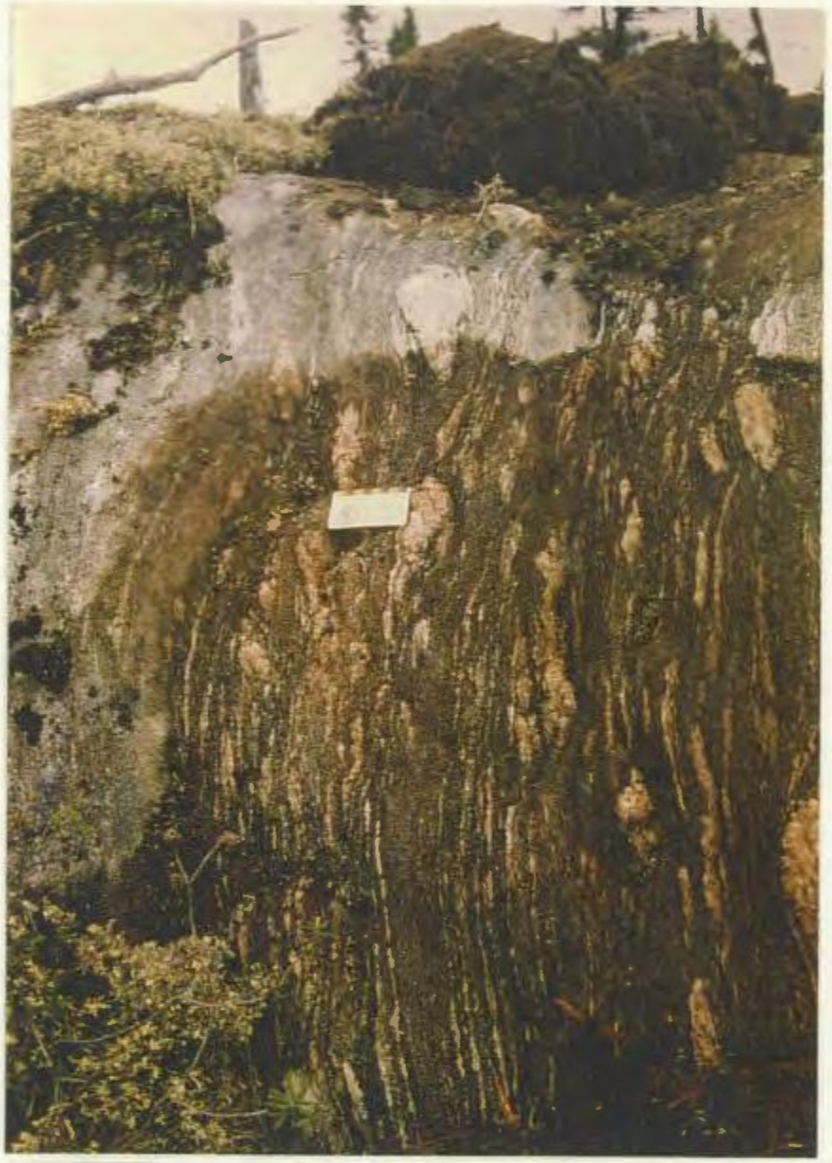

Plate 3.5 High strain in boudinaged biotite-quartzofeldspathic gneiss along the Lac Gull shear zone. Although kinematic indicators are generally symmetrical, local dextrally rotated plagioclase porphyroclasts suggest that shear sense is north side (right side of photograph) up. Card for scale (7cm). View looking west.

amphibolite and white to pink weathering granite. Asymmetrical shear sense indicators are rare and are extensively annealed, although dextrally rotated anatectic veins with down-dip quartz stretching lineation were locally observed (Plate 3.6), which translates into top-to-the-south movement along the shear zone.

3.5 THRUST SHEET STRATIGRAPHY

The Gueslis, Lac Don, Lac Gull and Lac Lamêlée shear zones underlie four thrust sheets with distinctive variations in the Knob Lake Group stratigraphy. Stratigraphic columns for each thrust sheet, shown in Figure 3.3 are based on the Knob Lake Group stratigraphic sequence (Section 2.0 and Figure 2.1) observed within the respective thrust sheet. The thicknesses of the lithological units as drawn in the stratigraphic columns are only approximate estimates and do not take into account the substantial thickening and thinning around fold closures and along strike. In the following sections, the thrust sheets are compared with respect to their stratigraphic sequence, lateral extent, and the effects of polyphase deformation.

A brief description of the stratigraphy of each thrust sheet, beginning in the northern part of the field area, follows.

3.5.1 Gueslis Thrust Sheet

The Gueslis thrust sheet is bounded to the north (structural top) by the Lac Audréa shear zone and to the south along its base by the Gueslis shear zone

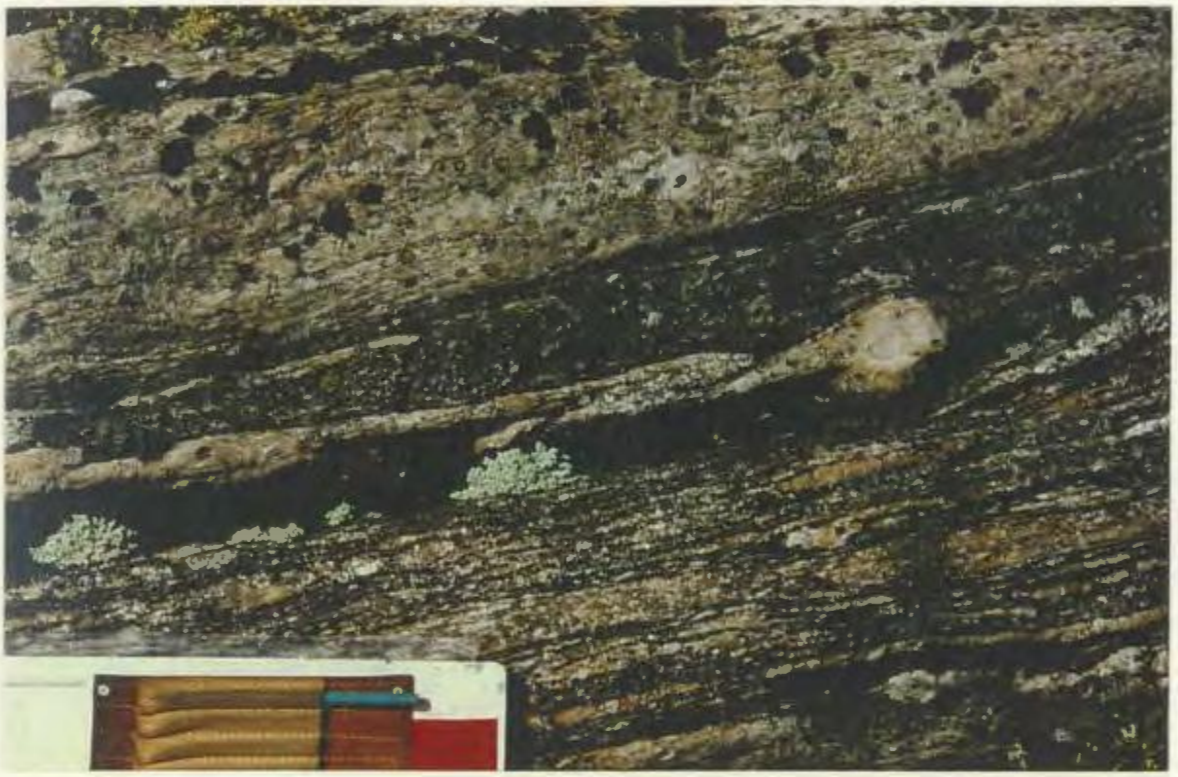

Plate 3.6 Well layered biotite quartzofeldspathic gneiss with interleaved amphibolite and rare, dextrally rotated granitic anatectic vein with down-dip quartz stretching lineation. Sense of displacement is inferred to be top-to-the-south.

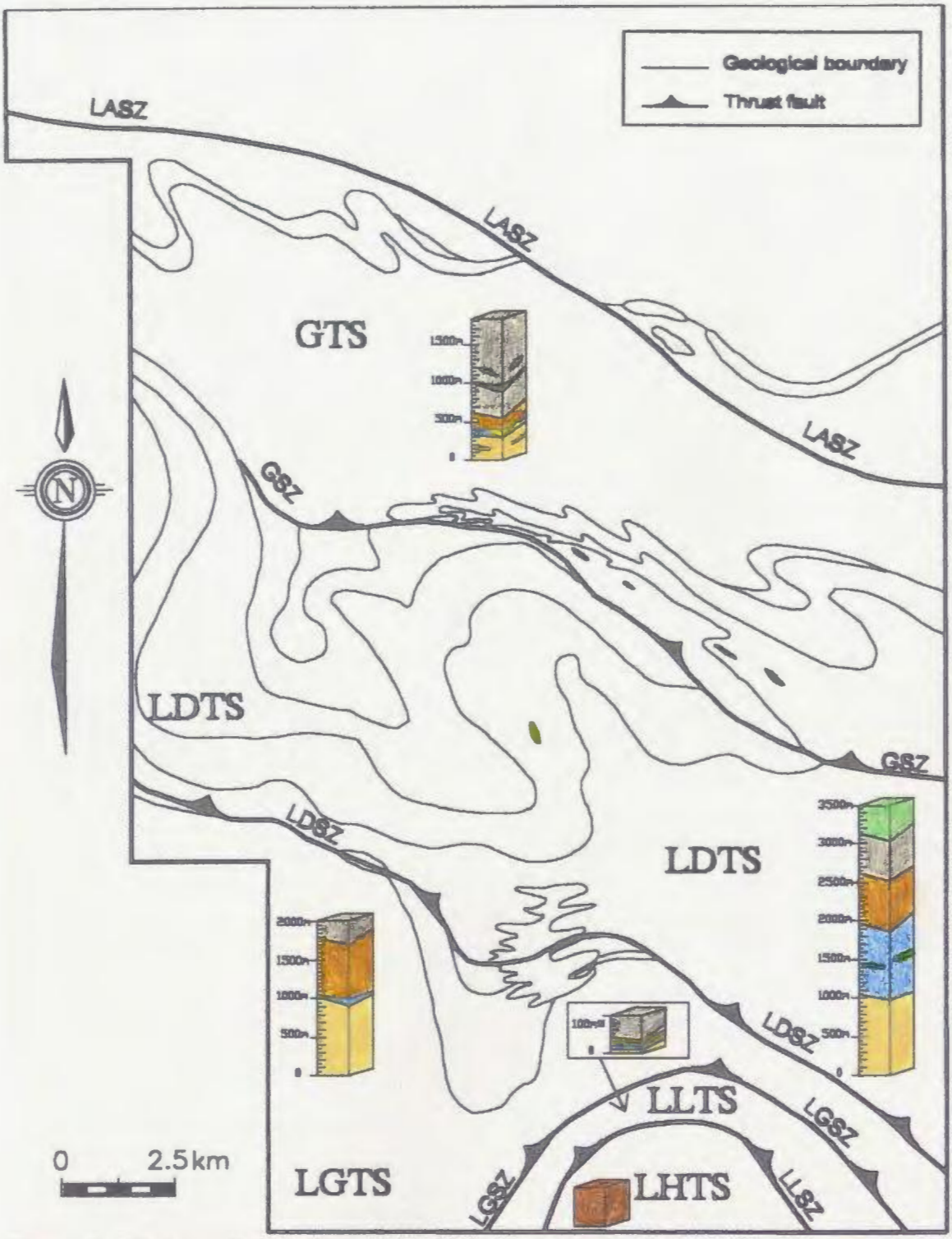

Figure 3.3 Schematic stratigraphic columns illustrating the variations in the Knob Lake Group stratigraphy and unit thickness within each thrust sheet in the field area. The thickness of the lithological units are measured from cross-sections and are approximate (refer to Figure 3.1 for abbreviations and legend).

(see Figure 3.1). As illustrated in Figure 3.3, the stratigraphy of the thrust sheet comprises, from bottom to top: (a) a few hundred metres of quartzofeldspathic gneiss of the Attikamagen Formation; (b) a discontinuous thin dolomitic marble unit less than 50 m thick (Denault Formation); (c) a thin (maximum 200 m) unit of oxide iron formation (Sokoman Formation) comprising 'lean iron formation' (quartzite with thin subordinate layers of specular hematite and magnetite) and locally with minor quartz pebble conglomerate (Wishart Formation); and (d) a thick section (1-1.5 km, top not seen) of migmatitic biotite ± garnet schists and gneisses of the Menihek Formation. Sparse boudinaged metamorphosed gabbro dykes occur in the Attikamagen, Denault and Menihek formations (see Figure 3.1).

North of the Lac Audréa shear zone the area is largely underlain by quartzofeldspathic gneisses of the Attikamagen Formation, but in the absence of stratigraphic marker units, it is not possible to estimate its thickness.

3.5.2 Lac Don Thrust Sheet

The Lac Don thrust sheet is bounded to the north (structural top) by the Gueslis shear zone and to the south (bottom) by the Lac Don shear zone (see Figure 3.1). The stratigraphy of the thrust sheet is distinguished by a succession, shown in Figure 3.3, from bottom to top: (a) a thick (probably >1 km, base not seen) section of quartzofeldspathic biotite ± garnet migmatitic gneisses of the Attikamagen Formation; (b) a thick (~800-1000 m) unit of well layered to massive

dolomite and calcite marble with subordinate quartz and calc-silicate minerals; (c) a thick (~800-1000 m) unit of iron formation, including carbonate, silicate carbonate and minor oxide varieties; (d) about 500 m or less of biotite-rich quartzofeldspathic schists and gneisses of the Menihek Formation; and (e) a thin (<500 m) unit of coarse boulder conglomerate (Lac Gull formation).

3.5.3 Lac Gull Thrust Sheet

Along its northern margin, the Lac Gull thrust sheet (see Figures 3.1 and 3.3) is overlain by the Lac Don thrust sheet along the Lac Don shear zone, and it is bounded to the south by the Lac Gull shear zone. In the area mapped by the author the stratigraphy of the thrust sheet comprises ~800-1000 m of quartzofeldspathic gneisses (Attikamagen Formation), a thin unit (<100m) of marble (Denault Formation), a thick (~500-800 m) unit of silicate-carbonate iron formation (Sokoman Formation), and a thin layer (~50-100 m) of quartzofeldspathic schists and gneisses of the Menihek Formation.

3.5.4 Lac Lamêlée Thrust Sheet

The Lac Lamêlée thrust sheet in the south of the map area exhibits an extremely condensed, but complete stratigraphy of the Knob Lake Group. Units of quartzofeldspathic gneiss, marble with calc-silicates, quartzite, oxide iron formation and pelitic gneiss, comprising the Attikamagen, Denault, Wishart, Sokoman and Menihek formations respectively (see Figures 3.1 and 3.3), are generally less than 10 m thick, but are nonetheless continuous around a major

map-scale isoclinal fold structure. All the units possess a well-developed layer-parallel foliation ($S_0//S_1$), but strain is not extreme and the thin succession is interpreted to be largely an original feature.

3.5.5 Lac Hippocampe Thrust Sheet

The Lac Hippocampe thrust sheet extends well to the south of the study area, where it has not been examined in detail but is reported to consist of "segregated biotite ± hornblende gneiss" (Clarke, 1967, 1977) (see Figures 3.1 and 3.3). Within the study area, it consists of well layered quartzofeldspathic biotite (± garnet) gneisses with amphibolite and minor pink granite. Strain is variable in this unit, with the well layered straight gneiss character being predominant near the Lac Lamêlée shear zone.

On the basis of the abundance of amphibolite, and its 'segregated' character, the unit is tentatively interpreted as a slice of strongly reworked Archean basement with minor Proterozoic granitoid intrusions, but this remains to be verified geochronologically.

3.6 COMPARISON OF THE STRATIGRAPHIES OF THE THRUST SHEETS

As the previous paragraphs indicate, and acknowledging the imprecision of the thickness estimates and the probability of considerable tectonic thickening and thinning locally, there are nonetheless important differences in thickness and lithological composition of several units in different thrust sheets. The most significant of these differences are: (a) variation in thickness of the marble from

<50 m to 800-1000 m; (b) variation in the facies of iron formation from oxide facies to silicate-carbonate facies, with concomitant variation in thickness from <10 m to 800-1000 m; (c) variation in the thickness of the Menihek Formation, from <100 m to 1-1.5 km. These original stratigraphic differences indicate that the present structural configuration is simply not the result of imbrication of a short section of strata with a laterally consistent, layer-parallel 'pancake' stratigraphy. They imply the existence of important sedimentary facies contrasts within individual units between adjacent thrust sheets.

The structural juxtaposition and imbrication of the same units with contrasting sedimentary facies could indicate either: (a) that thrust sheets represent an assembly of facies brought together from initially widely separated parts of the shelf-rise sequence; or (b) that the shelf was characterized by significant local topography in the form of horsts and graben that controlled sedimentation (i.e. variation of stratigraphic thickness and facies change) locally. While (a) is not impossible and can be tested by metamorphic studies, previous work in the northern part of the Kaniapiskau Supergroup north of the Grenville Front in the Labrador Trough (Wardle and Bailey, 1981) and also south of the Grenville Front near Wabush (van Gool, 1992) indicates that there was significant local topography within the Knob Lake Group basin that produced a primary control on the distribution of sedimentary facies, and so (b) may be the more likely alternative. This has been assumed in the construction of Figure 2.1.

3.7 PHASES OF DEFORMATION IN THE STUDY AREA

In the following sections the characteristic features of the fabrics within the units of the Knob Lake Group are described, followed by an evaluation of the major structural features within each thrust sheet (Sections 3.8 and 3.9), structural overprinting relationships (Section 3.10), and an examination of the overall large-scale structural geometry of the study area (Section 3.11). On the basis of field- and map-scale observations collected by the author, at least four phases of deformation have been identified. However, not all these phases of deformation can be unambiguously correlated on a regional scale, so a brief note on the assignment of structural elements to a particular phase of deformation is appropriate here.

In general, assignment of a structural element to a particular structural event (D_1, D_2, etc.) can only be reliably made where several generations of superimposed fabric elements are seen together, a situation that is restricted to relatively few outcrops in the study area. Thus it is necessary to extrapolate from these key outcrops to those in which only one or two generations of fabric elements are present. Based on the subparallel relationship between bedding (S_0) and the S_1 foliation ($S_0//S_1$) that is observed in most outcrops, it is assumed that D_1 is a regionally penetrative deformation and that F_1 folds are isoclinal structures that have an associated penetrative axial planar fabric. Where identified, D_2 appears to have been a somewhat less penetrative deformational event than D_1.

as F_2 folds are generally tight rather than isoclinal in shape and the associated axial planar fabric (S_2) is restricted to ductile lithologies. Thus, in the absence of overprinting relations, layer parallel fabrics and isoclinal folds are interpreted as D_1 structural elements, whereas more open folds with less well developed axial planar fabrics are interpreted as D_2 elements. However, it is quite possible that in areas of high D_2 strain, F_2 folds could have become isoclinal and S_2 fabrics penetrative, resulting in obliteration of D_1 structures and rendering D_2 and D_1 fabric elements locally indistinguishable. In general, there is no way of distinguishing these possibilities.

The third phase of folding (F_3) is only locally preserved, and is expressed as recumbent refolding of outcrop scale D_1 and D_2 structures. The last phase of folding, F_4, resulted in upright steeply plunging map-scale folds that are best expressed in the southern part of the study area, where local F_2/F_4 fold interference structures are observed. Interference between F_3 and F_4 structures is not seen in the field area on account of their mutually exclusive geographic distributions. They are distinguished on the basis of their orientations, which imply their formation was due to differently oriented stress fields. However, the relative chronology between F_3 and F_4 is unknown.

Although F_1, F_2 etc. denotes a local structural sequence, it is not intended to imply that F_1 folds were formed everywhere before F_2 structures developed. F_1 and F_2 are both interpreted to have developed under a similar stress field, and it

is likely that the two structural generations developed in a single deformational event that progressed at different rates in different parts of the area. With respect to the later phases of deformation, which developed in differently oriented stress fields, it is likely that they post dated D_1-D_2. Finally it must also be noted that any errors incurred in the numerical assignment of the generation of D_1 or D_2 structures do not greatly influence the interpretation of the overall structural architecture, but do however influence the models of the structural evolution of the area presented in Chapter 6.

In the study area, linear fabrics are generally poorly preserved, probably due to later annealing. Lineations in quartzofeldspathic gneisses are in part defined by elongate trains of quartz veins that exhibit a bimodal grain size due to subgrain formation, a typical recrystallization product of quartz ribbons, implying a major component of strain parallel to the lineation. A weak stretching lineation defined by quartz (see Plates 2.8 and 2.9) and pyroxene elongation is preserved in the oxide and silicate-carbonate iron formations (Sokoman Formation) respectively, and a similar feature is expressed by calc-silicate minerals in marble (see Plate 2.6) of the Denault Formation, and by stretched quartz grains in granitic layers parallel to S_1 in gneisses and schists of the Attikamagen and Menihek formations (see Plate 3.4).

Based on the observation that penetrative fabrics are D_1 (see below), it is assumed that most linear fabrics are L_1 features. However, quartz stretching

lineations are also associated with thrust faults, which as described below, are post D_1 structures such that quartz stretching lineations cannot be unambiguously used to constrain a particular phase of deformation. Therefore stretching lineations are not distinguished in terms of L_1, L_2 or L_3 on the map but are designated L_x. In a few places where both F_1 and L_x structures are present in the same outcrop, they are subparallel, implying that F_1 structures were rotated into the L_1 stretching direction during high strain deformation. A similar problem exists with respect to the definition of a foliation as $S_0//S_1$ or S_2. The distinction can generally be made in the hinge zone of an F_2 fold, but is ambiguous elsewhere. As a result, all foliations were given the same symbol in Figure 3.4. The orientations of fabrics, folds and lineations are shown in Figures 3.4 to 3.6 respectively, and a summary of the large-scale structural features is shown in Figure 3.7. Outcrop locations are shown in Appendix A_1.

3.7.1 Primary (D_0) Structures

The oldest planar structure in most rocks is a compositional layering that can locally be shown to be relict bedding (S_0) (see Plates 2.3 and 3.2). However in many areas, S_0 cannot be identified with certainty, and the oldest fabric is a composite compositional layering and tectonic fabric, interpreted to be $S_0//S_1$ (Plate 3.7) (see Plates 2.1 and 2.2). Younging directions are determined from the stratigraphic sequence in the Knob Lake Group (see Figures 2.1 and 3.3) on the assumption that the local stratigraphy is similar to that in the less deformed and

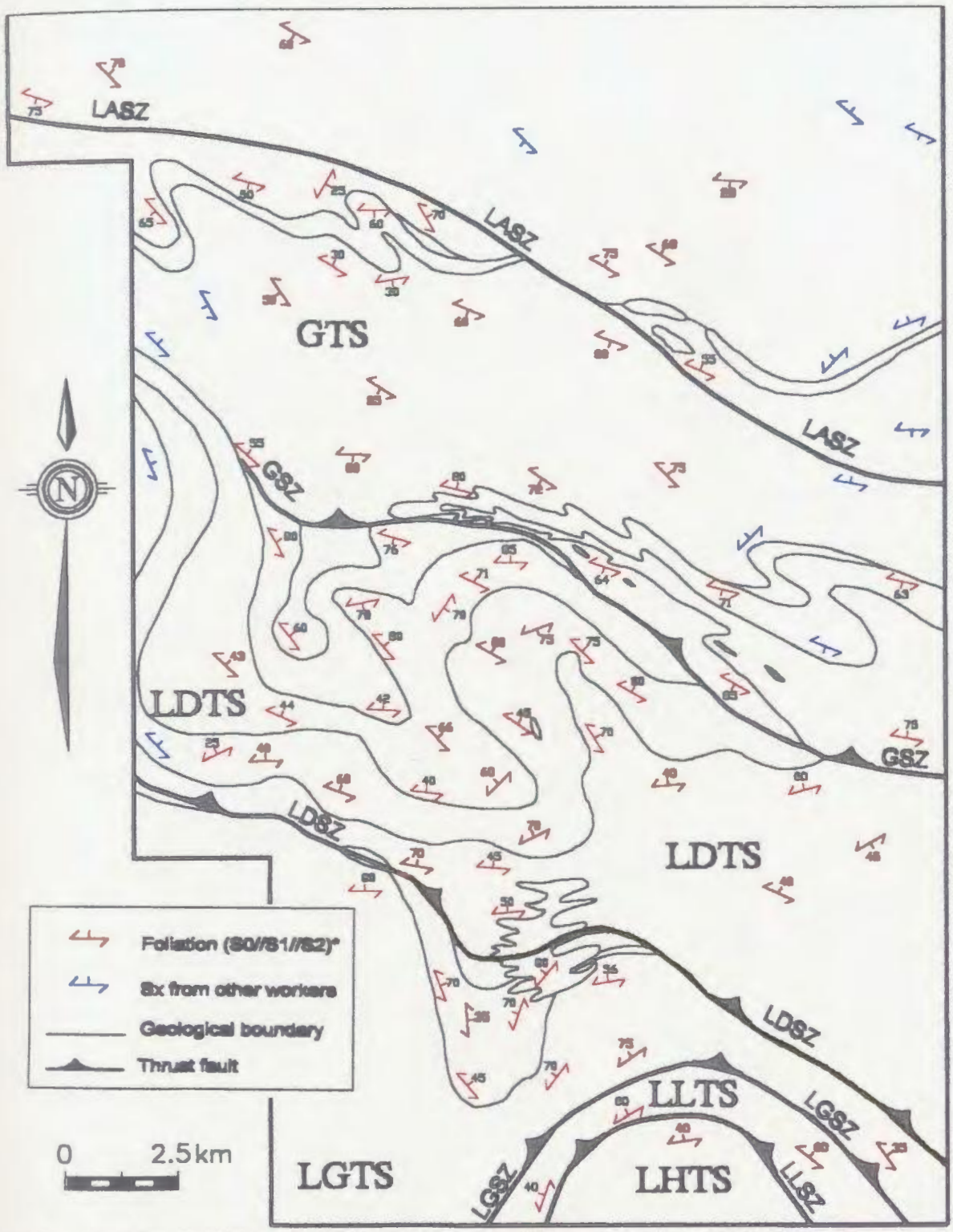

Figure 3.4 Geological map of the study area illustrating the distribution of lithologic units and planar fabrics (S_1 and S_2) in the Knob Lake Group (refer to Figure 3.1 for abbreviations).

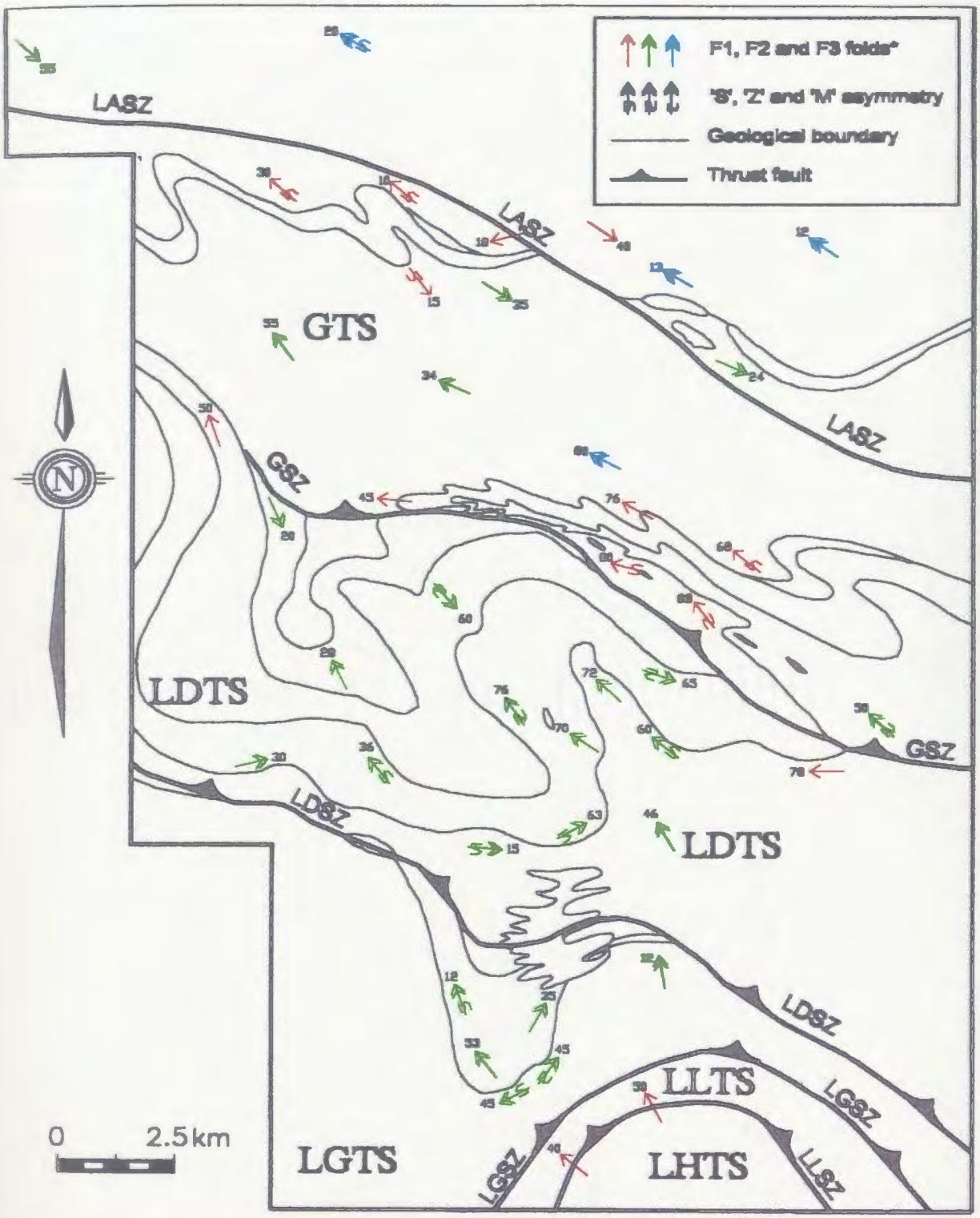

Figure 3.5 Geological map illustrating the distribution of measured fold axes in the study area. F_4 folds are map-scale structures and are not shown on this figure (refer to Figure 3.1 for abbreviations).

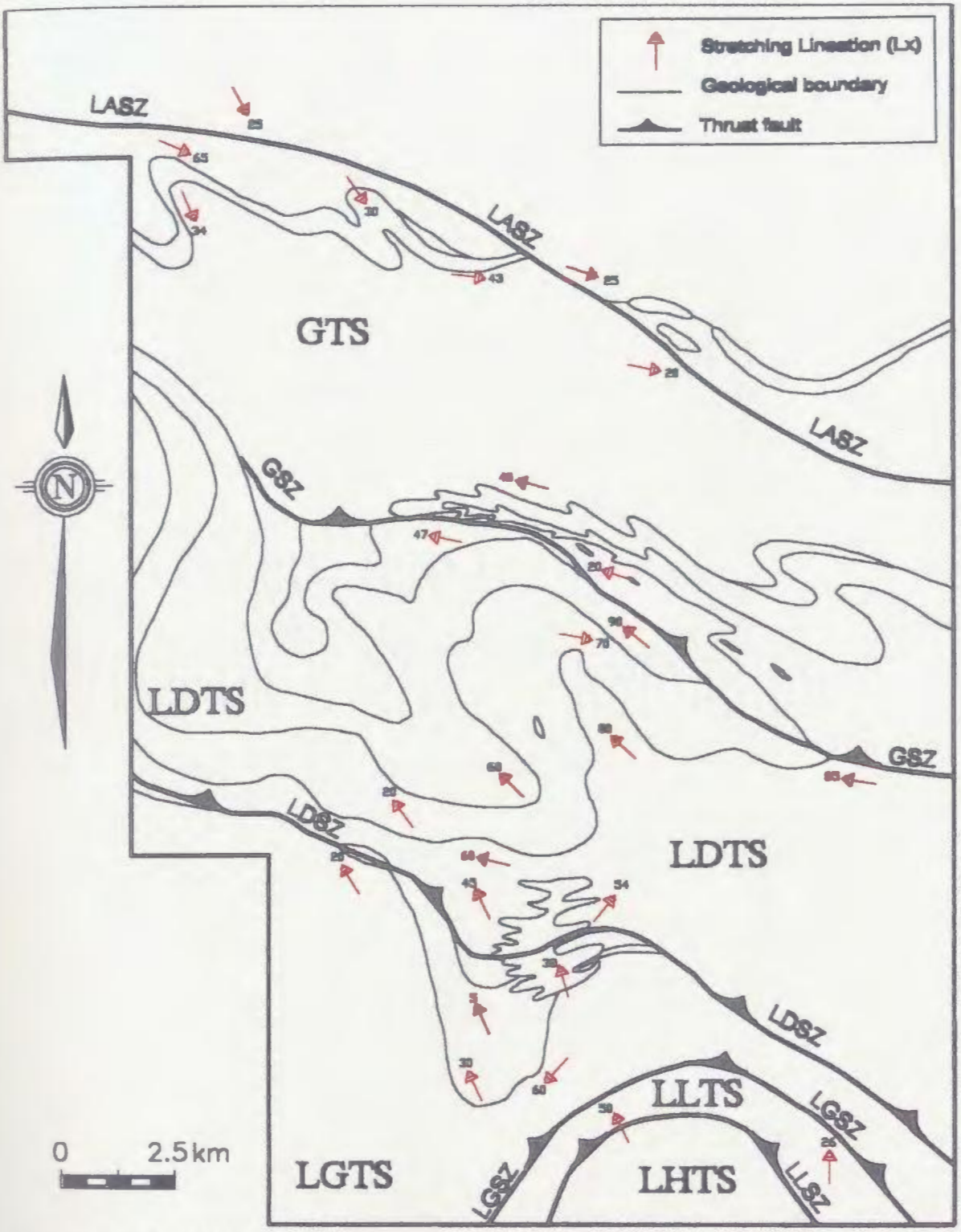

Figure 3.6 Geological map illustrating the distribution of measured linear fabrics (L_x) in the study area (refer to Figure 3.1 for abbreviations).

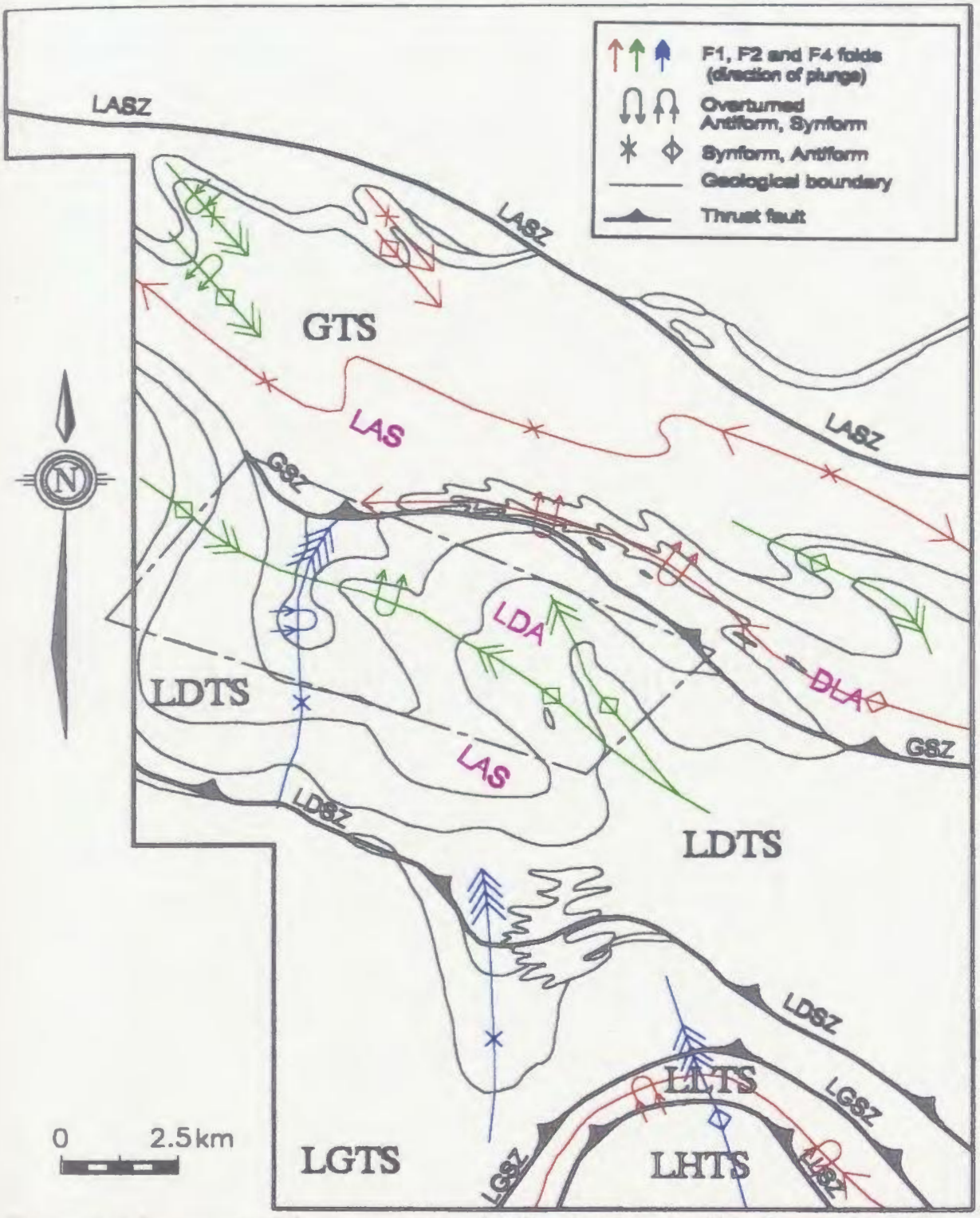

Figure 3.7 Summary of the large-scale ductile structures within the study area (refer to Figure 3.1 for abbreviations). The box shows the location of the block diagram shown in Figure 3.9.

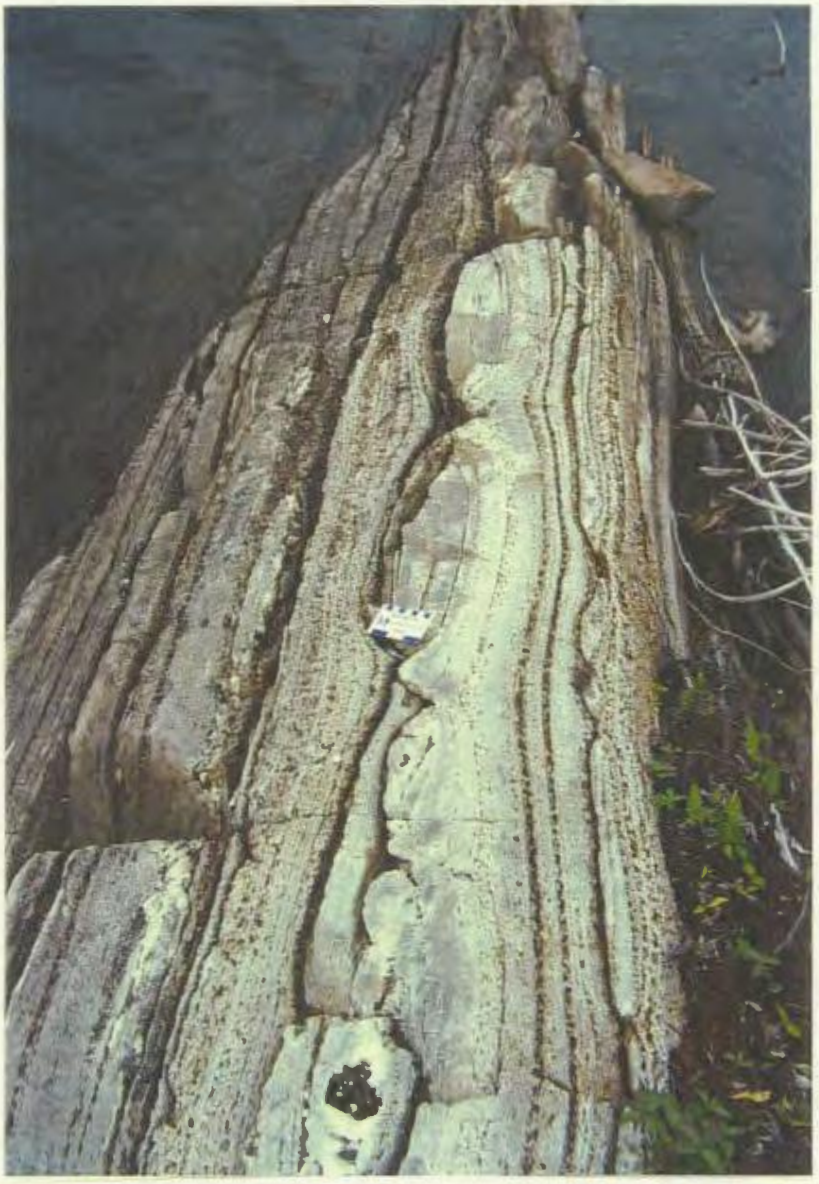

Plate 3.7 Boudinage in quartz-rich 'lean' iron formation (Sokoman Formation) on the western side of Lac Gull, showing $S_0//S_1$ and implying a very large layer -parallel D_1 strain.

metamorphosed parts of the Knob Lake Group to the north of the Grenville Front. This assumption, which has been shown to be valid in the Labrador City-Wabush area some 80 km to the north (van Gool, 1992), yields consistent results in the study area and provides an important constraint to interpret the effects of Grenvillian polyphase deformation, including the characterization of the thrust sheets.

3.7.2 D_1 Structures

The first phase of Grenvillian deformation (D_1) recognized in the field area is expressed as a regionally developed metamorphic foliation (S_1), typically a penetrative schistosity or migmatitic layering (Figure 3.4), and also by less common intrafolial folds (F_1; Figure 3.5) and lineations (L_x; Figure 3.6). S_1 planar structures are well developed at outcrop-scale, although variable in style according to lithology. The single strong fabric present in many outcrops of the Attikamagen and Menihek formations, inferred to be. $S_0//S_1$, is expressed as a gneissic layering (see Plates 2.1, 2.2 and 2.10) that is also enhanced by elongate quartz and/or feldspar grains, and commonly by the preferred orientation of micas. Near the thrust sheet boundaries, the gneisses of the Attikamagen and Menihek formations are more severely strained and contain abundant attenuated and boudinaged leucocratic veins parallel to the S_1 foliation (Plate 3.8) (see

Plate 3.8 Layered garnet-biotite gneiss (Menihek Formation) with coarse-grained quartzofeldspathic veins interpreted to be of anatectic origin. Note that the veins are deformed into a planar fabric that is subparallel to relict compositional layering defined by quartz-rich layers (best observed at top of photograph). Thus the relict layering and the veins define $S_0//S_1$ at this outcrop. A second fabric, S_2, defined by the preferred orientation of biotite in the mica-rich layers, is oblique to $S_0//S_1$, implying that the outcrop is located in an F_2 hinge region. Small-scale F_2 folds of an anatectic vein margin can be observed in the upper middle of the photograph (see sketch). Note that the garnet porphyroblasts occur in both the veined and unveined parts of the unit and overgrows all fabrics. Launcher for scale (15 cm).

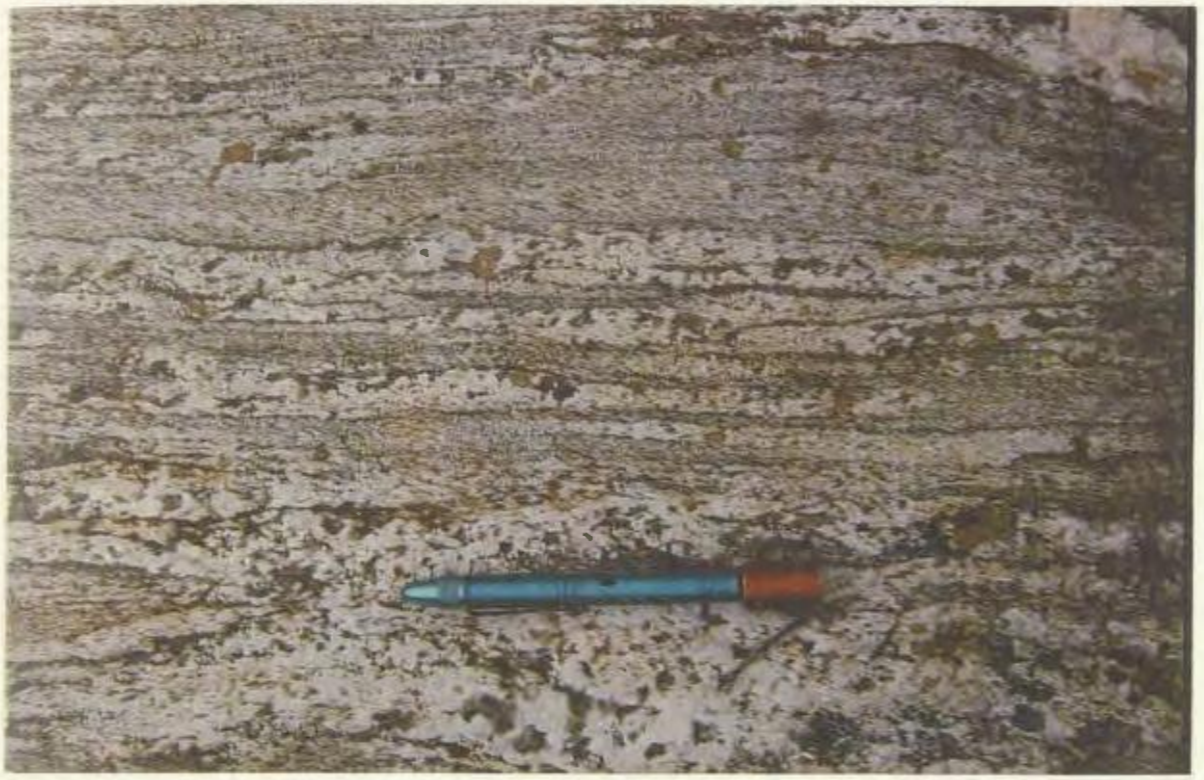

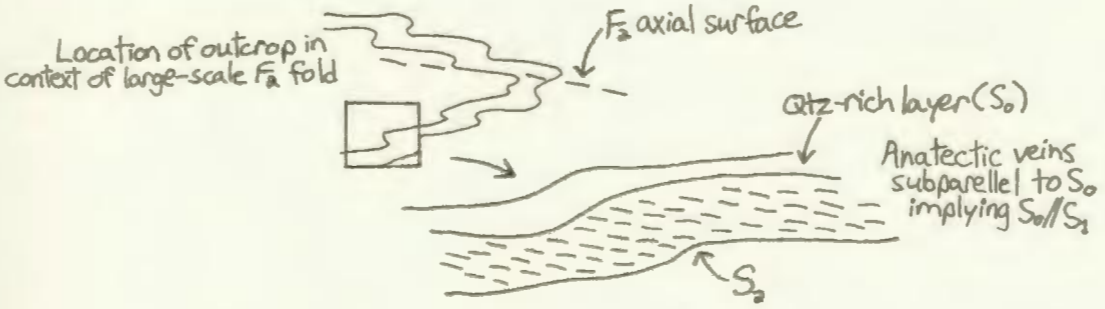
Location of outcrop in context of large-scale F_2 fold
F_2 axial surface
Qtz-rich layer (S_0)
Anatectic veins subparellel to S_0 implying $S_0 // S_1$
S_2

Plates 3.1, 3.2, 3.3 and 3.7). The boudins, commonly with characteristic tails formed by trains of subgrains, indicate a strong component of layer parallel stretching. In the marble and iron formation of the Denault and Sokoman formations respectively, the S_1 fabric is commonly less well defined mineralogically due to extensive later annealing and may be difficult to clearly distinguish from lithological layering (Plates 2.4 and 2.9). However, extreme ductility of quartz layers (e.g. Plate 2.5) also implies very large D_1 strain in these units.

Small-scale F_1 folds have been identified in all units of the Knob Lake Group, but although widespread, they are relatively uncommon (see Plates 2.5, 2.7A). Small-scale F_1 folds with wavelengths of a few centimetres, are tight to isoclinal features with S_1 axial surfaces (sub-) parallel to S_0 away from the hinge zones. Sheared-off limbs are characteristic (e.g. Plates 3.9, 3.10 and 3.11), and in areas of high strain F_1 folds are locally preserved as isolated boudinaged F_1 fold hinges within the penetrative shear zone fabric (see Plate 3.2). Many F_1 folds have asymmetric 'S' or 'Z' shapes when viewed down plunge, however, 'M'-shapes such as illustrated in Plates 3.9 and 3.11 also occur, and imply the existence of F_1 folds with larger wavelengths. Several map-scale F_1 folds have also been identified within the study area (Section 3.8) and it is likely that others are present, but have been so strongly transposed as to be unrecognizable.

Evidence of folding of the combined $S_0//S_1$ planar fabric is commonly

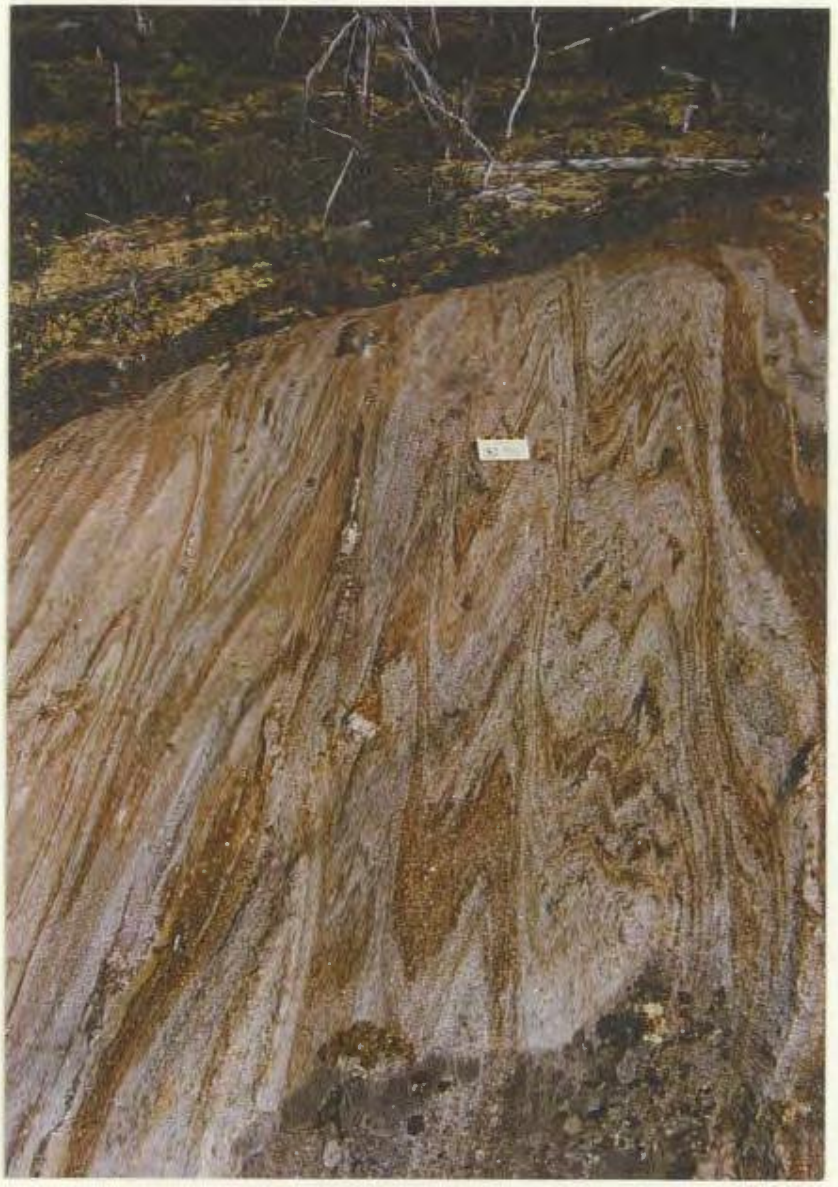

Plate 3.9 Tight to isoclinally folded pelitic to semi-pelitic biotite-muscovite-garnet-kyanite quartzofeldspathic schist of the Attikamagen Formation. The (F_1) folds, which fold compositional layering (S_0), are M-shaped on the left side of photo but display an S-asymmetry on the right side where sheared-off limbs are prevalent. Scale card in cm, view to east.

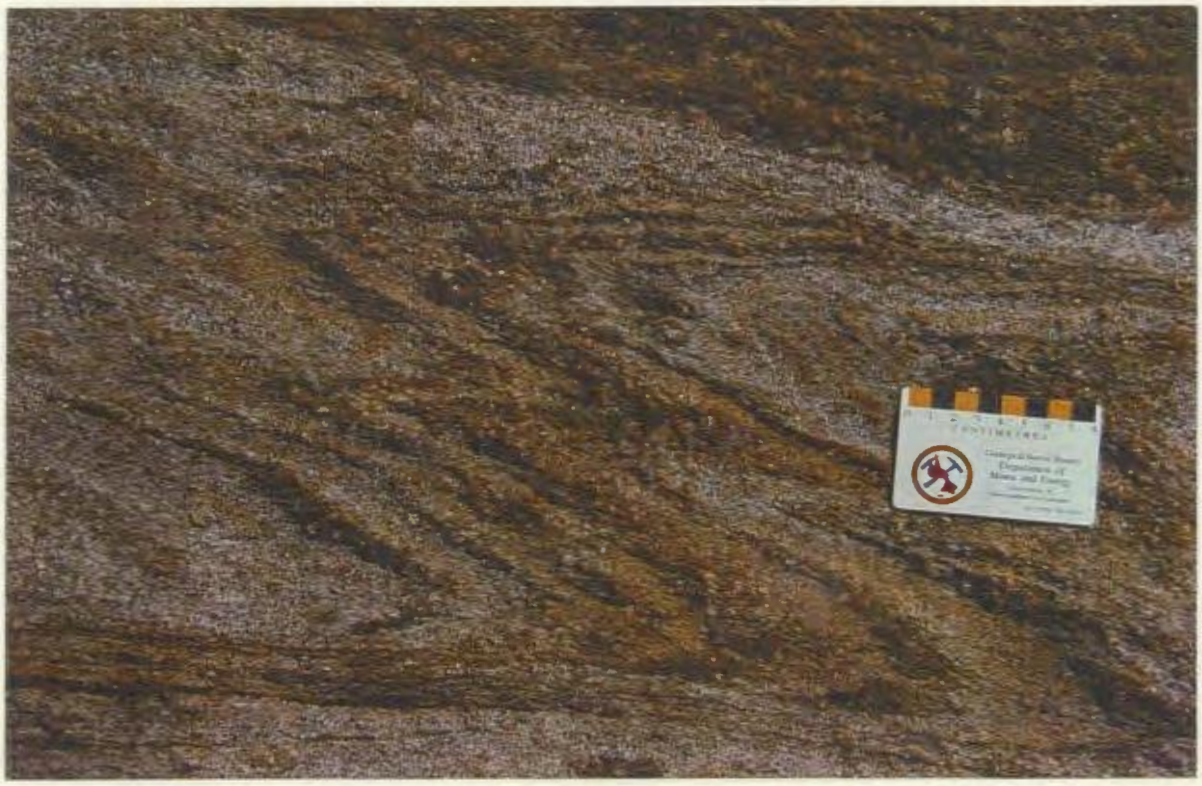

Plate 3.10 Detail view of an area in the upper right of Plate 3.9 illustrating the well developed axial planar foliation (S_1) defined by biotite as well as the tightly folded compositional layering (S_0). The S_1 fabric, in conjunction with those in Figures 3.4 and 3.5, suggests that these structures lie in the core of a large-scale NW-plunging F_1 anticline.

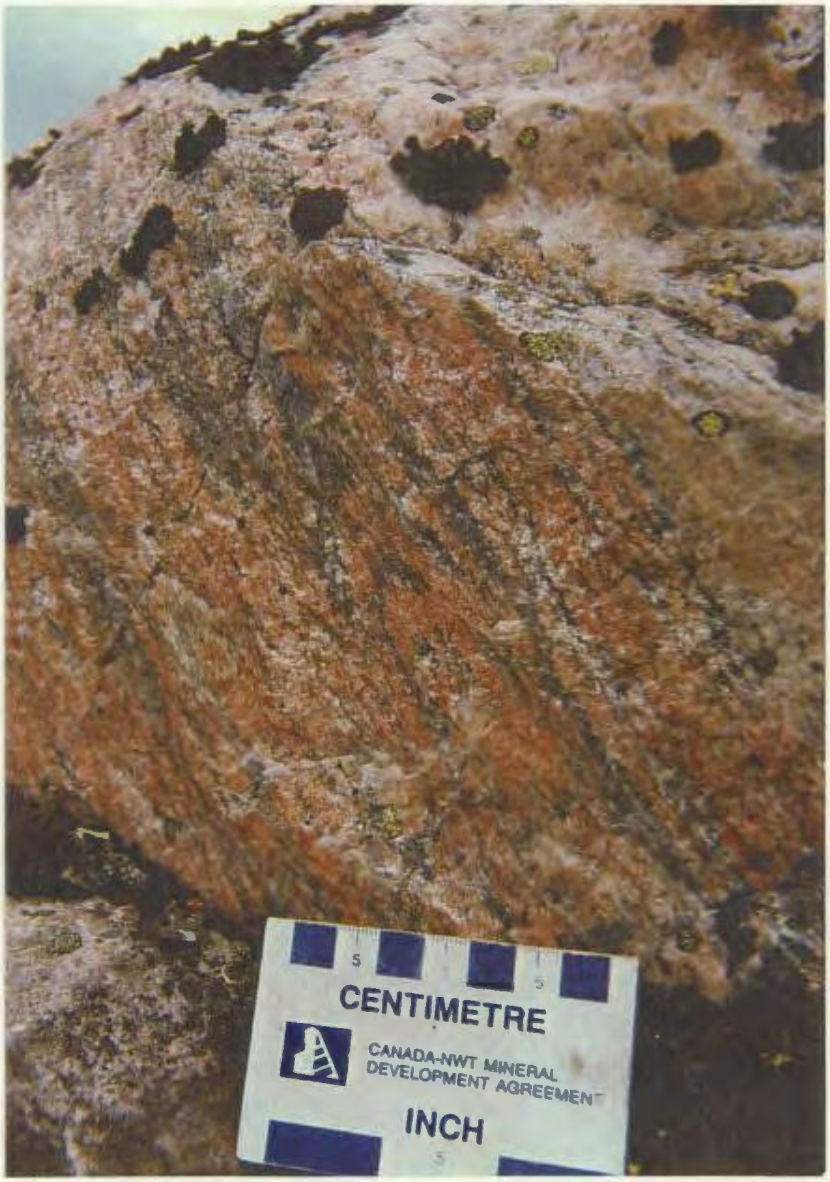

Plate 3.11 Oblique section through isoclinal F_1 folds defined by quartz ribbons in granite along the Lac Don shear zone, north of Lac Gull. View looking northwest.

observed in outcrop and inferred from the map pattern. These post-D_1 structures are typically more open in profile than F_1 folds and generally do not have a penetrative axial planar fabric in the more competent lithologies. On the basis of orientation, it is likely that these post-F_1 fabrics were formed in three distinct stress fields, and constitute three distinct deformational episodes. The three orientations are: (a) variably plunging, NW-SE trending folds with steep axial surfaces, (b) rare NW-trending recumbent folds, and (c) variably plunging, northerly trending folds with steep axial surfaces.

As shown by the fold interference patterns (see Figure 3.7 and Section 3.10), the NW-SE -trending structures with steep axial surfaces are interpreted to predate the other two orientations of post-D_1 folds. These are therefore referred to as F_2 folds. From regional correlations, the large-scale north-trending folds are considered to be the youngest structures, they are therefore referred to as F_4 structures. The rather sparse recumbent folds are by default defined as F_3.

3.7.3 D_2 Structures

As previously noted, the style of the F_2 outcrop-scale folds is variable according to lithology. Gneisses of the Attikamagen and Menihek formations contain D_1 leucocratic veins deformed by D_2, and locally by D_3 (Plates 3.12 and 3.13), whereas micaceous schists contain small- to medium-scale, open F_2 folds that crenulate the D_1 penetrative fabric (see Plate 2.10). F_2 folding of thin $S_0//S_1$ surfaces in marble of the Denault Formation varies in style from isolated tight to

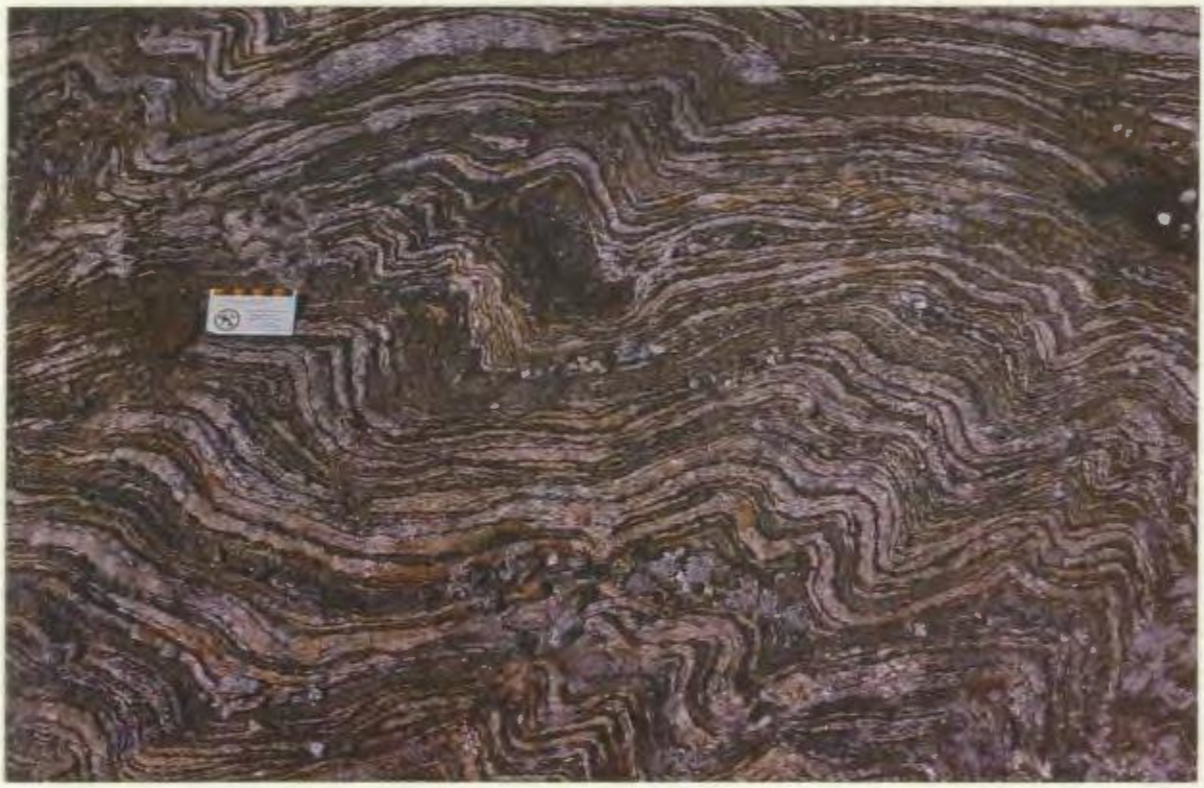


CENTIMETRE
INCH

isoclinal folds (Plate 3.14) to fold trains with axial planes at a high angle to the S_1 foliation (see Plate 2.5). Map scale, ESE to WNW -trending tight to open D_2 folds dominate the central part of the map area (see Figures 3.4 to 3.6).

3.7.4 D_3 Structures

Tight -to isoclinal refolding of the $S_0//S_1$ fabric by outcrop-scale northwest-trending recumbent D_3 structures (Plate 3.15) has been observed in several locations in the Gueslis thrust sheet. F_3 folds are distinguished from F_1 and F_2 folds by their shallow axial surfaces and subhorizontal fold axes, whereas F_1 and F_2 folds generally have steep axial surfaces.

3.7.5 D_4 Structures

Evidence of the fourth phase of deformation (F_4) is limited to the southern part of the study area, where the presence of large-scale N-trending fold axes with kilometer scale wavelengths is inferred from the map pattern (see Figure 3.7). Outcrop evidence of F_4 folding is rare, but is locally observed in iron formation in the Lac Gull thrust sheet (see Plate 2.8). In general, D_4 is inferred to account for some of the considerable variation of the plunge and trend of F_2 fold axes (especially in Lac Don thrust sheet), and refolded S_1 fabrics.

3.8 STRUCTURE OF THRUST SHEETS

In this section, the structural relationships displayed on maps, sketches and photographs form the basis for the interpretation of the large-scale polyphase ductile deformation structures. The style of deformation is strongly non-cylindrical,

rendering interpretation of structural data plotted on lower hemisphere equal area stereoplots very imprecise, and it is not presented here. Another complication, as discussed in Section 3.7, involves the uncertainty in the numerical assignment of structural features.

3.8.1 Gueslis Thrust Sheet

As described above, the Gueslis thrust sheet is subdivided by two major structures. In the north, the Lac Audréa syncline is characterized by a large, subhorizontal E-W trending F_1 syncline that is refolded by WNW-ESE -trending, variably plunging F_2 folds, and the complementary structure, the Duck Lake anticline, lies to the south (see Figure 3.7). Small-scale NW-trending, NE-verging, moderately dipping to recumbent F_3 structures were locally recognized near 'A' and the location of Plate 3.14 (see Figure 3.2). F_4 structures are not recognized within the Gueslis thrust sheet.

As shown in Figures 3.4 and 3.6, shallow SE-dipping S_1 bedding-parallel fabrics and lineations in gneisses of the Attikamagen and Menihek formations along the northern limb of the Lac Audréa synform wrap around 'lean iron formation' (quartzite with thin subordinate layers of specular hematite and magnetite) and locally with minor quartz pebble conglomerate (of the Sokoman and Wishart formations respectively), which is folded and exhibits pinch and swell along its length. In the largest swell, which outcrops on top of the treeless hill just south of Lac Audréa, S_0 can be identified locally in quartzite and quartz-rich 'lean'

iron formation, where it is at high angles to the regional ESE-WNW trend of the unit implying it is the locus of an F_1 fold hinge. The lack of an S_1 axial planar fabric is interpreted to be a function of the competence of these units. These features combined with the map pattern suggests that the swell is an F_1 antiform-synform pair that plunges 15-30^0 towards the ESE (see Figure 3.7). From the structural information available, which was obtained without the locational precision of plane tabling, two structural configurations are possible (Figure 3.8), both with the regional younging direction towards the WSW. In (a) the stratigraphy is overturned, giving rise to an antiformal synform and a synformal antiform pair, whereas in (b) the stratigraphy is the right way up and the folds comprise a normal antiform-synform pair. Although the structural information is inadequate to definitively distinguish between the two alternatives, there is no other evidence for widespread overturning of the stratigraphy in the Gueslis thrust sheet, so (b) is considered the more likely interpretation.

The Duck Lake anticline in the southeastern part of the Gueslis thrust sheet (see Figure 3.7) is outlined by the outcrop pattern of marble and discontinuous iron formation (Denault and Sokoman formations) separating schists of the Attikamagen and Menihek formations. Within the Attikamagen Formation, in the hinge of the fold, relict bedding (S_0) is isoclinally folded and overprinted by a NW-trending S_1 axial planar foliation (see Plates 3.9, 3.10 and Figures 3.4, 3.5), indicating that this is a large-scale F_1 structure that plunges

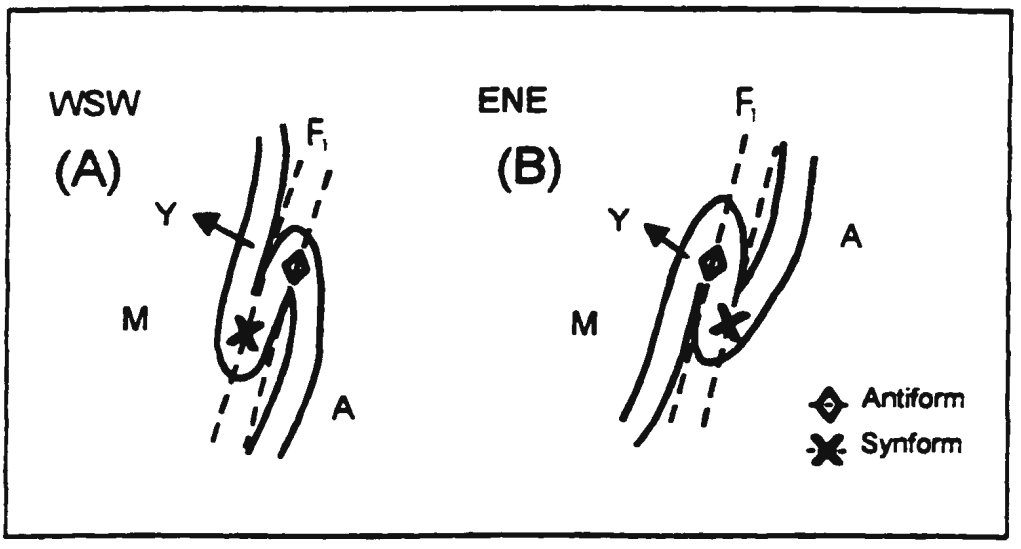

Figure 3.8 Two possible schematic cross-sections through the F_1 fold pair, defined by quartzite and iron formation (Wishart and Sokoman formations), south of Lac Audréa. In A) the stratigraphy is overturned, whereas in B) it is the right way up. B is considered the most likely interpretation. Abbreviations: A - Attikamagen Formation; M - Menihek Formation; Y - younging direction indicated by arrow.

shallowly to moderately towards the WNW (see Figure 3.7). The S_1 fabric, as shown in Plate 3.10, is axial planar to the folds and Plate 3.9 illustrates that there are many ductile shear zones, probably with small individual displacements, subparallel to the S_1 foliation. This suggests that D_1 deformation involved a significant overall component of simple shear. In an adjacent outcrop, bedding -cleavage (S_0-S_1) angular relationships are in accord with the shape and asymmetry of closure of the large-scale F_1 fold (see Figures 3.4 and 3.7). These field observations, on the basis of lithological trends and S_1 axial planar foliation, suggest that the Lac Audréa syncline and Duck Lake anticline are a NW-trending, and WNW -plunging F_1 syncline/anticline pair.

3.8.2 Lac Don Thrust Sheet

The Lac Don structure comprises a large F_2 anticline/syncline pair. Measured structural data, including S_1 fabrics, F_2 fold axes and lineations (see Figures 3.4, 3.5 and 3.6) from the Lac Don thrust sheet, indicate that the map-scale F_2 folds define a NW-trending, SE-plunging, SW-vergent tight to isoclinal fold structure that has been refolded by north-trending map-scale F_4 folds (see Figure 3.7). The resulting large F_2/ F_4 basinal interference structure is sketched in Figure 3.9. Preservation of the Lac Gull formation, the youngest unit in the map area, is due to its location in the core of the basinal structure. The continuity of the Lac Audréa synclinal structure suggests that displacement on the western extension of the Gueslis shear zone is minimal.

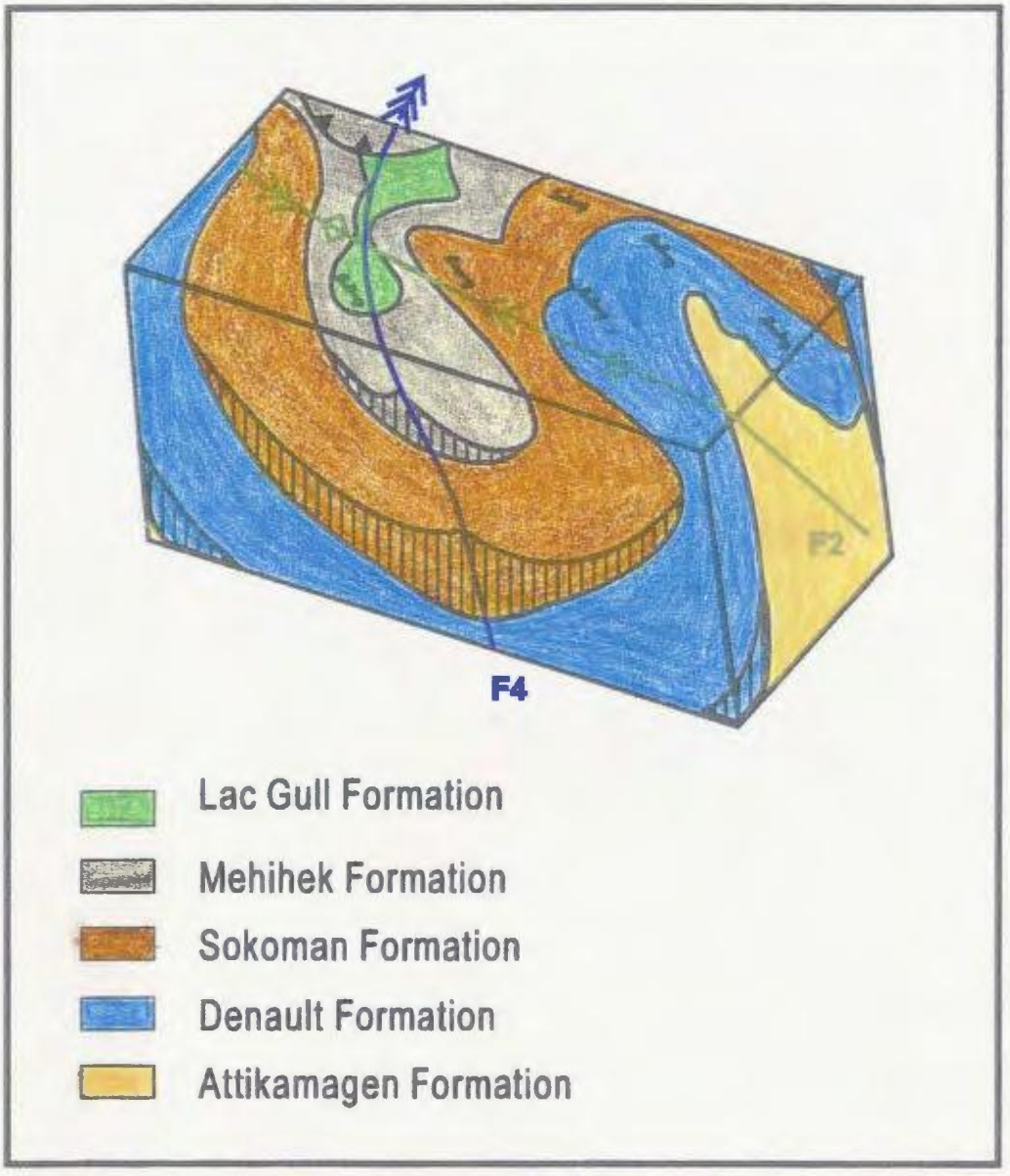

Figure 3.9 Block diagram of the NW-trending, SW-verging D_2 Lac Don anticline -syncline pair that has been refolded by N-trending F_4 folds. The resulting F_2/ F_4 basinal interference structure in the Lac Don thrust sheet may account for the preservation of the pebble conglomerate (Lac Gull formation).

3.8.3 Lac Gull Thrust Sheet

In the Lac Gull thrust sheet, the $S_0//S_1$ planar fabric dips and youngs northward (see Figure 3.4). South of Lac Gull, $S_0//S_1$ in silicate-carbonate iron formation (Sokoman Formation) is deformed into a km-scale north-plunging F_4 syncline (see Figures 3.4 and 3.7). Outcrop -scale F_4 folds are locally expressed as a crenulation or buckling of the $S_0//S_1$ fabric in iron formation (see Plate 2.8) and as re-folding of F_1 folds defined by anatectic veins in the gneisses of the Attikamagen Formation. NNW-trending quartz stretching lineations plunge 15-30^0 (see Figure 3.5).

3.8.4 Lac Lamêlée Thrust Sheet

In the thin Lac Lamêlée thrust sheet, the stratigraphy youngs inwards from both sides of the synform defining a very tight map-scale isoclinal fold that is inferred to be an F_1 structure (see Figure 3.7). This F_1 fold is inferred to have been originally ~E-W trending and overturned towards the south, and on account of the continuity of the structure outside the area of the map (Clarke, 1967) must have a subhorizontal axis. The F_1 structure has been refolded by a map-scale, N-plunging F_4 antiform, as is shown in Figure 3.7.

3.8.5 Lac Hippocampe Thrust Sheet

The structure in this thrust sheet has not been examined in detail, but where examined, the units within it display a single strong tectonic fabric that is parallel to layering. Based on reinterpretation of Clarke (1967, 1977), these

structural trends are folded around the same map-scale, N-plunging F_4 fold that was described in the Lac Lamêlée thrust sheet. The age of the 'segregated ± biotite ± hornblende gneisses' (Clarke, 1967, 1977) in this thrust sheet is uncertain, but they are suspected to represent the reworked Archean basement of the Knob Lake Group, with all Archean structures having been thoroughly overprinted during the Grenvillian Orogeny and are now largely cryptic. Radiometric dating to resolve this problem, although outside the scope of this thesis, is in progress (by T. Rivers).

3.9 RE-INTERPRETATION OF PUBLISHED MAPS ADJACENT TO THE STUDY AREA

In the previous sections, the outcrop- and map-scale structures observed within the field area were described, and in this section those results are used as a guide for the compilation and reinterpretation of the structure of the surrounding areas mapped by Phillips (1958, 1959), Murphy (1959) and Clarke (1967). These map areas were not subject to structural analysis at the time, although they were subsequently incorporated into the regional synthesis of Duffel and Roach (1959) and Roach and Duffell (1974). However the latter authors did not recognize the existence of thrust sheets, so this study represents the first attempt at a modern structural analysis of the area. The compiled areas lie immediately to the west, southwest, east and south of the author's field area respectively (Figure 3.10). They are not accessible by road and the author was not able to visit them, so the

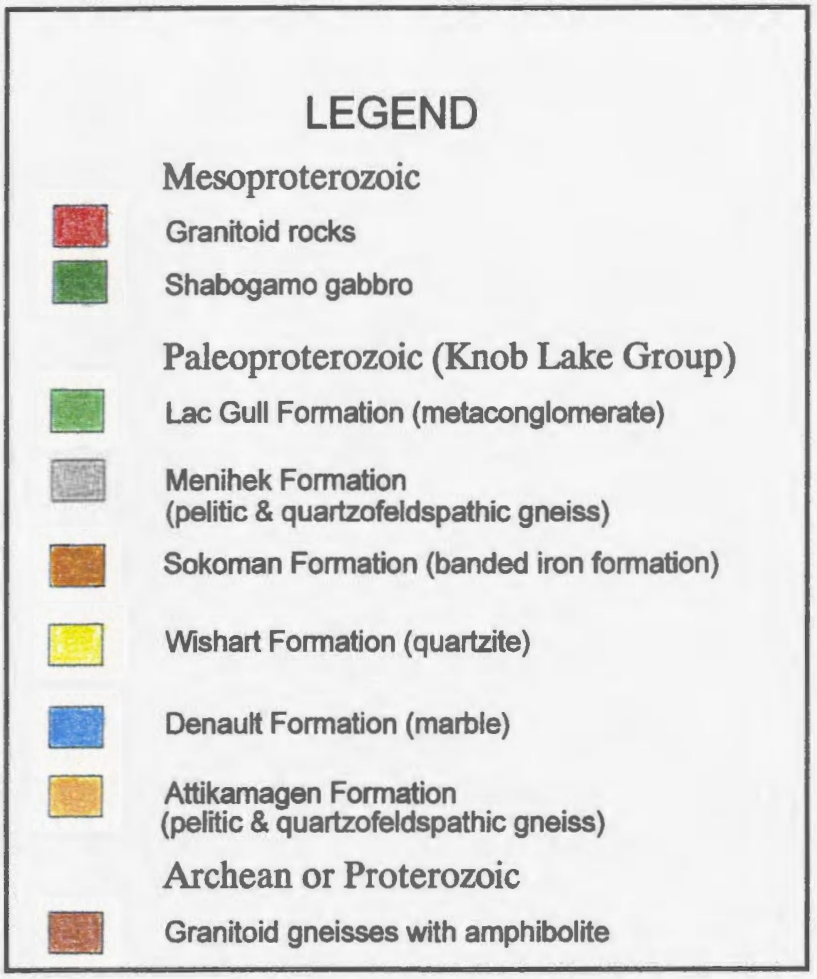

Figure 3.10 Compilation of previous mapping in the surrounding area using the style and nature of deformation observed in the area mapped by the author. In most areas the structural dip of the lithological units is inferred from variation of stratigraphic thickness, as sketched in the cross sections. For simplicity, all geological contacts and thrust boundaries are shown by solid lines. Areas mapped by previous workers are outlined by grey coloured boxes. Structural measurements by the author are shown in red. Abbreviations: G-LDTS - Gueslis-Lac Don thrust sheet, LGTS - Lac Gull thrust sheet, LLTS - Lac Lamêlée thrust sheet, NLHTS - North Lamêlée Hill thrust sheet, LKTS - Lac Kendrick thrust sheet, LHTS - Lac Hippocampe thrust sheet, LASZ - Lac Audréa shear zone, GSZ - Gueslis shear zone, LDSZ - Lac Don shear zone, LGSZ - Lac Gull shear zone, LLSZ - Lac Lamêlée shear zone, NLHSZ - North Lamêlée Hill shear zone, LKSZ - Lac Kendrick shear zone. Coloured legend is applicable for Figures 3.11 to 3.15.

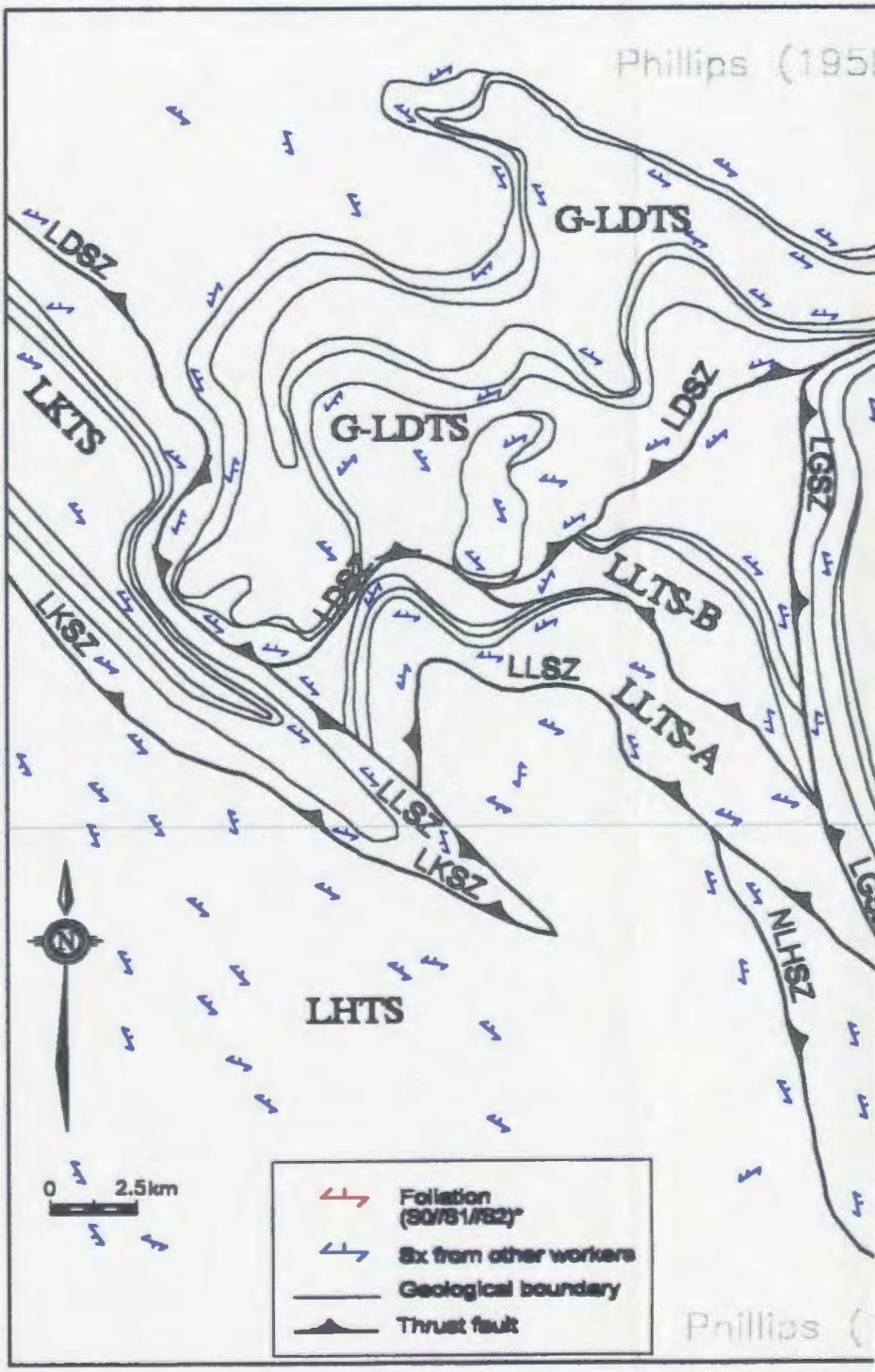
Phillips (195
G-LDTS
LDSZ
LKTS
G-LDTS
LDSZ
LGSZ
LLTS-B
LDSZ
LKSZ
LLSZ
LLTS-A
LLSZ
LKSZ
NLHSZ
LHTS
N
0
2.5km
Foliation (S0/S1/S2)*
Sx from other workers
Geological boundary
Thrust fault
Phillips (

Figure 3.10

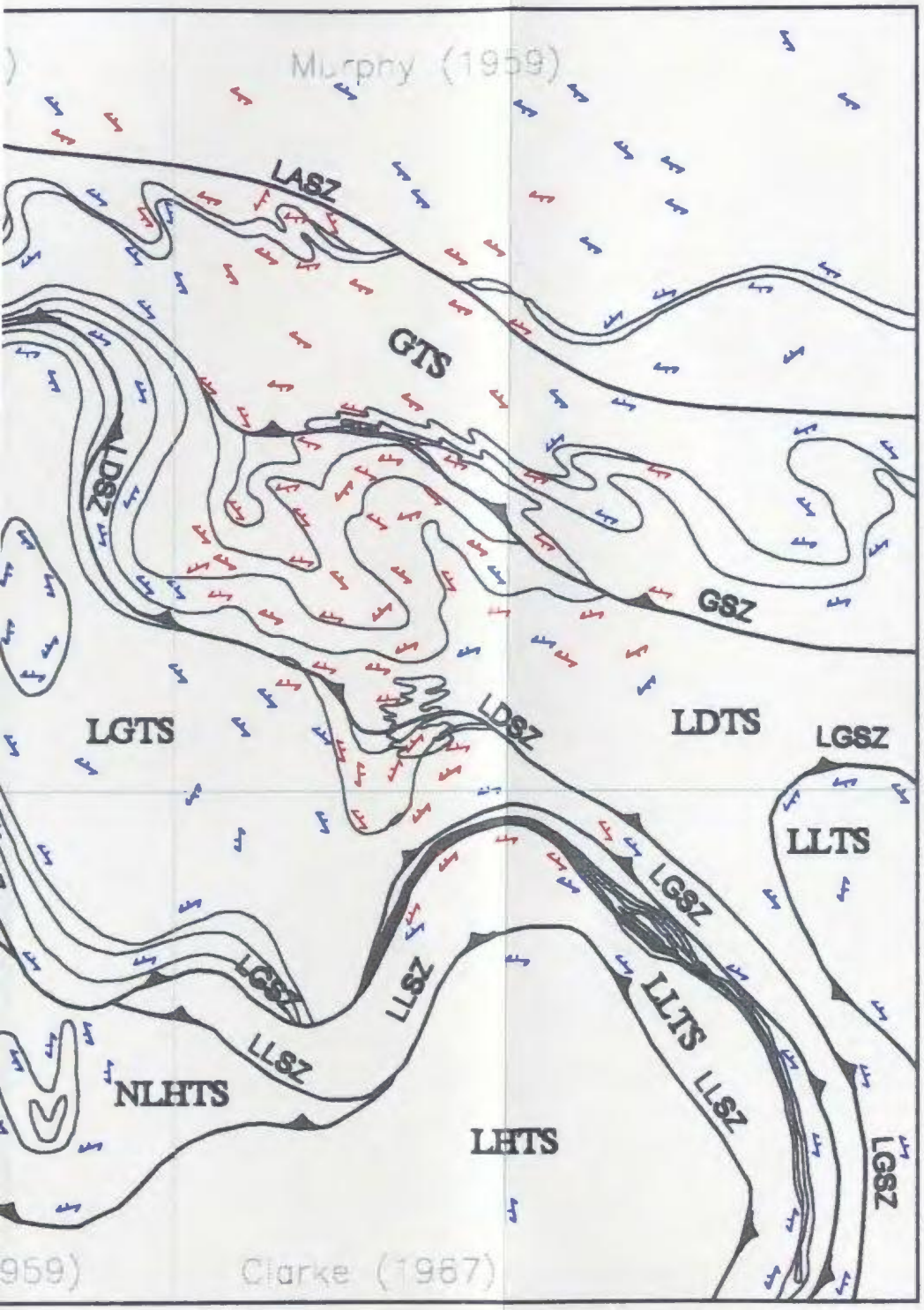
Murphy (1959)
LASZ
GTS
LDSZ
GSZ
LGTS
LDSZ
LDTS
LGSZ
LLTS
LGSZ
LGSZ
LLSZ
LLTS
LLSZ
LLSZ
NLHTS
LHTS
LGSZ
959)
Clarke (1967)

interpretation is therefore strongly reliant on the information on the existing maps (Appendix A_2). The structural data on the maps published by these workers include strikes and dip directions but not dip magnitudes. The lack of dip information means that it is not possible to determine the true dips and thicknesses of the stratigraphic units (Figure 3.11), and in the cross-sections.

Using the methods described in Sections 3.4 and 3.5 *i.e.* the local Knob Lake Group stratigraphy and the stratigraphic younging direction, the area was divided into thrust sheets. The distinctive character of the lithological units and the existence of sufficient outcrop in much of the area permitted the establishment of major structures. Four of the five previously described thrust sheets are interpreted to extend into this area, implying that the thrust sheets have substantial along strike continuity (at least 20 km) and two additional thrust sheets were recognized (described below). In each thrust sheet, the map-scale structural features were inferred from the pattern defined by lithological contacts, and the locations of the proposed thrust faults are based on the distribution of the lithologies, and as such represent the minimum number of these features in the area. It is certainly possible that intra-formational thrust faults have been missed. The stratigraphy within each thrust sheet is shown in Figure 3.11. Major structures within each thrust sheet are discussed in Section 3.9, followed by an examination of the map-scale fold interference patterns in Section 3.10.

In order to interpret the geometry of the major structures, schematic

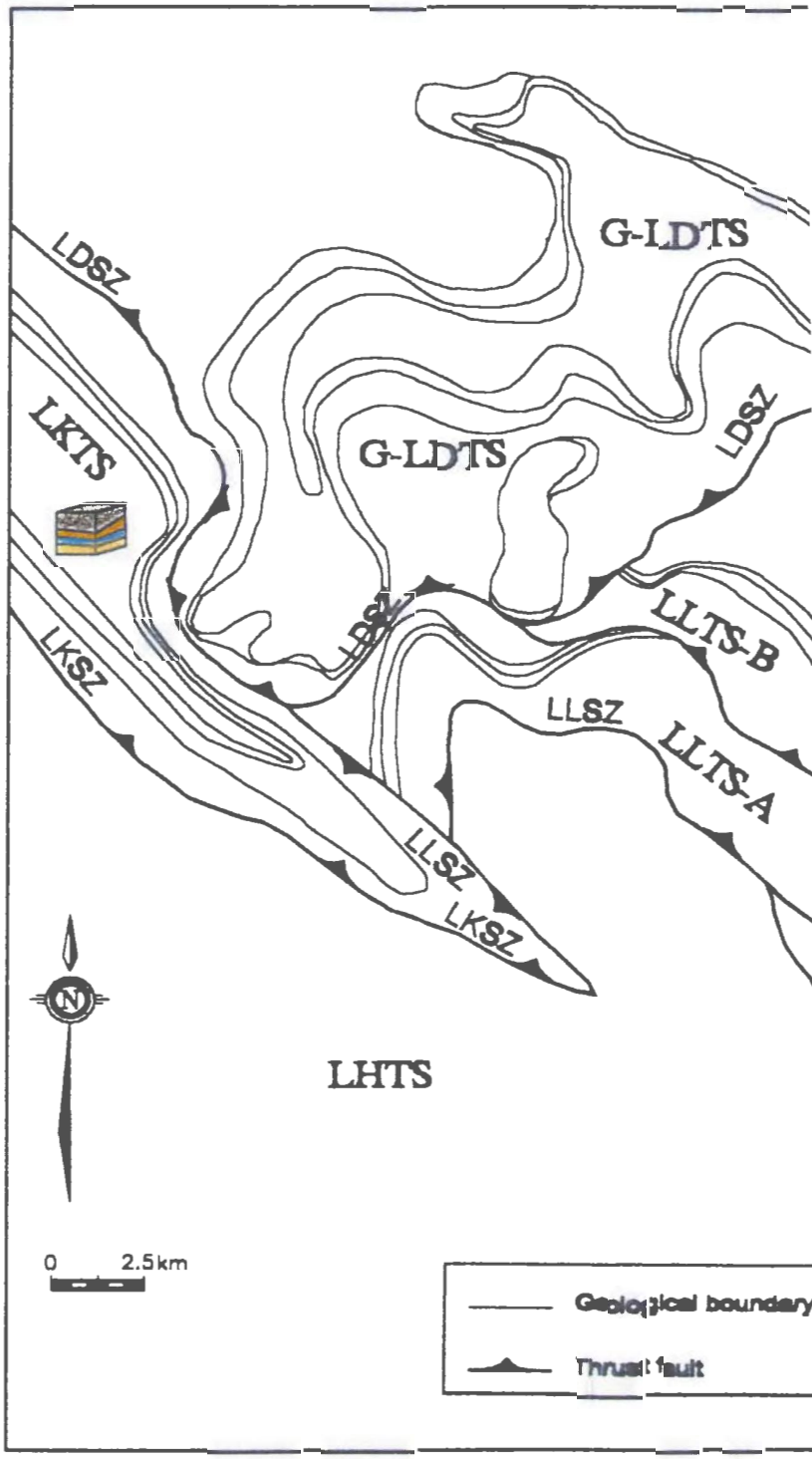

Figure 3.11 Schematic stratigraphic columns illustra
lithological thickness in each thrust sheet based on
the lithological units are measured from cross-sectio
legend.

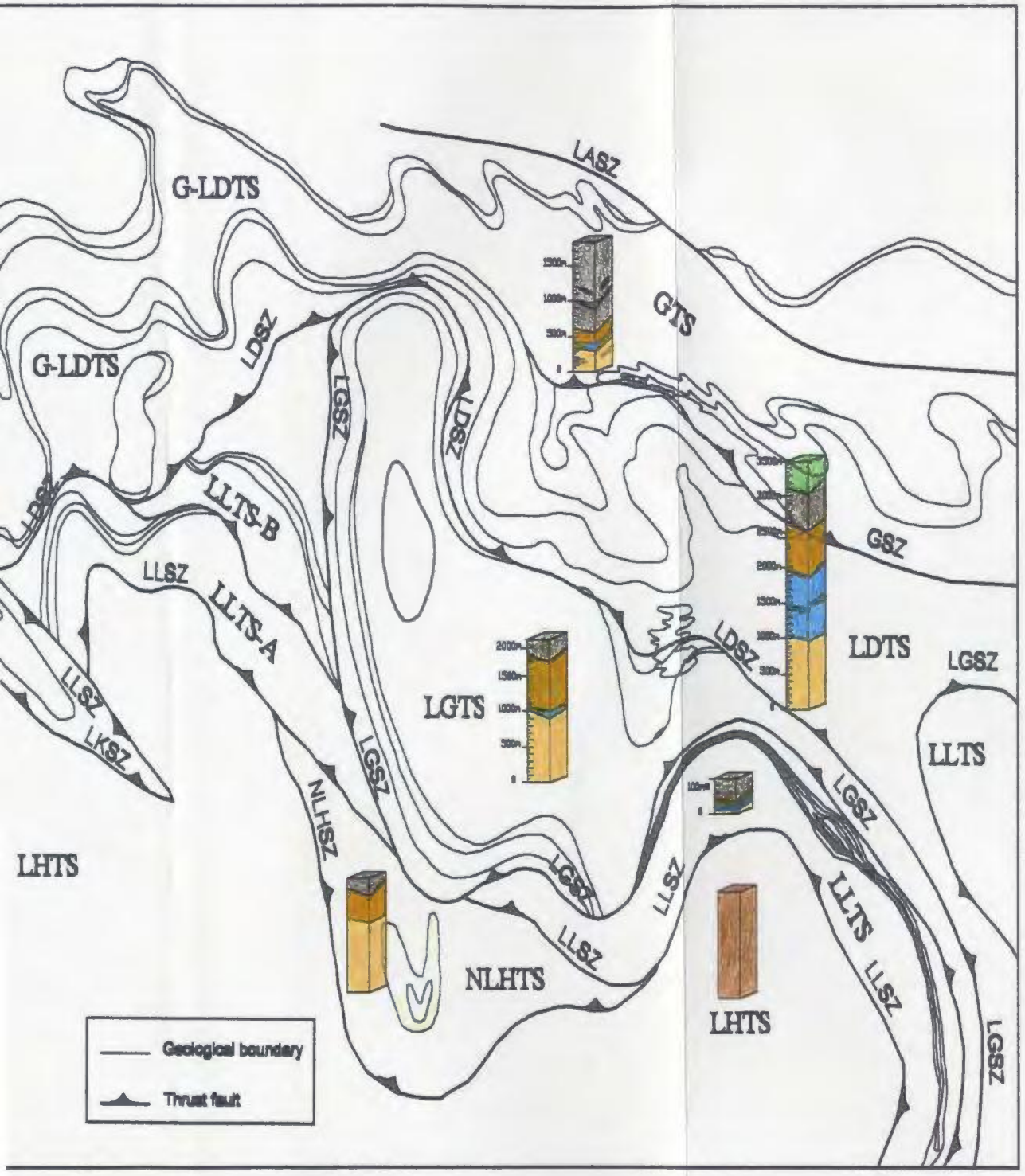

natic stratigraphic columns illustrating the variations in the Knob Lake Group stratigraphy and
ss in each thrust sheet based on the reinterpretation of maps of previous workers. The thicknesses of
s are measured from cross-sections and are approximate. Refer to Figure 3.10 for abbreviations and

cross-sections were drawn across each thrust sheet (locations shown in Figure 3.11). Orientations of the cross-sections were chosen so as to best illustrate the major structures of the thrust sheet and due to the complexity of the deformation pattern, several are not oriented perpendicular to the orogenic front. The cross -sections are schematic and cannot be rigorously balanced due to the ductile nature of the deformation in all units.

3.9.1 Gueslis-Lac Don Thrust Sheet

As shown in Figures 3.10 and 3.11, there is no stratigraphic or structural evidence for the continuation of the Gueslis shear zone much beyond the western extent of the author's field area, so the westerly continuation of the Gueslis thrust sheet, which merges with the Lac Don thrust sheet, is referred to as the Gueslis -Lac Don thrust sheet. In this area, reinterpretation of the lithological younging directions and structural trends from Phillips' (1958) map suggests that the Gueslis-Lac Don thrust sheet extends some 20 km to the west of the author's map area The stratigraphy of the northern part of the thrust sheet appears similar to that described for Gueslis thrust sheet, whereas the stratigraphy of the southern part, with its thicker marble and carbonate iron formation, is more similar to that in Lac Don thrust sheet. As in the Gueslis thrust sheet, the Gueslis-Lac Don thrust sheet is dominated by the F_1 Lac Audréa synform. This large-scale upright F_1 structure has been refolded by smaller-scale upright plunging WNW -ESE trending F_2 folds (Figures 3.12A and 3.12B).

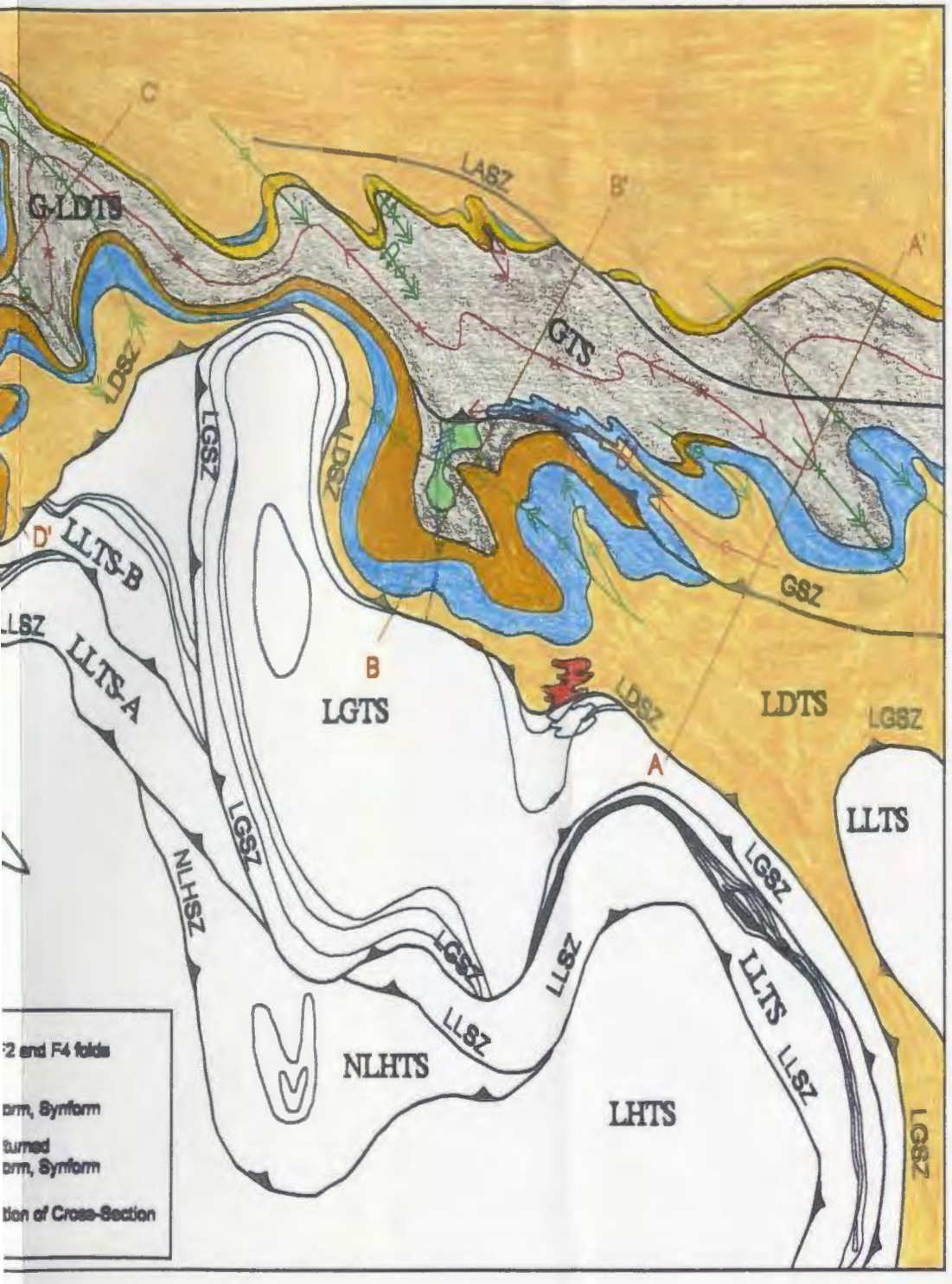

l schematic cross-sections (B) through the Gueslis-Lac Don thrust sheet. Refer to
legend.

A

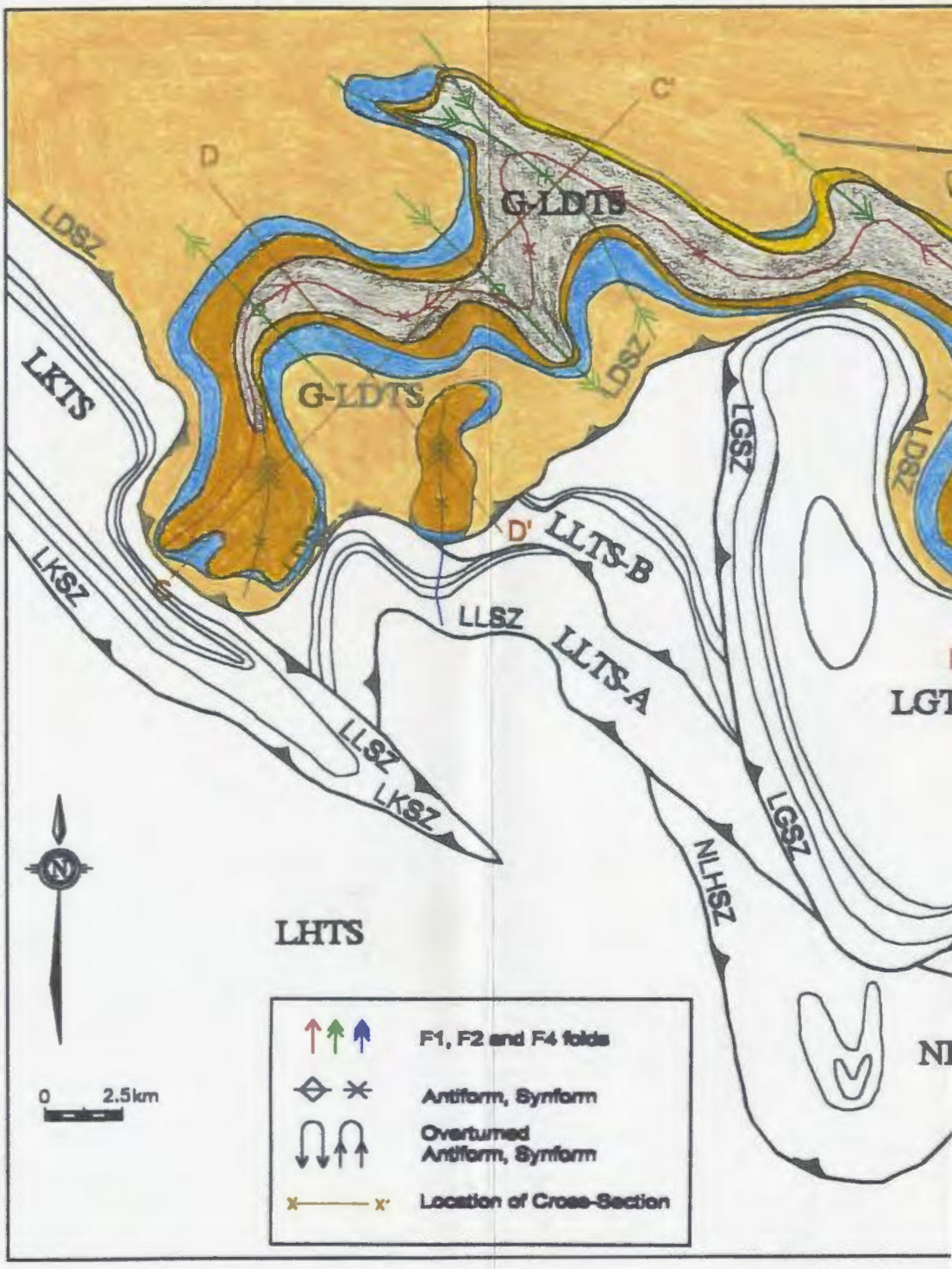

Figure 3.12 Geologic map (A) and schematic cross-sections (B) throug
Figure 3.10 for abbreviations and legend.

B

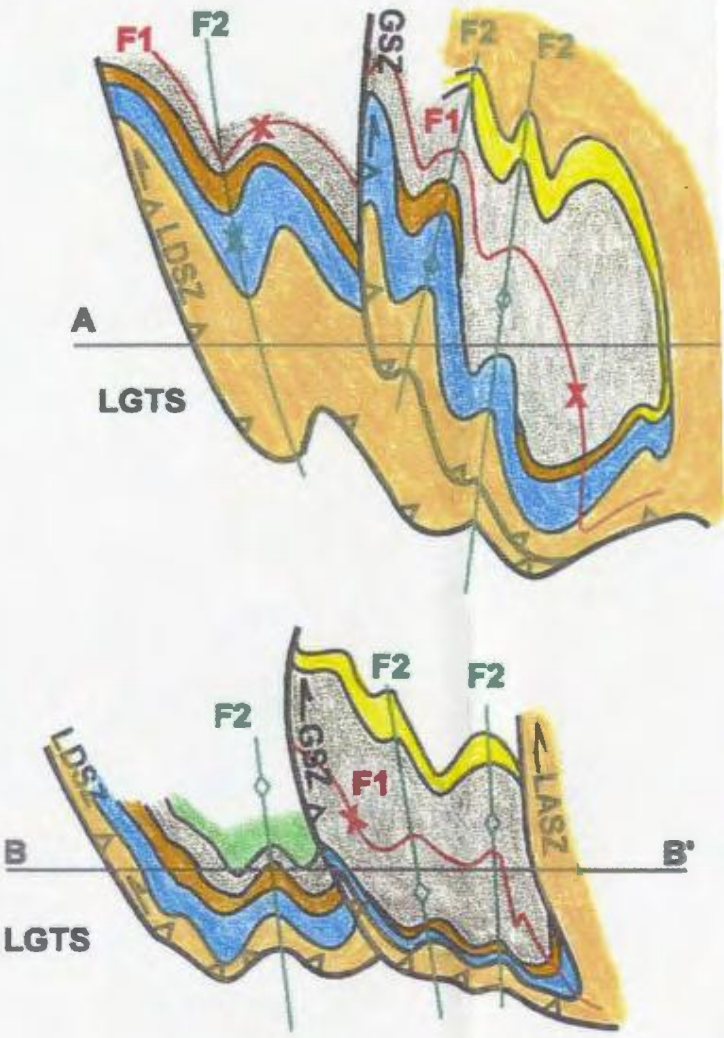

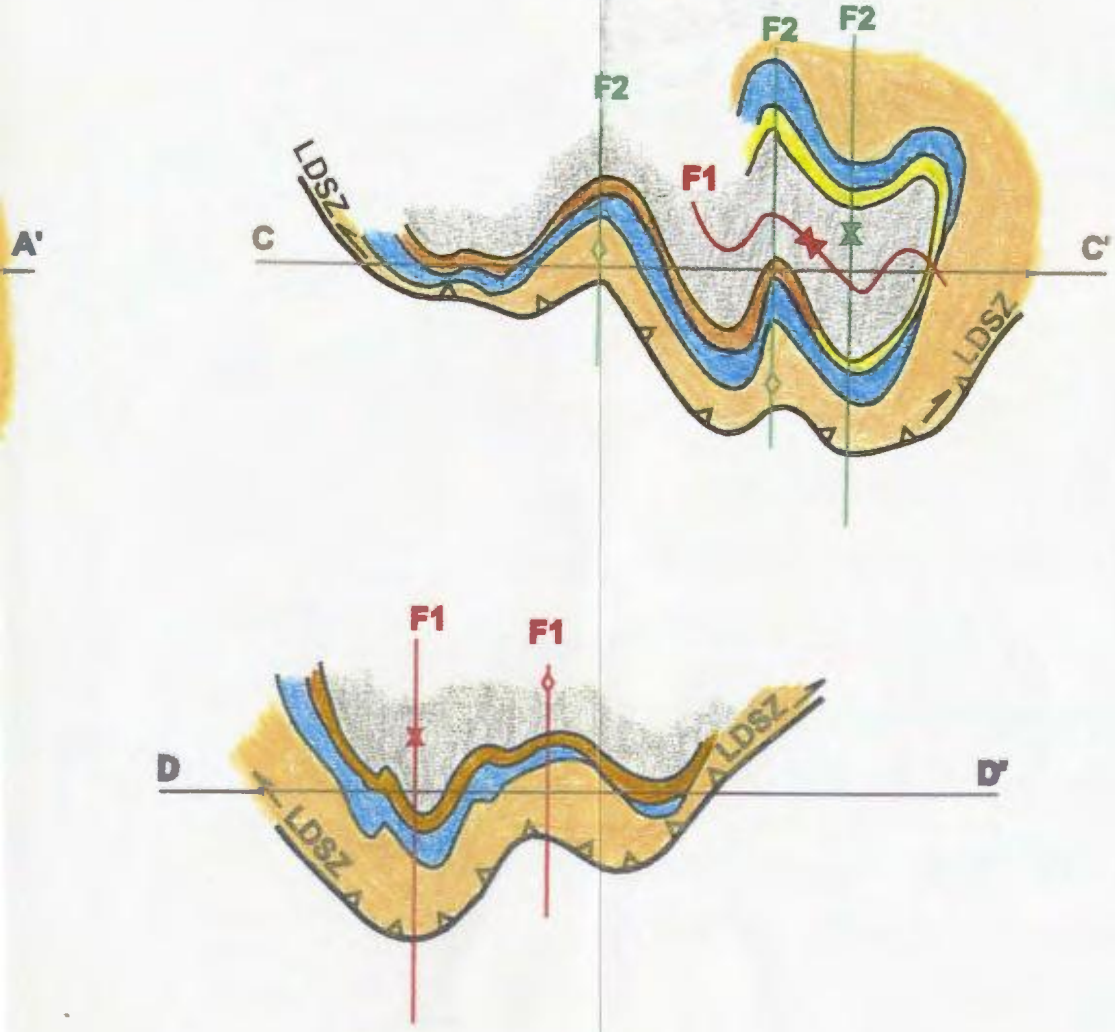
F2
F2
F2
F1
LDSZ
LDSZ
C
C'
A'
F1
F1
LDSZ
LDSZ
D
D'

Four schematic cross-sections across the Gueslis-Lac Don thrust sheet outline the geometry of the major structures (Figure 3.12B). Cross sections A-A', B-B' are oriented NNE-SSW, at high angle to the axial surface of the F_1 Lac Audréa synform and perpendicular to the axial surfaces of the smaller F_2 folds. These cross-sections therefore show approximate profile views of both these structures. Cross-section C-C' is also oriented NNE-SSW, but in this case is approximately parallel to the F_1 axial surfaces and therefore shows only the F_2 structures. Cross-sections A-A', B-B' and C-C' show that the F_1 Lac Audréa synform is a tight to isoclinal synclinal structure and Figure 3.12A shows that it may originally have been curved fold axial surface. F_2 folds are SE-trending, variably plunging structures superimposed on the larger F_1 syncline. Fold interference between F_1 and F_2 structures in the vicinity of cross-sections A-A' and B-B' has resulted in a modified hook pattern (Type 3 fold interference, Ramsay, 1967) that forms when the axial surfaces of the two generations of folds are at high angle to each other, and in this case the two generations of fold axes are subparallel. Fold interference between F_1 and F_2 structures (cross-section C-C'), where the axial surfaces of the two fold generations are approximately perpendicular, has resulted in a modified dome and basin pattern (Type 1 fold interference, Ramsay, 1967).

Cross-section D-D' is oriented subparallel to the axial surfaces of the F_2 folds and perpendicular to the axial trace of the F_1 Lac Audréa syncline and

therefore shows an approximate profile view of the latter. The shallower dips of the units in much of the cross-section (as determined qualitatively by the wider outcrop patterns of the platformal units) suggest that folding in the closure of the Lac Audréa syncline was more open here than elsewhere in the map area. Also shown in cross-section D-D', the shallow north-trending basinal areas of iron formation are inferred to be due the additional effects of F_4 fold interference (see Figures 3.12A & B), but this does not appear to be widespread elsewhere in the Gueslis-Lac Don thrust sheet.

3.9.2 Lac Gull Thrust Sheet

To the west of the area mapped by the author, the distinctive stratigraphic sequence (see Figure 3.11) and structural trends (see Figure 3.10) can be traced on the maps of Phillips (1958, 1959) and defines a large, east-dipping recumbent F_1 antiform that is refolded by a series of N-S trending, variably plunging, upright F_4 folds that die out towards the northern edge of the thrust sheet (Figure 3.13A). The large-scale structure of the F_1/F_4 fold interference in Lac Gull thrust sheet is imaged in a series of E-W cross-sections perpendicular to the predominant strike (Figures 3.13A & B).

These cross-sections show that the east- to south-dipping stratigraphy along the northwestern margin of the thrust sheet youngs towards the northwestern margin of the thrust sheet. In contrast, the stratigraphy along the southwestern margin of the thrust sheet is southwest-younging and northeast

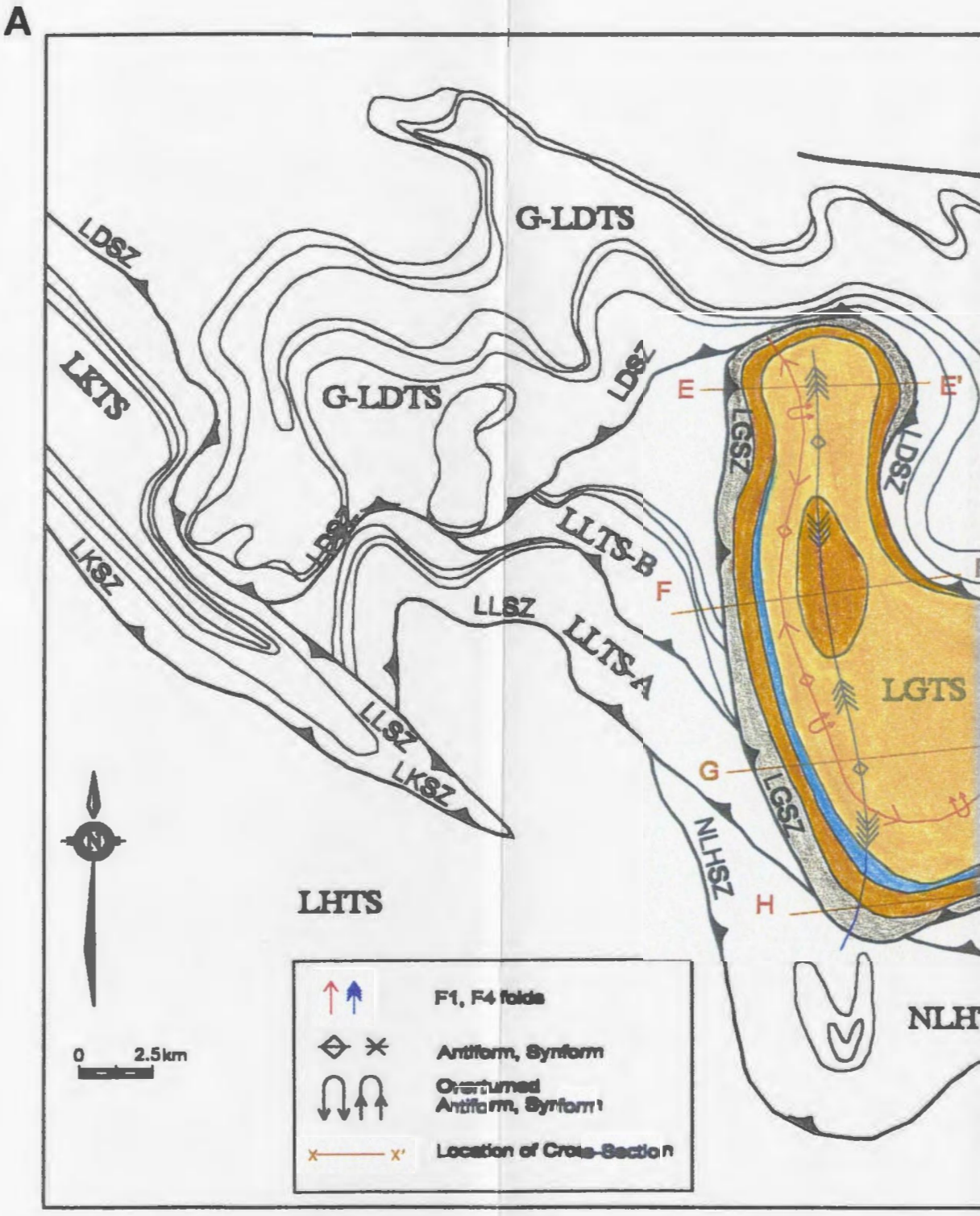

Figure 3.13 Geologic map (A) and schematic cross-sections (B) through th
for abbreviations and legend.

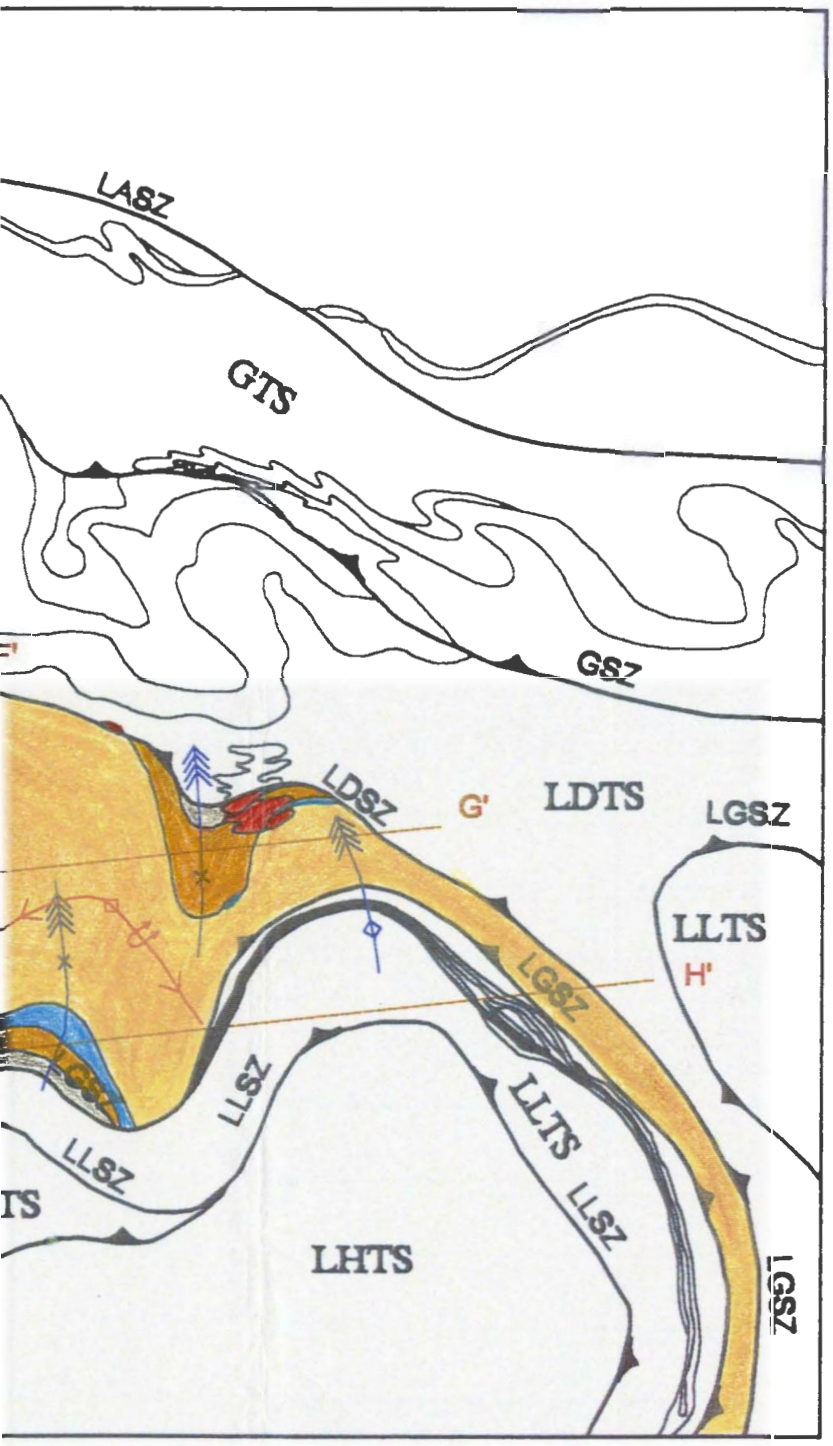

e Lac Gull thrust sheet. Refer to Figure 3.10

B

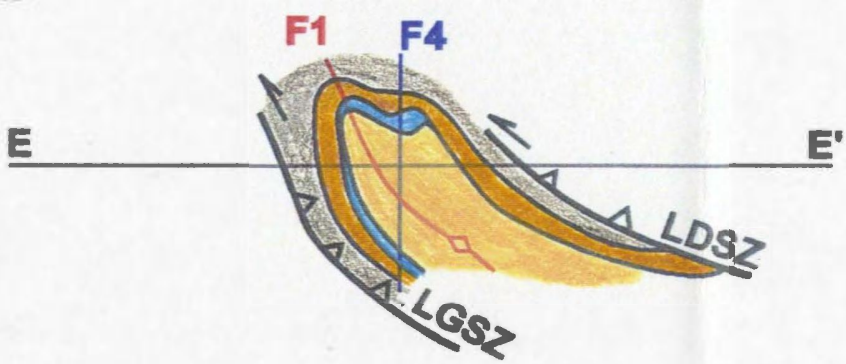

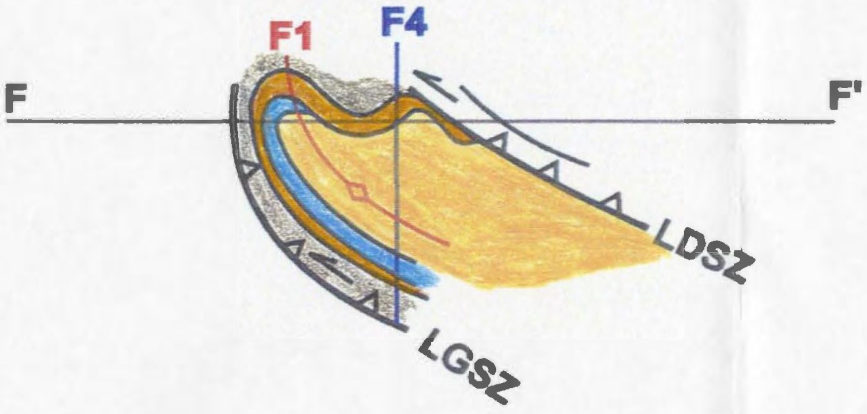

H

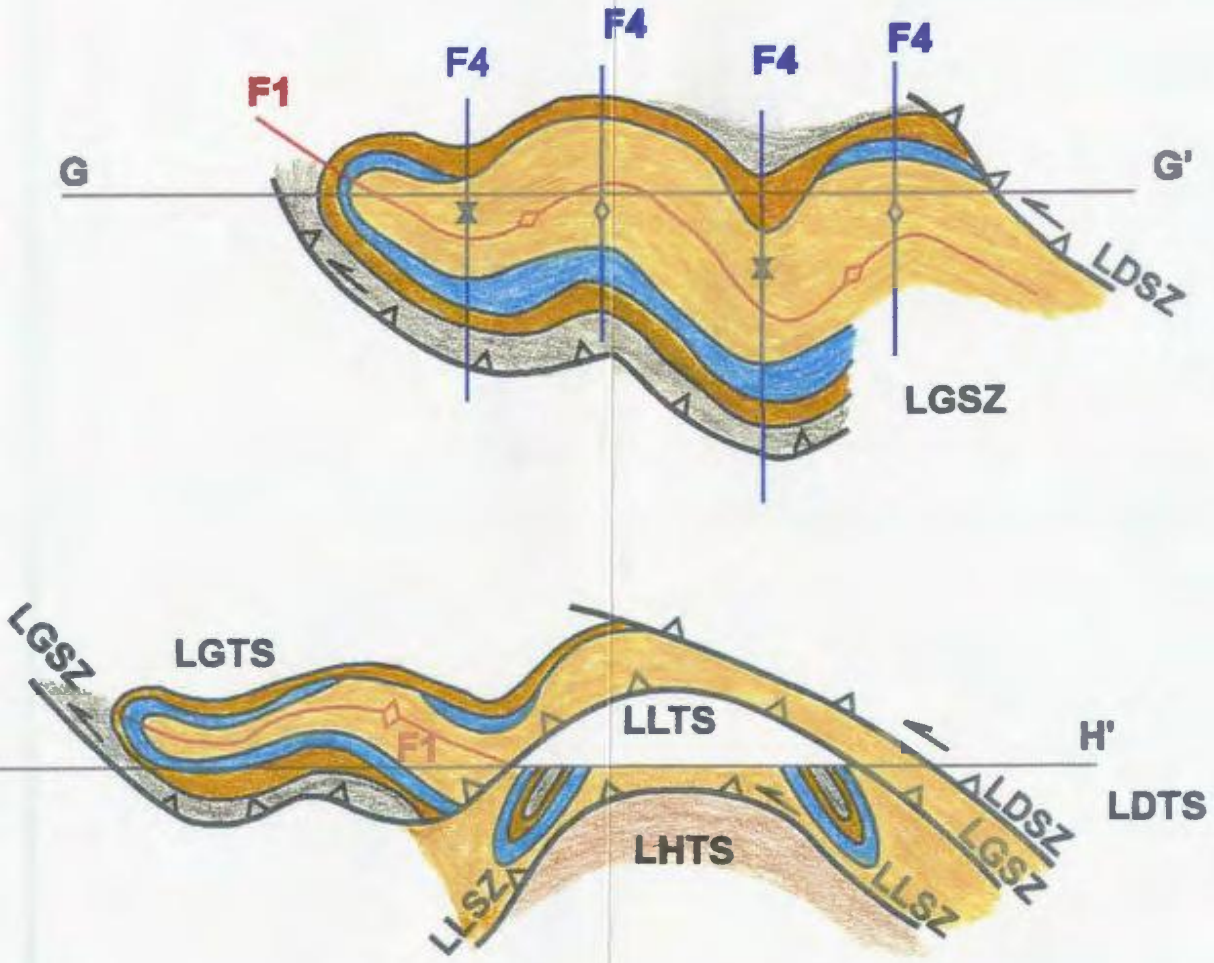
F4
F4
F4
F4
F1
G
G'
LDSZ
LGSZ

LGSZ
LGTS
LLTS
F1
H'
LDSZ
LDTS
LGSZ
LHTS
LLSZ
LLSZ

-dipping. This indicates that the thrust sheet comprises a major recumbent F_1 fold and that parts of both the upper and lower limbs of the fold are exposed. The overall plunge of the F_1 fold is inferred to be subhorizontal because of the lateral continuity of the structure is in excess of 20 km. The trace of the axial surface of the F_1 structure is shown in Figures 3.13A & B. All stratigraphy to the east of the axial trace youngs upward and is the right way up, whereas that to the west of the axial trace it youngs downward and is overturned.

The structural setting of the large basinal-shaped body of silicate -carbonate iron formation (Sokoman Formation) in the centre of the thrust sheet is poorly understood and the area has not been visited by the author. As mapped by Phillips (1958), the iron formation overlies gneisses of the Attikamagen Formation. A possible interpretation of the structure is shown in cross-section F-F' (Figures 3.13A & B) assuming that the contact between the gneisses and the iron formation is stratigraphic, but an alternative (more complex) possibility is that the gneiss/iron formation contact is tectonic and that the iron formation at Disc Hill is a klippe structurally detached from the underlying gneisses. In either case, the shape of the iron formation appears to be the result of structural overprinting by F_4 folds, as is shown schematically in Figures 3.13A & B.

3.9.3 Lac Lamêlée Thrust Sheet

As described above, the Lac Lamêlée thrust sheet in the area mapped by the author is dominated by a large-scale, north-verging, gently plunging F_1

A

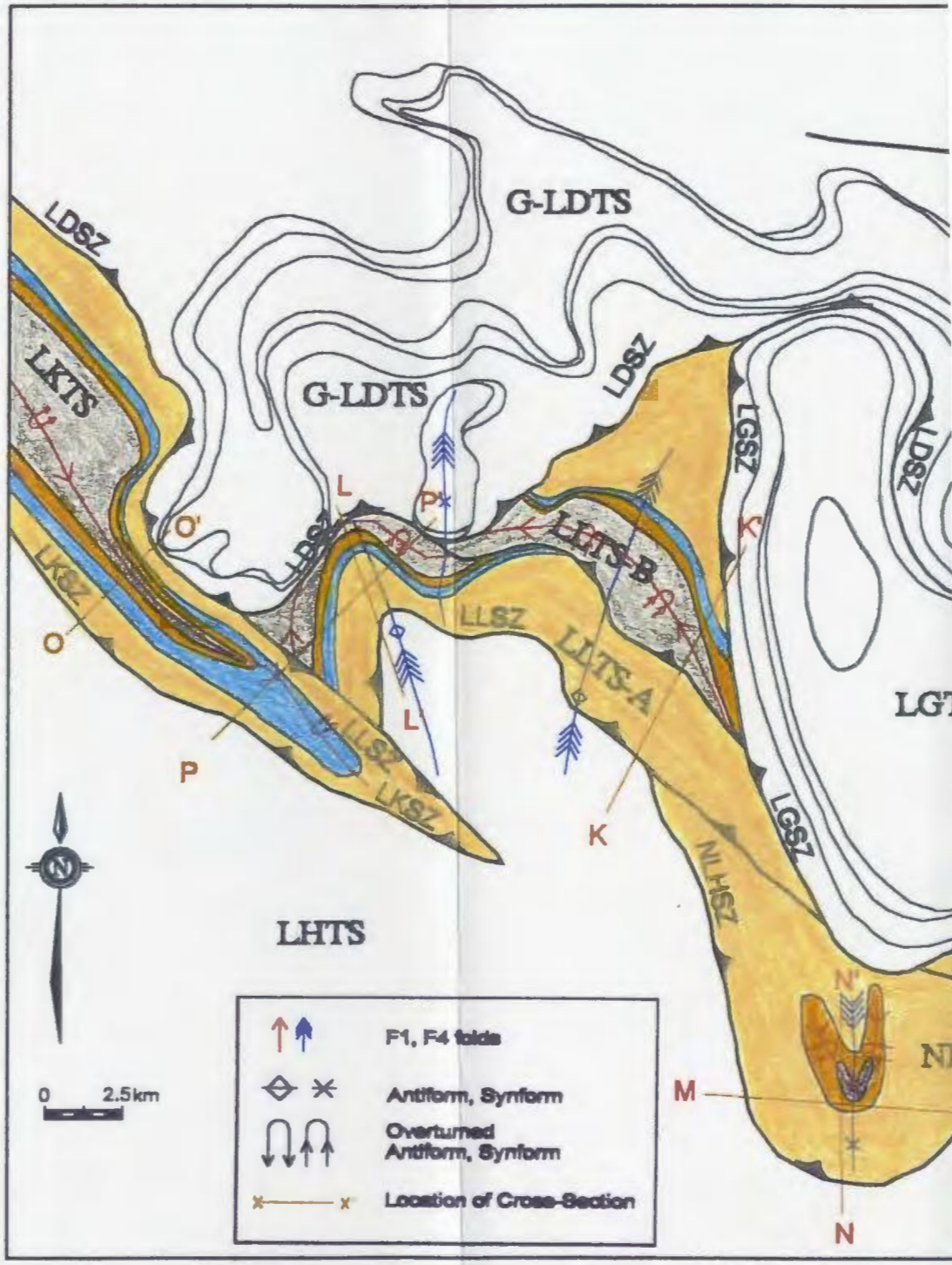

Figure 3.14 Geologic map (A) and schematic cross-sections (B and C) t
North Lamêlée Hill thrust sheets. Refer to Figure 3.10 for abbreviations

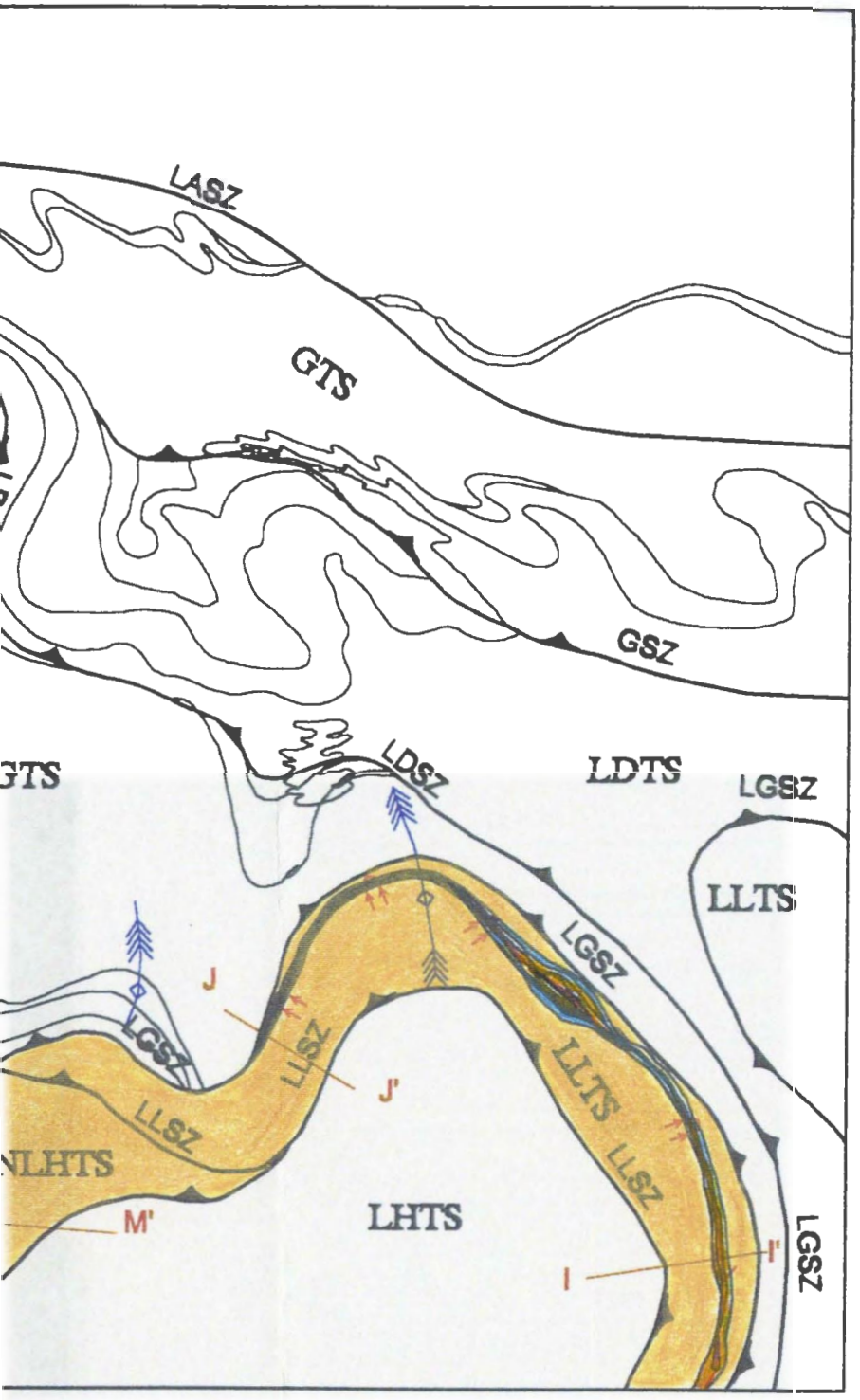

) through the Lac Lamêlée, Lac Kendrick and
s and legend.

B

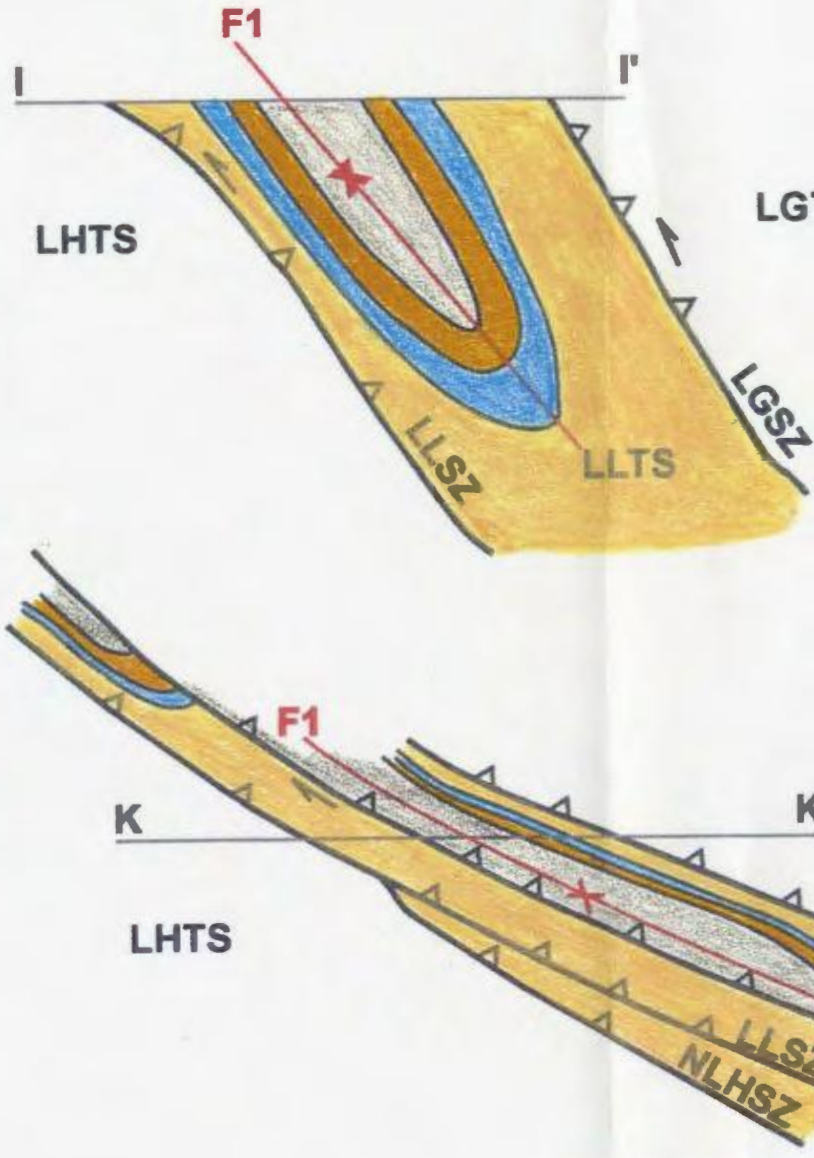

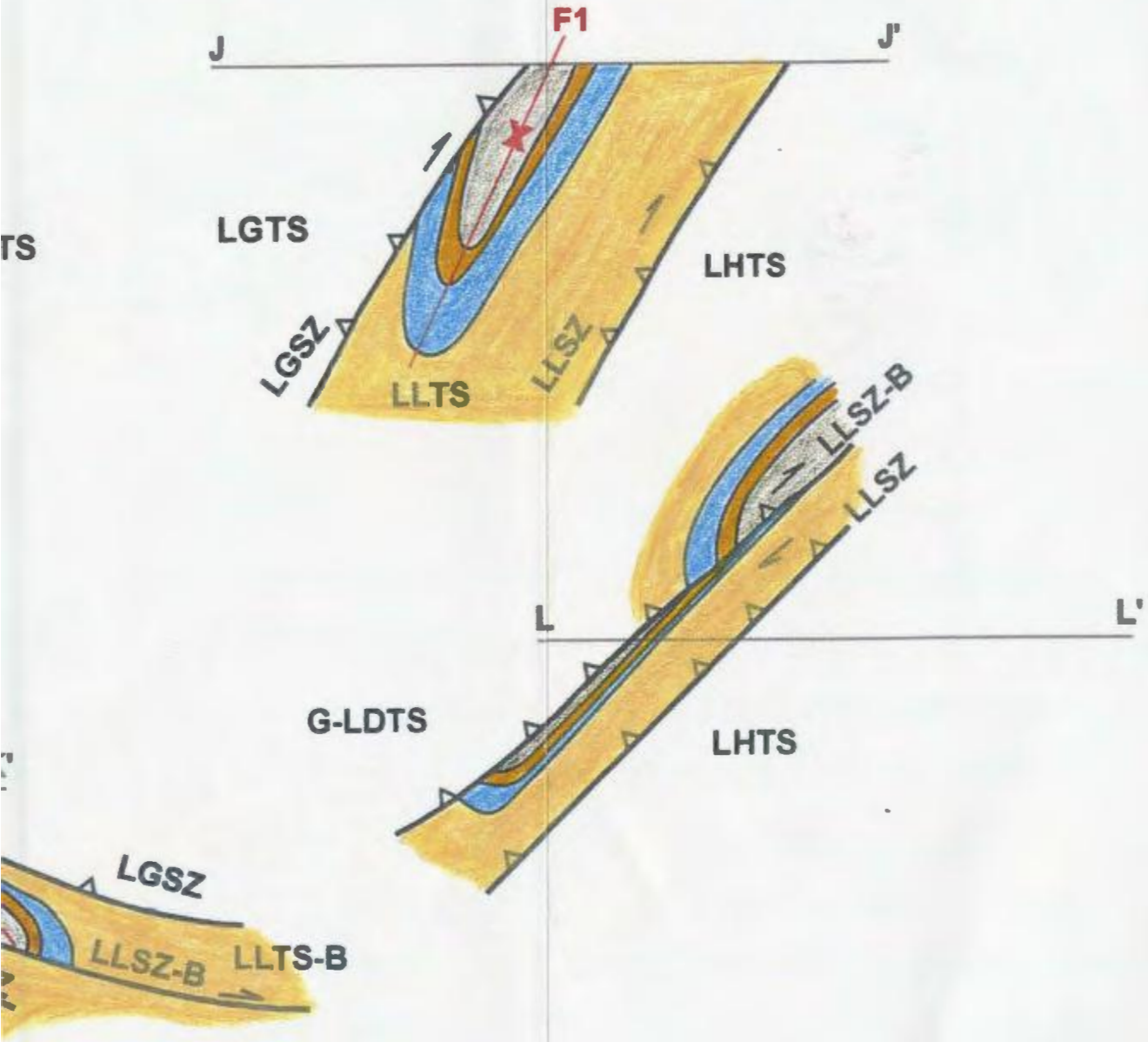
F1
J
J'
LGTS
LHTS
LGSZ
LLSZ
LLTS
LLSZ-B
LLSZ
L
L'
G-LDTS
LHTS
LGSZ
LLSZ-B
LLTS-B

C

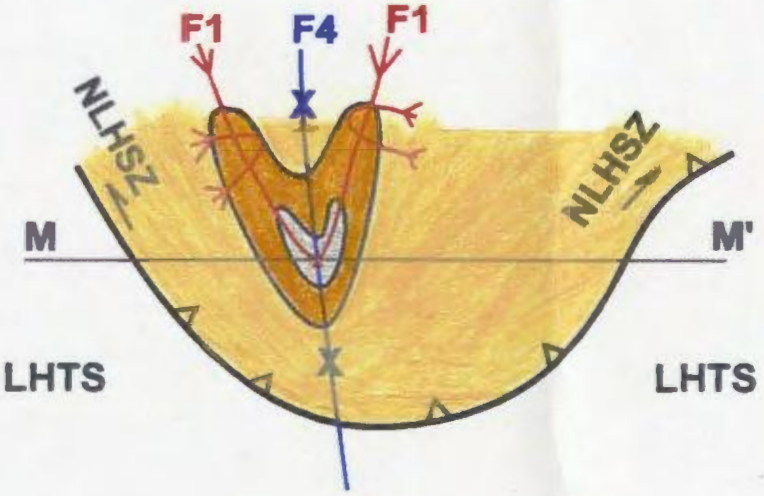
F1
F4
F1
NLHSZ
NLHSZ
M
M'
LHTS
LHTS

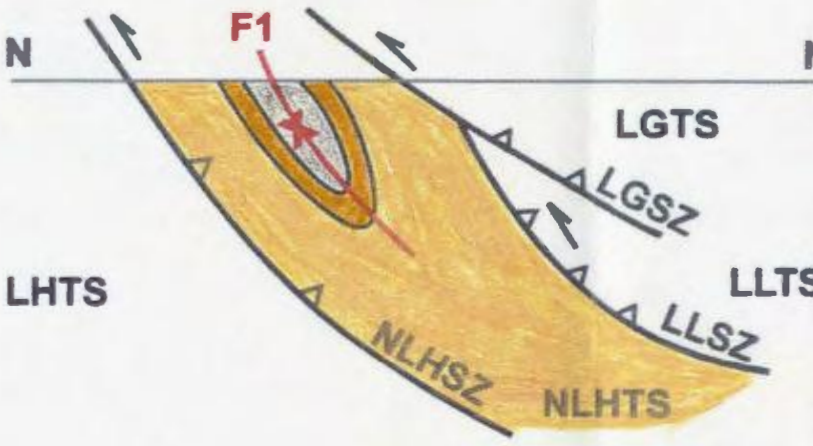
N
F1
LGTS
LGSZ
LHTS
LLTS
LLSZ
NLHSZ
NLHTS

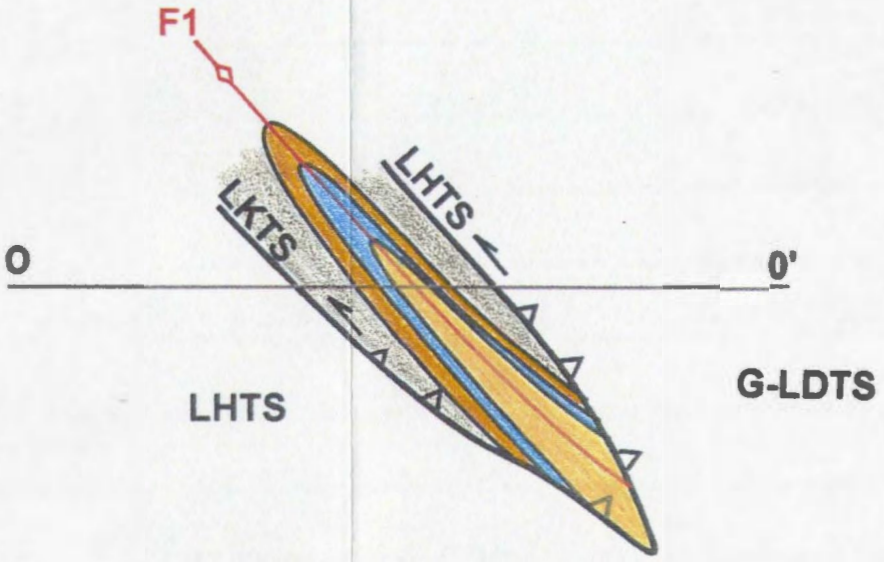
F1
LHTS
LKTS
O
O'
LHTS
G-LDTS

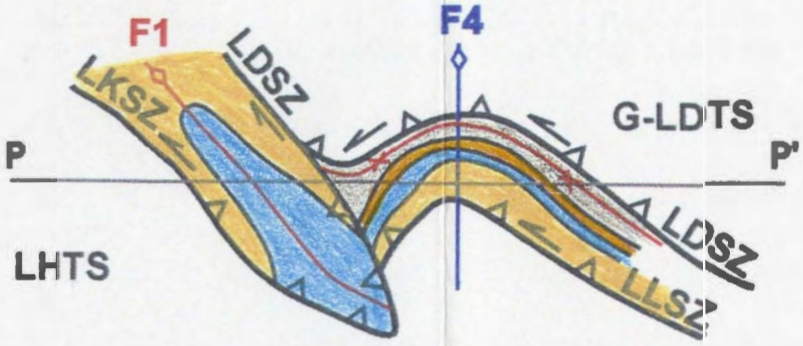
F1
F4
LDSZ
LKSZ
G-LDTS
P
P'
LDSZ
LLSZ
LHTS

syncline that is refolded by map-scale N-trending F_4 folds (Figure 3.14A) (see Figures 3.10 and 3.11). West of the area mapped by the author, the Lac Lamêlée thrust sheet is inferred to extend under the Lac Gull thrust sheet. Where it appears west of Lac Gull thrust sheet, the Lac Lamêlée thrust sheet is dissected into two shallowly north-dipping thrust sheets (LLTS-A and LLTS-B) by an out-of-syncline thrust that is shown in cross-sections K-K' and L-L' (Figure 3.14B). The platformal stratigraphy (see Figure 3.11) of the upper limbs of the fold youngs downward in cross-section K-K' whereas the stratigraphy of the lower limb youngs upward in cross-section L-L' suggesting that they are part of a single disrupted isoclinal fold structure comparable with that seen in cross-sections I-I' and J-J' (Figures 3.14A & B).

Foliation trends shown on Clarke (1967) in the gneissic rocks of the Attikamagen Formation suggest that there are several km-scale N-NNE trending F_4 folds that affected the Lac Lamêlée thrust sheet, the antiforms giving rise to the exposure at the current erosion level where it is surrounded by structurally higher units.

3.9.4 North Lamêlée Hill Thrust Sheet

Structurally underlying the Lac Lamêlée thrust sheet, the North Lamêlée Hill thrust sheet is composed of quartzofeldspathic gneisses (Attikamagen Formation) with a crescent-shaped body of iron formation (Sokoman Formation) surrounding a small core of pelitic gneisses (Menihek Formation) (Figures 3.10

and 3.11). The structural interference pattern was analyzed by Roach and Duffel (1974) and the interpretation here is broadly in agreement with theirs. The main structure is considered to be a result of refolding of an approximately E-W trending, N-dipping and gently plunging isoclinal F_1 fold by a tight, N-trending, N-plunging F_4 synform (Figures 3.14A & C: cross-sections M-M' and N-N'). Thus this structure has a similar structural pattern to the Lac Lamêlée thrust sheet, with the difference that the F_4 folding is tighter, resulting in less lateral continuity of the F_1 structure at the erosion surface.

3.9.5 Lac Kendrick Thrust Sheet

The Lac Kendrick thrust sheet, which is defined entirely on the basis of reinterpretation of the map of Phillips (1958), consists predominantly of silicate-carbonate iron formation (Sokoman Formation), pelitic and semi-pelitic schists and gneisses (Attikamagen and Menihek formations) and marble of the Denault Formation (see Figures 3.10 and 3.11). The map pattern suggests a structurally-isolated NNW-trending, NNE-dipping, SW-vergent anticline completely detached from adjacent synclines. Since the area was not visited by the author, it is not possible to determine whether the major structure is the result of F_1 or F_2 deformation. However, as is shown in cross-sections O-O' and P-P' (Figures 3.14A & C), Lac Kendrick and Lac Lamêlée thrust sheets occupy the same structural level in the thrust stack, and the overall structure is similar to the F_1 syncline in the Lac Lamêlée thrust sheet, suggesting that the Lac Kendrick

structure may also be the result of large-scale F_1 folding. In contrast, the Lac Kendrick thrust sheet does not appear to have been significantly refolded by F_4 structures.

3.9.6 Lac Hippocampe Thrust Sheet

The lack of distinctive Knob Lake group stratigraphy within this thrust sheet precludes a detailed interpretation of its internal structure. The Lac Hippocampe thrust sheet is therefore unique in that it is principally defined by foliation trends (from Clarke, 1967) in the 'segregated' gneisses that are folded into the same N-NNE trending F_4 folds noticed in the Lac Lamêlée thrust sheet (Figure 3.15).

3.10 MAP-SCALE INTERFERENCE PATTERNS

Figure 3.16 and Table 3.1 are a summary of the major phases of deformation (F_1, F_2, F_4) in each of the thrust sheets. Several patterns are immediately evident. (1) F_2 is restricted to the Gueslis-Lac Don thrust sheet in the northern part of the map area. (2) F_4 folds have similar orientations throughout the area, but are more strongly developed and more steeply plunging in the southern thrust sheets. (3) F_1 folds are inferred to have had originally similar orientations in Gueslis-Lac Don, Lac Lamêlée, North Lamêlée Hill and Lac Kendrick thrust sheets (i.e. E-W trending horizontal inclined folds developed about N-dipping axial surfaces). However F_1 folds were recumbent with probably N-S trending axes in Lac Gull thrust sheet. This suggests that the F_1 folds in the

Figure 3.15 Geologic map of the Archean basement domina
S_x foliation folded into N to NNW-trending F_4 folds. Refer to

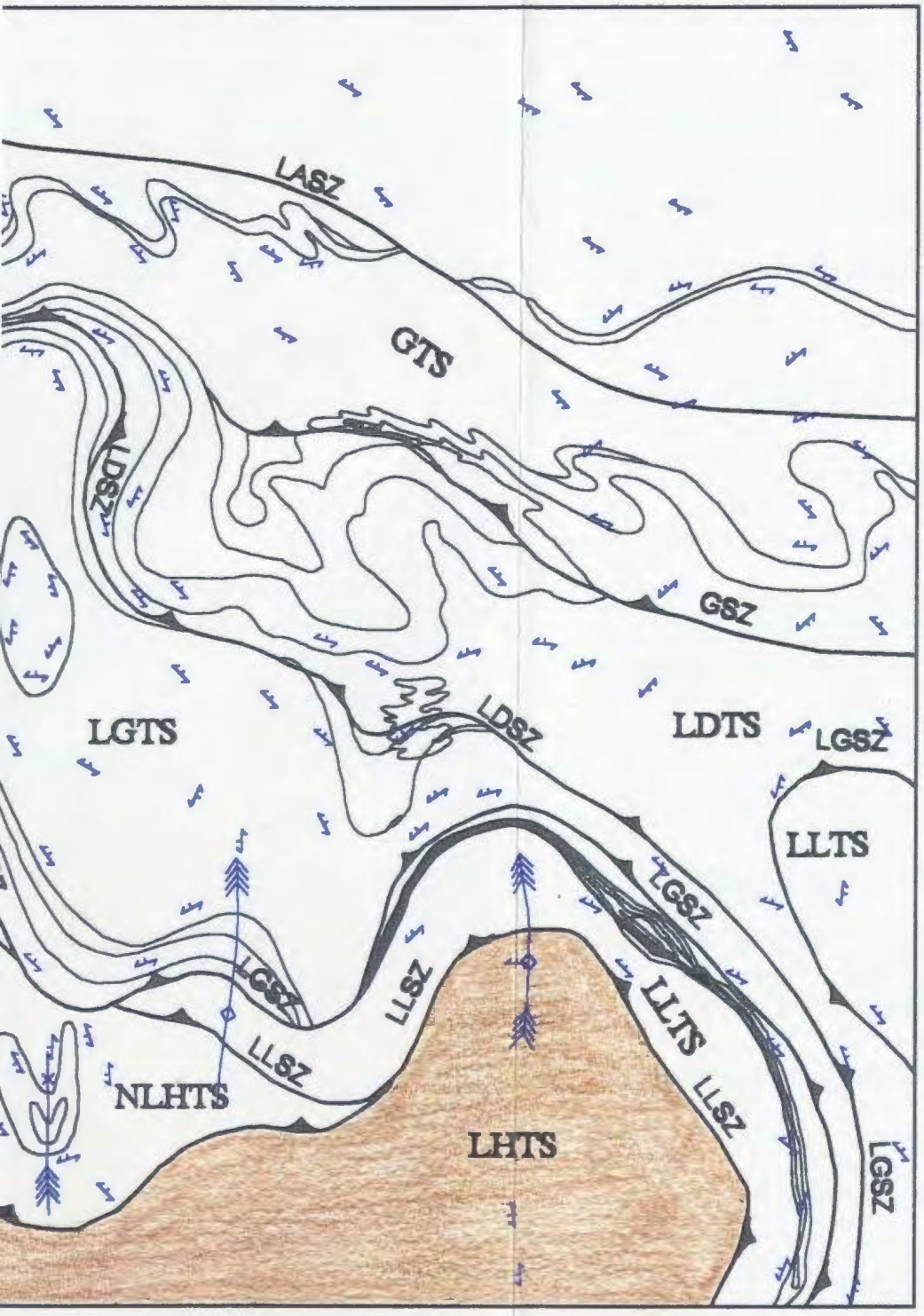

ted Lac Hippocampe thrust sheet. Major structures are an
Figure 3.10 for abbreviations and legend.

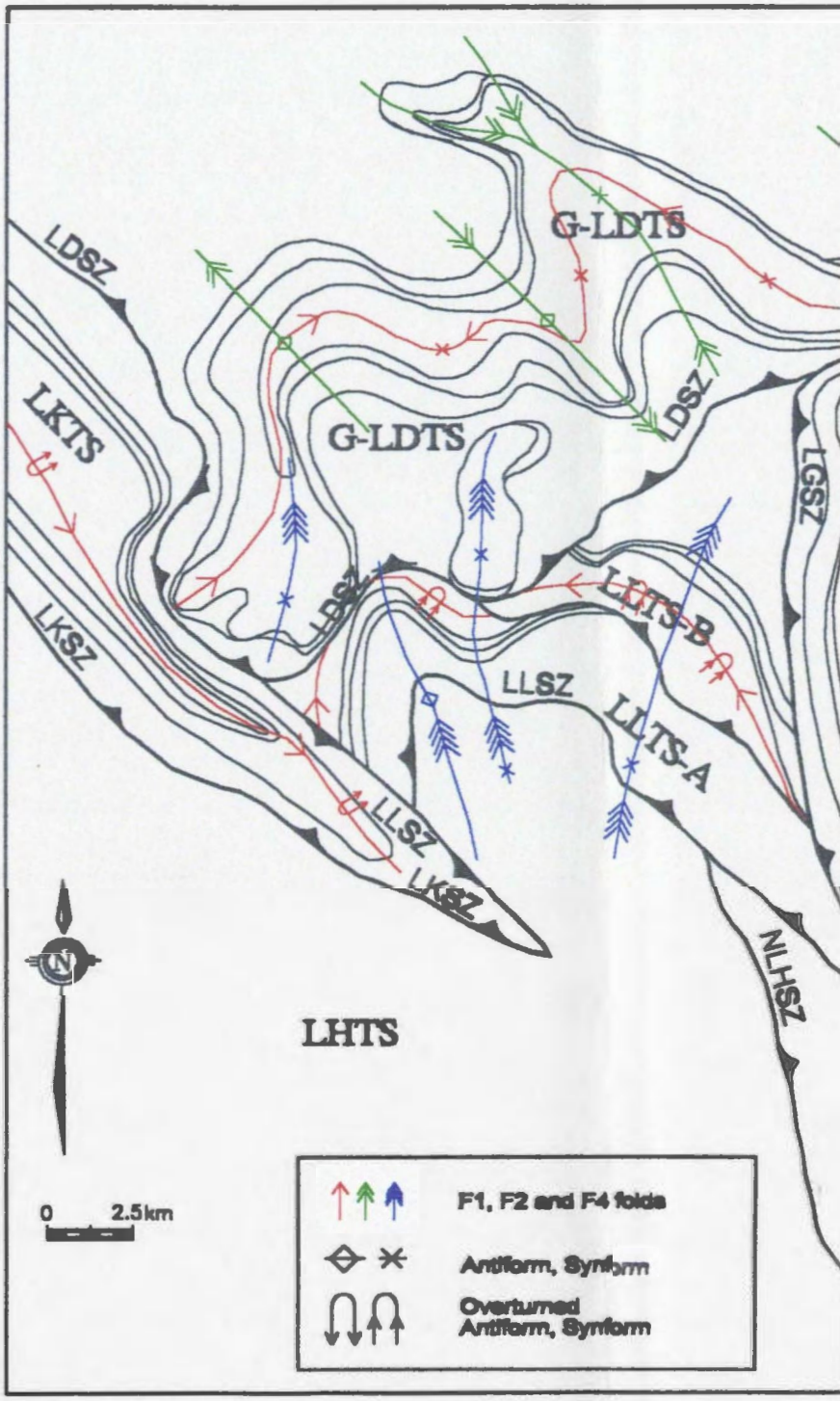

Figure 3.16 Summary of map-scale deformation in the co
map-scale. Refer to Figure 3.10 for abbreviations and leg

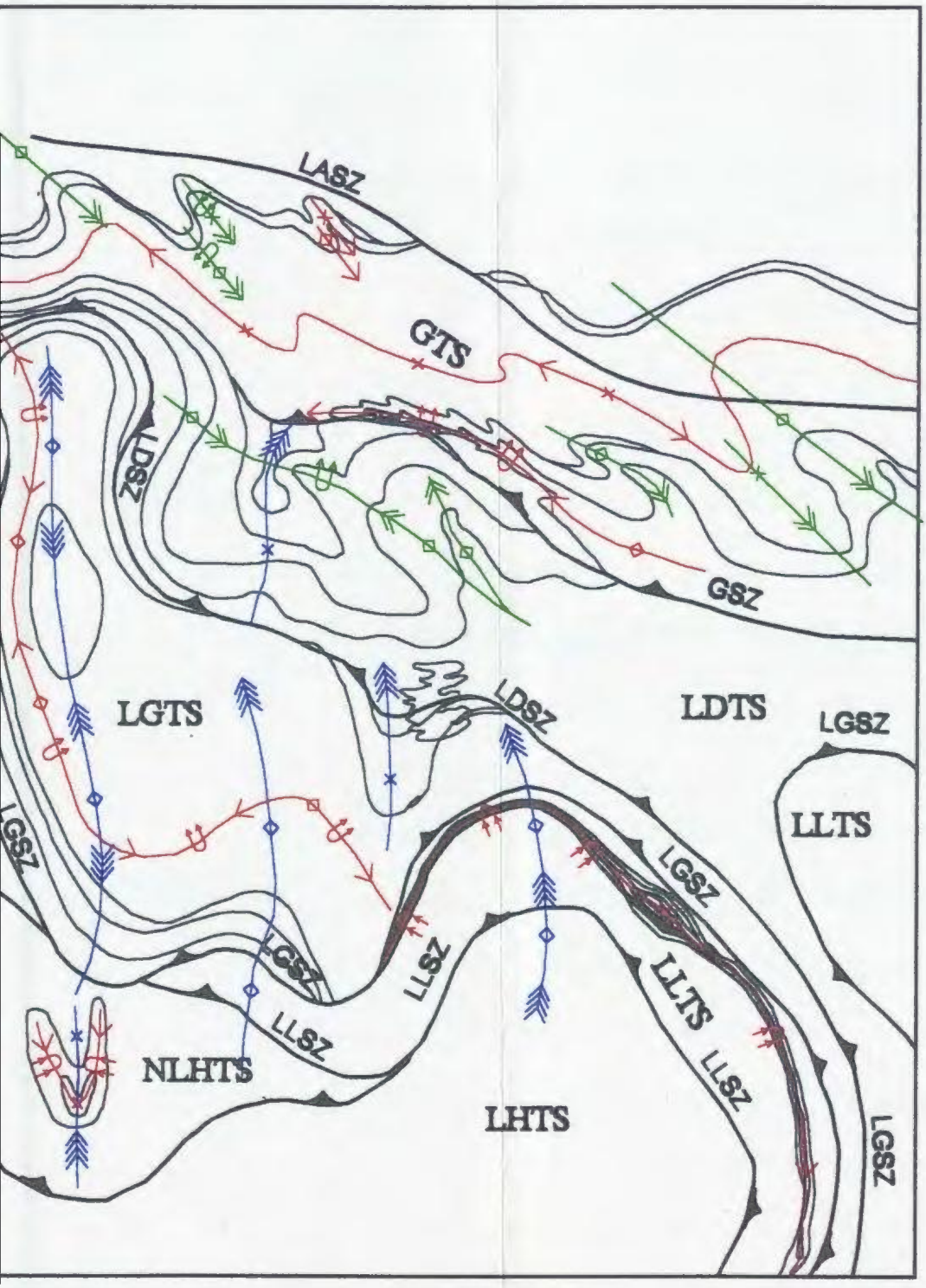

ompiled field area. F_3 folds are not shown as they are not of
gend.

Table 3.1 Distribution and orientation of map-scale structures by thrust sheet. Orientations for folds and axial planar fabrics were visually estimated from Figure 3.16. F_1 and F_2 fold orientations were estimated by unfolding younger superposed deformation. F_3 folds are rare and were found mainly in the G-LDTS. Abbreviations: Fold Desc. - Fold description in terms of the orientation of the fold axis and fold axial surface.

Thrust Sheet	F_1	F_2	F_4
Gueslis-Lac Don	S_1: 020-100°/60°N F_1: 0°->020-100°	S_2: 130°/90° F_2: 50°->130°	S_4: 360°/90° F_4: 20-60°->360°
Fold Desc.	Horizontal inclined	Plunging upright	Plunging upright
Lac Gull	S_1: subhorizontal F1: 0°->360°		S_4: 360°/90° F_4: variable <30°-> 180 to 360°
Fold Desc.	Recumbent		Plunging upright
Lac Lamêlée	S_1: ~090°/50°N F_1: ~0°->090°		S_4: 360°/90° F_4: 40°->360°
Lac Kendrick			
Fold Desc.	Horizontal inclined		Plunging upright
North Lamêlée Hill	S_1: ~090°/50°N F_1: ~0°->090°		S_4: 360°/90° F_4: 50°->360°
Fold Desc.	Horizontal inclined		Plunging upright

Lac Gull thrust sheet formed under a different stress field than the other F_1 structures.

Several types of fold interference patterns were developed in response to the superposition of folds of different generation and orientation (Figure 3.16). In the Gueslis-Lac Don thrust sheet fold interference patterns are principally due to the superposition of F_2 and F_1. The major F_1 structure (Lac Audréa syncline) has a half wavelength of about 5 km, whereas the overprinting F_2 folds have half wavelengths in the order of 2 km. This difference in size affects the nature of the interference pattern, as does the axial curvature of the Lac Audréa syncline. F_2 folds are upright plunging, SE-trending structures with the angle between F_2 and F_1 varying between ~30-90^0. S_1 is steeply N-dipping, whereas S_2 is vertical, and this combined geometry leads to variable fold interference between Type 3 (in the east) and Type 1 (in the west) (Ramsay, 1967).

In the Lac Gull thrust sheet, the major fold interference is between F_1 and F_4, with in this case the two sets of fold axes being subparallel and the axial surfaces at high angles (Figure 3.16). In the end-member case where the two sets of fold axes are precisely parallel and the two sets of axial surfaces are perpendicular, no interference pattern results. However, the presence of a weakly developed dome and basin (Type 1) pattern in the middle of the Lac Gull thrust sheet implies that the two sets of fold axes are not precisely parallel. In addition, the F_4 folds are not penetratively developed throughout this thrust sheet, which

may account for the non-text-book development of the fold interference pattern.

Map-scale fold interference in Lac Lamêlée and North Lamêlée Hill thrust sheets is also between F_1 and F_4 structures (Figure 3.16). F_1 and F_4 fold axes are approximately perpendicular; the strike of S_1 and axial surface of the F_4 folds are at high angles, but S_1 is inclined whereas the axial surfaces of F_4 folds are upright. The type of fold interference is best illustrated by the fold pattern within the North Lamêlée Hill thrust sheet which is a modified 'mushroom' pattern (Type 2, Ramsay 1967). The trace of the Lac Lamêlée synform, which extends outside of the field area, forms another such structure on a much larger scale.

3.11 ARCHITECTURE OF THE THRUST STACK

Having discussed the geometry of the individual thrust sheets, it is appropriate to consider the architecture of the thrust stack as a whole. No evidence for extension has been found in any of the shear zones, so all are inferred to be thrust features (although as noted previously, pervasive annealing has obliterated most kinematic indicators).

All the thrust sheets contain a strong $S_0//S_1$ fabric and shear zones bounding the thrust sheets are both parallel to and truncate this fabric. This suggests that the shear zones have a ramp-flat geometry and that they formed during or after penetrative F_1 isoclinal folding. A syn-D_1 age of thrusting is implied by the out-of-sequence thrust that bisects the Lac Lamêlée thrust sheet in the western part of the map area (into LLTS-A and LLTS-B, see Figures 3.14A & B).

On the other hand, a syn- to post-D_2 age is inferred for thrust motion on the Gueslis shear zone, which truncates the limbs of the major F_2 fold in Lac Don thrust sheet. Several of the thrust faults are folded by map-scale F_4 folds, implying that F_4 post-dated thrusting. Timing relationships between F_3 folding and thrust movement have not been determined. Stacking relationships across thrust sheet boundaries are summarized in Table 3.2.

The majority of the thrusts dip to the north and are south-vergent. The northerly dip and southerly vergence of this part of Gagnon terrane are diametrically opposed to the south (-southeasterly) dips and north (-northwesterly) vergence of the Grenville front fold-thrust belt at the northern margin of Gagnon terrane, both near Wabush (Rivers, 1983a; van Gool, 1992) and farther east (Brown et al., 1992). North (-northwesterly) tectonic transport is also well known from elsewhere along the Grenville Front (e.g. Rivers et al., 1993), so that south-verging structures are the exception, and are inferred to be a result of back-thrusting in the author's field area.

On the basis of the stacking sequences outlined in Table 3.2, it is inferred that the oldest thrusts are those in the south and that thrusting becomes progressively younger towards the north. The most southerly thrust sheet in the area is the Lac Hippocampe thrust sheet, which as noted earlier, is tentatively interpreted to be composed of variably reworked Archean basement rocks ('segregated gneisses' of Clarke, 1967, 1977). The oldest thrust in the study area

Table 3.2 Summary of shear zone relationships. Abbreviations: GTS - Gueslis thrust sheet, LDTS - Lac Don thrust sheet, LGTS - Lac Gull thrust sheet, LLTS - Lac Lamêlée thrust sheet, NLHTS - North Lamêlée thrust sheet, LHTS - Lac Hippocampe thrust sheet.

Shear Zone	Attitude	Stacking	Comments
Lac Audréa	Vertical	-	Late feature ?. Minor displacement.
Gueslis	Steeply N-dipping	GTS/LDTS	Scissor displacement. Movement dies out to west. GTS emplacement was syn-post F_2.
Lac Don	Steeply N-dipping	LDTS/LGTS; G-LDTS/LLTS; G-LDTS/LKTS	LDTS emplacement was post F_1 - pre F_4.
Lac Gull	Subhorizontal to gently E-dipping	LGTS/LLTS; LGTS/NLHTS	LGTS completely overlaps LLTS and lies directly on NLHTS locally. LGTS emplacement is pre-F_4.
Lac Lamêlée	Moderately N-dipping	LLTS/LHTS; LLTS/NLHTS	LLTS emplacement is pre-F_4.
Lac Kendrick	Moderately NE-dipping	LKTS/LHTS	

thus brought a slice of reworked basement rocks into the thrust stack and subsequent deformation involved backthrusting, principally in the Knob Lake Group cover sequence, as these units were transported towards the south over the Lac Hippocampe thrust sheet. Chapter 6 consists of a permissive tectonic model to explain the structural pattern.

3.12 STRUCTURAL SUMMARY

(1) The area has been subdivided into seven thrust sheets, each with a distinctive stratigraphy.

(2) Evidence of four phases of deformation has been described, of which three (F_1, F_2 and F_4) produced map-scale structures.

(3) D_1 structures include isoclinal folds and penetrative S_1 foliation. F_1 folds had approximately E-W trending axes and were horizontal inclined structures in most thrust sheets, except in Lac Gull thrust sheet in which they were recumbent.

(4) F_2 folds are upright variably SE-plunging structures that are restricted to the north of the map area.

(5) F_3 folds are sporadically developed small-scale structures on the steep limbs of F_1 and F_2 folds in the northern thrust sheets. These folds are believed to be the result of vertical shortening of the steep limbs of F_1 and F_2 folds.

(6) F_4 folds are large-scale upright variably plunging, north-trending folds that are best developed in the south of the map area.

(7) A wide range of structural interference features is developed in the

study area due to superposition of folds of different generation.

(8) Kinematic indicators are scarse due to extensive syn- and post-kinematic recrystallization.

(9) The thrust stack on a whole dips towards the north and verges towards the south, and is inferred to have developed by back-thrusting.

(10) The basal thrust sheet, the Lac Hippocampe thrust sheet, is inferred to be a basement wedge, over which all other thrust sheets were backthrust towards the south.

CHAPTER 4: METAMORPHISM

4.1 INTRODUCTION

This chapter comprises a thin section-based study of mineral assemblages, microstructures (i.e. the relationship between mineral growth and deformation) garnet zoning profiles and geothermobarometry that together serve to outline the metamorphic characteristics of the thrust sheets. The emphasis is on metapelitic rocks since these rocks contain mineral assemblages that are the most diagnostic of the P-T conditions. However, the metamorphic mineral assemblages of the calc-silicate, marble, iron formation and igneous rocks, although less diagnostic, are also presented. Where there are contrasts between metamorphic characteristics in different thrust sheets, these are noted in the text. All mineral abbreviations used in the text are those of Kretz (1983), and abbreviations for thrust sheets are the same as those in Chapter 3. Locations of samples described in the text are shown in Figure 4.1.

4.2 PETROGRAPHIC MINERAL DESCRIPTIONS

Maximum phase mineralogical assemblages of each lithologic unit in the field area are described below and mineral assemblages observed in each thin section are presented in Tables 4.1 and 4.2 according to lithology and thrust sheet.

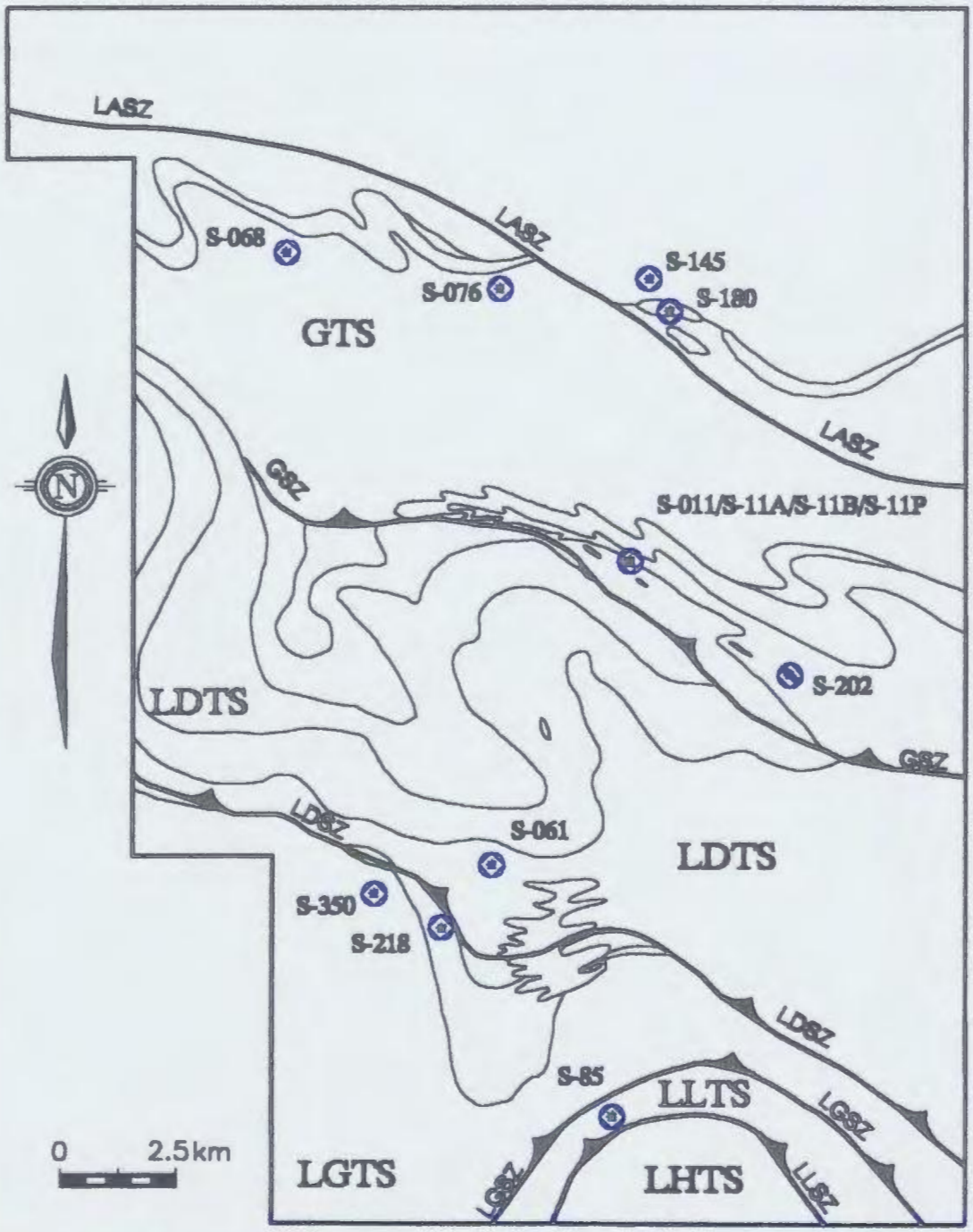

Figure 4.1 Map of sample locations described in text. Corresponding mineral assemblages are shown in Tables 4.1 and 4.2. Abbreviations: GTS - Gueslis thrust sheet, LDTS - Lac Don thrust sheet, LGTS - Lac Gull thrust sheet, LLTS - Lac Lamêlée thrust sheet, GSZ - Gueslis shear zone, LASZ - Lac Audréa shear zone, LGSZ - Lac Gull shear zone, LLSZ - Lac Lamêlée shear zone.

Table 4.1: Mineral assemblages in non-pelitic rocks.

Denault Formation

	Sample #	Qtz	Cal-Dol	Cpx	Hbl	Opx	Grt	Bt	Ol
GTS	S-41X	X		X		X	X	X	
	S-68		X	X		X			X
	S-107F		X	X		X			
	S-108			X		X			
LDTS	S-11N		X		X	X		X	
LGTS	S-210		X	X		X			
	S-238B	X	X	X		X			
	S-238C		X	X	X	X			
LLTS	S-82C		X	X		X			

Wishart Formation

	Sample #	Opx	Kfs	Ms	Grt	Bt	Qtz
GTS	S-119	X	X	X	X	X	X

Sokoman Formation

	Sample #	Qtx	Gru	Opx	Hbl	Ms	Grt	Bt	Pl	Ol
GTS	S-47C	X			X	X	X	X	X	
LDTS	S-11P	X	X	X	X		X	X	X	
LGTS	S-154	X		X		X				X

Gabbroic[1], Granitic[2] and Garnet Amphibolite[3] Rocks

	Sample #	Grt	Bt	Pl	Qtz	Hbl	Ol	Opx	Cpx	Kfs
GTS[1]	S-180	X	X	X	X	X	X	X	X	
	S-202	X	X	X	X	X	X	X	X	
LDTS[1]	S-58	X	X	X	X	X				
LDTS[2]	S-11B	X	X	X	X				X	X
GTS[3]	S-145	X	X		X			X	X	

Table 4.2: Mineral assemblages in Attikamagen and Menihek formations.

	Sample #	Grt	Bt	Pl	Qtz	Ms	Kfs	Ky	Opx	L*
GTS	S-39	X	X		X	X(r)				
	S-43	X	X	X	X	X(r)	X			
	S-47A	X	X	X	X	X(r)	X			
	S-70	X	X	X	X	X(p&r)				
	S-75	X	X		X	X(r)	X			
	S-76	X	X	X	X	X(r)	X			X
	S-94	X	X	X	X					
	S-107	X	X	X	X	X(r)				
	S-118	X	X	X	X	X(r)	X			
	S-119	X	X		X	X(r)	X			
	S-139	X	X	X	X	X(r)				
	S-147	X	X	X	X	X(r)				
	S-185	X	X	X	X	X				
	S-186	X	X	X	X	X(r)	X			
	S-187	X	X	X	X	X(r)	X			X
	S-197	X	X	X	X	X(r)	X			
LDTS	S-11A	X	X	X	X		X		X	
	S-58A	X			X	X				
	S-61	X	X	X	X		X		X	X
LGTS	S-211	X	X	X	X					
	S-218	X	X	X	X		X	X		
	S-228A	X	X	X	X					
	S-350	X	X	X	X		X			X
LLTS	S-085B		X		X	X	X	X		
	S-85B	X	X		X	X	X	X		
	S-85C	X	X	X	X	X	X			
	S-91	X	X	X	X					
	S-264A	X	X	X	X					

p: primary
r: retrograde
L*: granitic liquid was not always observed in thin section due to sample size.

4.2.1 Denault Formation

The Denault Formation comprises carbonate and calc-silicate lithologies layered in scales ranging from <1cm to several metres. The mineralogy of this unit in the study area comprises: carbonates (dolomite and calcite), quartz, diopside, tremolite -actinolite, phlogopite and forsterite (Table 4.1). The most common sub-assemblages are Do-Di and Qtz-Di, with the maximum phase assemblage Do-Di-Fo occurring in a single sample (S-068) from the Gueslis thrust sheet. Staining for carbonates has not been carried out, so it is not known if the sub-assemblage Fo-Cal was stable. Colourless to light green tremolite-actinolite amphibole occurs in variable abundance in most samples and is inferred to be a retrograde phase replacing diopside. In several samples, diopside porphyroblasts are recrystallized into aggregates of subgrains giving rise to a granular appearance in thin section.

4.2.2 Wishart Formation

The Wishart Formation is a relatively pure quartzite containing 95% quartz and up to 5% hematite (Table 4.1) and minor phases including muscovite, biotite, garnet, orthopyroxene, rutile and zircon.

4.2.3 Sokoman Iron Formation

As described in Chapter 2, the Sokoman Formation consists of two types of iron formation. Silicate-carbonate iron formation comprises variable proportions of carbonates (siderite, dolomite and Fe-dolomite), quartz, ortho and

clinopyroxene, magnetite and grunerite (Table 4.1). Apatite and spinel are minor phases and secondary goethite is common. The observed maximum phase assemblage is: Qtz-Mag-Sid-Cpx-Opx-Gru (sample S-11P).

Oxide iron formation consists of quartz, specular hematite and magnetite. Observed assemblages are: Qtz-Hem, Qtz-Mag and Qtz-Hem-Mag.

4.2.4 Attikamagen And Menihek Formations

The quartzofeldspathic and pelitic rocks of the Attikamagen and Menihek formations are discussed together as these units are compositionally and mineralogically indistinguishable in the field (Section 2.1). The emphasis is placed here on the maximum phase peak mineral assemblages. Minor retrograde phases (especially muscovite) are common, but generally do not obscure the interpretation of peak mineral assemblages. Quartzofeldspathic compositions predominate in both formations and are composed of the assemblage: Qtz-Pl-Bt$\pm$Grt$\pm$Kfs$\pm$Ms$\pm$L with accessory tourmaline, Fe-Ti oxide and zircon. Evidence of partial melting (L) is widespread in all thrust sheets in the form of discontinuous granitoid veins and sweats, most of which are deformed and aligned parallel to the main foliation (e.g. Plates 3.8, 3.13). The granitoid veins are granitic to granodioritic in composition and are leucocratic, containing much lower abundances of mafic minerals (mostly biotite and/ or garnet) than the adjacent restite.

Pelitic rocks in the Attikamagen and Menihek formations are relatively

sparse in the study area, but occur in all thrust sheets.

(a) Pelites in Gueslis thrust sheet are composed of the maximum phase assemblage: Qtz-Ms-Bt-Grt-Kfs-Pl-L (S-76: Table 4.2). K-feldspar (microcline) occurs commonly in assemblages also containing abundant muscovite, indicating that bulk compositions (in the Menihek Formation) in this thrust sheet are K-rich. The pelitic rocks do not show evidence of partial melting, in contrast to more quartzofeldspathic compositions discussed above.

(b) In the Lac Don thrust sheet, the observed maximum phase mineral assemblage consists of: Qtz-Bt-Grt-Pl-Kfs-L (S-61: Table 4.2). A sample of metapelite was also collected from the Sokoman Formation in LDTS (S-11A: Table 4.2). The metapelite forms a thin (<50 cm) layer within the silicate -carbonate iron formation. The assemblage in this sample (S-11A) is: Qtz-Bt-Grt-Pl-Opx-Carb. No muscovite or melt (L) are present in this sample, but biotite is abundant. Carbonate is a minor phase.

(c) In LGTS, the observed maximum phase assemblages are: (1) Qtz-Ky-Kfs-Bt-Grt -Pl and (2) Qtz-Bt-Grt-Pl-Kfs-L (samples S-218 and S-350 in Table 4.2 respectively). In assemblage (1), kyanite and K-feldspar are in close association and are inferred to be in equilibrium; prograde muscovite is absent. In assemblage (2) the rock is segregated into leucosome and restite, with alkali feldspar (perthite) occurring in both leucosome and restite. The leucosome is granite, being composed of Qtz-Kfs-Pl-Bt.

(d) In LLTS the maximum phase peak assemblage consists of: Qtz-Ms-Grt-Ksp -Bt-Ky with accessory tourmaline (sample S-85B). Kyanite (partially replaced by muscovite) is inferred to have been in equilibrium with K-feldspar and muscovite, the latter being abundant in the matrix (Plate 4.1).

In summary, pelitic rocks in the Gueslis and Lac Don thrust sheets are characterised by the stable sub-assemblage Ms-Qtz, coexisting with Grt-Bt-Kfs (in GTS) and Grt-Bt (in LDTS), the difference implying a K_2O-richer bulk composition in the Gueslis thrust sheet. Muscovite is absent and orthopyroxene is present in pelite in iron formation in LDTS. In LGTS, the sub-assemblage Ms-Qtz is not stable, being replaced by the chemically equivalent mineral pair Ky-Kfs. In the LLTS, the four phases Ms-Qtz-Ky-Ksp are inferred to have been in stable equilibrium, implying univariant conditions on the reaction boundary. Figure 4.2 shows a synopsis of maximum phase peak assemblages in each of the thrust sheets, projected in AFM diagrams. Assemblages lacking both muscovite and K-feldspar cannot be plotted in this projection.

Assuming that other variables (especially a_{H2O}) were constant, the mineral assemblages in pelites suggest that the highest grade conditions in the study area were attained in LGTS and the lowest grade conditions were in GTS and LDTS. LLTS displays evidence of intermediate P-T conditions. The presence of Opx in the pelitic layers within the iron formation in LDTS, in what is interpreted on other criteria to be an amphibolite-facies thrust sheet (Ms-Qtz stable), is

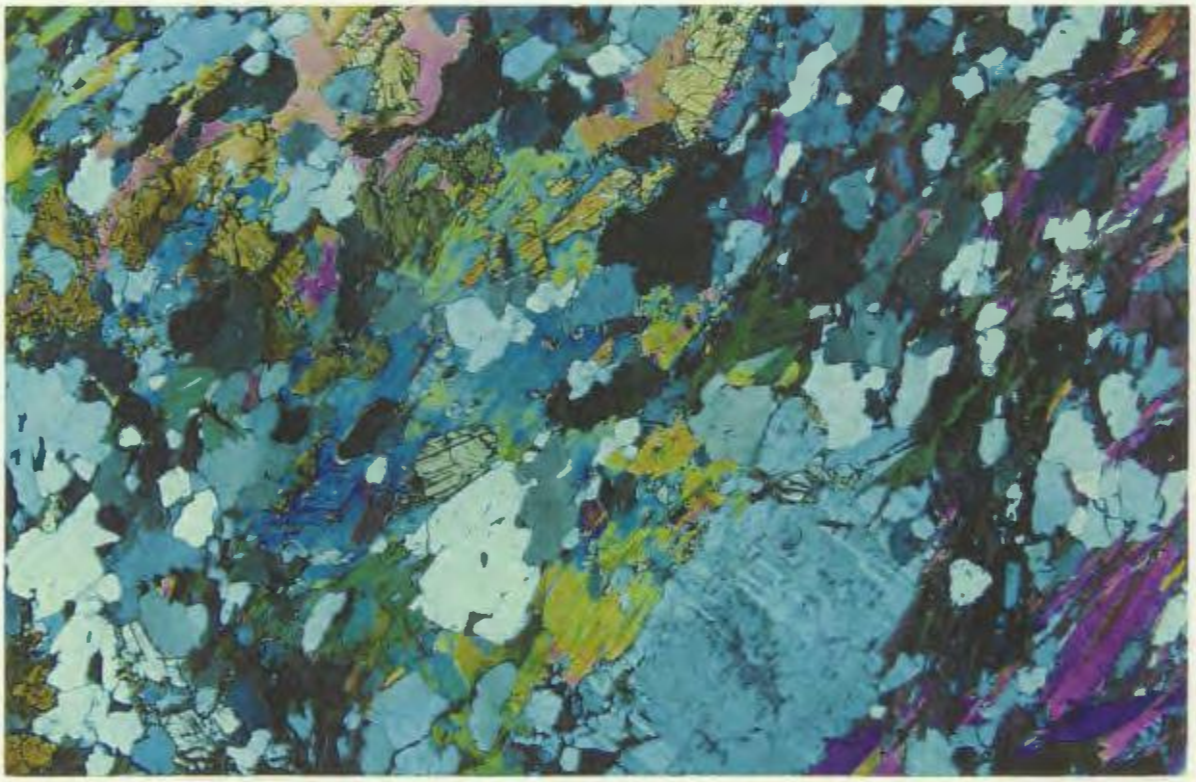

Plate 4.1 Photomicrograph of kyanite and quartz replacement by muscovite and K-feldspar in a quartz-rich muscovite-kyanite schist (Sample S-85B). Cross-polarized light. Width of Plate is 0.8 mm.

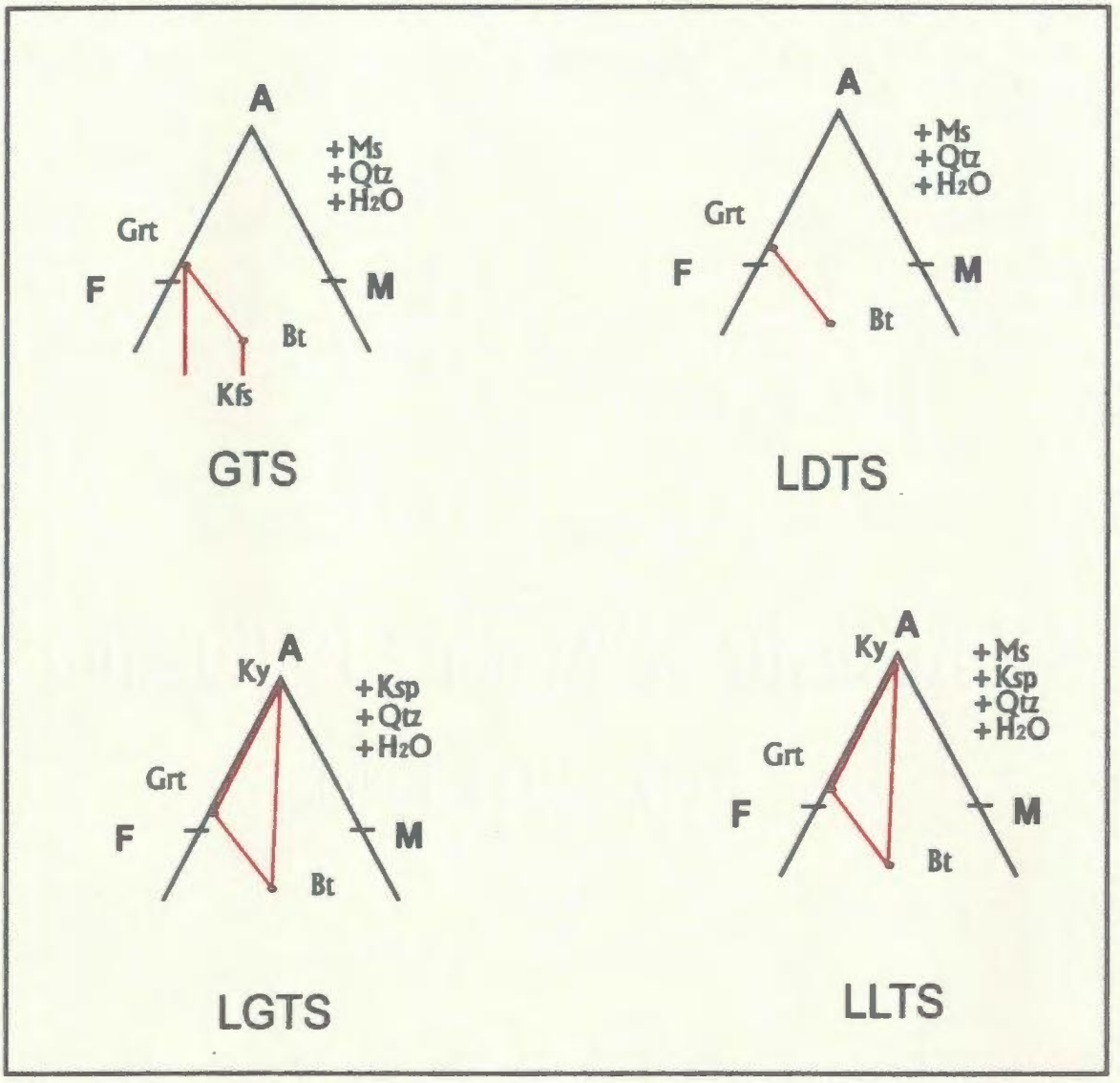

Figure 4.2 Schematic AFM diagrams projected from muscovite and/or K-feldspar. These represent the maximum phase assemblages observed in quartzofeldspathic and pelitic rocks of the Attikamagen and Menihek formations in different thrust sheets in the study area. Abbreviations for mineral names after Kretz (1983).

inferred due to depression of a_{H2O} by CO_2 during metamorphism (carbonate present in assemblage) and/or by the Fe-rich nature of the bulk composition.

The interpretation of melting reactions between pelitic and quartzofeldspathic rocks is more subtle. Pelitic rocks in GTS and LDTS do not show evidence of partial melting, whereas quartzofeldspathic rocks commonly contain leucosomes of assumed anatectic origin. In LGTS, in contrast, there is evidence of melting in aluminous (kyanite-bearing) compositions and in a single sample evidence was found for K-feldspar (perthite) as a restite as well as a leucosome phase. The significance of these observations is discussed later.

4.2.5 Granitic Rocks

Several granitic bodies intrude the supracrustal gneisses. The two larger bodies (Figure 4.2) consist of medium-grained, weak to moderately foliated, homogeneous biotite granodiorite to granite. The mineral assemblage of the sample S-11B (Table 4.1) consists of Qtz-Pl-Kfs-Cpx-Grt-Bt and contains accessory minerals, including hornblende, magnetite and ilmenite.

4.2.6 Garnet Amphibolites

All rocks containing garnet and hornblende are included here as the microstructural character of hornblende-rich calc-silicate rocks is similar to amphibolites derived from the retrogression of gabbroic rocks. They are composed of variable amounts of garnet, hornblende, clinopyroxene, biotite and plagioclase with subordinate epidote, sphene, calcite-dolomite, apatite and

opaque minerals (Table 4.1). The maximum phase assemblage Qtz-Grt-Bt-Cpx-Opx occurs in a single sample (S-145: Table 4.1). The most commonly observed assemblage is Qtz-Grt-Bt±Pl±Opx.

4.2.7 Shabogamo Gabbro

The field area hosts two gabbroic intrusions that are tentatively correlated with the Shabogamo Gabbro (Figure 4.2). The larger body, east of Lac Audréa, is massive and retains relict igneous minerals which are separated by coronas and/or pseudomorphed by metamorphic minerals. The most common and maximum phase assemblage (samples S-180, S-202 in Table 4.1) is Pl-Grt±Ol±Opx±Cpx, which contains minor amounts of biotite and hornblende, and trace amounts of ilmenite, rutile exsolution in orthopyroxene, corundum inclusions in plagioclase, and opaque minerals. Similar textures in Shabogamo gabbros have been described by Rivers and Mengel (1988), Indares (1993) and Indares and Rivers (1995).

4.3 RELATIVE TIMING OF PORPHYROBLAST GROWTH AND DEFORMATION

In the following sections, the characteristic microstructural relationships between garnet porphyroblasts, their inclusion patterns and the minerals defining the matrix foliation in metapelitic rocks of the Attikamagen and Menihek formations are described to provide constraints on the relative timing of metamorphic and structural events. Comparisons between thrust sheets indicate

significant differences, so the text below is organised to reflect this.

There has been considerable debate in the literature on the interpretation of relative time relationships between metamorphism and deformation using porphyroblast-matrix microstructural criteria. Some authors have favoured the concept of rotating porphyroblasts (Zwart, 1962; Spry, 1969; Rosenfeld, 1970; Schonenveld, 1977), whereas others have proposed that the microstructures developed by overgrowth of a folded fabric in a heterogeneous strain field (Bell, 1985; Bell et al., 1986; Jamieson and Vernon, 1987; Plint and Jamieson, 1989; Vernon, 1989; Williams, 1994). It seems likely that both mechanisms are feasible, but there is little doubt that porphyroblasts with spiral inclusions trails (snowball garnets) developed by porphyroblast rotation (Williams, 1997). The microstructures in the study area cannot be unambiguously interpreted as a result of either mechanism, however, and so inferences concerning the mode of formation of the structures are not made here.

4.3.1 Gueslis Thrust Sheet

Fabrics in metapelitic samples from the Gueslis thrust sheet are typically defined by the preferred orientation of muscovite and by the dimensional orientation of quartz and feldspars. Four styles of porphyroblast-fabric relations were observed (Figure 4.3). In all cases, the main foliation (S_e- external foliation) wraps around the garnet porphyroblasts. In (B), the external foliation (S_e) is continuous with the internal foliation (S_i) in the garnet porphyroblast, whereas in

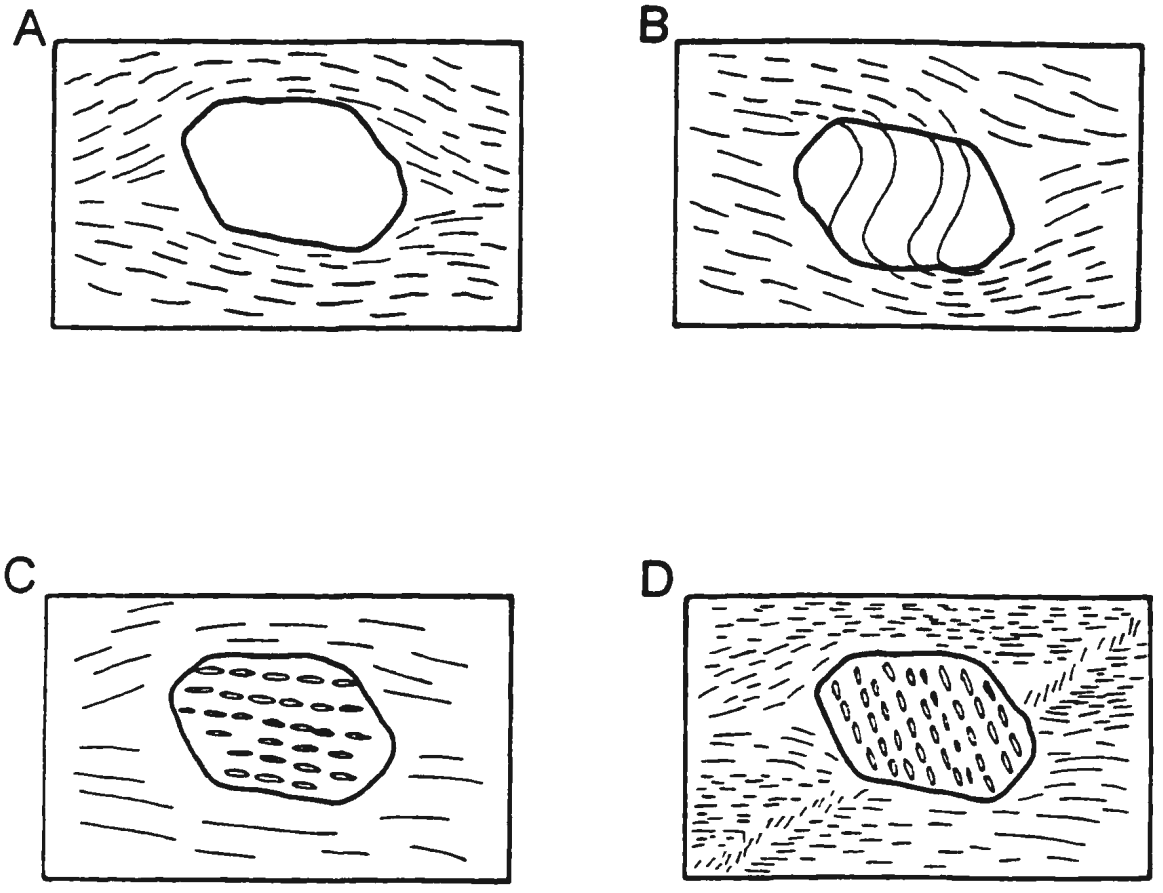

Figure 4.3 Schematic representation of garnet porphyroblasts-fabric relations in GTS. Garnet porphyroblasts are typically elongate parallel to the S_e foliation. In (A) the garnet contains no internal fabric; in (B) the internal fabric (S_i) is at high angle to S_e and is continuous with it; in (C) S_i is parallel to S_e outside the porphyroblast; and in (D) S_i is at a high angle to S_e and S_e is deformed by a late kink fold.

(C) and (D) the two foliations are discontinuous. Types (A), (C) and (D) are the most commonly observed.

These relationships suggest that the main foliation (S_e) is a combined S_1/S_2 fabric and that S_i is the relict S_1 fabric. The various angular relationships between S_i and S_e suggest that S_1 and S_2 were subparallel in (C) but at an angle in (D) (Plate 4.2). Figure 4.3B indicates that in some samples there is a little mineralogical expression of the S_2 fabric, suggesting that D_2 strain was variable. The S_e fabric is crenulated into open microfolds in some samples, inferred to be a result of post-D_2 deformation.

There is petrographic evidence that annealing was variable throughout the GTS. In several samples, the micas defining the main fabric are bent and retain internal strain, whereas in others individual crystals are undisturbed and some are at a high angle to the fabric.

4.3.2 Lac Don Thrust Sheet

Garnet prophyroblasts from the Lac Don thrust sheet are generally similar to those illustrated in Figure 4.4, since those garnets do not contain an internal fabric (S_i). As in Gueslis thrust sheet, the main foliation (S_e) wraps around the garnet porphyroblasts, and is locally crenulated. By analogy with Gueslis thrust sheet, these textural relationships suggest that the main fabric is a combined S_1/S_2 feature which is locally crenulated by post-D_2 deformation. However the absence of an internal fabric (S_i) in the samples examined renders discrimination between S_1 and S_2 cryptic.

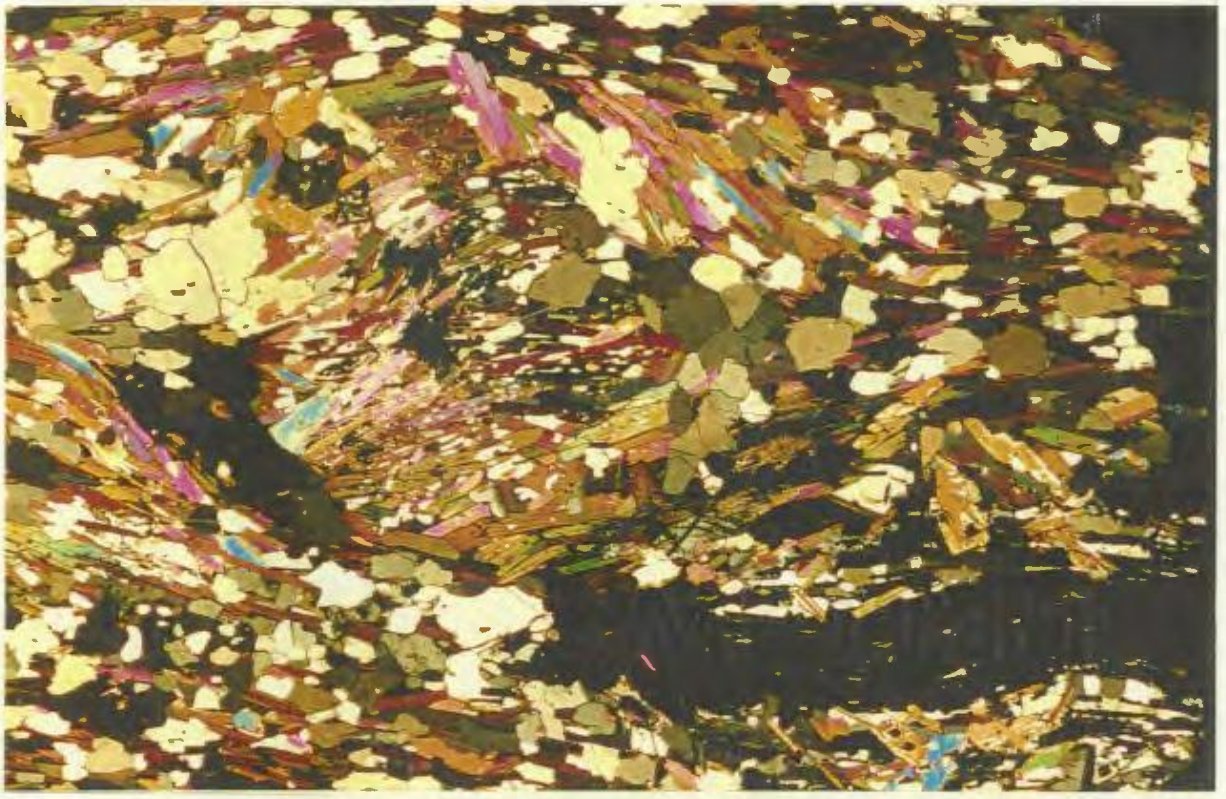

Plate 4.2 Photomicrograph of two garnet porphyroblasts (S-107) from Gueslis thrust sheet. The central garnet porphyroblast is replaced by retrograde muscovite and biotite; garnet is resorbed and has an internal fabric of fine- and medium grained biotite and muscovite (S_1) which is locally at an angle to the muscovite and biotite ($S_1//S_2$) foliation in the matrix. At the lower right corner, the second garnet porphyroblast is elongate parallel to the matrix fabric and appears to have overgrown $S_1//S_2$. Cross-polarized light. Width of the image is 1.0 mm.

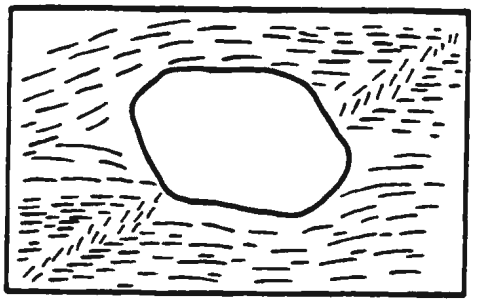

Figure 4.4 Schematic representation of garnet porphyroblast-fabric relations from the LDTS. Garnet porphyroblasts are partially overgrown by muscovite and biotite (S_1) which wrap around the garnet porphyroblast and are locally crenulated by D_2, suggesting garnet growth during the early (-to middle) part of S_1.

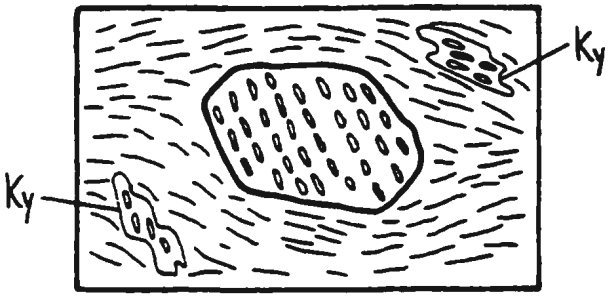

Figure 4.5 Schematic representation of garnet porphyroblast-fabric relations from the LGTS. The matrix fabric (S_1), consists of biotite, quartz and locally muscovite (not shown). Kyanite porphyroblasts contain an internal fabric which is parallel to the matrix S_1 foliation and is locally crenulated (D_2). These inclusion fabrics suggest that garnet growth in the LGTS occurred during early -to syn D_1 and growth terminated prior to D_2.

4.3.3 Lac Gull Thrust Sheet

Porphyroblast-fabric relations for both garnet and kyanite can be observed in the Lac Gull thrust sheet. Kyanite porphyroblasts have an internal fabric, S_i which is aligned both parallel and oblique to the main fabric (S_e)(Plate 4.3). In sample (S-218), the inclusion fabric (S_i) in the garnet porphyroblasts is oblique to the main fabric (S_e) and is parallel to that in the kyanite porphyroblasts (Figure 4.5).

These relationships suggest that S_i is the relict S_1 and that S_e is an S_2 fabric and that kyanite grew during both D_1 and D_2.

4.3.4 Lac Lamêlée Thrust Sheet

Garnet porphyroblasts in LLTS contain an internal foliation (S_i) parallel to S_e outside the porphyroblasts (Figure 4.6). S_e also wraps gently around the porphyroblasts. Relict kyanite porphyroblasts (Sample S-85B) are aligned parallel to S_e. These relations suggest that S_i is S_1 and that S_e is S_2, as in other thrust sheets. Several samples show evidence of post-D_2 crenulation deformation oriented at a range of angles to S_2.

4.3.5 Summary

Points that emerge from petrography with respect to the relative timing of metamorphism and deformation are as follows.

(1) Garnets and other porphyroblastic phases commonly show evidence of an internal fabric (S_i) that may be straight or curved and either parallel or oblique to the external matrix foliation (S_e).

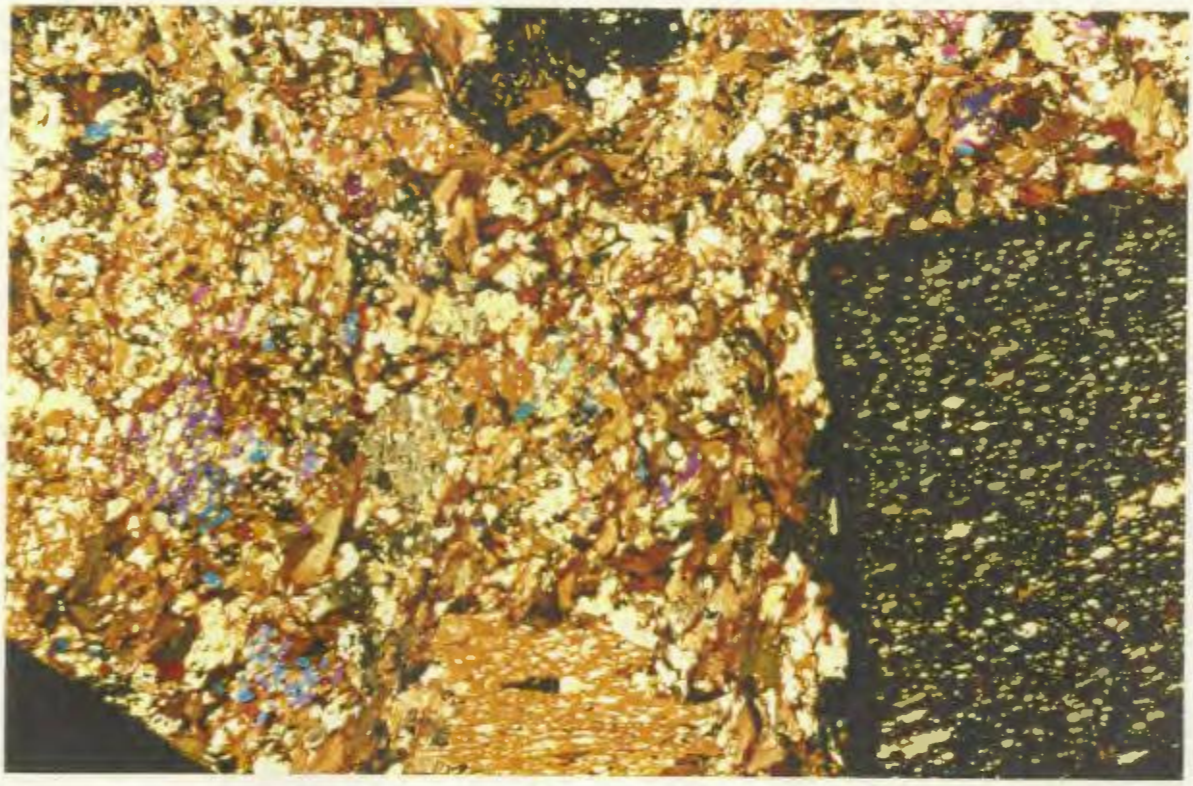

Plate 4.3 Photomicrograph of garnet (bottom right) and kyanite (centre bottom) porphyroblasts in pelitic schist from Lac Gull thrust sheet (S-218). Both garnet and kyanite porphyroblasts have a straight internal fabric (S_i) defined by elongate quartz inclusions. S_i is at high angle to the matrix fabric (S_e) suggesting that S_i is S_1, and S_e is the S_2 fabric. Cross-polarized light. Width of the image is 0.6 mm.

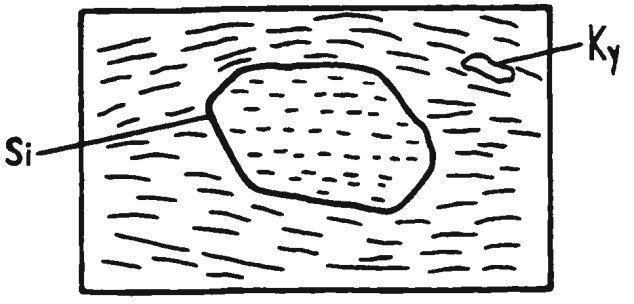

Figure 4.6 Schematic representation of a garnet porphyroblast-fabric relations from the LLTS. The garnet porphyroblasts contain an internal foliation (S_i) which is parallel to the external fabric (S_e). This suggests that S_i is S_1 and that S_e is the combined $S_1//S_2$ fabric. Post D_2 crenulations occur locally in the matrix.

(2) Spiral inclusion fabrics were not observed.

(3) The main regional fabric (S_e) was mapped as $S_0//S_1$ in the field, but examination of the metapelites in thin section indicates that it is at least S_2, with S_i in garnets (and other porphyroblastic phases) representing the relict S_1 foliation.

(4) In several rocks examined, $S_0//S_1$ and S_2 are approximately coplanar, but in others there is a large angle between $S_0//S_1$ and S_2. This may indicate variable rotation of $S_0//S_1$, or may indicate that F_2 folds were isoclinal. Criteria to distinguish these possibilities were not seen in most outcrops.

(5) Textural relationships indicate that most porphyroblast (e.g. garnet) growth took place after D_1 and before D_2. However evidence of syn- to post D_2 growth is also seen. This suggests that the peak of metamorphism was approximately synchronous with D_1 and D_2.

4.4 P-T ESTIMATION OF MINERAL ASSEMBLAGES IN METAPELITIC AND QUARTZOFELDSPATHIC ROCKS

This section focuses on the pelitic and quartzofeldspathic rocks as these contain mineral assemblages most suitable for P-T studies. The following diagnostic maximum phase mineral assemblages have been recognised in the different thrust sheets in thin section (Section 4.2.4):

(P)	Ms-Qtz-Grt-Bt-Kfs-Pl-L	GTS
(Q)	Qtz-Grt-Bt-Kfs-Pl-L	LDTS
(P)	Ms-Qtz-Grt-Bt-Kfs-Ky	LLTS
(P)	Qtz-Grt-Bt-Kfs-Ky-Pl	LGTS
(Q)	Qtz-Grt-Bt-Kfs-Pl-L	LGTS

where (P) = pelitic and (Q) = quartzofeldspathic rocks.

Other assemblages involving granitic liquid (L) are possible, but were not observed in thin section. In the field it is evident that most quartzofeldspathic rocks have undergone extensive partial melting (e.g. Plates 3.8, 3.13); however some muscovite-rich units did not show evidence of melting, suggesting that certain melt reactions were exceeded, whereas others were not. In the following sections, an attempt is made to relate observed mineral assemblages (both in the field and in thin section) to qualitatively inferred P-T conditions in each thrust sheet. The presence of L as part of the assemblage was evident in the field in some areas, but it was not observed in all thin sections due to sample size. L was assumed to be part of these assemblages in the use of the P-T grid below (Figure 4.7).

The assemblages can be modelled in the system KFMASH containing the minerals quartz, K-feldspar, muscovite solid solution (muscovite with celadonite component: Ms_{ss}), kyanite, biotite solid solution (Bt_{ss}), H_2O fluid phase and granitic liquid of variable composition. A schematic P-T grid, calculated for a bulk rock X_{Mg} of 0.5 and fluid-absent conditions ($a_{H2O}<1$) is presented in Figure 4.6 (modified from Vielzeuf and Holloway, 1988). Obviously such a P-T grid is schematic, but it is nonetheless useful for comparative purposes if the bulk compositions and fluid activities do not vary significantly within the field area. The assumption of a bulk rock $X_{Mg}=0.5$ is probably not unrealistic and the H_2O activity was likely <1 in these rocks, since intergranular H_2O would likely have dissolved in the leucosomes, reducing a_{H2O} in the coexisting restite. Minor changes in a_{H2O}

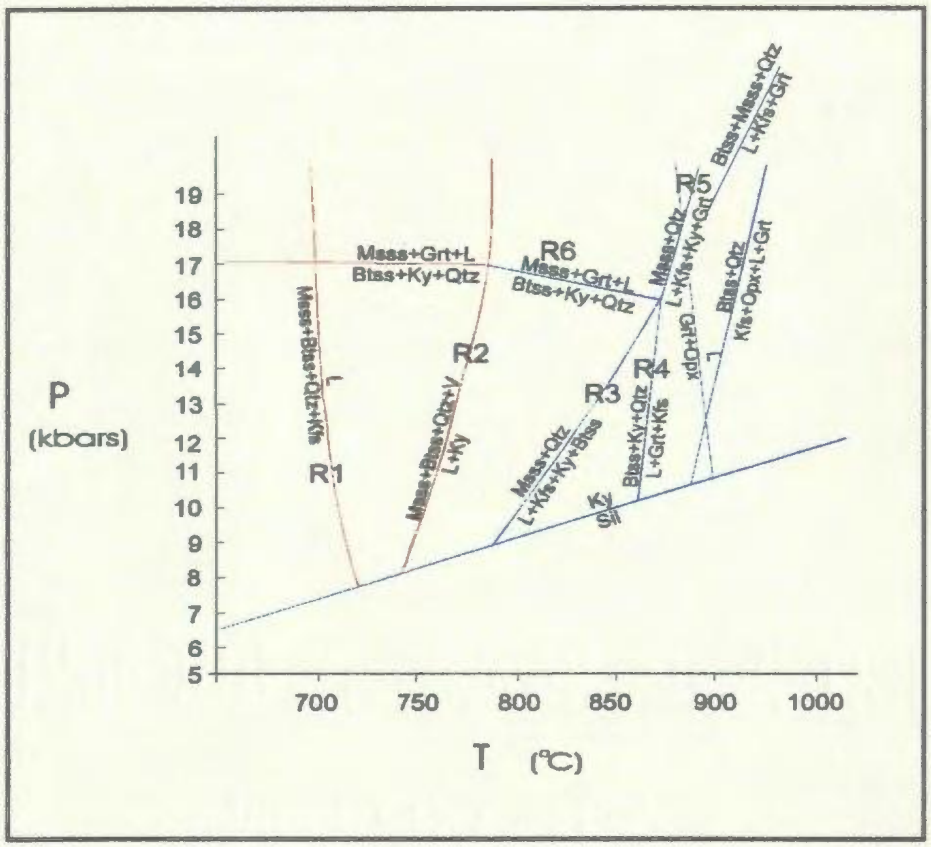

Figure 4.7 Schematic petrogenetic grid for quartz-saturated melting in metapelitic and metagreywacke (X_{Mg} ~0.5) in the model KFMASH system (after Vielzeuf and Holloway, 1988). R1 and R2 (shown in red) involve an H_2O bearing fluid phase (V) whereas R3-R6 (in blue) are fluid-absent reactions. Higher grade metamorphic zones are preserved in the more southern thrust sheets.

will cause some displacement of melt reactions, but will not dramatically alter the topology of the grid. The other significant simplification in the model system is the absence of Ca and Na. Plagioclase is an important phase in melt reactions in pelitic and quartzofeldspathic rocks, but is excluded from the KFMASH model system. Addition of albite would reduce the temperature of the melt reactions by ~50°C, whereas addition of anorthite would increase the temperature by about the same amount (Thompson and Tracy, 1979: Vielzeuf and Holloway, 1988).

Despite these shortcomings, the P-T grid provides a useful qualitative start for the metamorphic analysis.

4.4.1 Assemblage: Ms_{ss}-Bt_{ss}-Qtz-Kfs(-Pl)+L

Local field evidence suggests that quartzofeldspathic rocks locally experienced considerable partial melting, probably by a melting reaction such as (Thompson and Tracy, 1979; Vielzeuf & Holloway, 1988):

$Ms_{ss}+Bt_{ss}+Qtz+Kfs(+Pl)+V=L$ R1

This reaction would likely have proceeded until all intergranular H_2O fluid was consumed in some samples. In other samples, the absence of muscovite or K-feldspar in the restite suggests that these phases were the first to be consumed. Approximate minimum temperatures required for this reaction to proceed are between 680-725°C.

4.4.2 Assemblage: Ms_{ss}-Bt_{ss}-Qtz (-Pl)-Ky+L

Although not observed in thin section, the coexistence of kyanite and liquid (L) in an assemblage with biotite and muscovite was observed in the field,

implying that the P-T conditions for reaction R2 may have been exceeded.

$Ms_{ss}+Bt_{ss}+Qtz+V\ (+Pl)=L+Ky$ R2

The presence of vapour (V) as a reactant in reaction R2 is compatible with the inference of consumption of all K-feldspar in reaction R1, leaving the remaining reactants stable to higher temperatures. This reaction likely consumed the remaining intergranular H_2O, reducing a_{H2O} to well below unity. It would represent the transition between fluid-present and fluid-absent melting. This reaction occurs over the range 750-760^{0}C in the kyanite field in the model system.

4.4.3 Assemblage: Bt_{ss}-Ms_{ss}-Qtz (-Pl)-Ky-Kfs±L

The occurrence of the sub-assemblage Ky-Kfs-L implies that the vapour-absent dehydration melting reaction (Thompson and Tracy, 1979; Vielzeuf and Holloway, 1988):

$Bt_{ss}+Ms_{ss}+Qtz\ (+Pl)=L+Kfs+Ky$ R3

was exceeded. Muscovite is absent in all kyanite-K-feldspar bearing samples suggesting that it was consumed by reaction R3. This reaction occurs at temperatures in excess of 800^{0}C in the kyanite field in the model system (Figure 4.7).

4.4.4 Sub-Assemblage: Bt_{ss}±Ms_{ss}-Qtz (-Pl)-ky-Grt±Kfs± L

The presence of garnet in some leucosomes could be a result of one of three reactions (Thompson and Tracy, 1979; Vielzeuf and Holloway, 1988):

$Bt_{ss}+Ky+Qtz\ (+Pl)=L+Grt+Kfs$ R4

$Bt_{ss}+Ms_{ss}+Qtz$ (+Pl)=L+Grt+Kfs R5

$Bt_{ss}+Ky+Qtz=Ms_{ss}+Grt+L$ R6

The restite assemblage (Qtz-Grt-Kfs-Bt_{ss}±Ms_{ss}±Pl) in samples with garnet-bearing leucosomes suggests that the P-T conditions were in excess of 850°C in the kyanite field. Ky-Ksp-Grt and Ms_{ss}-Grt were not definitely recorded in equilibrium with L in any samples, so there is no evidence that reactions R5 and R6 were exceeded in the field area.

4.5 QUALITATIVE ESTIMATION OF P-T CONDITIONS IN DIFFERENT THRUST SHEETS

In the following sections the diagnostic mineral assemblages in metapelitic rocks observed within each thrust sheet are used to constrain P-T conditions using the petrogenetic grid in Figure 4.7.

4.5.1 Gueslis and Lac Don Thrust Sheets

Quartzofeldspathic rocks in Gueslis and Lac Don thrust sheets contain abundant leucosomes, whereas more pelitic compositions (especially in GTS) do not display much evidence of partial melting. The assemblage Qtz-Ms-Bt-Grt±Kfs in rocks that lack leucosomes implies that P-T conditions are on the left hand side of R1 on Figure 4.7 (i.e. T<700°C). This conclusion is enhanced by the lack of the assemblage Ky-Kfs-L, despite these minerals occurring individually in the thrust sheet.

4.5.2 Lac Gull Thrust Sheet

The sub-assemblage Ky-Ksp in pelitic restite was observed in a single

sample from the LGTS (Table 4.1). Assuming that this assemblage was in equilibrium with granite leucosomes (L) then reaction R3 would have been exceeded, implying temperatures of 800-850°C in the in the field area (Figure 4.7).

4.5.3 Lac Lamêlée Thrust Sheet

The sub-assemblage Ms-Qtz-Ky-Kfs in pelitic restite, assumed to be in equilibrium with L, implies P-T conditions of R3 (i.e. temperatures of approximately 850°C) (Figure 4.7).

4.5.4 Summary

Mineral assemblages and the schematic P-T grid suggest that temperatures in the Gueslis and Lac Don thrust sheets were below ~725°C, whereas temperatures in Lac Gull and Lac Lamêlée thrust sheets were higher, in the range of 800-850°C assuming that the inferred reactions are applicable. Petrogenetic grid constraints indicate that pressure was greater than 7 kbars in all thrust sheets and less than 17 kbars. These constraints do not take into account possible variations in a_{H2O} or X_{Mg} between samples.

4.6 P-T PATHS AND THERMOBAROMETRY

4.6.1 Introduction

In high grade rocks, the interpretation of garnet zoning and application of thermobarometry to appropriate mineral assemblages can provide constraints on P-T paths and metamorphic conditions. Thermobarometry is applied to mineral assemblages for which continuous reactions sensitive to changes in P-T

conditions can be written. By using analysed mineral compositions and the simultaneous solution of pressure and temperature sensitive reactions, the pressures and temperatures of some stage of the metamorphism can be calculated. Most geothermobarometers involve garnet. If garnet grains are large enough so that zoning is preserved, this may provide a means to qualitatively constrain the evolving P-T path as the zoning reflects variations in P-T conditions during garnet growth or cooling.

4.6.2 Garnet Zoning and P-T Paths: Theory

Under greenschist or amphibolite facies conditions, garnet growth zoning is preserved due to the lack of effective intra- and intergranular diffusion (Selverstone and Spear, 1985; Spear, 1988, 1991, 1993; Florence and Spear, 1989; Spear et al., 1990; Spear and Florence, 1992). Growth zoning is expressed as a series of concentric rims, every rim having been in equilibrium with the matrix minerals and reflecting the P-T conditions at that stage of growth. In this context, the final rim composition will reflect the maximum P-T conditions, provided that garnet only grows during prograde metamorphism and that retrograde diffusion has not occurred. Typical features of growth zoning profiles include: (a) a bell-shaped chemical composition profile of the Xsps (Mn) content (Hollister, 1966) due to the gradual depletion of Mn from the matrix minerals, a process that is largely independent of pressure and temperature since Mn is preferentially incorporated into garnet; (b) in assemblages with biotite, garnet typically displays decreasing Fe/(Fe+Mg) ratios from core to rim which reflect the

change in Mg/Fe partitioning between garnet and biotite with increasing temperature during progressive metamorphism (Spear, 1988, 1991, 1993; Spear and Cheney, 1989; Spear et al., 1990, 1991). Grossular zoning depends upon the grossular-forming reactions. For instance, in pelitic rocks, where grossular typically forms by consumption of the anorthite component of plagioclase during garnet growth, the Xgrs isopleths have a positive slope in P-T space, with X_{grs} increasing toward the higher pressure or lower temperature conditions. Therefore, if the temperature evolution is known, Xgrs can also be interpreted in terms of pressure evolution.

Prolonged exposure to high temperatures (T>650°C), sufficient to increase diffusion rates, results in the homogenization of growth zoning at the scale of individual garnet grains. According to Spear (1988, 1990, 1991, 1993) and Spear et al. (1991) the degree of homogenisation depends upon: (a) the size of the garnet, and (b) the length of time at high temperature conditions. Homogenization leads to flattened or smoothened chemical diffusion profiles. Xsps trends become averaged between core and rim compositions. Flat Fe/Fe+Mg profiles, due to exchange between garnet and other ferromagnesian phases (e.g. biotite), reflect maximum temperature conditions. Ca trends are the last to be affected by homogenisation due to the lower diffusion rate of Ca in garnet, a result of its greater ionic radius (Spear et al., 1991; Spear and Florence, 1992; Spear, 1993).

During cooling from high temperatures (T>650°C) diffusion rates are typically sufficient to allow garnet rims to re-equilibrate with adjacent matrix

minerals (e.g. biotite) (Spear and Florence, 1992; Spear, 1989, 1993). As in the case of homogenisation, retrograde zoning is diffusion controlled, but since diffusion is less effective at lower temperatures these effects are commonly limited to grain rims. Common retrograde zoning trends are: (a) increasing Fe/Fe+Mg ratios toward garnet rims, reflect continued Fe-Mg exchange between garnet and ferromagnesian phases e.g. biotite during cooling and/ or the effect of discontinuous pyrope-almandine consuming reactions (Spear, 1991, 1992, 1993; Spear et al., 1991; Spear and Florence, 1992), and (b) increased Mn at the garnet rim, due to consumption of garnet rims as Mn is not easily accepted into the structure of surrounding minerals (Thompson and Algor, 1977; Tracy, 1982; Cygan and Lasaga, 1985). Finally, if significant decompression occurs during the early stages of retrogression, grossular is consumed to form plagioclase and therefore Xgrs decreases at the rims.

4.6.3 Studied Samples

A limited number of pelitic samples containing assemblages suitable for geothermobarometry was found in the field area, despite an intensive search. After detailed examination of thin sections, two rocks were chosen for further analysis. An examination of garnet zoning profiles and thermobarometry was carried out on two samples, S-11 and S-218, from the Gueslis and Lac Gull thrust sheets respectively. Sample locations are shown in Figure 4.2.

Sample S-11 from a pelite layer in silicate -carbonate iron formation (Section 2.2.4), contains the assemblage Opx-Grt-Pl-Qtz suitable for the

application of the Grt-Opx thermometry and Grt-Opx-Pl-Qtz barometry, whereas sample S-218, which is from the Menihek Formation (Section 2.2.5), contains the assemblage Grt-Bt-Pl-Ky-Qtz suitable for the application of Grt-Bt thermometry and Grt-Ky-Pl-Qtz (GASP) barometry (see Table 4.2). Microstructures in these samples, described in Section 4.2.1.5, 4.3.1 and 4.3.3 indicate that these are equilibrium assemblages.

4.6.4 Analytical Conditions

Major element analyses of biotite, garnet, plagioclase, and orthopyroxene in the two samples were obtained using the Cameca SX-50 electron microprobe in EDS mode at Memorial University. Operating conditions were an acceleration potential of 15 kV, beam current of 20 nA, and 1-2 μm beam spot size except for analyses of plagioclase in which a beam current of 10 nA and a 4-6 μm beam size were used to avoid Na loss. Counting times were 100 seconds (live time). Measured intensities were converted into element weight percent using the ZAF computer correction procedure. Probe results are reported below (Tables 4.3 to 4.8), as weight percent oxides, stoichiometric formulas and proportions of mineral endmembers.

Biotite, plagioclase and orthopyroxene core and rim compositions were analyzed adjacent to, and at increasing distance from, garnet. The largest garnets were analyzed by 2 or 3 rim-core-rim microprobe traverses in order to detect and interpret zoning for thermobarometric calculations. Microprobe points along those traverses were spaced at 100 μm intervals in the core and near the

rims. Where the chemical zoning was more pronounced, the spacing was at 25 mm intervals. Garnet zoning profiles were constructed in terms of molar fractions and Fe/(Fe+Mg) ratios and were divided into sectors on the basis of molar fraction trends.

4.6.5 Mineral Compositions: S-11

4.6.5.2 Orthopyroxene

Orthopyroxene compositions are listed in Table 4.3 Orthopyroxene is essentially a binary solution of En and Fs, with compositions in the range of Fs_{60-55}. Fe-Mg zoning is minor, with some grains showing a slight increase of En towards the rims.

4.6.5.2 Plagioclase

Plagioclase compositions are listed in Table 4.4. Most analyses range between 85-95% Ab, 7-15% An and <2% Or. The zoning patterns analyzed at various distances from garnet are not consistent. Some plagioclases have cores slightly enriched in anorthite whereas others have cores slightly depleted in anorthite. The zoning variations may be attributed to garnet (grossular) growth, such that plagioclase becomes more albitic at rim (Section 4.6.3.1), or garnet consumption, resulting in the release of Ca from grossular may have been added to plagioclase rim composition (Section 4.6.3.3).

4.6.5.3 Garnet

Representative garnet analyses are listed in Table 4.5. Garnet in S-11 is almandine-rich, consisting of 68-78% Alm, 5-16% Prp, 11-17% Grs and 1-4% Sps

Table 4.3: Representative orthopyroxene rim-core-rim compositions, S-11 (cations are on a 6(0) basis).

Smpl #	SiO_2	Al_2O_3	FeO	MgO	MnO	CaO	Total	Si	Al	Fe	Mg	Mn	Ca	Total	En	Fs	Wo
1-1	50.25	0.42	34.44	14.08	0.36	0.20	99.79	1.99	0.02	1.14	0.83	0.01	0.01	4.00	0.42	0.58	0.00
1-2	50.27	0.40	34.21	14.03	0.26	0.39	99.55	1.99	0.02	1.13	0.83	0.01	0.02	4.00	0.42	0.58	0.00
1-3	51.57	0.59	31.93	13.98	0.35	0.22	98.74	1.98	0.02	1.12	0.85	0.01	0.01	4.01	0.44	0.56	0.01
1-4	50.27	0.49	34.14	14.48	0.39	0.25	100.03	1.99	0.02	1.11	0.87	0.01	0.01	4.00	0.43	0.57	0.00
1-5	50.03	0.38	33.41	14.66	0.28	0.28	99.05	1.99	0.02	1.11	0.85	0.01	0.01	4.00	0.44	0.56	0.00
1-6	50.10	0.43	33.31	14.31	0.27	0.35	98.86	1.99	0.02	1.14	0.81	0.01	0.01	3.99	0.43	0.56	0.00
2-1	49.91	0.49	34.19	13.63	0.35	0.34	99.16	1.99	0.02	1.17	0.79	0.01	0.02	4.00	0.41	0.58	0.00
2-2	49.50	0.40	34.74	13.20	0.40	0.41	98.87	1.98	0.03	1.15	0.80	0.01	0.02	4.00	0.40	0.59	0.01
2-3	49.74	0.62	34.62	13.53	0.37	0.45	99.53	1.99	0.03	1.06	0.89	0.01	0.01	3.99	0.41	0.59	0.00
2-4	50.87	0.55	32.30	15.27	0.37	0.34	99.79	1.99	0.02	1.13	0.84	0.01	0.01	4.00	0.46	0.54	0.00
3-1	50.23	0.40	34.04	14.26	0.34	0.22	99.54	2.00	0.02	1.12	0.84	0.01	0.01	3.99	0.43	0.57	0.00
3-2	50.06	0.43	33.46	14.11	0.35	0.27	98.71	1.99	0.02	1.13	0.84	0.01	0.01	4.00	0.43	0.57	0.00
3-3	49.93	0.38	33.80	14.21	0.34	0.17	98.90	1.99	0.02	1.14	0.82	0.01	0.02	4.00	0.43	0.57	0.00

Core compositions used for thermobarometry represent the most refractory compositions, and are not necessary in the geometrical centre of the grain.

Table 4.4: Representative plagioclase rim-core-rim compositions, S-11 (Cations are on a 8(0) basis).

Smpl #	SiO_2	Al_2O_3	CaO	Na_2O	K_2O	Total	Si	Al	Ca	Na	K	Ab	An	Kfs
1-1	63.34	21.42	2.80	9.61	0.17	98.33	3.71	1.40	0.23	0.88	0.02	0.85	0.14	0.01
1-2	63.43	21.22	2.58	9.48	0.15	97.82	3.79	1.40	0.19	0.94	0.01	0.86	0.13	0.01
1-3	64.89	21.19	2.14	10.11	0.13	98.47	3.85	1.36	0.14	1.02	0.01	0.89	0.10	0.01
1-4	65.86	20.60	1.52	10.95	0.14	99.04	3.89	1.35	0.11	1.02	0.00	0.92	0.07	0.01
2-1	66.27	20.76	1.46	11.10	0.09	99.75	3.87	1.38	0.14	1.03	0.02	0.93	0.07	0.01
2-2	66.24	20.79	1.60	11.07	0.16	99.99	3.80	1.38	0.15	0.97	0.02	0.92	0.07	0.01
2-3	65.09	20.85	1.71	10.50	0.16	98.94	3.82	1.42	0.16	0.97	0.01	0.91	0.08	0.01
2-4	65.44	21.42	1.84	10.41	0.09	99.37	3.81	1.39	0.14	0.99	0.01	0.91	0.09	0.01
2-5	65.18	21.03	1.62	10.64	0.08	98.68	3.78	1.40	0.19	0.97	0.01	0.92	0.08	0.00
2-6	64.73	21.16	2.08	10.49	0.07	98.65	3.77	1.41	0.21	0.96	0.00	0.90	0.10	0.00

Core compositions used for thermobarometry represent the most refractory compositions, and are not necessary in the geometrical centre of the grain.

by mole ratio. Zoning is complex, and is shown for a representative grain in Figure 4.12. The radial zoning profile has been divided into three sectors labelled A1, A2 and B in Figure 4.8 (B is recognized only on one side of the profile). Sector A1 is characterized the following features:

(a) XSps declines radially from a peak of about four mole percent in the centre to about one mole percent at the contact with A2.

(b) XGrs shows a similar, though less marked trend to XSps with values declining from XGrs=17% to XGrs=15% away from the garnet centre.

(c) XPrp increases outwards, XAlm shows an irregular trend and XFe (=Fe/Fe+Mg) decreases outwards.

Sector A2 is characterized by an abrupt decline in XAlm and rapid increase in XPrp, minor decrease in XGrs and minor increase in XSps. XFe declines abruptly. These trends (Figure 4.8) correspond to a period of increasing T with decreasing P. Sector B is narrow and is characterized by reversals in most of the trends noted in sector A2. The zoning pattern of Sps and Grs in sector A1 indicate the presence of relict growth zoning, whereas sectors A2 and B represent superimposed diffusion zoning.

4.6.6 Qualitative Interpretation of Mineral Zoning: S-11

The zoning profile of sample S-11 records evidence of garnet growth during increasing P and T conditions, followed by a period of increasing T with decreasing P (sectors A and A2 respectively). A later period of partial homogenization and minor retrograde zoning is inferred from: (a) increasing XSps

Table 4.5: Representative garnet compositions, S-11 (cations on a 12(0) basis).

Smpl #	SiO_2	Al_2O_3	FeO	MgO	MnO	CaO	Total	Si	Al	Fe	Mg	Ca	Mn	Total	Alm	Prp	Grs	Sps	Adr
1	39.25	21.60	30.25	2.86	1.03	5.96	101.03	3.07	1.99	1.98	0.33	0.50	0.07	7.94	0.69	0.12	0.17	0.02	0.01
2	37.98	21.28	31.65	2.81	1.04	4.86	99.62	3.03	2.00	2.11	0.33	0.42	0.07	7.97	0.72	0.11	0.14	0.02	0.00
8	38.13	21.14	33.57	1.77	0.24	5.52	100.33	3.04	1.99	2.24	0.21	0.47	0.02	7.97	0.76	0.07	0.16	0.01	0.01
13	37.69	20.99	33.16	1.50	0.59	5.41	99.31	3.04	2.00	2.24	0.18	0.47	0.04	7.96	0.76	0.06	0.16	0.01	0.00
36	20.58	12.12	38.71	1.18	0.66	2.89	100.26	1.82	1.26	2.86	0.15	0.27	0.05	7.98	0.84	0.05	0.00	0.02	0.09
65	37.62	21.01	33.18	1.18	1.23	5.83	100.03	3.03	1.99	2.23	0.14	0.50	0.08	7.98	0.75	0.05	0.17	0.03	0.00
110	37.61	21.00	33.25	1.80	0.40	5.30	99.26	3.04	2.00	2.24	0.22	0.46	0.03	7.97	0.76	0.07	0.15	0.01	0.00
118	37.75	21.04	32.94	2.30	0.32	4.85	99.32	3.03	1.99	2.21	0.28	0.42	0.02	7.96	0.76	0.09	0.14	0.01	0.00
120	37.92	20.75	32.06	2.61	0.50	4.94	98.86	3.05	1.97	2.16	0.31	0.43	0.03	7.96	0.73	0.11	0.13	0.01	0.02
126	38.59	21.52	31.14	3.77	0.81	4.49	100.27	3.04	2.00	2.05	0.44	0.38	0.05	7.96	0.70	0.15	0.13	0.02	0.00
127	38.53	21.45	31.04	4.02	0.75	4.11	99.81	3.05	2.00	2.05	0.47	0.35	0.05	7.96	0.70	0.16	0.12	0.02	0.00
129	38.49	21.65	31.18	3.84	0.81	4.01	99.91	3.04	2.02	2.06	0.45	0.34	0.05	7.96	0.71	0.16	0.12	0.02	0.00
130	38.29	21.75	30.04	3.47	1.04	5.37	100.06	3.02	2.02	1.98	0.41	0.45	0.07	7.96	0.68	0.14	0.15	0.02	0.00

Garnet compositions used for thermobarometry are labelled in Figure 4.8 and Figure 4.10.

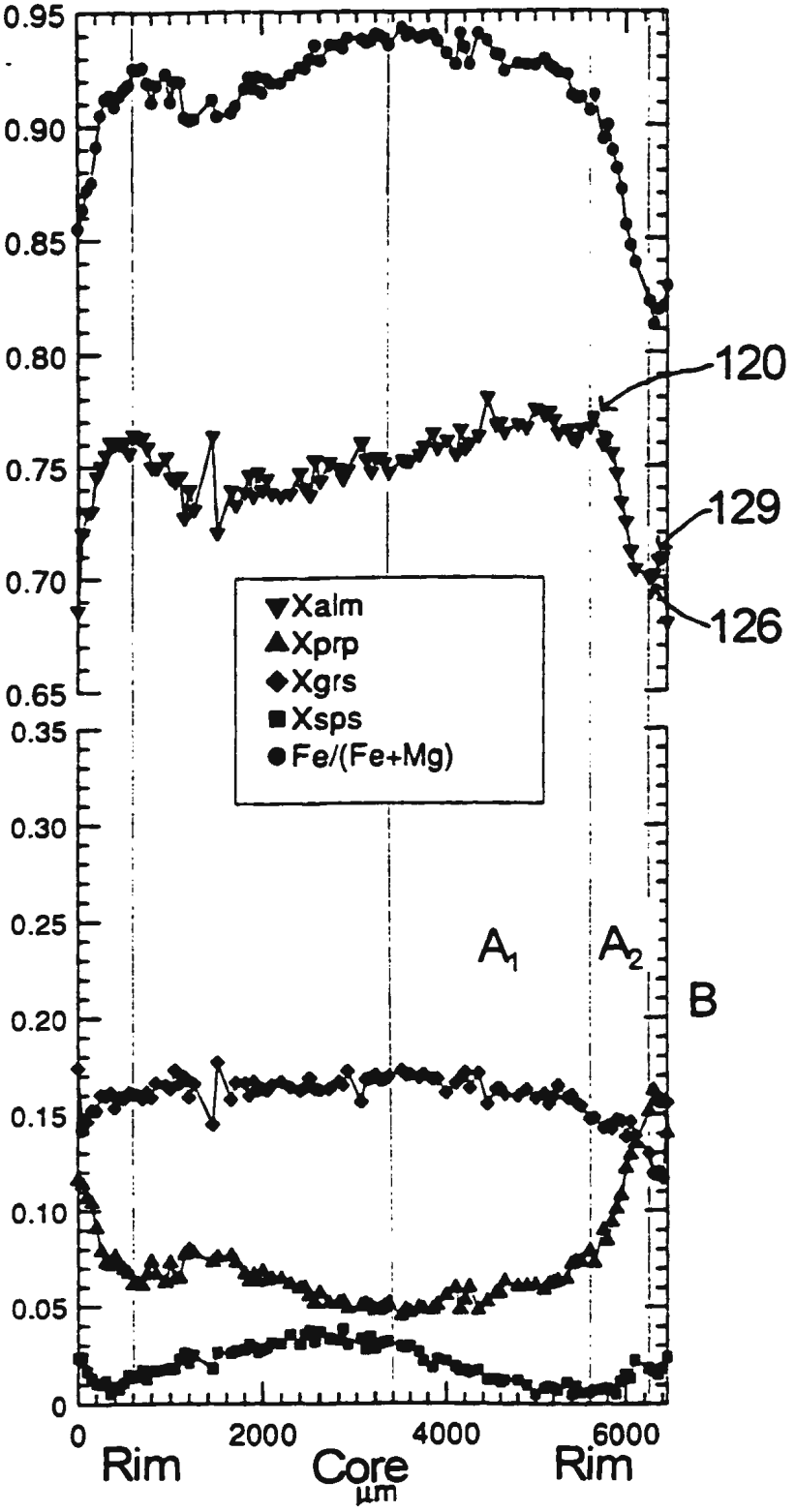

Figure 4.8 Zoning profile of garnet in sample S-11. Vertical lines separate sectors labelled A1, A2, B, as discussed in text.

at the garnet rim, (b) the lack of symmetry between XAlm and XPyp, and (c) the irregular Fe/Fe+Mg ratios. Garnet consumption is suggested by increasing XSps at the grain margin.

4.6.7 Mineral compositions: S-218

4.6.7.1 Biotite

Representative biotite analyses are listed in Table 4.6 with respect to mole fractions of the end members annite, phlogopite, and siderophyllite. Compositional variation is very minor and no detectable variation of composition with respect to proximity to garnet has been detected.

4.6.7.2 Plagioclase

Plagioclase analyses are listed in Table 4.7. Plagioclase is Ab-rich (Ab_{84-90}) and has a very low content of Or in solid solution. A single analyses of alkali feldspar yielded a composition of Or_{87}-Ab_{13}. Microprobe traverses were conducted across a few plagioclase grains to test for zoning.

4.6.7.3 Garnet

Representative garnet analyses are listed in Table 4.8. Garnet is essentially an Alm-Prp solid solution (Alm_{51-71}, Prp_{16-43}), with minor Sps ($_{0.2-1.7}$) and Grs ($_{2.9-11.6}$) components. The spectacular shape of the zoning profile across a representative garnet is shown in Figure 4.9. The profile has been subdivided into six sectors labelled A1-A4 and B1-B2. Sectors A1 to A4 display evidence of growth zoning, whereas B1 and B2 are indicative of retrograde zoning and garnet resorption. The right hand half of the zoning profile, which shows more regular

Table 4.6: Representive matrix biotite compositions, S-218 (cations are on a 11(O) basis).

Smpl #	SiO_2	AL_2O_3	TiO_2	FeO	MgO	Na_2O	K_2O	Total	Si	Al^{IV}	Al^{VI}	Ti	Fe	Mg	Na	K
1-1d	35.39	16.69	3.39	10.05	14.46	0.48	9.40	89.98	2.74	1.26	0.27	0.20	0.65	1.67	0.07	0.93
1-2	38.04	17.70	3.42	10.42	15.80	0.61	9.35	95.30	2.77	1.23	0.28	0.19	0.63	1.71	0.09	0.87
1-3	37.04	17.50	3.18	10.27	15.29	0.66	9.03	93.20	2.76	1.24	0.29	0.18	0.64	1.70	0.10	0.86
1-4	37.77	18.00	3.53	10.46	15.78	0.48	9.40	95.43	2.74	1.26	0.28	0.19	0.64	1.71	0.07	0.87
1-5p	36.21	16.89	2.47	10.02	15.37	0.48	9.49	90.87	2.77	1.23	0.29	0.14	0.64	1.75	0.07	0.93
3-1p	35.93	16.90	3.12	9.58	14.71	0.30	9.17	89.92	2.77	1.23	0.30	0.18	0.62	1.69	0.04	0.90
3-2	35.66	17.14	2.96	9.84	14.82	0.63	9.03	90.24	2.74	1.26	0.30	0.17	0.63	1.70	0.09	0.89
3-3	37.84	17.94	3.08	9.79	15.98	0.45	9.57	94.76	2.76	1.24	0.31	0.17	0.60	1.74	0.06	0.89
3-4	38.16	18.25	2.73	10.74	15.59	0.62	8.70	94.83	2.78	1.22	0.34	0.15	0.65	1.69	0.09	0.81
3-5	36.22	17.30	2.98	10.00	14.77	0.50	9.07	91.05	2.76	1.24	0.31	0.17	0.64	1.68	0.07	0.88
3-6	36.38	17.22	2.89	9.90	14.95	0.65	8.72	91.05	2.76	1.23	0.31	0.17	0.63	1.70	0.10	0.85
3-7	38.28	17.93	3.05	10.29	16.34	0.48	9.46	95.90	2.76	1.24	0.29	0.17	0.62	1.76	0.07	0.87
3-8	37.15	17.49	3.01	10.16	15.40	0.38	9.25	92.87	2.77	1.23	0.31	0.17	0.63	1.71	0.05	0.88
3-9	38.10	17.67	3.15	10.47	15.89	0.54	9.51	95.35	2.77	1.23	0.29	0.17	0.64	1.72	0.08	0.88
3-10	37.68	17.74	2.99	10.57	15.74	0.61	9.37	94.79	2.76	1.24	0.29	0.17	0.65	1.72	0.09	0.88
3-12	38.30	17.94	3.03	10.55	16.22	0.52	9.58	96.15	2.77	1.24	0.29	0.16	0.64	1.74	0.07	0.88
3-13	32.94	15.34	2.74	8.18	13.06	0.77	7.99	81.17	2.80	1.20	0.34	0.18	0.58	1.65	0.13	0.87
3-15	32.61	15.01	2.80	8.19	13.06	0.48	8.16	80.41	2.80	1.20	0.32	0.18	0.59	1.67	0.08	0.89
3-16d	31.53	14.20	2.58	7.85	12.39	0.40	7.64	76.38	2.84	1.16	0.35	0.18	0.59	1.66	0.07	0.88

In the oxides all Fe is calculated as FeO;
d: distal to garnet;
p: proximal to garnet.

chemical trends is described in point form.

(a) XSps displays an outward decrease through sectors A1 to A4. In sectors B1 and B2, in contrast, there is a minor increase in XSps.

(b) XAlm decreases from A1 to A3 and increases from B1 to B2. XPrp shows an antithetic trend. Fe/(Fe+Mg) declines in sectors A1 to A4, and increases in sectors B1 and B2.

(c) XGrs declines gradually from A1 to A2, increases slightly between A2 and A3, and declines from A3 to B2.

Table 4.7: Representative plagioclase rim-core-rim compositions, S-218 (cations are on a 8(0) basis).

Smpl #	SiO_2	Al_2O_3	CaO	Na_2O	K_2O	Total	Si	Al	Ca	Na	K	Ab	An	Kfs
1-1	59.07	22.82	2.88	9.14	0.31	94.93	2.76	1.26	0.14	0.83	0.02	0.84	0.15	0.02
1-2	65.86	20.90	2.12	10.32	0.20	99.51	2.91	1.09	0.10	0.88	0.01	0.89	0.10	0.01
1-3	65.62	21.11	2.12	10.75	0.22	99.80	2.89	1.10	0.10	0.92	0.01	0.89	0.10	0.01
4-1	65.47	20.97	2.42	10.32	0.15	99.52	2.90	1.09	0.11	0.88	0.01	0.88	0.11	0.01
4-2	65.44	21.00	2.24	10.54	0.20	99.46	2.90	1.10	0.11	0.90	0.01	0.89	0.10	0.01
4-3	65.24	21.23	2.22	10.04	0.24	99.05	2.89	1.11	0.11	0.86	0.01	0.88	0.11	0.01
4-4	65.74	21.26	2.16	11.05	0.16	100.25	2.89	1.10	0.10	0.94	0.01	0.89	0.10	0.01
4-5	64.98	21.45	2.55	10.44	0.14	99.63	2.87	1.12	0.12	0.90	0.01	0.87	0.12	0.01

Core compositions used for thermobarometry represent the most refractory compositions, and are not necessary in the geometrical centre of the grain.

Table 4.8: Representative garnet compositions, S-218 (cations on a 12(0) basis).

Smpl #	SiO_2	Al_2O_3	FeO	MgO	MnO	CaO	Total	Si	Al	Fe	Mg	Ca	Mn	Total	Alm	Prp	Grs	Sps	Adr
1	38.96	22.09	27.34	9.19	0.41	1.11	99.13	3.01	2.01	1.77	1.06	0.09	0.03	7.98	0.60	0.36	0.03	0.01	0.00
2	39.27	22.03	26.68	9.57	0.12	1.10	98.82	3.03	2.00	1.72	1.10	0.09	0.01	7.96	0.59	0.38	0.03	0.00	0.00
17	38.84	21.84	26.13	10.28	0.23	0.96	98.21	3.02	2.00	1.70	1.19	0.08	0.01	7.99	0.57	0.40	0.03	0.01	0.00
18	39.72	22.29	25.99	10.16	0.23	1.09	99.56	3.03	2.01	1.66	1.16	0.09	0.01	7.96	0.57	0.40	0.03	0.01	0.00
26	39.21	21.86	25.35	9.92	0.31	1.93	98.54	3.03	1.99	1.64	1.14	0.16	0.02	7.98	0.55	0.39	0.05	0.01	0.00
34	38.82	21.44	27.38	7.06	0.12	3.85	98.66	3.04	1.98	1.79	0.83	0.32	0.01	7.97	0.61	0.28	0.10	0.00	0.01
41	38.52	21.23	29.99	5.86	0.23	3.47	99.32	3.04	1.97	1.98	0.69	0.29	0.02	7.98	0.66	0.23	0.09	0.01	0.01
72	37.94	21.14	31.32	3.99	0.74	3.88	99.17	3.03	1.99	2.09	0.48	0.33	0.05	7.97	0.71	0.16	0.11	0.02	0.01
121	38.24	21.28	28.84	6.70	0.31	2.78	98.37	3.02	1.98	1.91	0.79	0.24	0.02	7.97	0.65	0.27	0.07	0.01	0.01
126	38.65	21.57	27.62	7.25	0.14	3.14	98.54	3.03	1.99	1.81	0.85	0.26	0.01	7.96	0.62	0.29	0.08	0.00	0.01
146	39.70	22.06	25.26	10.58	0.23	1.93	99.86	3.02	1.98	1.61	1.20	0.16	0.01	7.98	0.54	0.41	0.04	0.00	0.01
152	38.77	21.86	25.66	9.65	0.15	2.02	98.11	3.01	2.00	1.67	1.12	0.17	0.01	7.98	0.56	0.38	0.06	0.00	0.00
153	39.14	21.87	27.01	9.15	0.38	1.08	98.67	3.04	2.00	1.75	1.06	0.09	0.02	7.96	0.60	0.36	0.03	0.01	0.00

Garnet compositions used for thermobarometry are labelled in Figure 4.9 and Figure 4.11.

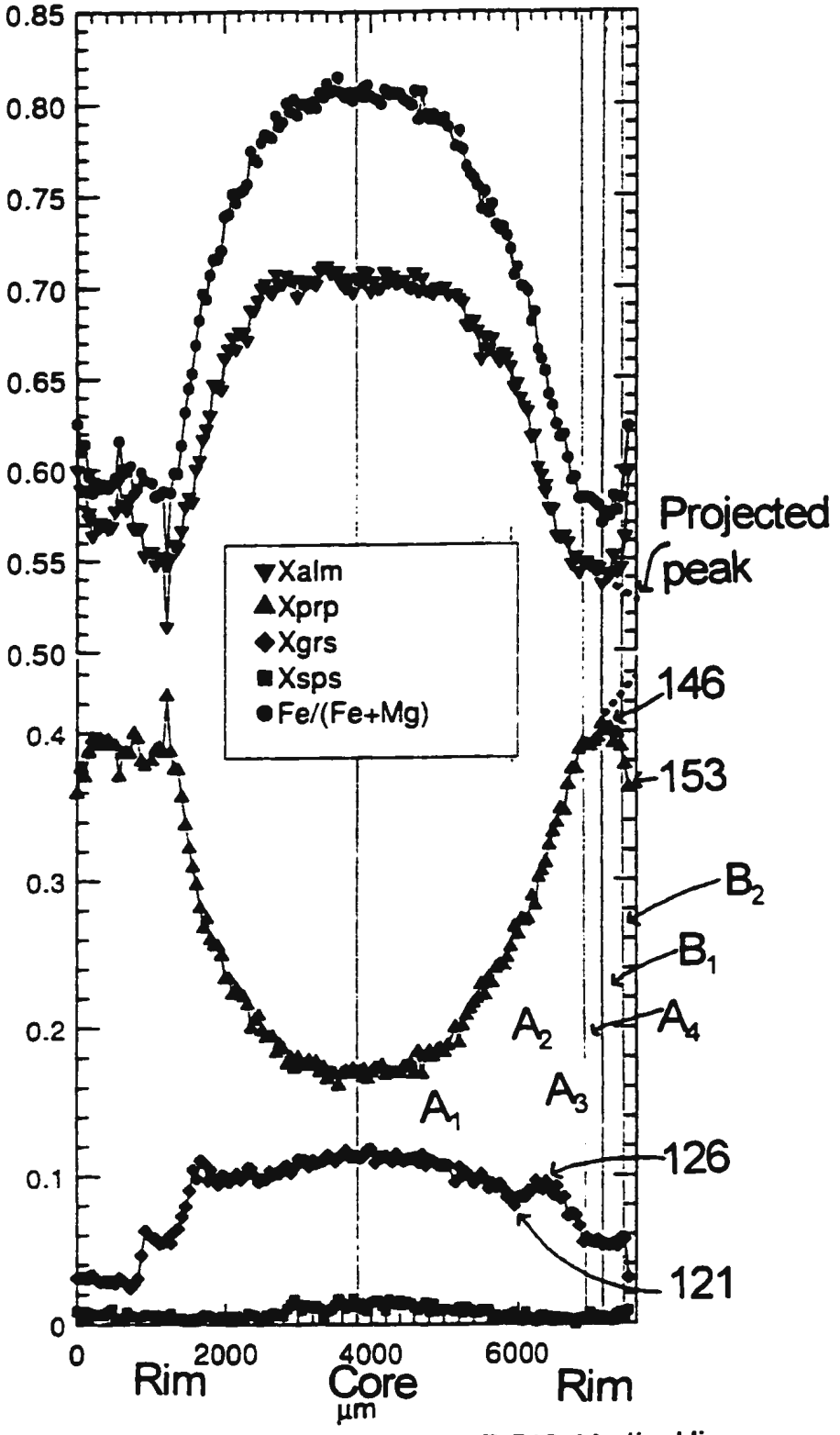

Figure 4.9 Zoning profile of garnet in sample S-218. Vertical lines separate Sectors (labelled A1 to A4, B1 and B2), as discussed in text.

4.6.8 Qualitative interpretation of zoning; S-218.

The assemblage in S-218 is Qtz-Bt-Pl-Kfs-Grt-Ky. This assemblage implies operation of the Fe/Mg exchange reaction between garnet and biotite, as well as the net transfer reaction involving the anorthite component of plagioclase, the grossular component of garnet, kyanite, and quartz. Assuming that the same assemblage was present during garnet growth, a qualitative interpretation of the garnet zoning profile in terms of variations in P and T can be made as follows:

(a) The trend of the Fe/(Fe+Mg) indicates increasing T through sectors A1 to A4 (prograde) with sectors B1 to B2 showing decreasing T (retrograde) and garnet resorption (increasing Mn towards rim).

(b) Slightly decreasing XGrs in sectors A1 to A4 (with minor perturbations) indicates that the slope of the P-T path was less than the slope of the isopleth for the reaction An=Grs+Ky+Qtz. Rapid decrease in XGrs in sections B1 to B2, in conjunction with decreasing T (see above) implies decreasing P.

The qualitative interpretation of the garnet zoning implies a moderate increase with P with increasing T during the prograde path, with a short retrograde path involving decreasing P and T, giving the P-T path a hairpin shape (maximum P and T achieved simultaneously).

4.7 GEOTHERMOBAROMETRY

4.7.1 Methods

In the pyroxene bearing sample (S-11), peak and retrograde temperature conditions were estimated using the Fe-Mg exchange reaction between garnet and orthopyroxene.

$$3MgSiO_3 + Fe_3Al_2Si_3O_{12} = 3FeSiO_3 + Mg_3Al_2Si_3O_{12}$$
enstatite almandine ferrosilite pyrope

Corresponding pressures were calculated by using the net transfer reaction:

$$3CaAl_2Si_2O_8 + 3Fe_2Si_2O_6 = Ca_3Al_2Si_3O_{12} + 2Fe_3Al_2Si_3O_{12} + 3SiO_2$$
anorthite ferrosilite grossular almandine quartz

In the metapelitic sample (S-218), peak and retrograde temperature conditions were estimated using the Fe-Mg exchange reaction between garnet and biotite:

$$Fe_3Al_2Si_3O_{12} + KMg_3AlSi_3O_{10}(OH)_2 = Mg_3Al_2Si_3O_{12} + KFe_3AlSi_3O_{10}(OH)_2$$
almandine phlogopite pyrope annite

Corresponding pressures were calculated using the net transfer reaction:

$$3\ CaAl_2Si_2O_8 = Ca_3Al_2Si_3O_{12} + 2Al_2SiO_5 + SiO_2$$
anorthite grossular kyanite quartz

A potential problem in the Grt-Bt thermometry is the possibility of Fe^{3+} in biotite, which cannot be evaluated from microprobe analyses by standard stoichiometric calculations. If significant Fe^{3+} is present, and all the analyzed Fe is assumed to be Fe^{2+}, temperatures are overestimated. However the studied sample contains graphite, implying a low f_{O2} environment, and Fe^{3+} values are expected to be minimal (Guidotti and Dyar, 1991; McMullin et al., 1991).

4.7.2 Selection Of Analyses

In order to perform thermobarometric calculations, it is crucial to use mineral compositions that represent equilibrium P-T conditions. Although equilibrium cannot be proved, it can reasonably be assumed if appropriate criteria are met. In this section, the selection of microprobe analyses for the estimation of peak and retrograde conditions for both pyroxene-bearing and metapelitic rocks is described. Since most phases except garnet exhibit only minor zoning, discussion is primarily directed towards garnet.

Peak P-T estimates require analyses of the composition of solution phases that were in equilibrium at the metamorphic peak (Spear, 1989, 1991, 1993; Spear et al., 1991; Spear and Florence, 1992). However garnet grains in both S-11 and S-218 exhibit retrograde zoning, therefore peak P-T cannot be unambiguously recovered. As the best approximation to peak P-T conditions, the composition at the junction between the growth and retrograde sections (A and B in Figures 4.8 and 4.9) is used. As a result, calculated 'peak' P-T's will be somewhat less than the actual peak by an unknown amount. The width of the retrograde rim serves as a qualitative estimate of the degree of underestimation of peak P-T.

Orthopyroxene in S-11 is slightly zoned, with the outward decrease in Fe being compatible with retrograde zoning. The Fe richest parts of the crystals (cores) are therefore assumed to be the best approximations to peak conditions, although this composition may or may not corespond to the geometrical centre of

the grain. Similarly plagioclase in both S-11 and S-218 is slightly zoned, with increasing Ca towards the rim, compatible with diffusion (retrograde) zoning during decompression. Thus the lowest Ca analyses in the core were used for estimates of peak P.

Individual biotite grains are unzoned, but a zonation of Fe/Mg compositions towards garnet is known from other studies (van Gool, 1992; Spear, 1993; Indares, 1995). Peak T is thus obtained from a biotite distal from garnet, and in general biotite peak compositions are best recovered from samples with a large biotite:garnet ratio (infinite reservoir concept). The biotite:garnet ratio in S-218 is ~4:1.

Retrograde T conditions represent the T at which retrograde geothermometric reactions ceased and retrograde P conditions represent the P at which the retrograde geobarometric reactions ceased. However it is known that in general Fe-Mg exchange reactions (eg. Grt-Bt, Grt-Opx) cease at lower T than net transfer reactions (eg. GOPQ, GASP) (Spear, 1992, 1993; Spear et al., 1991; Spear and Florence, 1992). Thus there is a potential for spurious retrograde P-T determinations unless the biotite and orthopyroxene reservoirs are sufficiently large that their compositions are virtually unaffected by the retrograde reaction. In this study retrograde P-T conditions were determined using the garnet rim compositions with the average of orthopyroxene and plagioclase rim compositions, and the average of matrix biotite compositions distal from garnet.

4.7.3 Quantitative P-T Results

Pressures and temperatures have been calculated using the TWQ computer program (Berman, 1991) and the solution models of Berman (1990) for garnet, Newton (1973) for orthopyroxene, McMullin et al. (1991) for biotite and Aranovich and Podlesskii (1989) for plagioclase, all of which are internally consistent with Berman's (1990) database. In the text, calculated temperatures and pressures have been rounded to the nearest 10^0C and 0.5 kbar.

4.7.3.1 Sample S-11

P-T estimates for sample S-11, using Grt-Opx and Grt-Opx-Pl-Qtz thermobarometry, are given below. Estimated peak P-T conditions from the right side of the profile (see Figure 4.8) are between 750-770^{0}C and 12-13 kbars, and those from the left side yielded lower conditions due to garnet consumption (see Figure 4.8). Calculated retrograde P-T conditions are between 670-710^{0}C and 8.5-10 kbar.

An approximate estimate of P-T conditions at some stage of the prograde metamorphic path can be made by combining garnet compositions from sector A1 with averaged orthopyroxene core and plagioclase core compositions from the matrix. This yields estimates of 510-540^{0}C and 6-9 kbar, but these results can only be considered approximate, being subject to several sources of error including retrograde reequilibration of orthopyroxene and plagioclase compositions. Nevertheless, the estimates are qualitatively in accord with a hairpin-shaped P-T, as is shown in Figure 4.10. They are also compatible with

the qualitative interpretation of the zoning profile and with the location of the XGrs and Fe/(Fe+Mg) reversals at the same distance from the garnet core, suggesting that peak P-T were achieved simultaneously. Thus the P-T path in Figure 4.10 reflects garnet growth over a range of temperatures, with partial preservation of growth zoning suggesting relatively short residence times at high T.

4.7.3.2 Sample S-218

P-T results for sample S-218 using Grt-Bt and Grt-Ky-Pl-Qtz mineral pairs are shown in Figure 4.11. Peak conditions, as determined from both sides of the garnet profile (see Figure 4.9), are between 750-800^{0}C and 12-15 kbar. Retrograde metamorphic conditions, are estimated between 600-690^{0}C and 8-10 kbar are assumed to be reasonably accurate due to the narrow retrograde rim on garnet.

An attempt was made to 'undo' the effects of retrograde diffusion zoning and visually project garnet compositions from the inner rim to the periphery of the garnet (see Figure 4.9) to obtain peak compositions before retrogression. Use of these projected composition estimates yields 'projected peak conditions' of 875-955^{0}C and 16.5-18 kbar. The estimated pressure range is comparable with pressure estimates elsewhere in southeast Gagnon terrane by Indares (1995), but the temperature estimates are incompatible with the mineral assemblage since at these temperatures biotite would be unstable with respect to orthopyroxene. In conclusion 'projected P-T estimates' are not considered to be reliable and are not considered further.

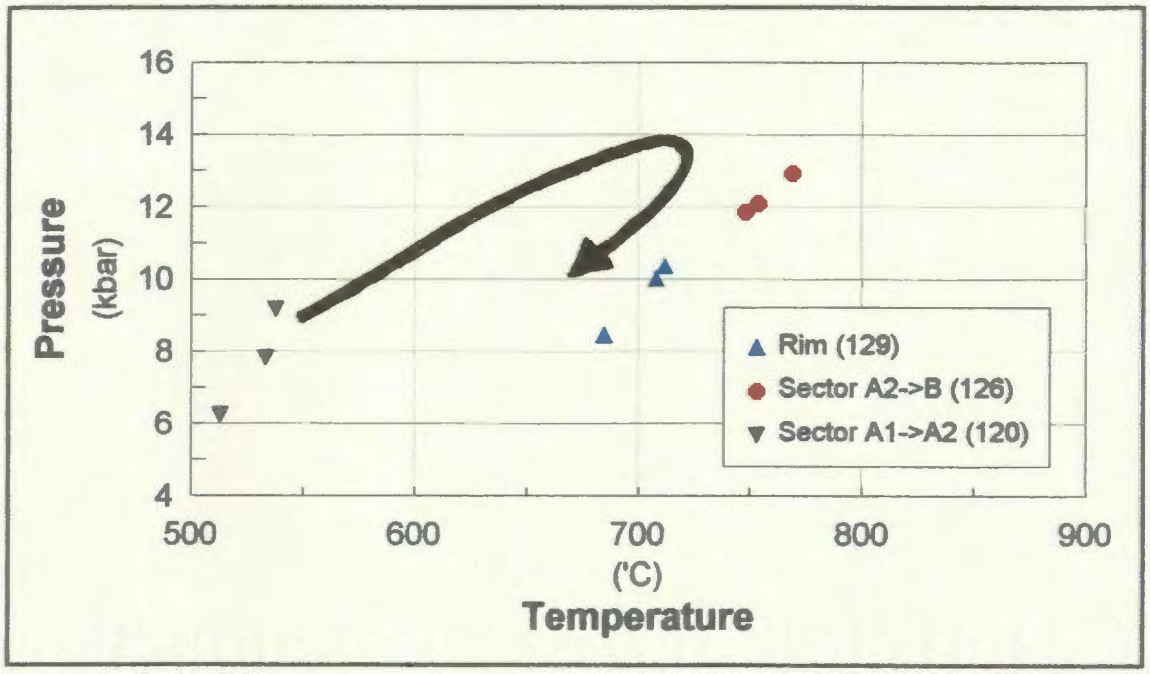

Figure 4.10 Grt-Opx and Grt-Opx-Pl-Qtz geothermobarometry in sample S-11 suggest peak P-T conditions between 750-770^{0}C and 12-13 kbars (red dots). Calculated retrograde P-T conditions using the garnet rim composition (blue triangles, see Table 4.5 and Figure 4.9) are between 670-710^{0}C and 8.5-10 kbar. P-T conditions calculated using the garnet compositions from sector A1 (black triangles) are considered to be too low (510-540^{0}C and 6.0-9.0 kbar). These results, combined with molar fraction trends, suggest partial homogenization at high temperature followed by rapid post-metamorphic peak exhumation. The location of sample S-11 is shown on Figure 4.1.

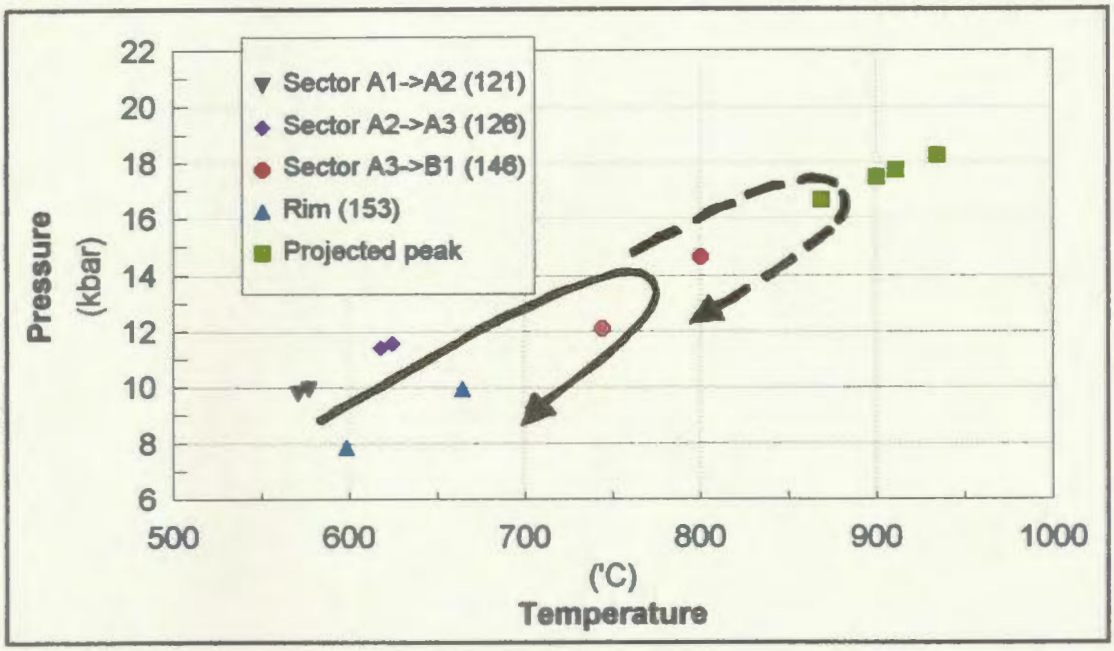

Figure 4.11 Grt-Bt and Grt-Ky-Qtz-Pl geothermobarometry in sample S-218 suggests rapid post-metamorphic peak uplift to lower temperatures. The hairpin shaped P-T-t path extends from 560-570°C and 10 kbar between sectors A1-A2 (black triangles, Table 4.8 and Figure 4.9) to P-T conditions of 750-800°C and 12-15 kbars using the garnet composition between sectors A3-B1 (red dots). An approximate estimate of P-T conditions at some stage of the prograde metamorphic path, at sector A2-A3 (purple diamonds), yielded an estimate of 610-640°C and 11-12 kbar. Although calculated P-T conditions from the garnet rim (blue triangles) are low (600-670°C and between 8-10 kbar), the amount of diffusional resetting due to retrogression is minimal (Figure 4.9). Hypothetical peak P-T conditions (green squares) using inferred compositions projected to the rims of the garnet grains (Figure 4.9) are between 875-955°C and 16.5-18 kbar. The sample location is indicated on Figure 4.1.

Preservation of garnet growth zoning at estimated peak temperatures of at least 710-800°C indicates that the total time spent at peak temperature must have been short. This inference is compatible with the hairpin-shaped P-T path and with the dramatic zoning profile in S-218. In particular, the concordance of the changes in the slope of the Fe/(Fe+Mg) and XGrs zoning trends (between sections A4 and B1 on Figure 4.9) suggest that maximum T and P were attained simultaneously. The narrow retrograde rims signify rapid cooling (i.e. rapid exhumation) along a hairpin-shaped P-T path.

4.7.4 Discussion and Comparison of Results

Thermobarometric results are presented in Table 4.9. Garnets in S-11 and S-218 grew under conditions of increasing P and T, which reached a minimum of 750-770°C and 12-13 kbars for S-11 from the Gueslis thrust sheet and 710-800°C at 12-15 kbars for S-218 from the Lac Gull thrust sheet. Given standard errors on P-T estimates of $\pm$50°C and $\pm$1 kbar, the results of the two samples are not significantly different from a statistical point of view. However it is interesting to note that garnets in S-11 are considerably more homogenized than in S-218, perhaps indicating that this sample experienced a P-T path with longer thermal relaxation during the initial stages of unloading. S-218, on the other hand, displays evidence of a very narrow retrograde rim suggesting that this thrust sheet was cooled and exhumed rapidly after attaining peak metamorphic conditions. A hairpin-shaped P-T path is consistent with these observations.

Table 4.9: Thermobarometric results.

	Sector A1-A2		Sector A2-A3		Sector Ax-B Peak		Sector B Rim		Sector Bx Projected Peak	
Sample	P (Kbar)	T (°C)	P (Kbar)	T (°C)	P (Kbar)	T (°C)	P (Kbar)	T (°C)	P (Kbar)	T (°C)
S-11	6-9	510-540			12-13	750-770	8.5-10	670-710		
S-218	10	560-570	11-12	610-640	12-15	750-800	8-10	600-690	16.5-18	875-955

Sectors represent the garnet composition used for thermobarometry, as indicated on the garnet zoning profiles (Figures 4.8 and 4.9) and P-T path (Figures 4.10 and 4.11).

4.8 CONCLUSION

This study of the metamorphic assemblages, microtextures and estimated P-T results has yielded several conclusions:

(a) Mineral assemblages in metapelitic rocks indicate that peak P-T conditions attained were not the same in each thrust sheet. In particular, the sub-assemblage muscovite-quartz is stable in LLTS, whereas the assemblage K-feldspar-kyanite-Liquid occurs in LGTS and muscovite-quartz-K-feldspar -kyanite occurrs in LLTS.

(b) On the basis of field relationships and microstructural relationships, the timing of deformation with respect to growth of garnet porphyroblasts is inferred to be syn -to post-D_1 and pre-syn D_2, and varied according to thrust sheet.

(c) P-T conditions estimated from two samples from Gueslis and Lac Don thrust sheets are in the range 710-800^{0}C and between 12-15 kbar. Of note is the fact that the P-T estimates for the two samples are similar, despite the different mineral assemblages in the two thrust sheets (see Section 4.7.4). This suggests that atleast one of the estimates does not represent peak conditions. Examination of the garnet zoning profiles in the two samples supports this interpretation, with the greater degree of post-peak homogenization in S-11 (GTS) suggesting that this thrust sheet underwent a longer residence time at high temperature, probably due to slow exhumation. In contrast, the zoning profile from S-218, with well preserved growth zoning despite the high metamorphic temperatures, is compatible with a hairpin-shaped P-T-t path suggesting rapid, tectonically-driven

exhumation. These P-T estimates and conclusions must be considered tentative because of the small number of samples analyzed.

CHAPTER 5: GEOCHRONOLOGY

5.1 INTRODUCTION

A cross-cutting granite was sampled in order to determine the age of the main metamorphism. The Grt-Cpx bearing pegmatitic granite (Section 2.2.8), which is intruded along the Gueslis shear zone (Section 3.4.2), is foliated and has well-defined boundaries that are generally concordant but locally cross-cut (see Plate 2.16) the main fabric ($S_0//S_1$) in the surrounding silicate - carbonate iron formation (Sokoman Formation). These field relationships suggest that granite emplacement was post-D_1 and pre-D_2. The sample location (SS-11B) is shown in Figure 4.1.

5.2 ANALYTICAL PROCEDURE

The standard techniques of crushing and grinding in a clean laboratory setting were followed. Mineral separation involved use of a Wilfley™ table, followed by heavy liquid separation, after which the heavy mineral separates were further magnetically separated using a Frantz™ LB-1 isodynamic separator. In selecting zircon crystals for analysis, the largest, clearest, most fracture-free grains were handpicked. Where this was not possible the altered margins and overgrowths were removed by air abrasion in pyrite following the method of Krogh (1982) to reduce the effects of surface-correlated Pb loss.

Isotope dilution was carried out by P. Valverde-Vaquero using a mixed ^{205}Pb-^{235}U tracer (Krogh and Davis, 1975), after which the samples were weighed

in Teflon micro-capsules and dissolved in a 0.5-1.0 ml HF and 5 drops 6N HNO_3 solution for five days at 220°C.

U and Pb were separated in ion-exchange columns, following the procedure outlined by Krogh (1973). The samples were then loaded into a single Re filament using H_3PO_4 and silica gel. Analyses were performed by G. Dunning using a VG 354 mass spectrometer. Data reduction and error propagation involved standard programs used in the geochronological laboratory at Memorial University.

5.3 RESULTS

Two fractions of crack-free, somewhat rounded, equant, colourless zircons were analysed. These are interpreted to be igneous morphologies. Zircons in both fractions were nonmagnetic and do not contain visible cores. Zircon grains in fraction 'Z1' contain numerous small inclusions, whereas in fraction 'A' were clear and did not contain inclusions.

The two fractions agree closely with each other and each is about 1% discordant, yielding $^{207}Pb/^{206}Pb$ ages of 993±2 and 997±2 Ma. A best-fit line through these points yields a U/Pb age of 995 ± 2 Ma, which is interpreted to be the age of igneous crystallization (Figure 5.1). Zircons in both fractions have high U and low Th contents, consistent with crystallization from hydrous S-type granite that developed as a result of Grenvillian crustal thickening. Uncorrected data are presented in Appendix B.

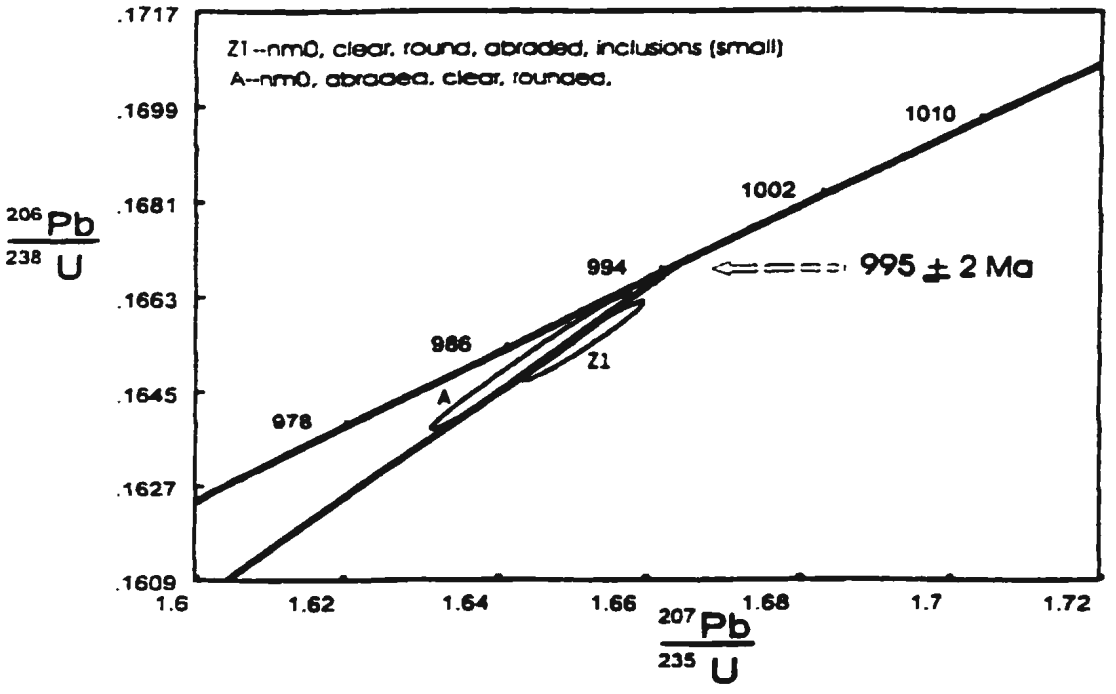

Figure 5.1 U/Pb concordia diagram for two fractions of abraded zircons from sample SS-11B, a syntectonic Grt-Cpx bearing S-type granite. $^{207Pb}/_{206Pb}$ ages of 993 ±2 and 997±2 Ma are each about 1% discordant. The U/Pb age of 995 ±2 Ma is interpreted to be the time of igneous crystallization which from field relations is interpreted to be syn -to post-D_1 and -pre D_2.

CHAPTER 6: TECTONIC MODEL FOR CENTRAL GAGNON TERRANE

6.1 INTRODUCTION: EXISTING TECTONIC MODEL FOR NORTHERN GAGNON TERRANE

Although a unique interpretation of the structural data is not possible, a hypothesis for the structural evolution can be proposed that is compatible with both the data and current models of thrust tectonics. Any model of the structural evolution of the map area must satisfy several constraints to be considered plausible. In addition to providing a reasonable method of generating the observed structural geometry, the model must be compatible with formation under the ambient metamorphic conditions (high pressure amphibolite facies in this case) and be consistent with current understanding of thrust tectonics in metamorphic fold-thrust belts. However, due to the very high strain in many rocks of the study area, no model of the Gagnon terrane can be more than schematic and permissive.

According to the existing thermotectonic model for the structural evolution of the northeastern part of Gagnon terrane (Rivers, 1983a; Brown et al., 1992; van Gool, 1992 and Rivers et al., 1993), northwest-directed thrust emplacement of the Molson Lake terrane on top of Gagnon terrane along a crustal ramp led to the development of fold-thrust belt in the latter. Based on the model of van Gool (1992), thrusting is inferred to have initiated within the graphitic Menihek Formation at the top of the Knob Lake Group. D_1 and D_2 fabrics, including D_1 and D_2 thrusts, the regional S_1 and S_2 planar fabrics, intrafolial F_1 folds and F_2 outcrop

-and map scale folds, are considered to have developed at this time (van Gool, 1992; Rivers et al., 1993)(Figure 6.1). These structures were confined to a thin-skinned, upper-level thrust system that progressively cut down through the supracrustal rocks resulting in their imbrication and accretion to the base of the thrust wedge (van Gool, 1992; Rivers et al., 1993)(Figure 6.2). Continued crustal convergence then led to the reactivation of Paleoproterozoic listric normal faults that had developed during the extensional phase of continent breakup and continent margin sedimentation on the Paleoproterozoic (Laurentia) continental margin (Figure 6.3). Such listric normal faults are presumed to have resulted in the large graben and horse structures on which the Knob Lake Group stratigraphic sequence was originally deposited (see Figure 2.1). Reactivation of these normal faults emplaced thick sheets of basement rocks into the base of the thrust wedge (van Gool, 1992; Rivers et al., 1993). The final stage of deformation is expressed by late Grenvillian (D_3) cross-folds (Roach and Duffell, 1974; Rivers, 1983a; Rivers and Chown, 1986; van Gool et al., 1988; van Gool, 1992) that are more pervasive towards the southeast.

Rivers (1983a, 1983b), Rivers and Chown (1986), Brown et al. (1992), van Gool (1992), Indares (1993, 1994, 1995) and Rivers et al. (1993) recognized that metamorphic grade increases towards the south in Gagnon terrane, suggesting that folding and thrusting resulted in the emplacement of higher grade thrust slices on top of lower grade slices and the development of an inverted metamorphic gradient through the thrust stack. van Gool (1992) suggested that

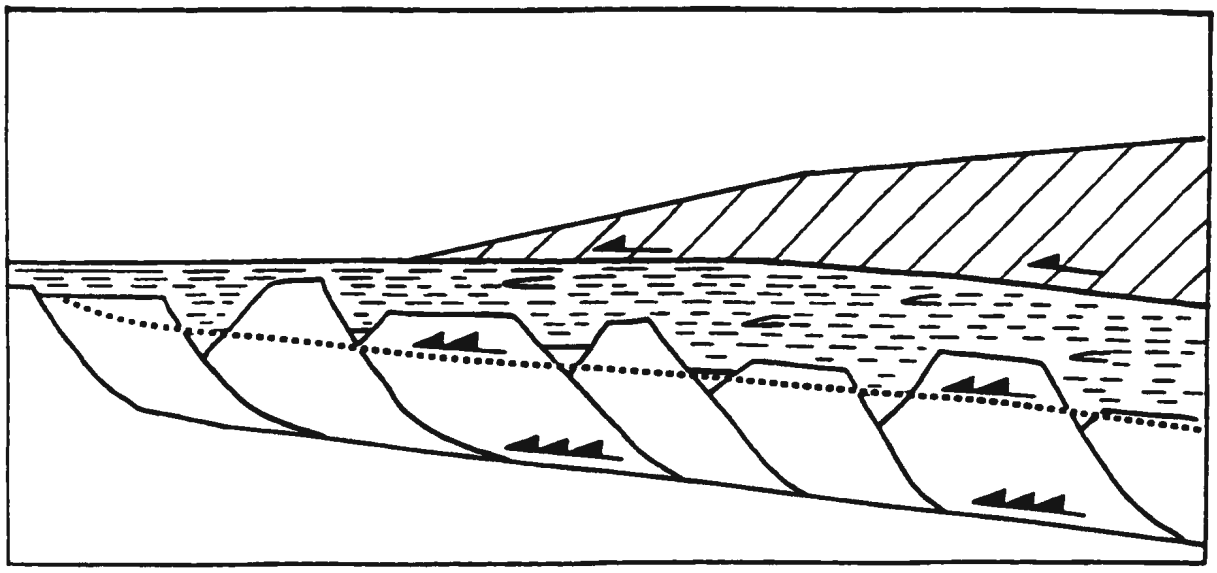

Figure 6.1 Based on the tectonic model for northeastern Grenville Province (van Gool, 1992; Rivers et al., 1993), northwest-directed overthrusting of the Molson Lake terrane over Gagnon terrane (thrust arrow with single tick) along a crustal scale ramp (e.g. Manicouagan Shear Belt, Rivers et al., 1993; Indares, 1994; Eaton et al., 1995). Overthrusting is inferred to have initiated development of critical topography and the formation of a fold-thrust belt within the upper levels of the Knob Lake Group metasedimentary sequence in Gagnon terrane (dashed area), such that it became progressively accreted to the base of the thrust stack (thrust arrows with double tick). Further thickening of the thrust wedge involved incorporation of basement rocks by inversion of the extended Paleoproterozoic continental margin (thrust arrows with three ticks) (van Gool, 1992; Rivers et al., 1993). D_1 and D_2 fabrics, including the regional S_1 planar fabric, intrafolial F_1 folds (represented by inverted 'v' shapes) and F_2 outcrop -and map scale folds, are thought to have developed at this time. Dashed line marks location of future thrusts. Ticks on thrust arrows indicate relative order of movement.

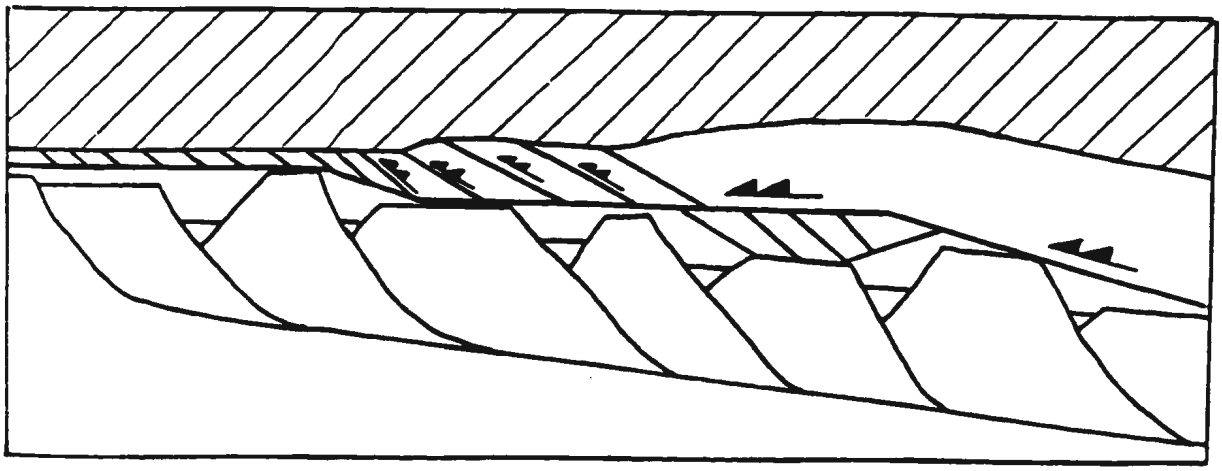

Figure 6.2 Detailed schematic cross-section of thin-skinned, upper-level thrust stack. Upper level thrusts were formed by accretion of supracrustal rocks to the base of the thrust wedge (van Gool, 1992). Modified from van Gool (1992) and Rivers et al. (1993).

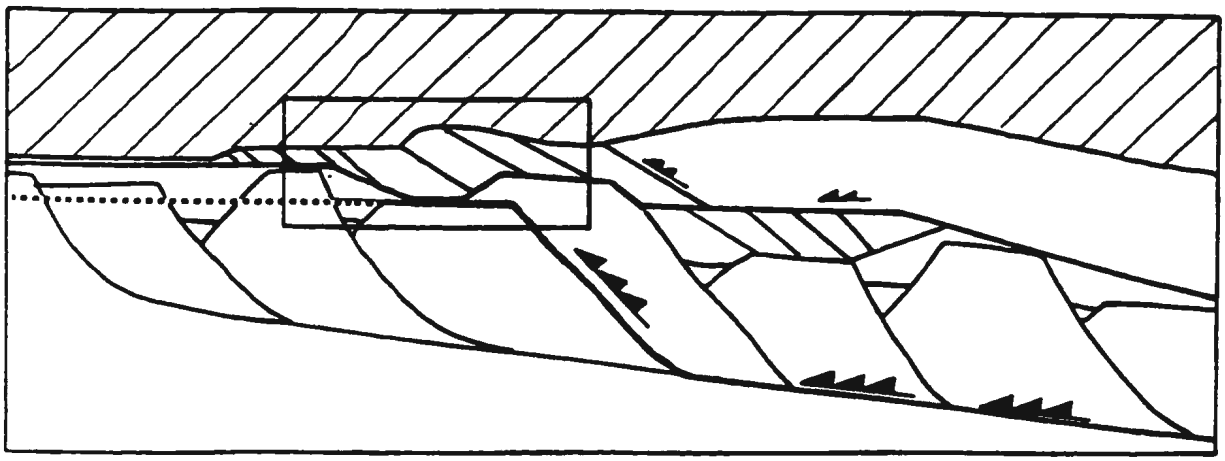

Figure 6.3 Detailed schematic cross-section of basement-involved thrusts. Continued crustal convergence led to the reactivation of listric normal faults that underlay the large graben and horse structures of the extensionally rifted Paleoproterozoic (Laurentia) continental margin on which the Knob Lake Group stratigraphic sequence was deposited (Figure 2.1). At some point, reactivated basement-involved thrusts (thrust arrows with three ticks) were accreted to the base of the thrust stack and inferred to have developed a northward dipping thrust ramp. Dashed line marks location of future thrusts. A detailed view of the area enclosed by the box is presented in Figure 6.4.

D_1 deformation, in Gagnon terrane, including the development of the main foliation, occurred under prograde metamorphic conditions when the rocks were in the footwall of the thrust wedge, whereas peak metamorphic conditions occurred during accretion to the base of the thrust shack. D_2 fabrics are inferred to have developed within thrust wedge rather than in the footwall (van Gool, 1992).

The occurrence of high pressure mineral assemblages and the predominance of ductility deformed rocks suggests that thrusting developed at mid to deep crustal levels (Rivers, 1983b; Brown et al., 1991, 1992; van Gool, 1992; van Gool and Cawood, 1994). In addition, hairpin-shaped P-T paths (van Gool, 1992) and the preservation of high pressure mineral assemblages (Rivers, 1983b; van Gool, 1992; Indares, 1993, 1994, 1995; Indares and Rivers, 1995; Indares and Dunning, 1997) suggest that post-peak metamorphic uplift and exhumation of deeply buried crust was not driven by simple static cooling associated with erosion (cf. England and Richardson, 1976), but must have been tectonically driven by uplift up a crustal-scale ramp (Rivers et al., 1993; Eaton et al., 1995).

6.2 COMPARISON WITH EXISTING MODEL

In the tectonic model of van Gool (1992) and Rivers et al. (1993), it was proposed that Molson Lake terrane was the structural load on Gagnon terrane during the Grenvillian Orogeny. Although the nearest outcrop of Molson Lake

terrane is at least 80 km away from the study area along the present erosion surface, this author follows this model in assuming that Molson Lake terrane, or some other thick thrust slice in a structurally equivalent position, was emplaced over Gagnon terrane from the southeast, thus creating a thrust wedge. Also following the existing model, it is assumed that the Gagnon terrane fold-thrust belt was accreted to this thrust wedge by basal accretion.

However, given these two initial points of similarity, the ensuing structural development of the fold-thrust belt in northern Gagnon terrane appears to have been different to that in the author's field area. The following points of difference are crucial. (i) Large-scale recumbent nappes, characteristic of the author's field area in central Gagnon terrane have not been recorded farther north. (ii) Most thrusts in the southern part of the author's map area dip towards the north and have southerly vergence, opposite to farther north in Gagnon terrane. (iii) Several major isoclinal folds (e.g. Lac Lamêlée synform, Lac Kendrick antiform) are overturned towards the south (i.e. backfolded) in the author's field area. (iv) The basal thrust sheet (Lac Hippocampe thrust sheet) comprises a wedge of inferred basement rocks. Such rock comprise only a minor part of the thrust wedge farther north. (v) Metamorphic grades are higher than in northern Gagnon terrane. From the structural field observations and metamorphic interpretations presented in Chapters 3 and 4, it seems reasonable to propose a revised tectonic model, based on that of Rivers and Chown (1986), van Gool (1992) and Rivers et al.

(1993), for the evolution of the fold-thrust and nappe belt in north-central Gagnon terrane. The contribution of this study to the evolving tectonic model is schematically illustrated in Figure 6.4 which is in continuation of Figures 6.1 to 6.3.

6.3 REVISED TECTONIC MODEL FOR CENTRAL GAGNON TERRANE

In this part of Gagnon terrane, provisionally termed the nappe belt (Rivers et al., 1993), Rivers and Chown (1986) reported large scale ductile interference structures defined by structural and stratigraphic trends in the Knob Lake Group sequence (e.g. Lac Gull thrust sheet, Figure 3.13A). According to their model, these recumbent nappes developed as a result of northwest-directed thrust emplacement of Molson Lake terrane over the foreland (Rivers and Chown, 1986; Rivers et al., 1993) resulting in progressive burial of Gagnon terrane. The rise in metamorphic grade due to crustal thickening was synchronous with polyphase ductile deformation of the Knob Lake Group sequence (KLG) and the upper part of the Archean basement gneisses.

In general, a cross-section across a collisional orogenic belt or foreland fold-and-thrust belt (e.g. Scandinavian Caledonides, Gee et al., 1985; Roberts and Gee, 1985; Stephens and Gee, 1985), shows a transition from thin thrust sheets in the foreland to strongly deformed nappe complexes of infolded basement and cover in the hinterland. The style and type of deformation within the fold-and-thrust belt is dependent primarily on the ambient rock temperature,

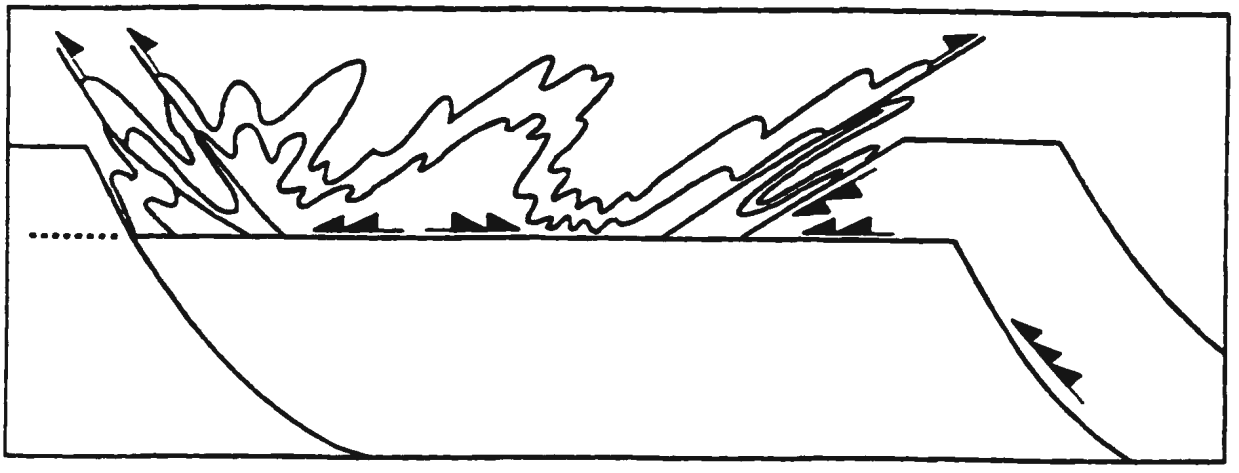

Figure 6.4 Detailed view of an area shown in Figure 6.3 illustrating the large scale fold structures, in the area now termed the Gagnon terrane nappe belt (Rivers et al., 1993). Forward propagation of the basement-involved thrust ramp (thrust arrows with three ticks and dashed line marking the location of future thrusts) is believed to have resulted in backthrusting (thrust arrows with double tick) and backfolding within the overlying Knob Lake Group. Backthrusting of the Knob Lake Group over the basement thrust wedge is also inferred to have developed northward dipping F_1 synclines (e.g. Lac Lamêlée syncline). Although not shown, the final stages of deformation are expressed by late (D_3) collapse structures and D_4 large scale cross-folds (Roach and Duffell, 1974; Rivers, 1983a; Rivers and Chown, 1986; van Gool et al., 1988; van Gool, 1992) that are more pervasive towards the southeast.

strain rate and degree of fluid involvement in the thrust sheets (Coward and Potts, 1985). Brittle deformation mechanisms are more prevalent in the upper thrust system (e.g. near the Grenville Front), whereas closer to metamorphic core (e.g. southern Gagnon terrane) the deformation can be a combination of brittle and ductile mechanisms depending on the ambient temperature and strain rate during movement (Hatcher and Williams, 1986).

The results of this study show that backfolding and backthusting are the prevalent styles of deformation within this part of the nappe belt of central Gagnon terrane. Map-scale backfolding and backthrusting were previously described by Rivers and Chown (1986) in the area near Mount Wright, where backfolds and the fanning of axial surfaces (D_2) were proposed to have developed as a result of a basement buttress that prevented the forward propagation of D_1 thrusts at -or near the basement -KLG interface. Elsewhere near the Grenville Front, backthrusting was locally recognized by Brown (1990), Brown et al., (1991) and van Gool (1992), where it was attributed to extension, a result of gravitational instability due to overthickening within the foreland-verging stack. However no evidence of extensional collapse was observed within the author's field area. As shown in the cross sections (see Figures 3.12 to 3.14), several major isoclinal folds (e.g. Lac Lamêlée synform, Lac Kendrick antiform) are overturned towards the south, and many thrusts, especially those in the southern part of the map area, dip towards the north and truncate folds implying

that they formed during both D_1 and D_2.

As described in Section 3.9.6, the most southerly thrust sheet in the area, the Lac Hippocampe thrust sheet, is inferred to comprise a wedge of variably reworked Archean basement rocks (Figure 6.4). On structural grounds it is reasonable to propose that the northerly movement of a thick, inferred basement wedge was the driving force for the orientation of this part of the fold-thrust belt. This wedge is interpreted to lie at the base of the thrust stack, and has created a wedge over which all other thrust sheets were backfolded and backthrust. Continued northerly movement of the thrust wedge is inferred to have caused the propagation of the thrusts towards the north with concurrent accumulation of N-dipping thrust sheets into the front of the thrust wedge, such that the oldest thrusts are those in the south and that thrusting becomes progressively younger towards the north. Some of the thrust faults may have involved reactivation of normal faults that controlled the original sedimentary architecture of the basin, as is illustrated schematically in a palinspastic section (see Figure 2.1). Basin inversion is a characteristic feature of high level fold-thrust belts (Coward and Potts, 1985) and was likely operative in the deep crust in Gagnon terrane as well.

D_3 Recumbent refolding of outcrop scale D_1 and D_2 structures is interpreted to be a late phase of Grenvillian deformation in central Gagnon terrane. It is presumed that the cessation or decrease of collisonal compressive forces may have decreased the rate of frontal accretion at the base of the thrust

wedge resulting in gravitational instability and collapse of the overthickened thrust wedge. The final stage of deformation is expressed by late Grenvillian (D_4) cross-folds (Roach and Duffell, 1974; Rivers, 1983a; Rivers and Chown, 1986; van Gool et al., 1988; van Gool, 1992) that resulted in the upright variably plunging map-scale folds that are best expressed in the southern part of the study area.

The metamorphic results from this study are broadly compatible with the revised tectonic model presented above. Mineral assemblages suggest some variation in metamorphic grade between thrust sheets, although the limited P-T estimates both indicate conditions of ~750^{0}C at 13kbars. Garnet zoning profiles from the more northerly thrust sheets (i.e. Lac Don) are more homogenized than those from Lac Gull thrust sheet, suggesting that P-T conditions remained at high temperatures for a prolonged period of time, i.e. experienced a P-T path with longer thermal relaxation during initial stages of unloading. In contrast, growth zoning in garnets from the Lac Gull thrust sheet is well preserved and profiles have only narrow rims affected by diffusional retrograde resetting. The inferred "hair-pin" shaped P-T path (Section 4.7.3) is consistent with the revised tectonic model presented above, suggesting that these rocks were part of a thick northward-tapering thrust wedge that was cooled and exhumed rapidly soon after attainment of peak metamorphic conditions (indicative of relatively fast unloading compatible with tectonically driven exhumation). The observation that peak

metamorphic conditions were syn D_1 and/or pre-syn D_2 also fits the general model, with post D_2 deformation taking place in the hanging wall of the thrust wedge (van Gool, 1992; Rivers et al., 1993).

These results are consistent with U/Pb geochronology from an S-type syntectonic (post-D_1 and pre-D_2) granite (Section 5.3), that developed as a result of Grenvillian crustal thickening.

6.4 CONCLUSION

Although the fold-thrust belt of Gagnon terrane immediately south of the Grenville Front has been well documented, there has not been a modern structural analysis of the nappe belt that tectonically overlies the foreland fold-thrust belt. The objective of this thesis was to investigate the structural and metamorphic relationships between mid- to deep crustal level folding and thrusting processes in the deeply eroded nappe belt in central Gagnon terrane. These results, when compared with the well-studied areas farther to the north and south, will limit the structural and metamorphic variations across the Gagnon terrane.

In summary the results of this study are as follows:

(a) The field area is characterized by large-scale recumbent nappes.

(b) The thrust stack on a whole dips towards the north and verges towards the south.

(c) Thrusting becomes progressively younger towards the north.

(d) The Lac Hippocampe thrust sheet is inferred to be a wedge composed of variably reworked Archean basement rocks over which all other thrust sheets were backthrust towards the south.

Metamorphic results from this study indicate that peak metamorphic conditions increased from north to south, and that the more northerly thrust sheets are presumed to have remained at higher temperatures for a prolonged period of time, and perhaps had experienced a P-T path with longer thermal relaxation during initial stages of unloading. In contrast, P-T results from the more southerly thrust sheets suggest that the rocks were overlain by a thick thrust wedge and then cooled and exhumed rapidly, soon after attaining their peak metamorphic conditions. A hairpin shaped P-T path is consistent with these observations.

This data is compatible with existing models for northeastern Grenville Province (Rivers, 1983a, 1983b; Rivers and Chown, 1986; Brown et al., 1992; van Gool, 1992; Rivers et al., 1993), and provides the first U/Pb age for deformation in the fold-thrust belt. According to the tectonic model, northwest-directed uplift of Molson Lake terrane along a crustal-scale ramp is interpreted to be responsible for the development of a foreland fold-thrust belt with an inverted metamorphic gradient in the thrust stack, and the preservation of grade mineral assemblages (Indares, 1993; Indares and Rivers, 1995; Indares and Dunning, 1997).

REFERENCES

Aranovich, L.Y. and Podlesskii, K.K., 1989. Geothermobarometry of high-grade metapelites: simultaneously operating reactions. In: J.S. Daly, R.A. Cliff and B.W.D. Yardley (eds.), Evolution of Metamorphic Belts. Geological Society of America Special Publication 43, pp. 45-62.

Baer, A.J., 1974. Grenville geology and plate tectonics. Geoscience Canada, 1: 54-61.

Baer, A.J., 1976. The Grenville Province in Helikian times: a possible model of evolution. Royal Society of London Philosophical Transactions, 280: 499-515.

Baer, A.J., 1981. A Grenvillian model of Proterozoic plate tectonics. In: A. Kroner (ed.), Precambrian Plate Tectonics. Elsevier, Amsterdam, pp. 353-385.

Bell, T.H., 1985. Deformation partitioning and porphyroblast rotation in metamorphic rocks: a radical reinterpretation. Journal of Metamorphic Geology, 3: 109-118.

Bell, T.H., Fleming, P.D. and Rubenach, M.J., 1986. Porphyroblast nucleation, growth and dissolution in regional metamorphic rocks as a function of deformation partitioning during foliation development. Journal of Metamorphic Geology, 4: 37-67.

Berman, R.G., 1990. Mixing properties of Ca-Mg-Fe-Mn garnets. American Mineralogist, 75: 328-344.

Berman, R.G., 1991. Thermobarometry using multi-equilibrium calculations: a new technique, with petrological applications. Canadian Mineralogist, 29: 833-855.

Brown, D., 1990. A structural analysis of the Grenville Front Zone, northeast Gagnon terrane, Labrador. M.Sc. thesis, Memorial University of Newfoundland, 190pp.

Brown, D., van Gool, J., Calon, T. and Rivers, T., 1991. The geometric and kinematic development of the Emma Lake thrust stack, Grenville Front, southwestern Labrador. Canadian Journal of Earth Sciences, 28: 136-144.

Brown, D., Rivers, T. and Calon, T., 1992. A structural analysis of a metamorphic fold and thrust belt, northeast Gagnon terrane, Grenville province. Canadian Journal of Earth Sciences, 29: 1915-1927.

Brown, R.L., Chappell, J.F., Moore, J.M., Jr., and Thompson, P.H., 1975. An ensimatic island arc and ocean closure in the Grenville Province of southeastern Ontario, Canada. Geoscience Canada, 2: 141-144.

Clarke, P.J., 1967. Preliminary Report on the Gras Lake-Félix Lake Area, Saguenay Electorial District. Ministère des Richesses Naturelles du Québec. Geological Report 129, 61pp.

Clarke, P.J., 1968. Basement gneisses in the Mount Wright-Mount Reed area, Quebec. Geological Association of Canada Proceedings, 19: 22-30.

Clarke, P.J., 1977. Preliminary Report on the Gagnon Area. Ministère des Richesses Naturelles du Québec. Geological Report 178, 79pp.

Connelly, J.N., van Gool, J. and Rivers, T., 1989. Molson Lake Terrane, a new terrane in the Parautochthonous Belt of the Grenville Province in southwestern Labrador. GAC-MAC Joint Annual Meeting, Montreal 1989, program with abstracts, 14: A23.

Connelly, J.N. and Heaman, L., 1993. U-Pb geochronological constraints on the tectonic evolution of the Grenville Province, western Labrador. Precambrian Research, 63: 123-142.

Corfu, F. and Easton, R.M., 1995. U-Pb geochronology of the Mazinaw terrane, an imbricate segment of the Central Metasedimentary Belt, Grenville Province, Ontario. Canadian Journal of Earth Sciences, 32: 959-976.

Corrigan, D., Culshaw, N.G. and Mortensen, J.K., 1994. Pre-Grenvillian evolution and Grenvillian overprinting of the Parautochthonous Belt in Key Harbour, Ontario: U-Pb and field constraints. Canadian Journal of Earth Sciences, 31: 583-596.

Coward, M.P. and Potts, G.J., 1985. Fold nappes: examples from the Moine Thrust zone. In: D.G. Gee and B.A. Sturt (eds.), The Caledonian Orogen - Scandinavia and Related Areas. John Wiley & Sons, New York, pp. 1147-1158.

Cygan, R.T. and Lasaga, A.C., 1985. Self diffusion of magnesium on garnet at 750 to 900°C. American Journal of Science, 285: 328-350.

Davidson, A., 1984. Identification of ductile shear zones in the southwestern Grenville Province of the Canadian Shield. In: A. Kroner and R. Greiling (eds.), Precambrian Tectonics Illustrated. E. Schweizerbart'sche Verlagsbuchhandlung, Stuttgart, pp. 263-279.

Davidson, A., 1986. Grenville Front relationships near Killarney, Ontario. In: J.M. Moore, Jr., A. Davidson and A.J. Baer (eds.), The Grenville Province. Geological Association of Canada Special Paper 31, pp. 61-74.

Davidson, A., 1990. Evidence for eclogite metamorphism in the southwest Grenville Province, Ontario. In: Current Research, Part C, Geological Survey of Canada, Paper 90-1C, pp. 113-118.

Davidson, A., 1991. Metamorphism and tectonic setting of gabbroic and related rocks in the Central Gneiss Belt, Grenville Province, Ontario. GAC-MAC Joint Annual Meeting, Toronto 1991, Field Trip A2 Guidebook, 57pp.

Davidson, A., Culshaw, N.G. and Nadeau, L., 1982. A tectono-metamorphic framework for part of the Grenville province, Parry Sound region, Ontario. In: Current Research, Part A, Geological Survey of Canada. Paper 82-1A, pp. 175-190.

Dewey, J.F. and Burke, K.C.A., 1973. Tibetan, Variscan and Precambrian basement reactivation: products of continental collision. Journal of Geology, 81: 683-692.

Dimroth, E., 1968. Evolution of the central segment of the Labrador Geosyncline, Part I: stratigraphy, facies and paleogeography. Neues Jahrbuch fur Geologie und Palaontologie Abhandjungen, 130: 247-274.

Dimroth, E., 1971. The evolution of the central segment of the Labrador Geosyncline, Part II: the ophiolitic suite. Neues Jahrbuch fur Geologie und Palaontologie Abhandjungen, 137: 209-248.

Dimroth, E., 1972. The Labrador Geosyncline revisited. American Journal of Science, 272: 487-506.

Dimroth, E., 1978. Labrador Trough area (54°30' - 56°30'). Ministère des Richesses Naturelles du Québec. Geological Report 193, 278pp.

Dimroth E., Barager, W.R.A., Bergeron, R. and Jackson, G.D., 1970. The filling of the Circum-Ungava geosyncline. In: A.J. Baer (ed.), Symposium on Basins and Geosynclines of the Canadian Shield. Geological Survey of Canada Paper 70-40, pp. 45-142.

Donaldson, J.A., 1966. Marion Lake Map-Area, New Quebec-Newfoundland. Geological Survey of Canada Memoir 338, 85pp.

Duffell, S. and Roach, R.A., 1959. Mount Wright, Quebec-Newfoundland. Geological Survey of Canada Map 6-1959.

Eaton, D.W., Hynes, A., Inderes, A. and Rivers, T., 1995. Seismic images of eclogites, crustal-scale extension, and Moho relief in the eastern Grenville province, Quebec. Geology, 23: 855-858.

England, P.C. and Richardson, S.W., 1977. The influence of erosion upon the mineral facies of rocks from different metamorphic environments. Geological Society of London Journal 134: 201-213.

Fahrig, W.F., 1967. Shabogamo Lake Map Area: Newfoundland-Labrador and Quebec 23G E $^{1}/_{2}$. Geological Survey of Canada Memoir 354, 23pp.

Fahrig, W.F., Christie, K.W. and Schwarz, E.J., 1974. Paleomagnetism of the Mealy Mountains anorthosite suite and of the Shabogamo gabbro, Labrador, Canada. Canadian Journal of Earth Sciences, 11: 18-29.

Florence, F.P. and Spear, F.S., 1989. Volume diffusion in garnet: effects on P-T path calculations. EOS, 70: 492.

Gastil, G. and Knowles, D.M., 1960. Geology of the Wabush area, southwestern Labrador and eastern Quebec, Canada. Geological Society of America Bulletin, 71: 1243-1254.

Gee, D.G., Guezou, J.C., Roberts, D. and Wolff, F.C., 1985. The central-southern part of the Scandiniavian Caledonides. In: D.G. Gee and B.A. Sturt (eds.), The Caledonian Orogen - Scandinavia and Related Areas. John Wiley & Sons, New York, pp. 109-134.

Green, A.G., Milkereit, B., Davidson, A., Spencer, C., Hutchinson, D.R., Cannon, W.F., Lee, M.W., Agena, W.F., Behrendt, J.C. and Hinze, W.J., 1988. Crustal structure of the Grenville Front and adjacent terranes. Geology, 16: 788-792.

Gross, G.A., 1968. Geology of iron deposits in Canada, vol. III: Iron ranges of the Labrador Geosyncline. Geological Survey of Canada, Economic Geology Report 22, 179pp.

Guidotti, C.V. and Dyar, M.D., 1991. Ferric iron in metamorphic biotite and its petrologic and crystallochemical implications. American Mineralogist, 76: 161-175.

Hanmer, S.K., 1984. The potential use of planar and elliptical structures as indicators of strain regime and kinematics of tectonic flow. In: Current Research, Part B, Geological Survey of Canada, Paper 84-1B, pp. 133-142.

Hatcher, R.D. and Williams, R.T., 1986. Mechanical model for single thrust sheets. Geological Society of America, 97: 975-985.

Hoffman, P.F., 1988. United plates of America, the birth of a craton: Early Proterozoic assembly and growth of Laurentia. Annual Revue of Earth Planet Sciences, 16: 543-603.

Hollister, L.S., 1966. Garnet zoning: an interpretation based on the Rayleigh fractionation model. Science, 154: 1647-1651.

Irving, E., Emslie, R.F. and Ueno, H., 1974. Upper Proterozoic paleomagnetic poles from Laurentia and the history of the Grenville Structural Province. Journal of Geophysical Research, 79: 5491-5502.

Indares, A., 1993. Eclogitized gabbros from the eastern Grenville Province: textures, metamorphic context and implications. Canadian Journal of Earth Sciences, 30: 159-173.

Indares, A., 1994. Lithotectonic characteristics of the eclogite-bearing Manicouagan shear belt, eastern Grenville Province. In: Abitibi-Grenville Transect, Lithoprobe Report 41, pp. 83-85.

Indares, A., 1995. Metamorphic interpretation of high-pressure metapelites with preserved growth zoning in garnet, eastern Grenville Province, Canadian Shield. Journal of Metamorphic Geology, 13: 475-486.

Indares, A. and Martignole, J., 1989. The Grenville Province south of Val-d'Or, Quebec. Tectonophysics, 157: 221-239.

Indares, A. and Rivers, T., 1995. Textures, metamorphic reactions and thermobarometry of eclogitized metagabbros: a Proterozoic example. European Journal of Mineralogy, 7: 43-56.

Indares, A. and Dunning, G., 1997. Coronitic metagabbro and eclogite from the Grenville Province of western Quebec: interpretation of U-Pb geochronology and metamorphism. Canadian Journal of Earth Sciences, 34: 891-901.

Jamieson, R.A. and Vernon, R., 1987. Timing of porphyroblast growth in the Fleur de Lys Supergroup, Newfoundland. Journal of Metamorphic Geology, 5: 273-288.

Kretz, R., 1983. Symbols for rock-forming minerals. American Mineralogist, 68: 277-279.

Krogh, T.E., 1973. A low contamination method for hydrothermal decomposition of zircon and extraction of U and Pb for isotopic age determinations. Geochemica et Cosmochimica Acta, 37: 485-494.

Krogh, T.E., 1982. Improved accuracy of U-Pb zircon ages by the creation of more concordant systems using air abrasion technique. Geochemica et Cosmochimica Acta, 46: 637-649.

Krogh, T.E. and Davis, G.L., 1975. The production and preparation of 205Pd for the use as a tracer for isotope dilution alalyses. Carnegie Institution of Washington Yearbook, 74: 416- 417.

McMullin, D.W.A., Berman, R.G. and Greenwood, H.J., 1991. Calibration of the SGAM thermobarometer for pelitic rocks using data from phase equilibrium experiments and natural assemblages. Canadian Mineralogist, 29: 889-908.

Moores, E.M., 1991. Southwest U.S.-East Antarctic (SWEAT) connection: A hypothesis. Geology, 19: 425-428.

Murphy, D.L., 1959. Preliminary Report on the Mount Wright area. Saguenay County. Ministère des Mines de Québec. Geological Report 380, 11pp. (with map No. 1260).

Newton, R.C., 1983. Geobarometry of high-grade metamorphic rocks. American Journal of Science, 283-A: 1-28.

Perreault, S., 1994. Géologie de la région du lac Gensart. Ministère des Ressources Naturelles. Gouvernement du Québec. Rapport MB 94-33, 45pp.

Phillips, L.S., 1958. Preliminary Report on the Tuttle Lake area, Saguenay County. Ministère des Mines de Québec. Geological Report 377, 7pp. (with map No. 1234).

Phillips, L.S., 1959. Preliminary Report on the Peppler Lake area (east half), Saguenay County. Ministère des Mines de Québec. Geological Report 401, 12pp. (with map No. 1290).

Plint, H.E. and Jamieson, R.A., 1989. Microstructure, metamorphism, and tectonics of the western Cape Breton Highlands, Nova Scotia. Journal of Metamorphic Geology, 7: 407-424.

Ramsay, J.G., 1967. Folding and Fracturing of Rocks. McGraw-Hill, New York, 568pp.

Rivers, T., 1978. Geological mapping of the Wabush-Labrador City area, southwestern Labrador. In: Report of activities for 1977, Mineral Development Divison, Newfoundland Department of Mines and Energy, Report 78-1, pp. 44-50.

Rivers, T., 1980. Geological mapping in the Wabush Lake area, southwestern Labrador. In: Current research, Mineral Development Division, Newfoundland Department of Mines and Energy, Report 80-1, pp. 206-121.

Rivers T., 1983a. The northern margin of the Grenville Province in western Labrador - anatomy of an ancient orogenic front. Precambrian Research, 22: 41-73.

Rivers, T., 1983b. Progressive metamorphism of pelitic and quartz-feldspathic rocks in the Grenville Province of western Labrador - tectonic implications of bathozone 6 assemblages. Canadian Journal of Earth Sciences, 20: 1791-1804.

Rivers, T., 1992. Contrasting styles of crustal shortening in northern Grenville Province. Friends of the Grenville workshop, 1992. Program and abstracts.

Rivers, T. and Chown, E.H., 1986. The Grenville orogen in eastern Quebec and western Labrador - definition, identification and tectonometamorphic relationships of autochthonous, parautochthonous and allochthonous terranes. In: J.M. Moore, Jr., A. Davidson and A.J. Baer (eds.), The Grenville Province. Geological Association of Canada Special Paper 31, pp. 31-50.

Rivers, T. and Mengel, F.C., 1988. Contrasting assemblages and petrogenetic evolution of corona and noncorona gabbros in the Grenville Province of western Labrador. Canadian Journal of Earth Sciences, 25: 1629-1648.

Rivers, T., Martignole, J., Gower, C.F. and Davidson, A., 1989. New tectonic divisions of the Grenville Province, Southeast Canadian Shield. Tectonics, 8: 63-84.

Rivers, T., van Gool, J. and Connelly, J., 1993. Contrasting styles of crustal shortening in the northern Grenville orogen. Geology, 21: 127-1130.

Roach, R.A. and Duffell, S., 1968. The Pyroxene granulites of the Mount Wright map-area, Quebec-Newfoundland. Geological Survey of Canada Bulletin 162, 83 pp.

Roach, R.A. and Duffell, S., 1974. Structural analysis of the Mount Wright map-area, southernmost Labrador Trough, Quebec, Canada. Geological Society of America Bulletin, 85: 947-962.

Roberts, D. and Gee, D.G., 1985. An introductiopn to the structure of the Scandanivian Caledonides. In: D.G. Gee and B.A. Sturt (eds.), The Caledonian Orogen - Scandinavia and Related Areas, John Wiley & Sons, New York, pp. 55-68.

Rosenfeld, J.L., 1970. Rotated garnets in metamorphic rocks. Geological Society of America Special Paper 129, 105pp.

Schoneveld, C., 1977. A study of typical inclusion patterns in strongly paracrystaliine rotated garnets. Tectonophysics, 39: 453-460.

Selverstone, J. and Spear, F., 1985. Metamorphic P-T paths from pelitic schists and greenstones in the southwest Tauern Window, eastern Alps. Journal of Metamorphic Geology, 3: 439-465.

Sinclair, A.J., 1961. Preliminary Report on the Peppler and Cailleteau Lakes area (west half), Saguenay County. Ministère des Mines de Québec. Geological Report 451, 11pp.

Spear, F.S., 1988. Metamorphic fractional crystallization and internal metasomatism by diffusional homogenization of zoned garnets. Contributions to Mineralogy and Petrology, 99: 507-517.

Spear, F.S., 1989. Petrologic determination of metamorphic pressure-temperature-time paths. In: F.S. Spear and S.M. Peacock (eds.), Metamorphic Pressure-Temperature-Time Paths. Short Course in Geology, American Geophysical Union, Washington, pp. 1-55.

Spear, F.S., 1991. On the interpretation of peak metamorphic temperatures in light of garnet diffusion during cooling. Journal of Metamorphic Geology 9: 379-388.

Spear, F.S., 1992. Thermobarometry and P-T paths from granulite facies rocks: an introduction. Precambrian Research, 92: 201-207.

Spear, F.S., 1993. Metamorphic Phase Equilibria and Pressure-Temperature-Time Paths. Mineralogical Society of America, Washington, 799pp.

Spear, F.S. and Cheney, J.T., 1989. A petrogenetic grid for pelitic schists in the system SiO2-Al2O3-FeO-MgO-K2O-H2O. Contributions to Mineralogy and Petrology, 101: 149-164.

Spear, F.S., Hickmott, D.D. and Selverstone, J., 1990. Metamorphic consequences of thrust emplacement, Fall Mountain, New Hampshire. Geological Society of America Bulletin, 102: 1344-1360.

Spear, F.S., Kohn, M.J., Florence, F.P. and Menard, T., 1991. A model for garnet and plagioclase growth in pelitic schists: implications for the thermobarometry and P-T path determinations. Journal of Metamorphic Geology, 8: 683-696.

Spear, F.S. and Florence, F.P., 1992. Thermobarometry in granulites: pitfalls and new approaches. Precambrian Research, 55: 209-241.

Spry, A., 1969. Metamorphic Textures. Pergamon Press, Oxford, 350pp.

Stephens, M.B. and Gee, D.G., 1985. A tectonic model for the evolution of the eugeoclinal terranes in the central Scandiavian Caledoniedes. In: D.G. Gee and B.A. Sturt (eds.), The Caledonian Orogen - Scandinavia and Related Areas. John Wiley & Sons, New York, pp. 953-978.

Stockwell, C.H., 1961. Structural provinces, orogenies, and time classification of rocks of the Canadian Precambrian Shield. In: J.A. Lowdon (ed.), Age Determinations by the Geological Survey of Canada. Report 2: Isotopic Ages. Geological Survey of Canada Paper 61-17, pp. 108-118.

Stockwell, C.H., 1964. Fourth report on structural provinces, orogenies, and time classification of rocks of the Canadian Precambrian Shield. In: Age Determinations and Geological Studies. Part II: Geological Studies. Geological Survey of Canada Paper 64-17, pp. 1-21.

Thompson, A.B. and Algor, J.R., 1977. Model systems for anatexis of pelitic rocks. 1. Theory of melting reactions in the system $KAlO_2$-$NaAlO_2$-Al_2O_3 -SiO_2-H_2O. Contributions to Mineralogy and Petrology, 63: 247-269.

Thompson, A.B. and Tracy, R.J., 1979. Model systems for anatexis of pelitic rocks. 2. Facies series melting and reactions in the system CaO-$KAlO_2$-$NaAlO_2$-Al_2O_3-SiO_2-H_2O. Contributions to Mineralogy and Petrology, 70: 429-438.

Tracy, R.J., 1982. Compositional zoning and inclusions in metamorphic minerals. Reviews in Mineralogy, 10: 355-397.

van Gool, J., 1992. The Grenville Front foreland fold-and-thrust belt in southwestern Labrador: Mid-crustal structural and metamorphic configuration of a Proterozoic orogenic thrust wedge. PhD. thesis, Memorial University of Newfoundland, 368 pp.

van Gool, J., Calon, T.J. and Rivers, T., 1987. Preliminary report on the Grenville Front Tectonic Zone, Bruce Lake area, western Labrador. In: Current Research, Part A, Geological Survey of Canada Paper 87-1A, pp. 435-442.

van Gool, J., Calon, T.J. and Rivers, T., 1988. Thrust tectonics along the Grenville Front Zone in western Labrador. GAC-MAC Joint Annual Meeting, St. John's 1988, program with abstracts, 13: A129.

van Gool, J. and Cawood, P., 1994. Frontal versus basal accretion and contrasting particle paths in metamorphic thrust belts. Geology 22: 51-54.

Vernon, R.H., 1989. Porphyroblast-matrix microstructural relationships: recent approaches and problems. In: J.S. Daly, R.A. Cliff and B.W.D. Yardley (eds.), Evolution of Metamorphic Belts. Geological Society of America Special Publication 43, pp. 83-102.

Vielzeuf, D. and Holloway, J.R., 1988. Experimental determination of the fluid absent melting relations in the pelitic system. Contributions to Mineralogy and Petrology, 98: 257-276.

Walton, M.S. and de Waard, D., 1963. Orogenic evolution of the Precambrian in the Adirondack Highlands, a new synthesis. Koninklijke Nederlandse Akademie van Wetenschappen Proceedings, 66: 98-106.

Wardle, R.J. and Bailey, D.B., 1981. Early Proterozoic sequences in Labrador. In: F.H.A. Campbell (ed.), Proterozoic Basins of Canada. Geological Survey of Canada Paper 81-10, supplement.

Wardle, R.J., Rivers, T., Gower, C.F., Nunn, C.A.G. and Thomas, A., 1986. The northeastern Grenville Province: new insights. In: J.M. Moore, Jr., A. Davidson and A.J. Baer (eds.), The Grenville Province. Geological Association of Canada Special Paper 31, pp. 13-29.

Williams, M.L., 1994. Sigmoidal inclusion trails, punctuated fabric development, and interactions between metamorphism and deformation. Journal of Metamorphic Geology, 12: 1-21.

Williams, P.F., 1997. Rotating garnets. GAC-MAC Joint Annual Meeting, Ottawa 1997, program with abstracts, 22: A158.

Wilson, M.E., 1918. The subprovincial limitations of pre-Cambrian nomenclature in the St. Lawrence basin. Journal of Geology, 26: 325-333.

Wilson, M.E., 1925. The Grenville pre-Cambrian subprovince. Journal of Geology, 33: 389-407.

Windley, B.F., 1984. The Evolving Continents. John Wiley & Sons, Chichester, 2nd ed., 399 pp.

Windley, B.F., 1986. Comparative tectonics of the western Grenville and western Himalaya. In: J.M. Moore, Jr., A. Davidson and A.J. Baer (eds.), The Grenville Province. Geological Association of Canada Special Paper 31, pp. 341-348.

Windley, B.F., 1989. Anorogenic magmatism and the Grenvillian Orogeny. Canadian Journal of Earth Sciences, 26: 479-489.

Wynne-Edwards, H.R., 1964. The Grenville province and its tectonic significance. Geological Association of Canada Proceedings, 15: 53-67.

Wynne-Edwards, H.R., 1969. Tectonic overprinting in the Grenville Province, southwestern Quebec. In: H.R. Wynne-Edwards (ed.), Age Relations in High-Grade Metamorphic Terrains. Geological Association of Canada Special Paper 5, pp. 163-182.

Wynne-Edwards, H. R., 1972. The Grenville Province. In: R.A. Price and R.J.W. Douglas (eds.), Variations in Tectonic Styles in Canada. Geological Association of Canada Special Paper 11, pp. 263-334.

Wynne-Edwards, H. R., 1976. Proterozoic ensialic orogenesis: the millipede model of ductile plate tectonics. American Journal of Science, 276: 927-953.

Zwart, H.J., 1962. On the determination of polymetamorphic mineral associations, and its application to the Bosost area (Central Pyrenees). Geol. Rundschau, 52: 38-65.

Appendix A_1: Outcrop locations in Field Area